DECEMBER 31, 1997

FINAL REPORT (Memo 9-5570-RMS-003/98)

CONTRACT NASW-4992
CRATERING EXPERIMENTS AND SCALING STUDIES

Computer Code Study of Asteroid Entry into Venusian Atmosphere: Pressure And Density Fields.

Principal Investigator:	Robert M. Schmidt
Institution:	Boeing Shock Physics ISDS
Address:	M/S 8H-05, P. O. Box 3999
City/State/Zip Code:	Seattle WA 98124
Telephone:	(253) 773-1113
	Fax: (253) 773-1249
E-Mail Address:	robert.m.schmidt@boeing.com

TABLE OF CONTENTS

LIST OF FIGURES page no.

ABSTRACT

Analysis of the cratering records on the Moon, Mercury, and Mars have shown similar size-frequency distributions of craters produced during the late heavy bombardment of the inner solar system (Strom, 1988). Venus provides a valuable data base of information on the impacting population for more recent time. Because of resurfacing events, the Venusian cratering record has been estimated to be only about 500 million years old, and for the most part is in pristine condition, thereby producing an opportunity to discover the properties (size/velocity distribution) of the objects that recently impacted its surface.

The Magellan IR mapping of the Venusian surface has produced an extremely high-quality set of crater topographies. The observed deficit of small craters is qualitatively explained by atmospheric effects on impactor breakup and the retardation effects of pressure on crater formation. Information about resurfacing history and impactor flux population can only be conjectured using arrant approximations for atmospheric effects on crater size scaling, such as assuming the absence of pressure effects or using other ad hoc approximations for this dependence. The recent work by Ivanov *et al.*(1986; 1992); Phillips *et al.*(1991;1992); Schaber *et al.* (1992) and others support the notion that atmospheric effects may have strongly influenced the Venusian cratering record. The work reported here looks at the potential synergism of aerodynamic entry and the gas dynamic flow fields that govern during the time scale and in the vicinity of crater formation.

INTRODUCTION

An essential requirement for proper interpretation of the Venus crater data set is better understanding of the role of a dense atmosphere on crater formation. The first crater observations were confirmed less than a decade ago and since then there have been a number of crater statistical studies looking at surface age and impactor fluxes, but the role of a dense atmosphere on crater formation and final crater size has never been accounted for.

Atmospheric effects on impact crater formation are very complex because they includes asteroid interactions with the atmosphere that in turn may have a synergistic effect on crater formation. The importance of atmospheric pressure effects has long been identified for explosive cratering by a number of investigators including Chabai, 1965; Johnson *et al.*, 1969; Herr, 1971; Schmidt *et al.*, 1986; Housen and Schmidt, 1990; Housen,*et al.*, 1992; and Schmidt *et al.*, 1992; 1993. In particular, the work by Housen *et al.*, (1992) provides the best correlation and scaling for the role of atmospheric pressure for explosive cratering at various depths of burst.

For impact cratering there is an additional synergistic effect of the impactor traveling through the atmosphere prior to hitting the surface. This creates a strong shock flow field setting up transient pressure and density variations across the surface. There have been a number of experiments to isolate different aspects of the impact cratering process. In

particular, small scale impacts for pressures less than 1 bar have been studied by Schultz and Gault (1979), Holsapple (1980) and Schultz (1990b; 1992). In another approach, Schmidt (1992; 1993) has used shallow-buried explosives to simulate impact cratering using a pressure chamber mounted on a centrifuge with pressure as high as 40 bars. We do not know how any of these reported effects scale or if they important in the interpretation of the Venusian crater record.

For large scale impact cratering these questions remain to be answered:

1) What is the shock pressure transient due to atmospheric entry?
2) What are the time scales of this overpressure compared to that of crater formation.
3) Does shock wave evacuate ambient gas?
4) How does disturbance scale with impactor size?
5) Effect of target boundary conditions?
6) Effect of entry incidence angle?
7) Does the transient crater lip lead or lag the dynamic pressure increase?
8) What is the overpressure and density at the ejecta plume leading the excavation?
9) Is there some time scale after which the remaining variation can be approximated by a constant pressure and density; and
10) if so, are they higher or lower than the initial undisturbed values?

APPROACH

In conjunction with Paul Hassig of iMALL Inc., we modified the MAZe code to examine various entry scenarios and simulation schemes. One of our objectives was to port the code to run on a MacIntosh at Boeing. This required quite a bit of extra work getting appropriate Fortran Update routines, etc. As it finally worked out, we update the program library on a SUN workstation and then compile on the Mac., not the most convenient but a workable solution using limited resources. We obtained the basic MAZe from Defense Special Weapons Agency (formerly Defense Nuclear Agency). MAZe is a CFD code developed to investigate the formation of dust, water, and ice clouds from nuclear and high explosives , including fireball expansion, airblast propagation, and boundary layer analysis (Hassig, *et al.*, 1991, 1992). Its relevant capabilities include adaptive zoning that automatically refines the grid where "needed" and TVD (Total Variation Diminishing) finite differencing. It employs a linearized Riemann solver, is second-order accurate, and flux limiting . Multiphase physics treats the mutual interactions between a gas mixture and the solid/liquid particles contained in that gas. ALE (Arbitrary Lagrangian Eulerian) grid techniques track the physical interface between different type materials. A recent application of interest using this code was the SL-9 Jovian atmospheric entry calculation by Hassig, P. J. *et al.*,(1994) in which a scheme for impactor breakup was implemented.

Modeling assumptions for the Venus atmosphere include: temperature profile from Seiff (1983) — 90 bar pressure, 733 K temperature at surface and treated as 100% CO2 modeled as a non-ideal gas EOS with variable gamma, of form P = rho (gamma -1) e , and requires gamma

versus T, and gamma versus e . For 111 K < T < 3000 K gamma is a look-up from gas tables (Keenan and Kaye, 1945) and for T > 3000 K, gamma = 1.15.

A previous relevant work (Hassig, P. J., 1991; Hatfield, *et al.*, 1992; Roddy, *et al.*, 1992;) examined the atmospheric response to a 10-km diameter asteroid travelling at 20km/s with normal impact on Venus. With these results, we set out to investigate how the atmospheric interaction on entry would scale with impactor size and interact with the cratering process. Our initial calculation was to repeat the one above, only for the normal entry of a 1-km diameter body. No provision for body deformation or breakup during atmospheric passage was implemented for these calculations. The intent here is to vary impactor size over an appreciable range to exercise the effect of the finite height of the atmosphere.

RESULTS

Normal Incidence Cases (2-D calculations)

As in the 10-km case above, the 1-km diameter calculation was started with the leading edge of the impactor located at 40 km above the Venusian surface and with U = 20km/s. For the 10-km body the calculated velocity at impact was 19.5 km/s compared to 15.7km/s for the 1-km body. Transit times through the atmosphere were 2.01 and 2.16 seconds respectively. Peak pressure on the leading edge of the impactor ramped up to 125 kbar for the large one and 75 kbar for the small one.

Using scaling laws for negligible atmosphere conditions from Schmidt and Housen (1987) as shown schematically in Fig. 1. to estimate crater sizes and times, we get the following comparison for the two events:

Impactor diameter (2a)	Transit time	Final crater radius (Rf)	Rf/a --	Formation time (Tf)	Growth (km, sec)
1-km	2.01 sec	3.9 km	7.8	18.2 sec	$R = 1.7\ t^{0.287}$
10-km	2.16 sec	26.5 km	5.3	47.5 sec	$R = 8.8\ t^{0.287}$

Figure 2 presents the transient pressure and density histories at crater's edge for the two calculations. The results for the 10-km impactor are shown on the left and are compared with those for the 1-km impactor on the right. The time origin of the plots is at 2 seconds which corresponds to the approximate impact time for both cases. The pressure has returned to ambient at about 29 seconds for the larger one and at about 11 seconds for the smaller one. Likewise, the density has returned to ambient at about 4.8 seconds for the larger one and at about 3.3 seconds for the smaller one and continues to fall to about an order of magnitude below ambient shortly thereafter. This suggests some simplification may be plausible for the cratering simulation problem. Once the shock passes, most of the crater excavation takes place at ambient pressure (92 bars), whereas the density is at least an order of magnitude below ambient density (< 10^{-3} g/cc) for the major portion of crater excavation. This indicates that drag effects should be considerably less than those estimated for undisturbed ambient conditions.

Coupling Parameter: $C \propto aU^{\mu}$

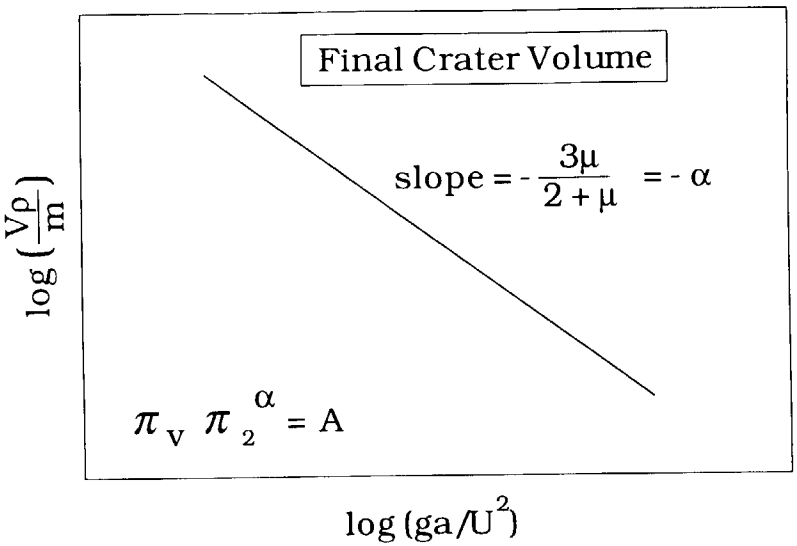

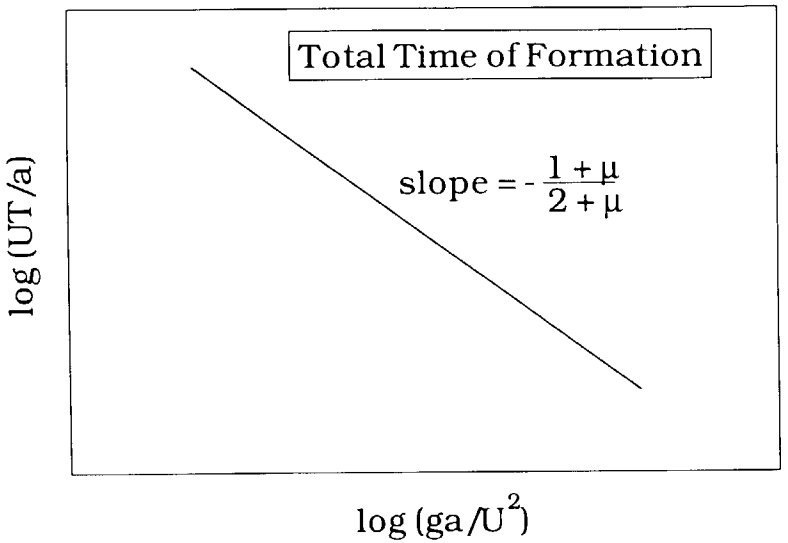

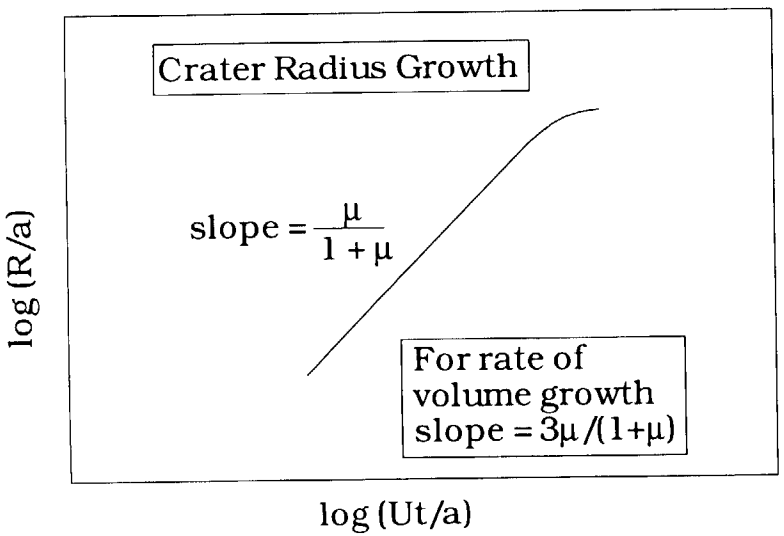

Dependence of exponents on material type

	α	μ	Crater Size	Form Time	Rate of Growth
Mom. Limit	3/7	1/3	0.429	0.571	0.250
Dry Soil	0.507	0.407	0.507	0.585	0.289
Wet Soil	0.600	0.500	0.600	0.600	0.333
Water	0.650	0.553	0.650	0.608	0.356
Energy Limit	3/4	2/3	0.750	0.625	0.400

Fig. 1 A schematic illustration of the generalized power-law scaling relationships, all of which depend upon a single scaling exponent, μ (or α) as developed by *Holsapple and Schmidt (1987) and Schmidt and Housen (1987).*

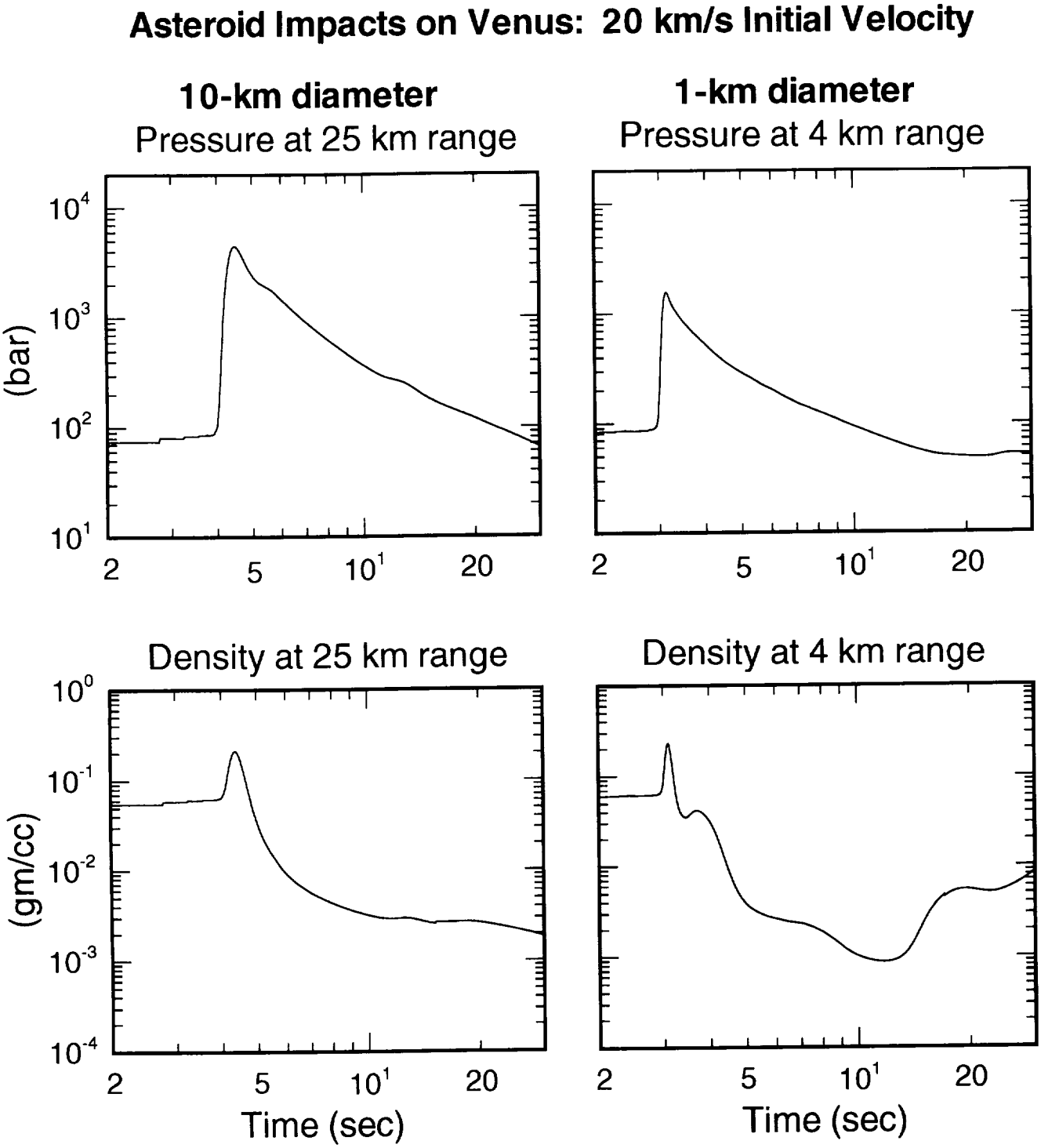

Fig. 2 Comparison of pressure and density arrival and decay at ranges approximating the final crater radii for a 10-km and a 1-km diameter impactor.

Figure 3 shows the propagation of the flow field scaled by the impactor radius usually referred to as cube root scaling. The results for the large impactor are shown by the bold curve and can be seen to produce a stronger disturbance due to the higher contact velocity and slightly out run those due to the smaller impactor represented by the thinner line. On a cube root basis, the final crater size for the larger event is at an R/a of 5.3, whereas the crater for the smaller event is at an R/a of 7.8. This difference is due to gravity. We can also examine the time scale of the flow field relative to the crater excavation time or crater radius as shown in Fig. 4. The times correspond to the same extent of relative crater excavation indicated by fixed values of range/final crater size. The heavy curve shown below the x-axis in each snapshot is the transient crater profile for negligible atmosphere calculated from the growth equation tabulated above. As can be seen in the first snapshot, when the transient crater radius is 23% of the final value, the large impactor (heavy line) creates a many thousandfold overpressure compared with a factor of about 80 for the smaller one (light line). For each, the region of overpressure extends out to the edge of the evolving crater. As the transient crater approaches half the final crater radius shown in the second snapshot, the shock wave has begun to pull out in front of the crater lip and the pressure is about equal for both; but, still an order of magnitude above ambient. Here the shock is further ahead for the smaller impactor. For the major part of the volume excavation, beyond 0.59 radius with approximately 80% of the volume excavation remaining, the pressure is nearing ambient. Note, that due to gravity, final radius/impactor radius for the larger impactor is at an (Rf/a) of only 5.3 compared to 7.8 for the smaller one. Consequently, it appears that the density variation more or less scales with evolving crater size as is shown in Fig. 5 for comparable scaled range, shown here for (r/Rf) equal to about 0.73±.03. The results for both impactors decay to values approaching earth ambient at about 20% of the final crater volume excavation (V/Vf).

Figure 6 shows a way to compare pressure history in a scaled sense for the two sizes. Since the smaller body is affected more by drag, it impacts at 15.7 km/s, whereas the larger one slows only slightly to 19.5 km/s. This is significant in that the decrease in velocity results in an increase in the effective value of $\pi_2 = ga/U^2$ when the impactor hits the surface If the normalized pressure ($2P/\rho U^2$) history is scaled by the crater time of formation, an apparent dynamic similarity is observed at fixed scaled range/crater radius (r/R_f) > 0.35 and beyond. Furthermore, in both cases the peak overpressure decays to ambient (90bars) at approximately $V/V_f = 0.5$ as shown in Fig. 6. This has important implications for determining the stages of crater formation that might be affected by shock overpressure.
It appears that the shock wave and high pressure regime occur over a very much shorter time scale and possibly can be neglected for crater excavation considerations.

The original 10-km impactor calculation performed by Hassig (1991) used a numerical artifact to create a "transparent" target allowing the impactor to pass through the surface. Hence, the calculated aerodynamic effects were due only to the entry shock wave. Concern was expressed that vaporization might provide a significant contribution to the flow field. Likewise, a compliant cratering surface would cause some vaporization while at the same time absorbing a lot of the kinetic energy in the form of coupling to the ground and in crater formation. To test the effects of these various boundary conditions, two additional calculations were run. One had a rigid surface, causing the impactor to arrest, rebound and vaporize upon

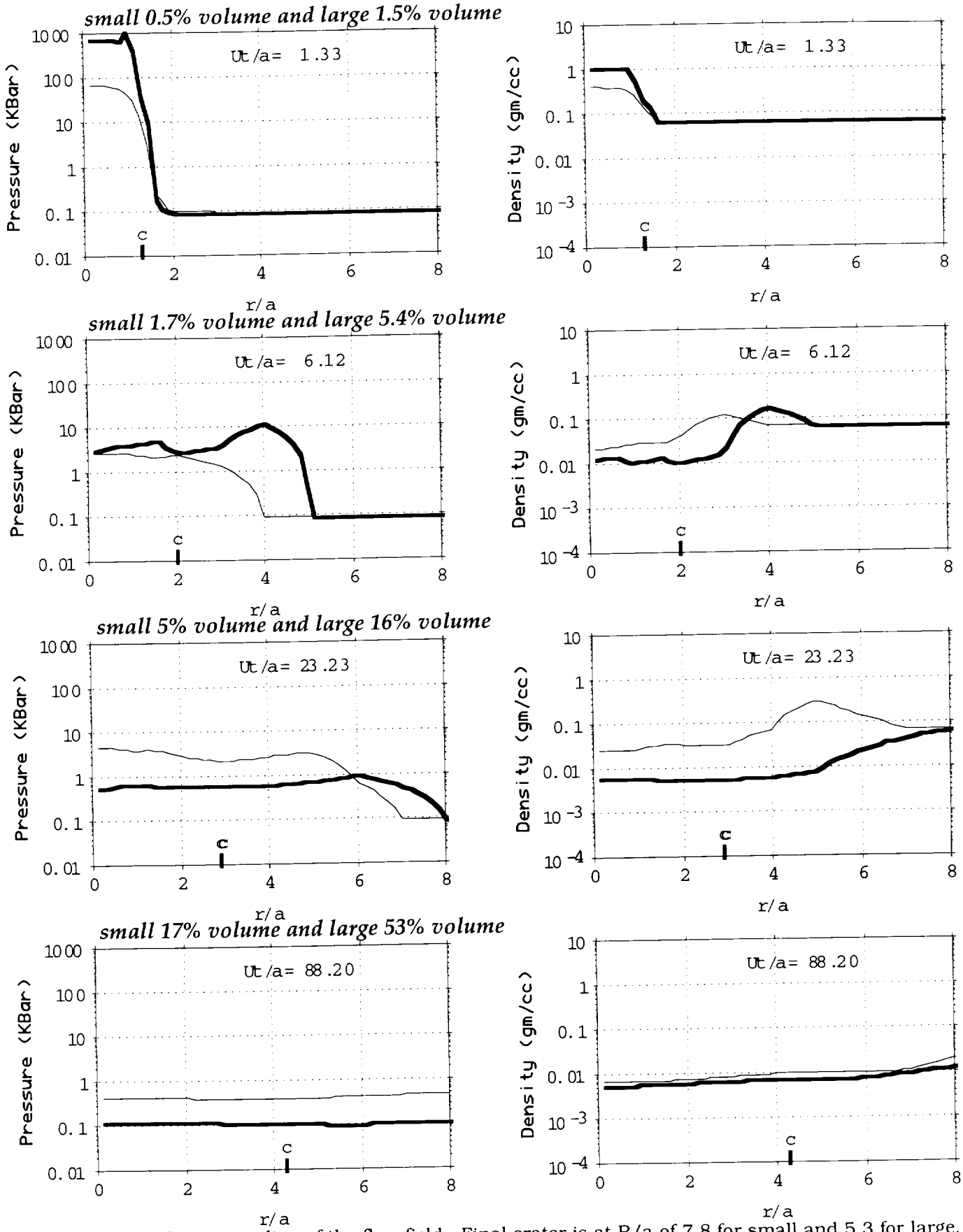

Fig. 3 Test for cube root scaling of the flow field. Final crater is at R/a of 7.8 for small and 5.3 for large.

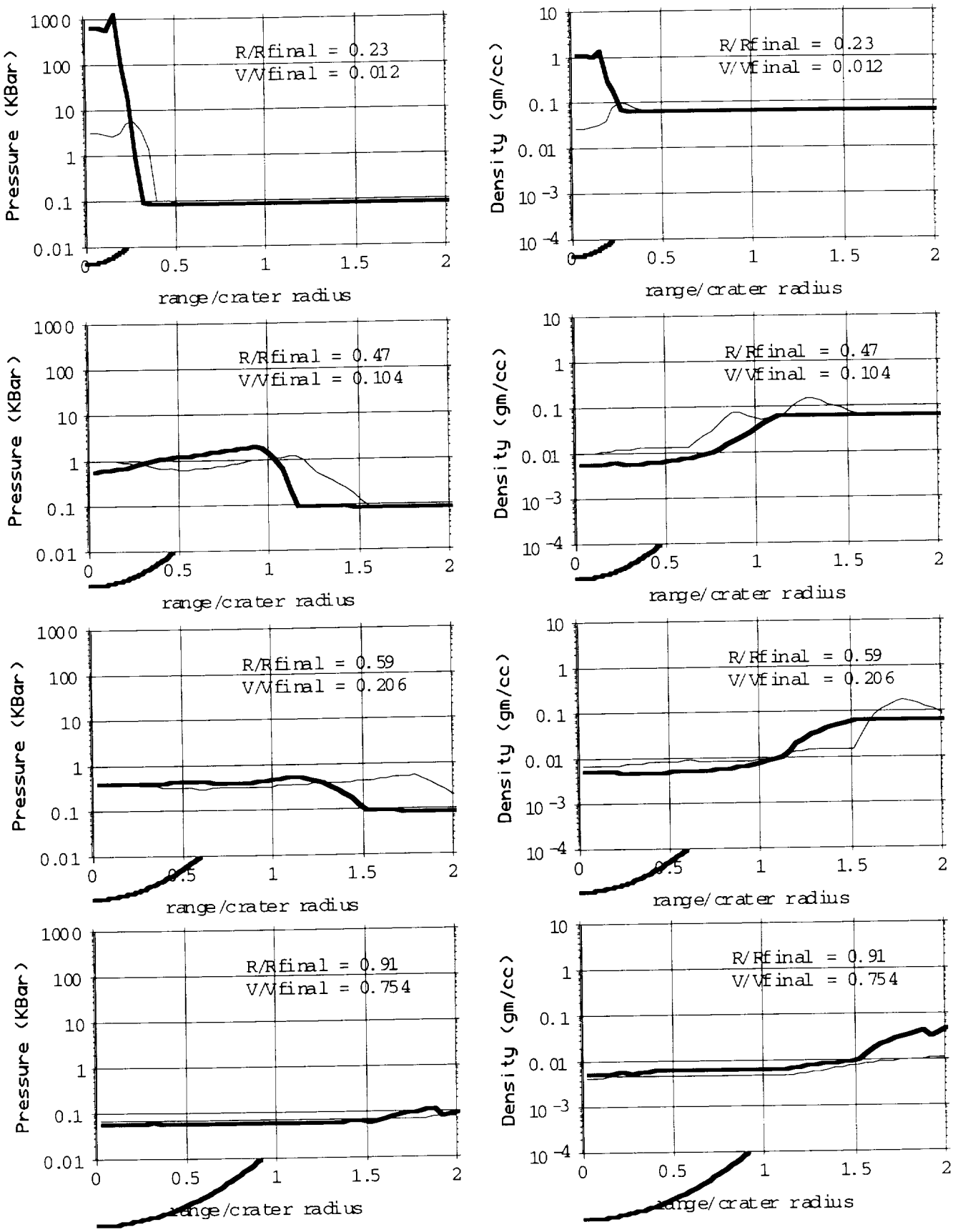

Fig. 4 Flow field dyanmics scaled by crater radius. Disturbance precedes crater for both events.

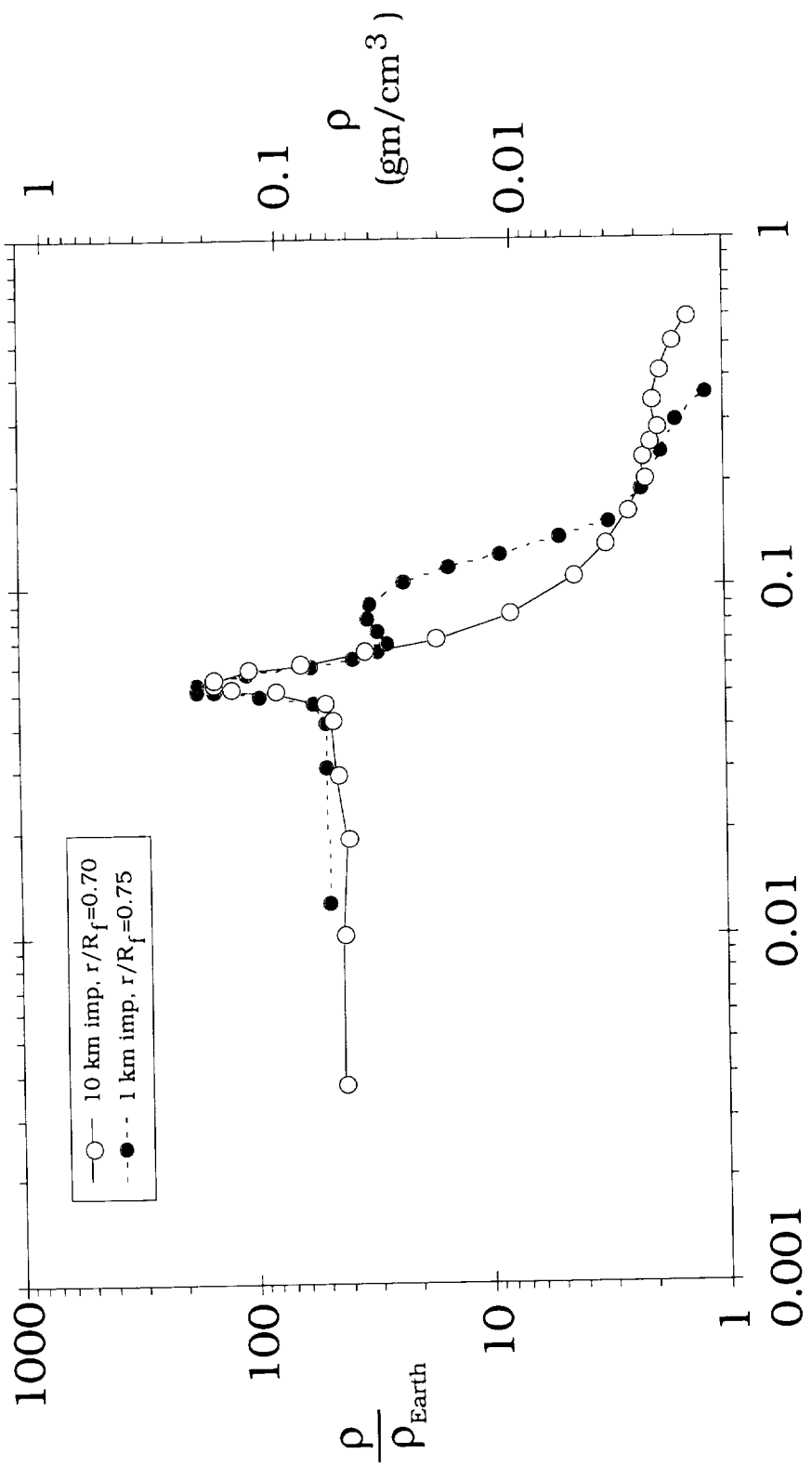

Fig. 5 Density profiles at fixed scaled crater radius.

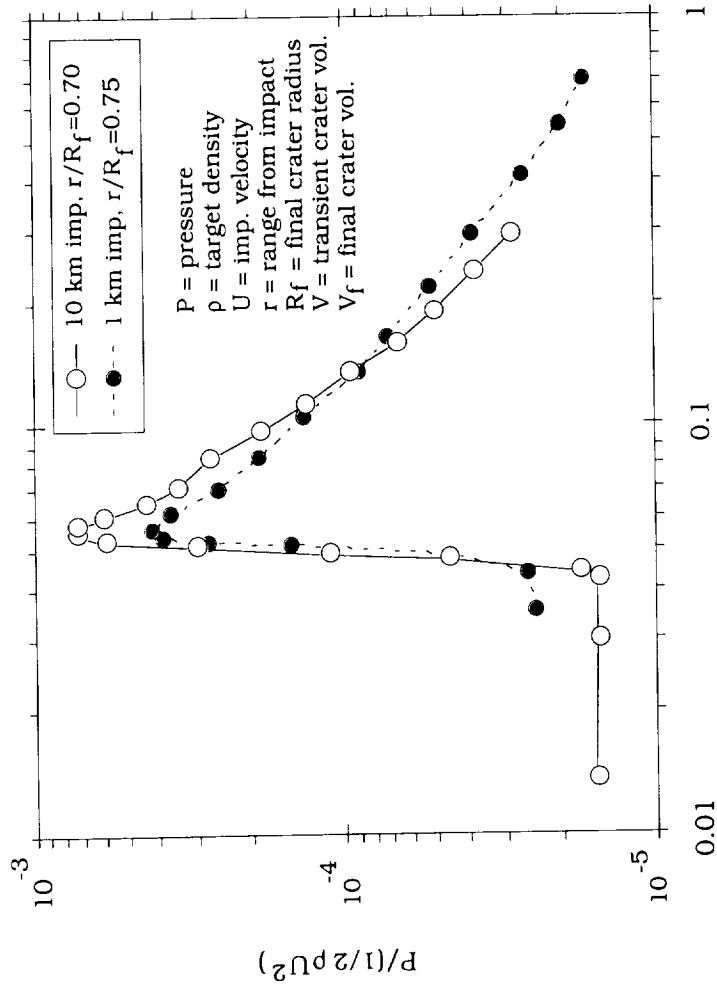

Fig. 6 Blast wave profiles at fixed scaled crater radius.

contact. The second used a coarsely-zoned quartz-like material to allow crater formation to take place. In the early time, close in, there were significant differences. However at the range of expected crater radius, the profiles all more or less coalesced as shown in Fig. 7. The rigid boundary showed higher peak shock pressures and density spikes and the cratering target showed the lowest peaks. However, over the time regime of interest for crater formation, there is no significant difference.

45° Incidence Case (3-D calculation)

A preliminary 3-D calculation was also preformed to explore the influence of incidence angle. To run such a problem on a personal computer such as a PC or a Mac did limit us to fairly coarse zoning. The 3-D calculation was performed with approximately 26,000 nodes on a 32 meg 486 computer, which was about at maximum capacity. The results are given as case VEN09 in the appendix and are shown for times out to 300 secs. The 3-D calculation was performed with some additional simplifications. There was no slow-down due to drag and the projectile was allowed to enter from a height from a height of 32 km. This resulted in a time of impact of about 2.26 seconds. Because of the coarser zoning necessary in the 3-D case, we reran the normal impact case with comparable zoning for normal impact, the results are compared in Figs. 8, 9 and 10. Figure 8 is the 3-D result for normal impact from case VEN09a showing pressure histories at ranges of 1, 2, 3, 4 and 5 km. These can be compared to the finer zoned 2-D case, VEN07 in Fig. 9 and the comparable coarser zoned 2-D case VEN07a in Fig. 10. Looking at the range of 5 km, there is some broadening of the pulse and the peak is down about 15% from the 2-D fine zone case. The coarser zoned 2-D seems to be down even more in amplitude, like 30%. At the 2-km range, the agreement is even a little bit better. At least by this comparison, we feel the pressure values should be pretty good with the coarser 3-D zoning. Fig. 11 is a map of peak pressure ratio scaled by ambient pressure Po = 92 bars. This figure can be compared directly with "*Fig. 8, part a*" from Takata *et al.* (1995) and reproduced here as Fig. 12. Her scaled range was divided by 2 to account the radius ratio of 2:1 between the two calculations, hers was for a 2-km diameter impactor, ours for a 1-km diameter impactor. The results are quite comparable for a first cut. This needs further verification with comparisons of other her other parameters plotted such as: (b) maximum shock density, (c) maximum horizontal gas velocity, (d) maximum induced dynamic pressure and (e) maximum temperatures. Figure 13 contains the same information plotted as the more common overpressure parameter. Figure 14 is the accompanying time of arrival for the maximum shock overpressure versus range.

Laboratory validation and simulation

Another problem area that was scoped using the code in a 2-D configuration was to examine different laboratory techniques to simulate impact cratering with large atmospheric pressure. Conventional two-stage light gas guns are limited to maximum impact velocities of 7 km/sec or less, particularly in the presence of a finite atmospheric pressure. At these velocities, the atmospheric interaction is much less important than at velocities of the range of 20 to 30 km/sec applicable to planetary impacts. Our code calculations for the 1-km diameter impactor show that half of the kinetic energy was deposited in the atmosphere for normal (90° to the

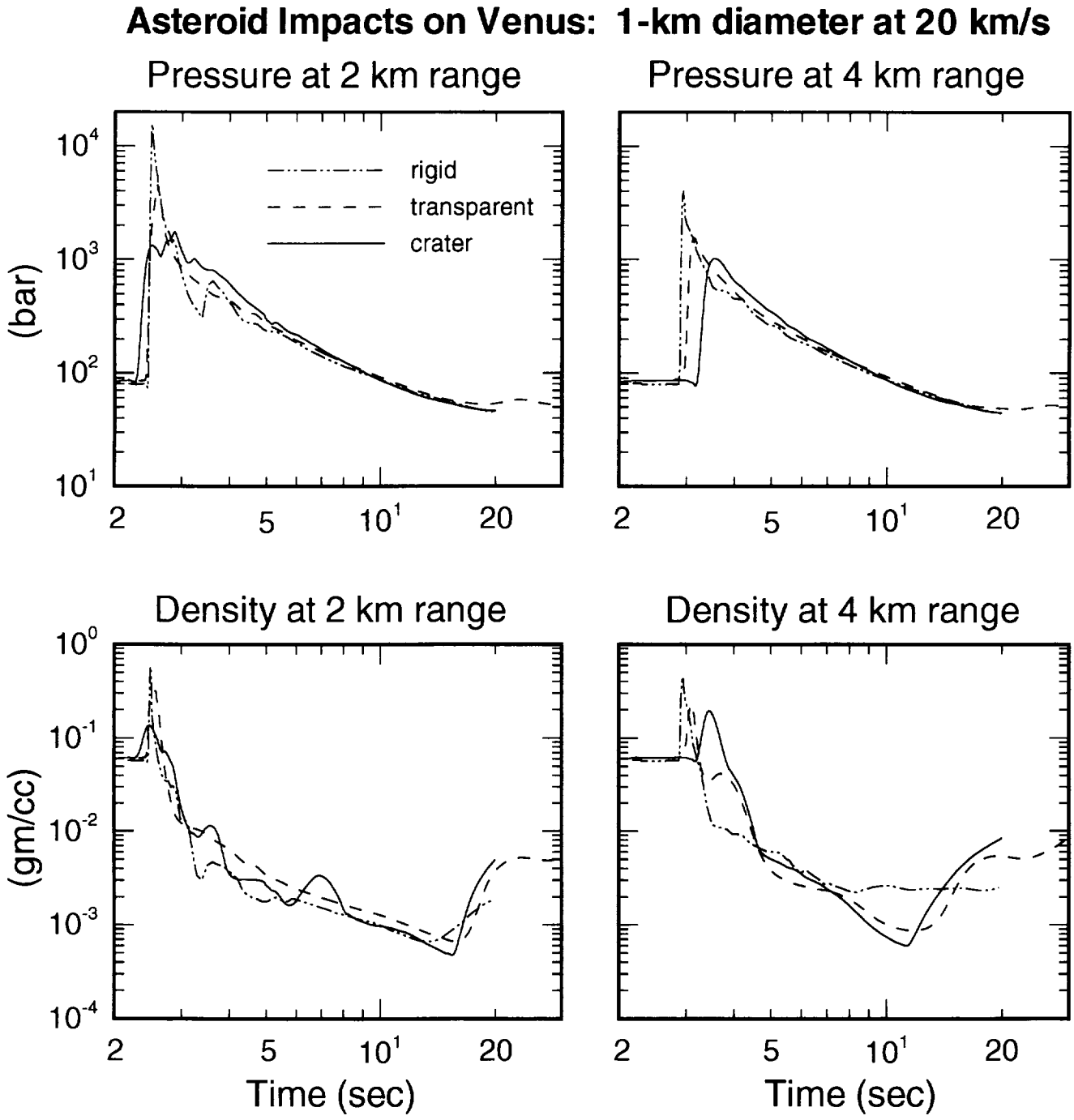

Fig. 7 Comparison of the effect of three different boundary conditions (rigid, "transparent," and cratering) on the calculated pressure and density histories at 2-km and 4-km ranges. For a 1-km diameter impactor the approximate final crater radius is 3.9 km.

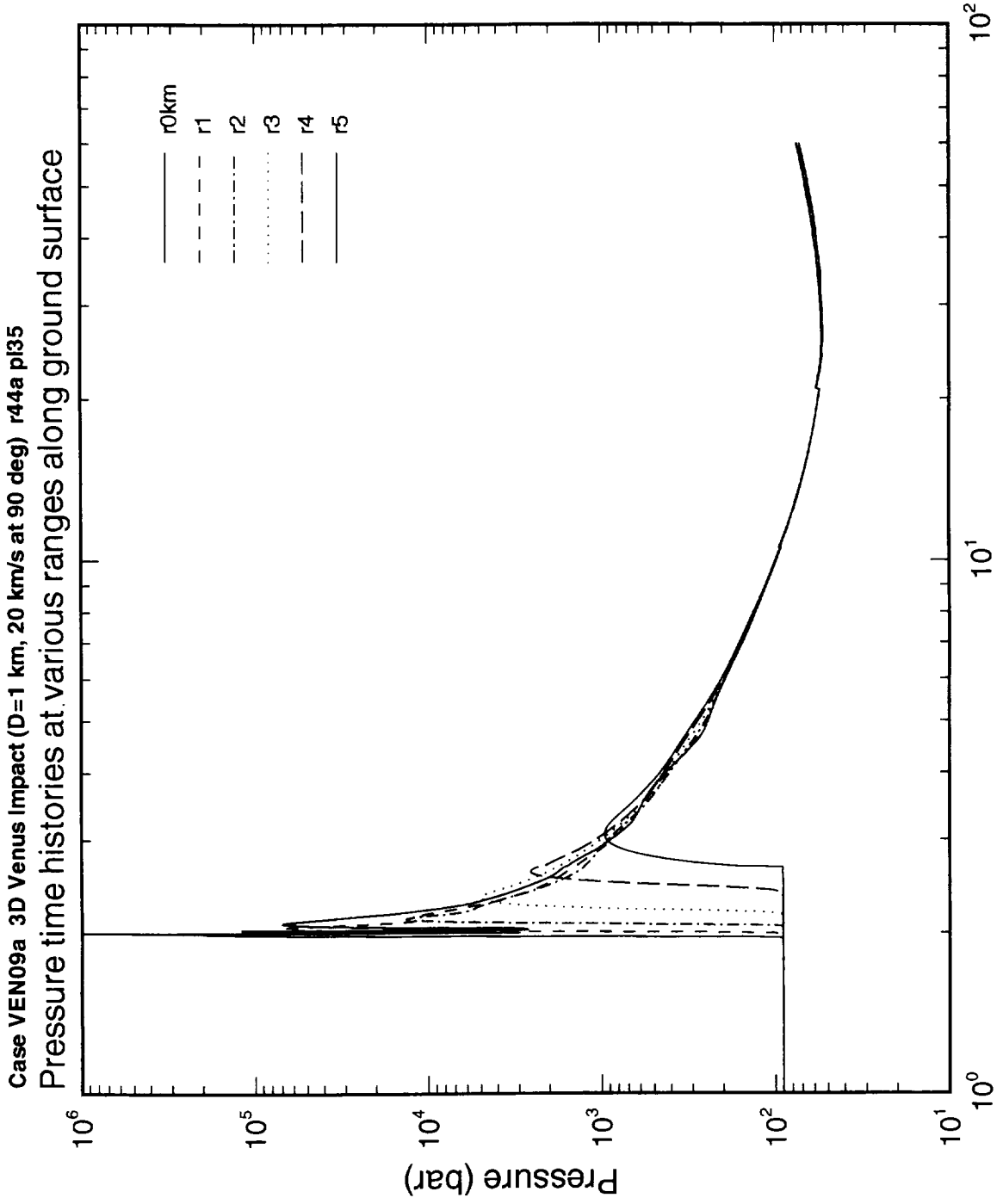

Fig. 8 Pressure histories at ranges of 1, 2, 3, 4 and 5 km from 3-D code calculation for normal impact, case VEN09a.

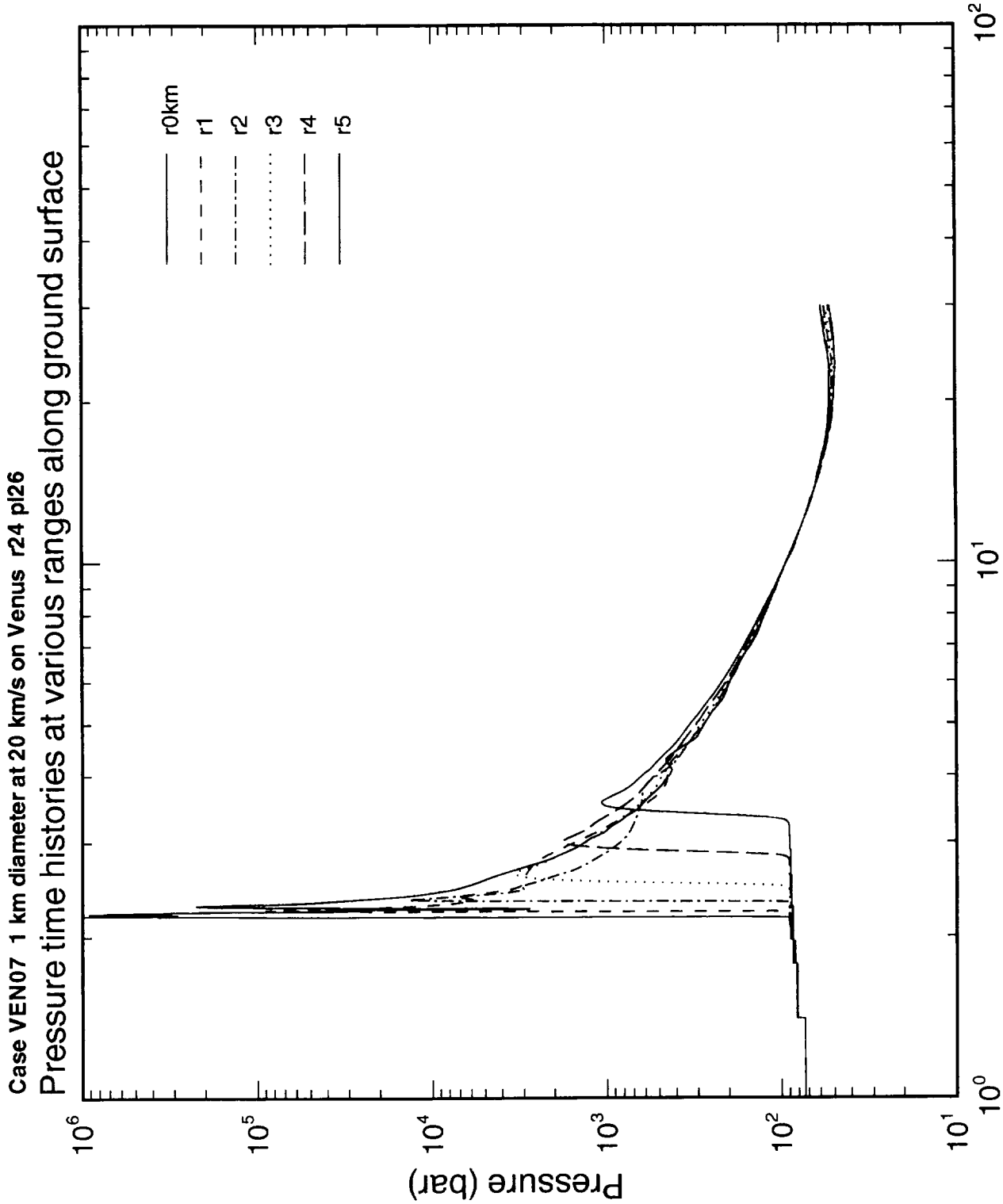

Fig. 9 Pressure histories at ranges of 1, 2, 3, 4 and 5 km from the finer zoned 2-D case, VEN07.

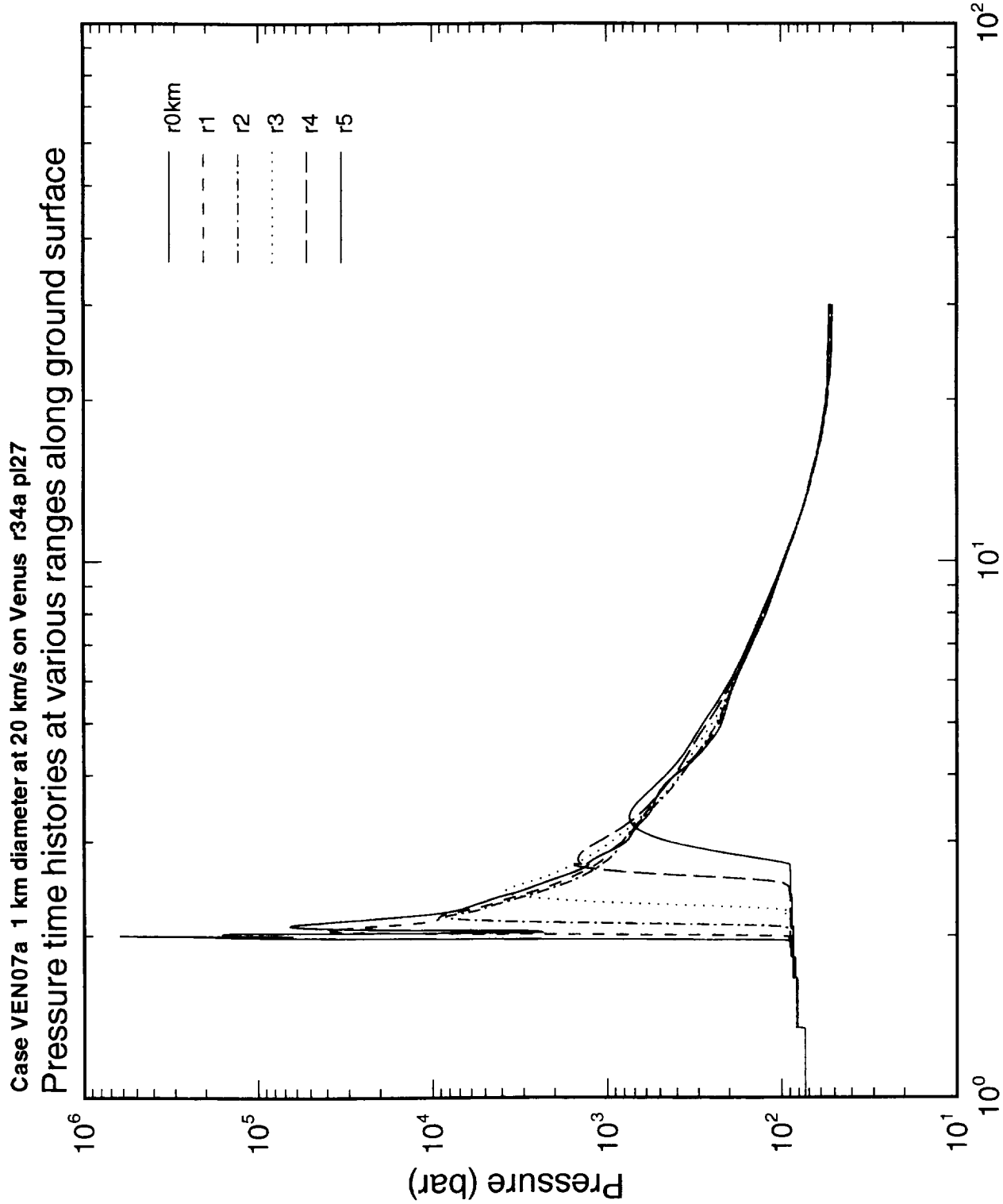

Fig. 10 Pressure histories at ranges of 1, 2, 3, 4 and 5 km from the coarser zoned 2-D case, VEN07a.

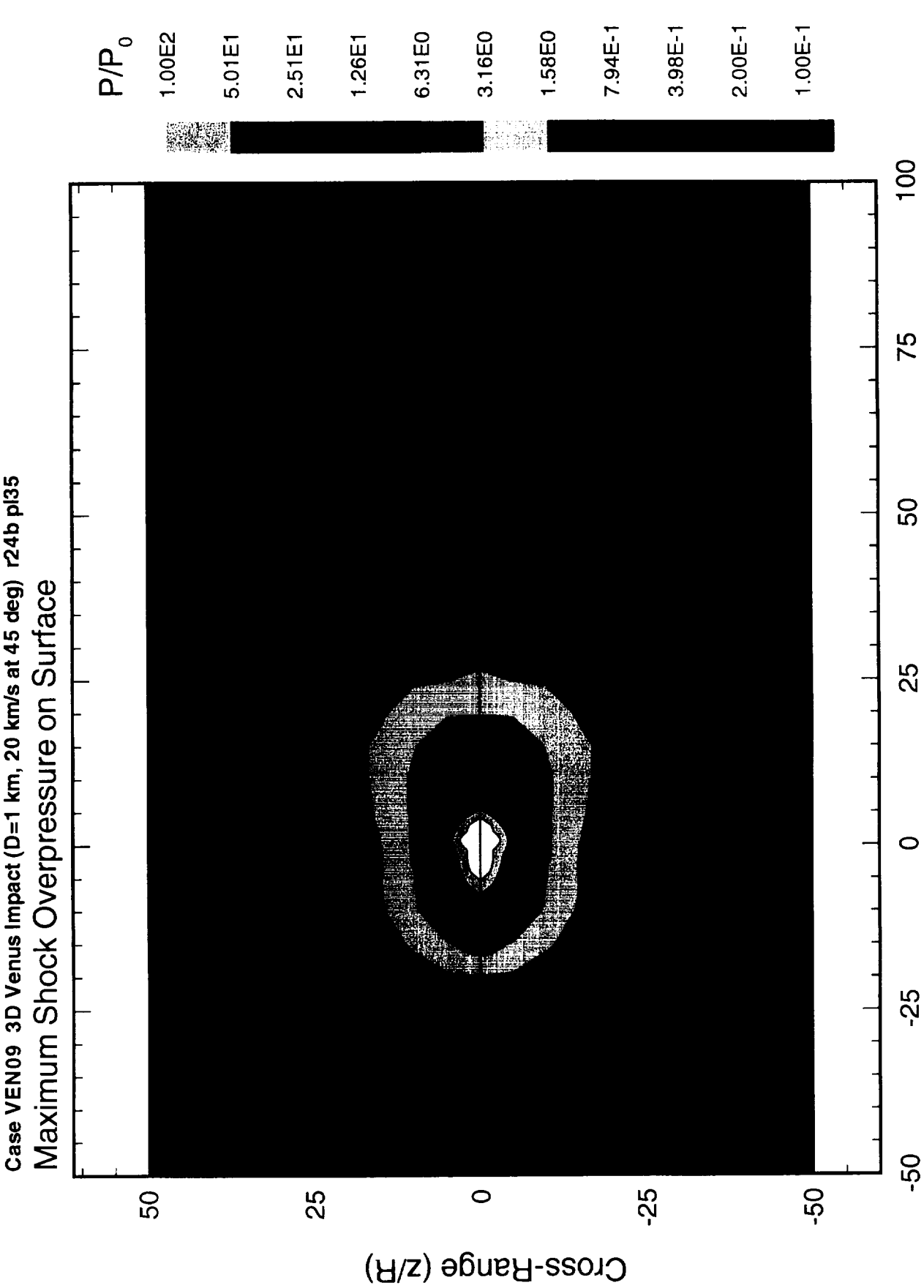

Fig. 11 Map of peak pressure ratio for 45° incidence normalized by ambient pressure Po = 92 bars.

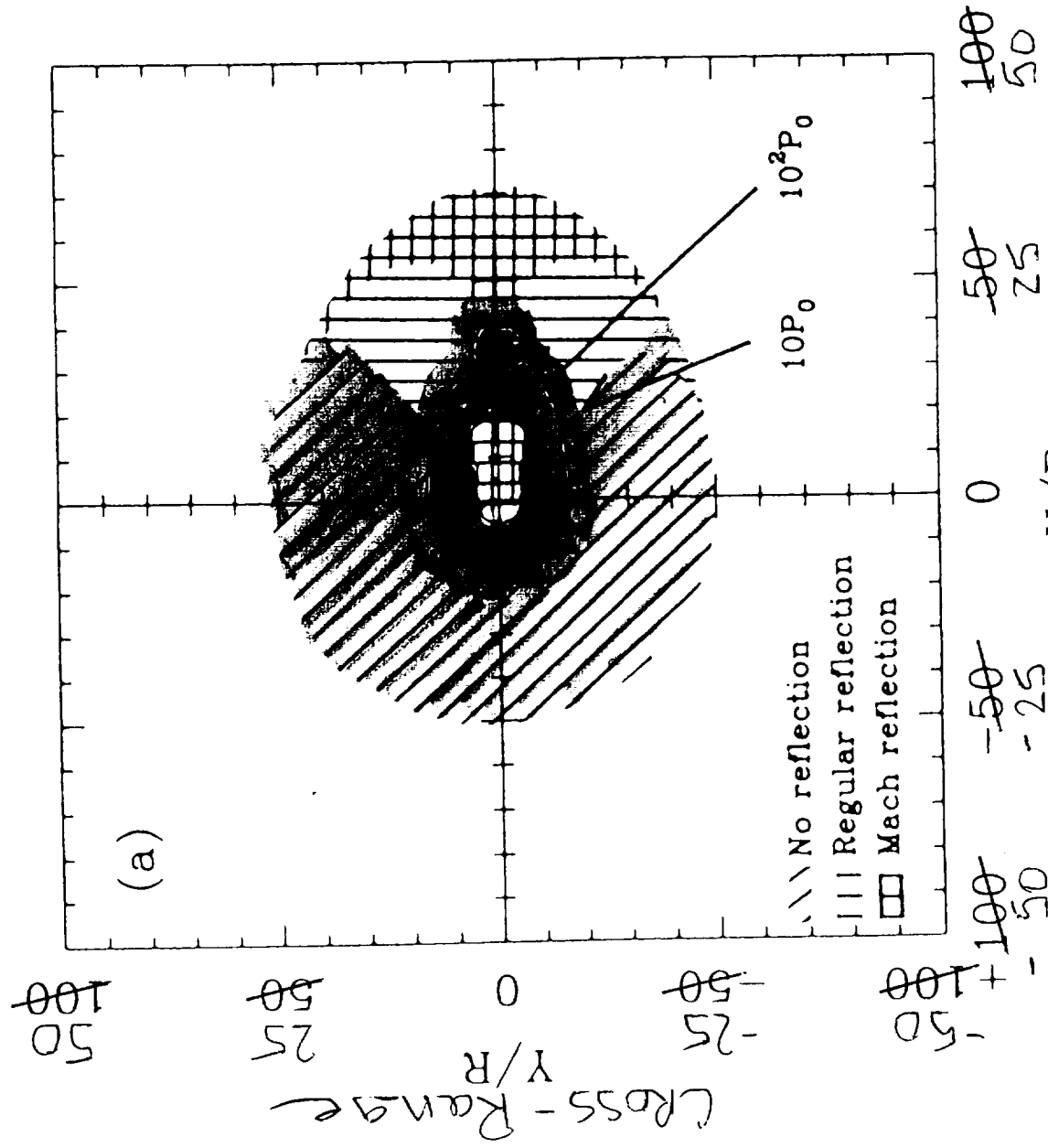

Fig. 12 Map of peak pressure ratio for 45° incidence normalized by ambient pressure Po = 92 bars from *Takata et al. (1995) "Fig. 8, part a"*

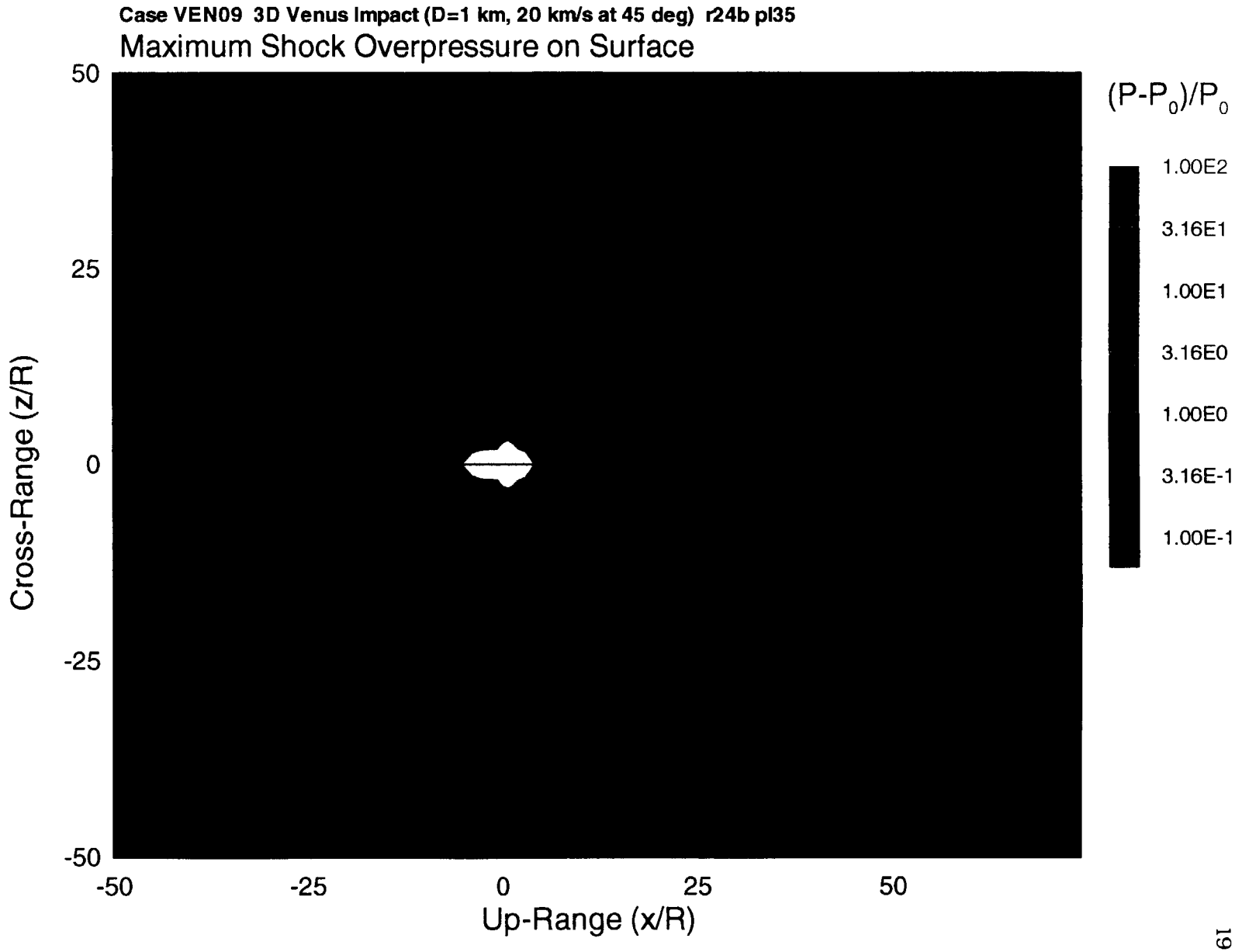

Fig. 13 Map of maximum shock overpressure ratio for 45° incidence, normalized by Po = 92 bars.

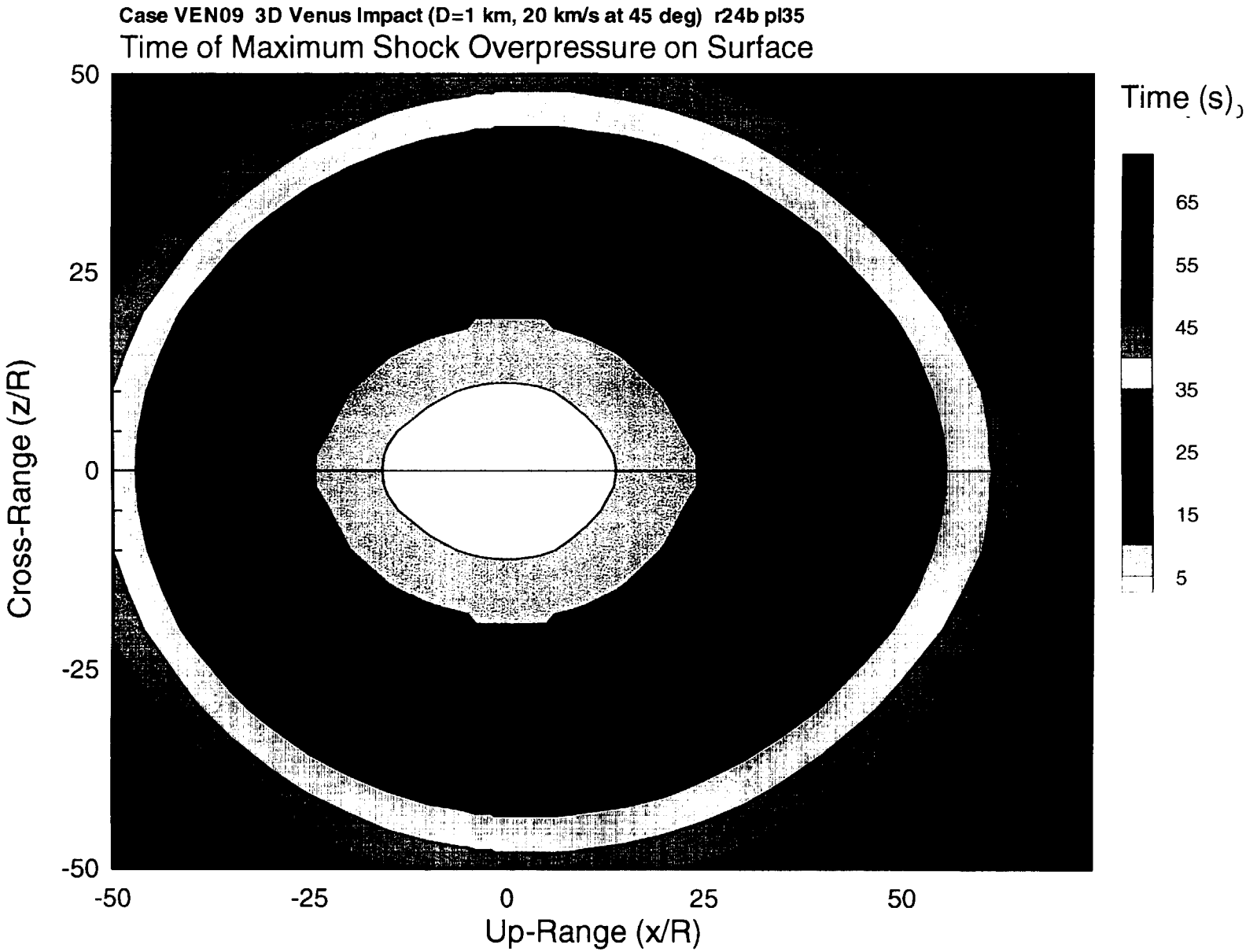

Fig. 14 Map of time of arrival for maximum shock overpressure on suface for 45° incidence.

target) incidence angle. As the angle is reduced to 45°, we expect even greater deceleration resulting in more gasdynamic shock pressure interaction. To simulate these higher speeds and pressure, we looked at test configurations as illustrated in Fig. 15. This is an economical set-up that relies entirely on a geometric array of small explosives. We have pictured a series of discrete detonators; that with a suitable sequential ignition source, can simulate any entry velocity of interest. However, as seen in the results of the MAZe calculations, entry through the Venus atmosphere takes on the order of 2 secs for a 20 km/sec impactor at normal incidence angle. At a 45-degree incidence this would increase to about 3 seconds due to the longer path length and additional deceleration. In either case this is small relative to the time of crater excavation, which is 20 seconds for the 1-km impactor and and 50 seconds for the 10-km impactor at normal incidence. To avoid the complication (and cost) of a ultra-fast ignition requiring sub microsecond timing , an alternative is to use explosive detonator cord with a nominal detonation speed of 7km/sec as shown in Fig. 16.

Energy dissipated in the atmosphere on entry for the two impactors.

Impactor attributes	1 km dia	10 km dia
a (km)	5.00E+04	5.00E+05
delta (g/cc)	2	2
mass (gm)	1.05E+15	1.05E+18
volume (km^3)	5.24E+14	5.24E+17
Uo (cm/s)	2.00E+06	2.00E+06
Uo^2	4.00E+12	4.00E+12
Eo (ergs)	2.09E+27	2.09E+30
Impact conditions		
Ui (cm/s)	1.57E+06	1.95E+06
Ui^2	2.46E+12	3.80E+12
Ei	1.29E+27	1.99E+30
delta E (ergs)	8.04E+26	1.03E+29
(delta E)/Eo	0.38	0.05

Using the value of "delta E" for the energy dissipated in the atmosphere from the above table, 4 cases were run.

Case VEN11 Line charge on Venus (8.04e26) r42a pl35 simulation of 1-km impactor
Case VEN11 Series of 9 explosions on Venus r43a pl35 simulation of 1-km impactor
Case VEN11 Line charge on Venus (1.03e29) r52a pl35 simulation of 10-km impactor
Case VEN11 Series of 9 explosions on Venus(1.03e29) r53a pl35 simulation of 10-km impactor

Results are cataloged in APPENDIX A. The energy was added directly to the air for the spherical charges. It was uniformly distributed out to 500 m radius for the small charges and out to 2.5 km for the large ones. Likewise for the line charges it was uniformly distributed out to 50 m for the smaller one and out to 5 km for the larger one.

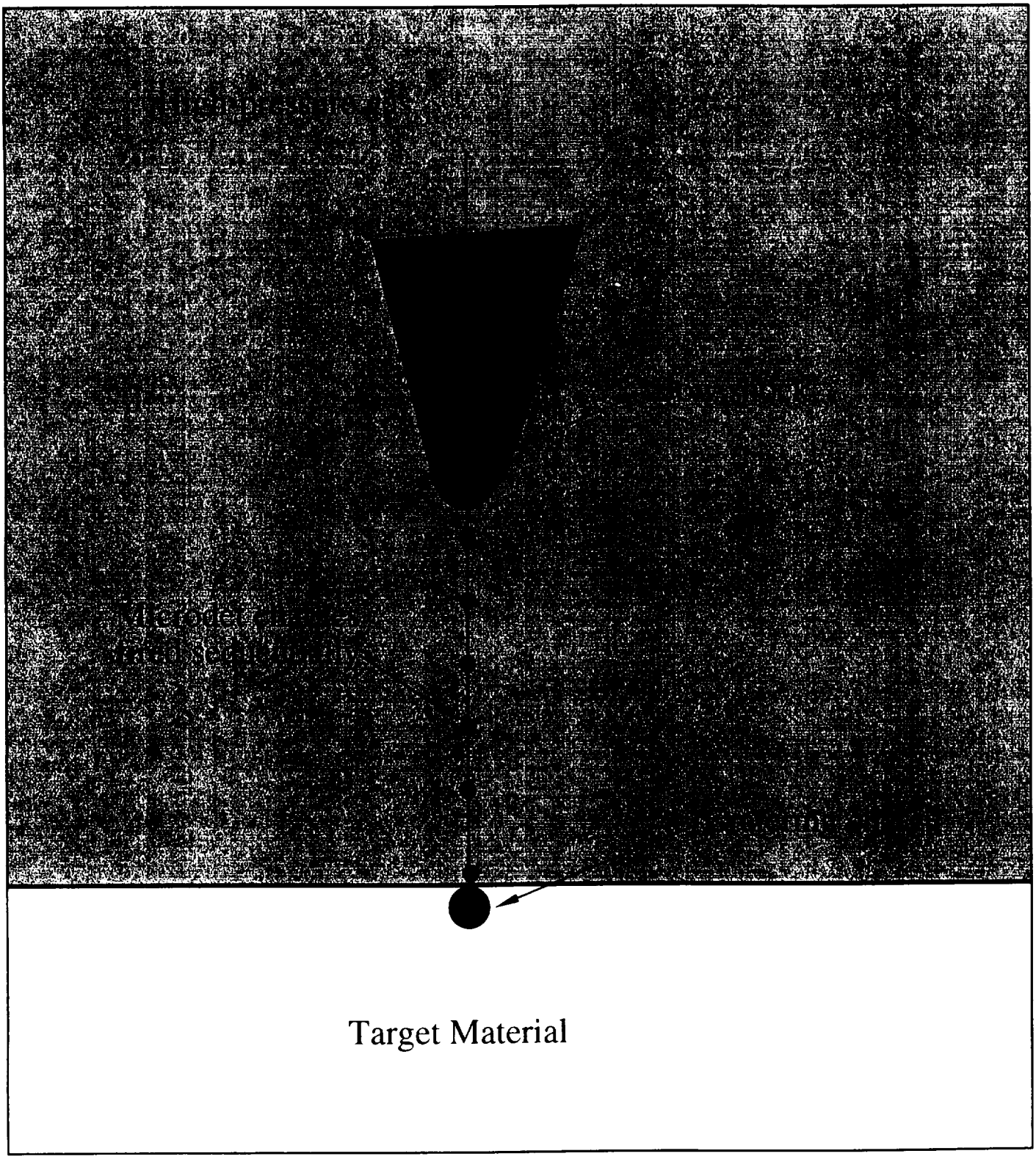

Fig. 15 Experimental technique to simulate entry shock transient dynamic pressure and density fields acting on the crater during formation for arbitrary angle of incidence. By timing and sizing the charge energy release it may be possible to simulate actual impact velocities of interest as large as 20km/sec or more.

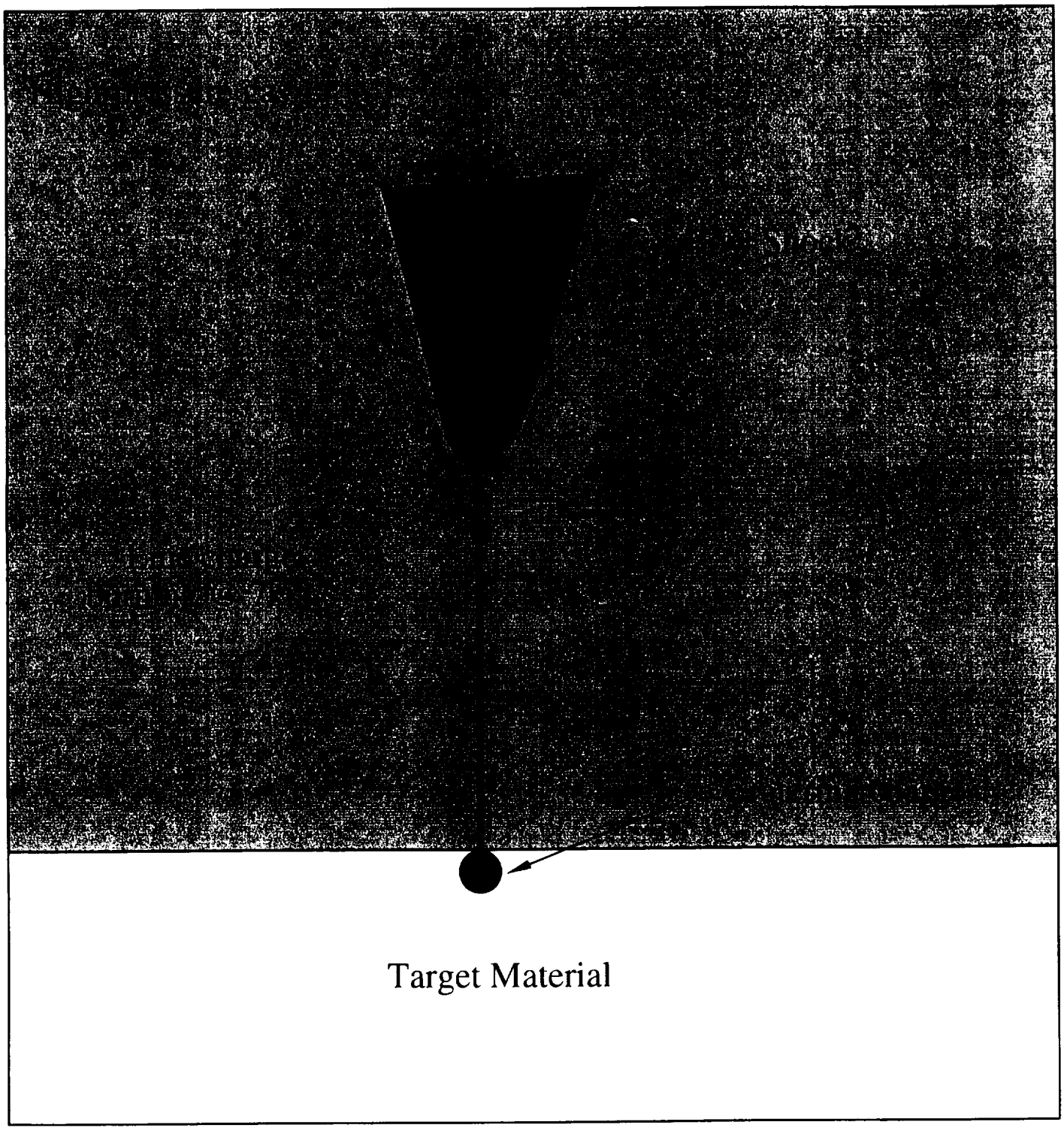

Fig. 16 Experimental technique to simulate entry shock transient dynamic pressure and density fields acting on the crater during formation for arbitrary angle of incidence. By sizing the line charge energy release it may be possible to create strong bow shock effect to test the code and observe the influence on cratering dynamics and final size.

CONCLUSIONS

1.) For cratering, it appears that the atmosphere pressure and density are nearly evacuated prior to the time scale of crater excavation. (See pressure and density histories at appropriate ranges for final crater size). This suggests that direct influence of large pressure and density may be negligible.

2.) The main influence of the dense atmosphere is to slow down bodies smaller than 10 km in diameter. This could skew the crater size counts because of the reduced impact energy for a given size impactor. The slow-down needs to be examined quantitatively for dependence upon angle of incidence.

3.) We appear to have preliminary agreement with the maximum shock pressure calculated by *Takata et al.(1995)* for the 45° case. More comparisons need to be made to verify agreement for other dependent quantities and angles of incidence.

4.) The simulation schemes provide a means to experimentally verify the code calculations and can be done at laboratory scale. It may also provide a means to simulate impact velocities above 7 km/sec.

APPENDIX A

The following table summarizes the calculations performed.
Output for the various cases is arranged in the following order.

Case Number	Diameter (km)	Velocity (km/s)	Boundary Condition	Remarks	page no.
VEN01	10	20	"transparent"	normal incidence	
VEN06	10	20	"transparent"	repeat of VEN01	26
VEN02	1	20	"transparent"	normal incidence	
VEN07	1	20	"transparent"	repeat of VEN02	49
VEN04	1	20	rigid	compare b.c. normal incidence	71
VEN05	1	20	crater	compare b.c. normal incidence	77
VEN09	10	20	"transparent"	45° incidence	82
VEN11r42a	1	line charge	rigid	2D simulation	107
VEN11r43a	1	9 charges	rigid	2D simulation	119
VEN11r52a	10	line charge	rigid	2D simulation	133
VEN11r53a	10	9 charges	rigid	2D simulation	147

10-km Diameter Impactor into Venus

20 km/s Initial Velocity time = 2 sec

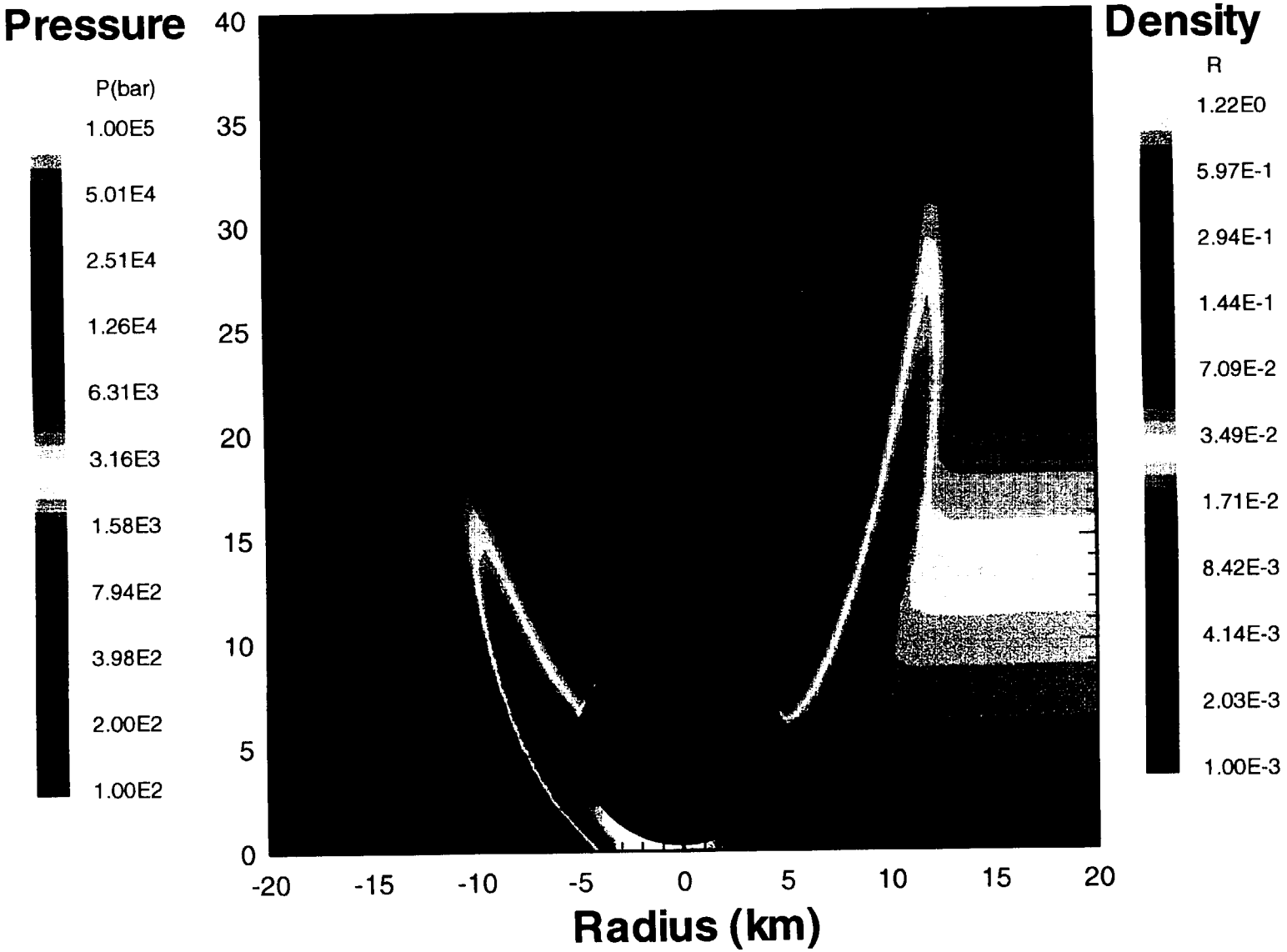

10-km Diameter Impactor into Venus

20 km/s Initial Velocity time = 20 sec

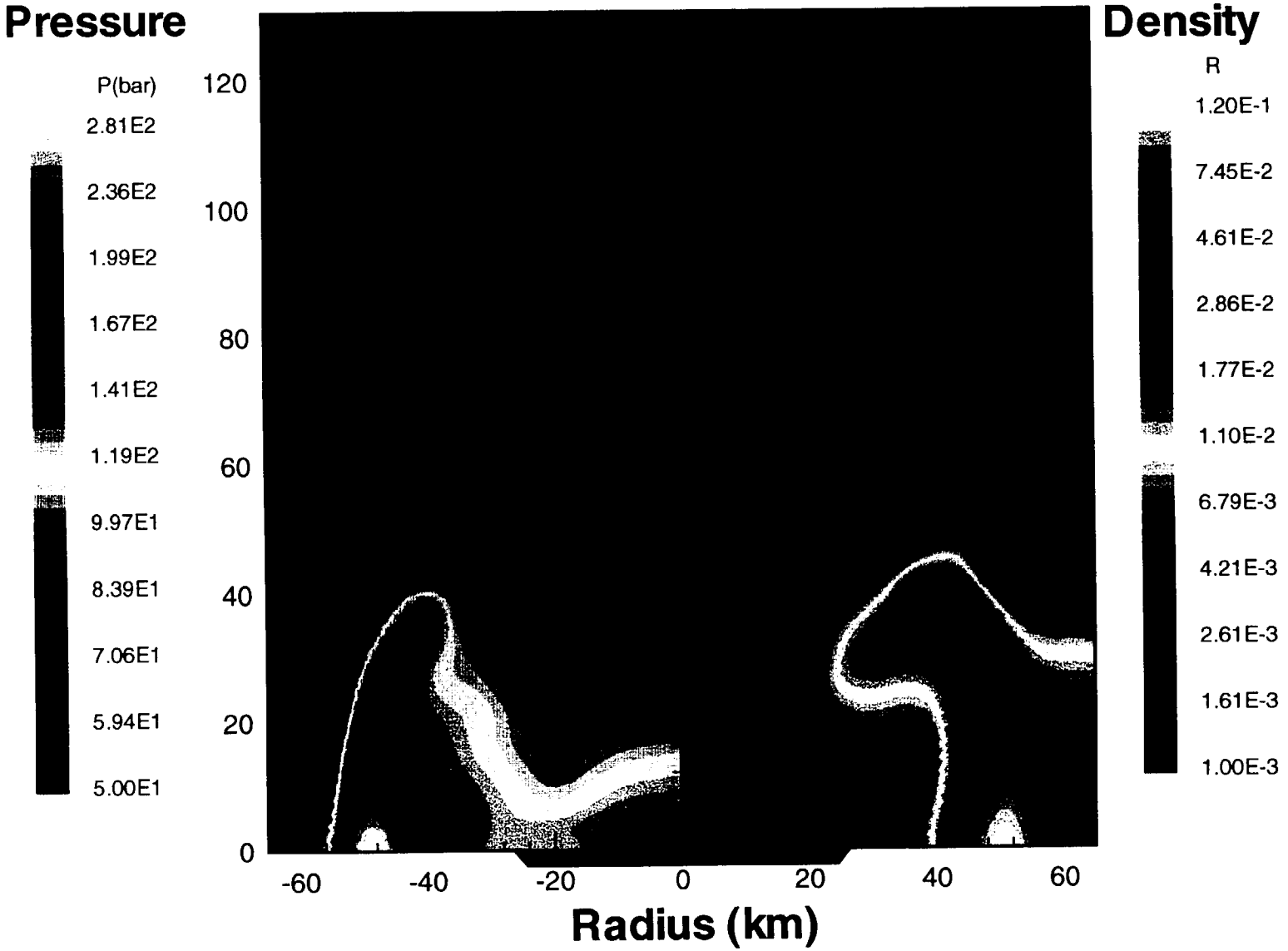

10-km Diameter Impactor into Venus

20 km/s Initial Velocity time = 20 sec

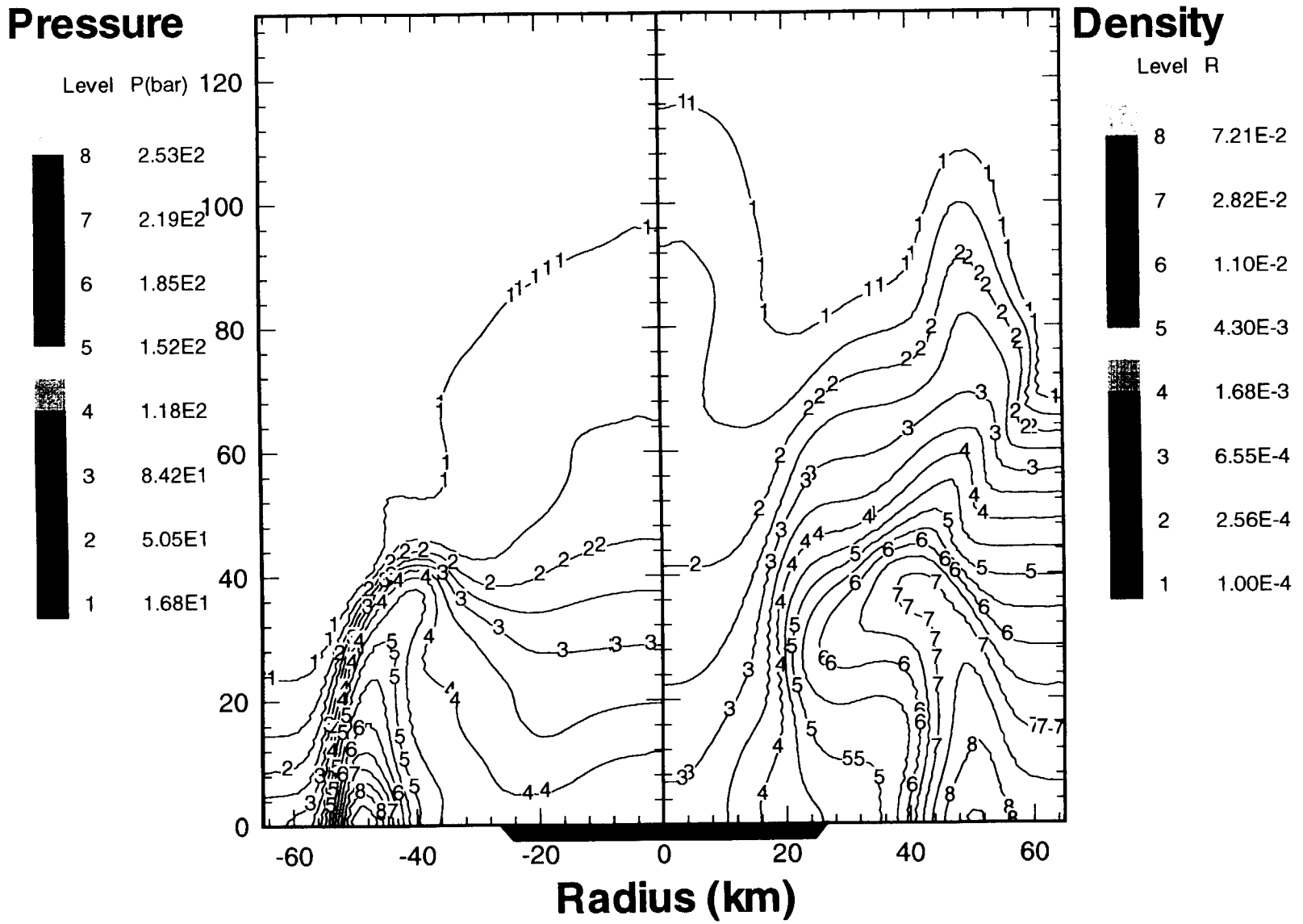

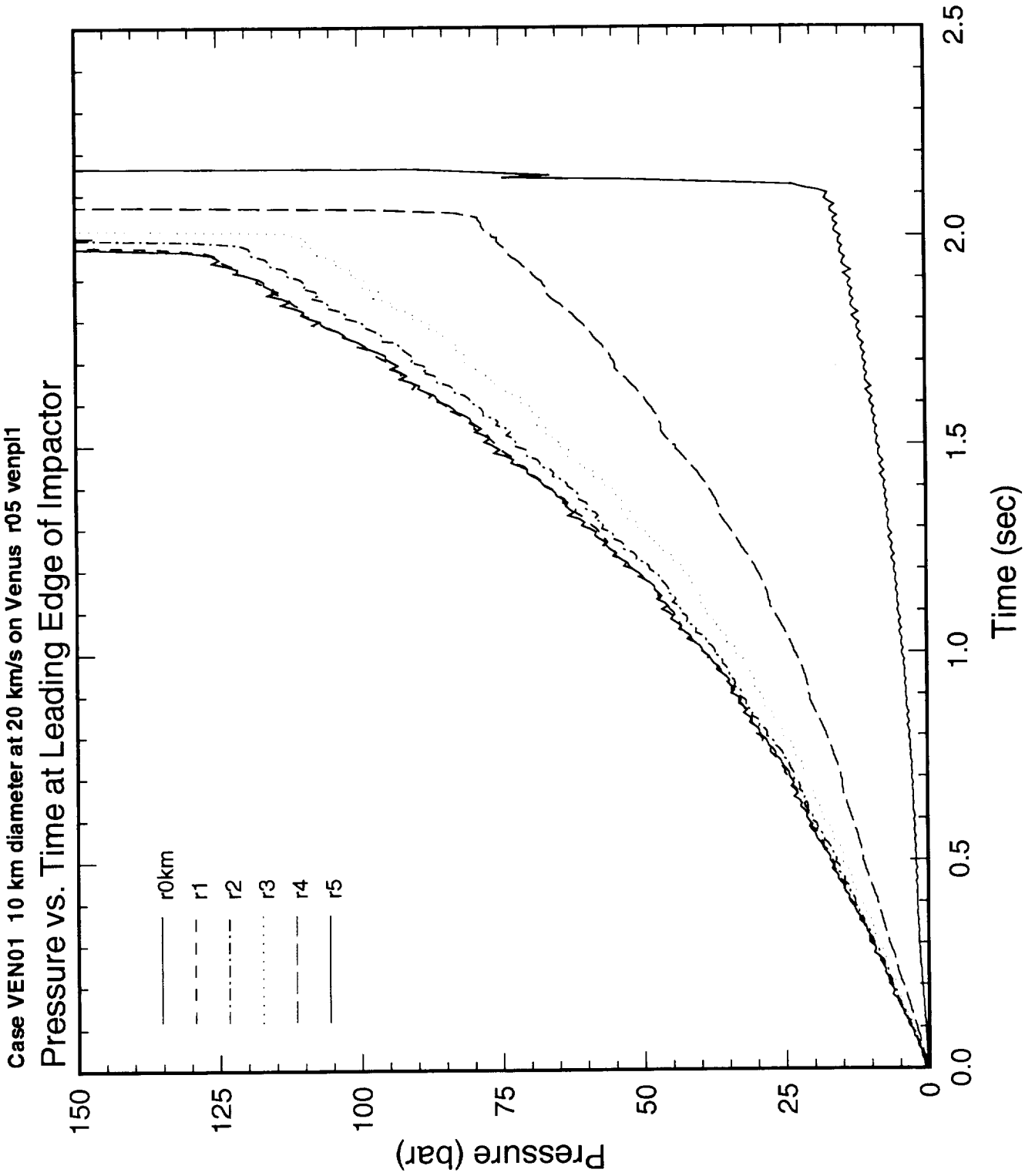
Case VEN01 10 km diameter at 20 km/s on Venus r05 venpl1
Pressure vs. Time at Leading Edge of Impactor
r0km
r1
r2
r3
r4
r5
Pressure (bar)
0
25
50
75
100
125
150
Time (sec)
0.0
0.5
1.0
1.5
2.0
2.5

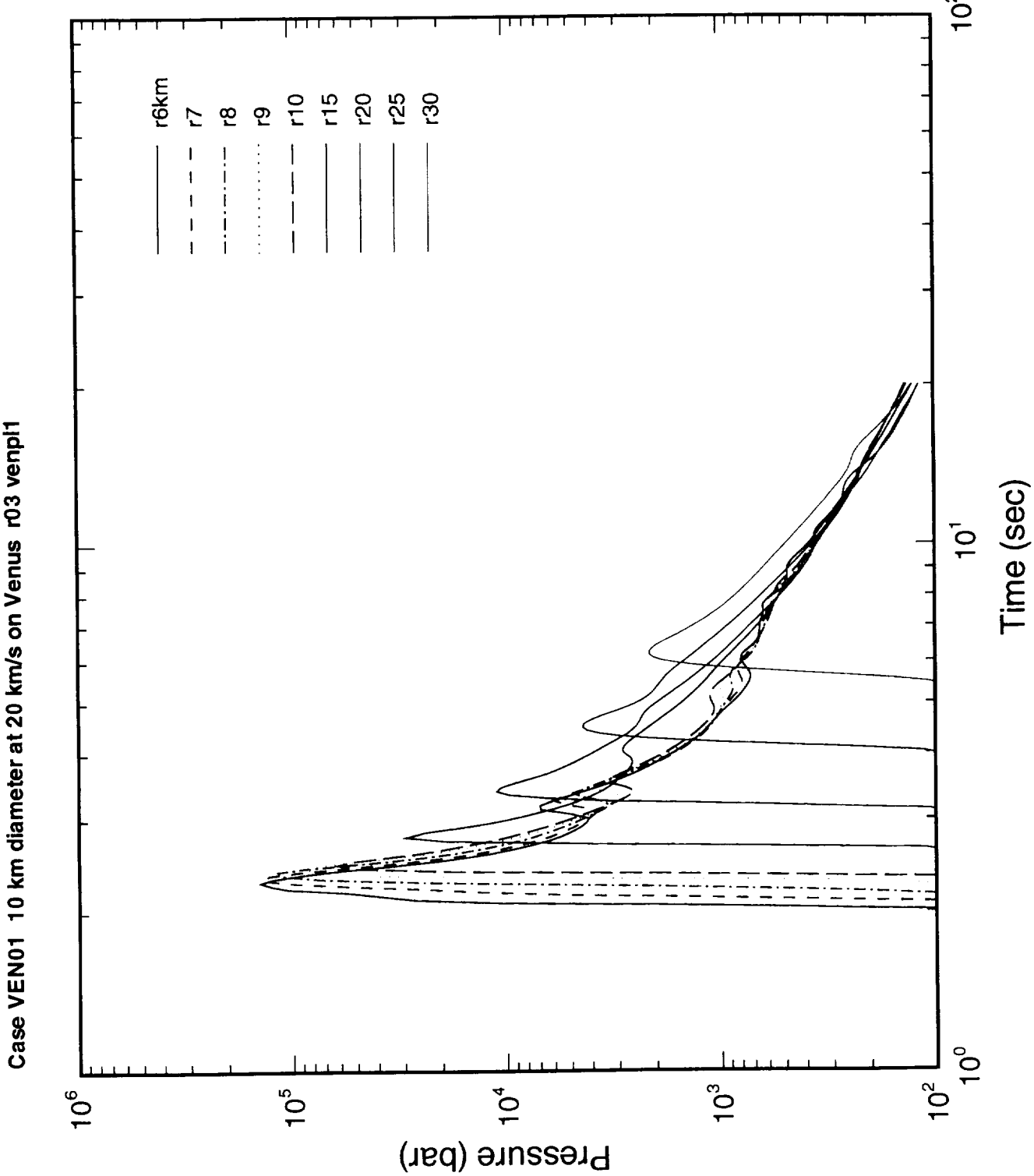
Case VEN01 10 km diameter at 20 km/s on Venus r03 venpl1
r6km
r7
r8
r9
r10
r15
r20
r25
r30
Pressure (bar)
Time (sec)
10^6
10^5
10^4
10^3
10^2
10^0
10^1
10^2

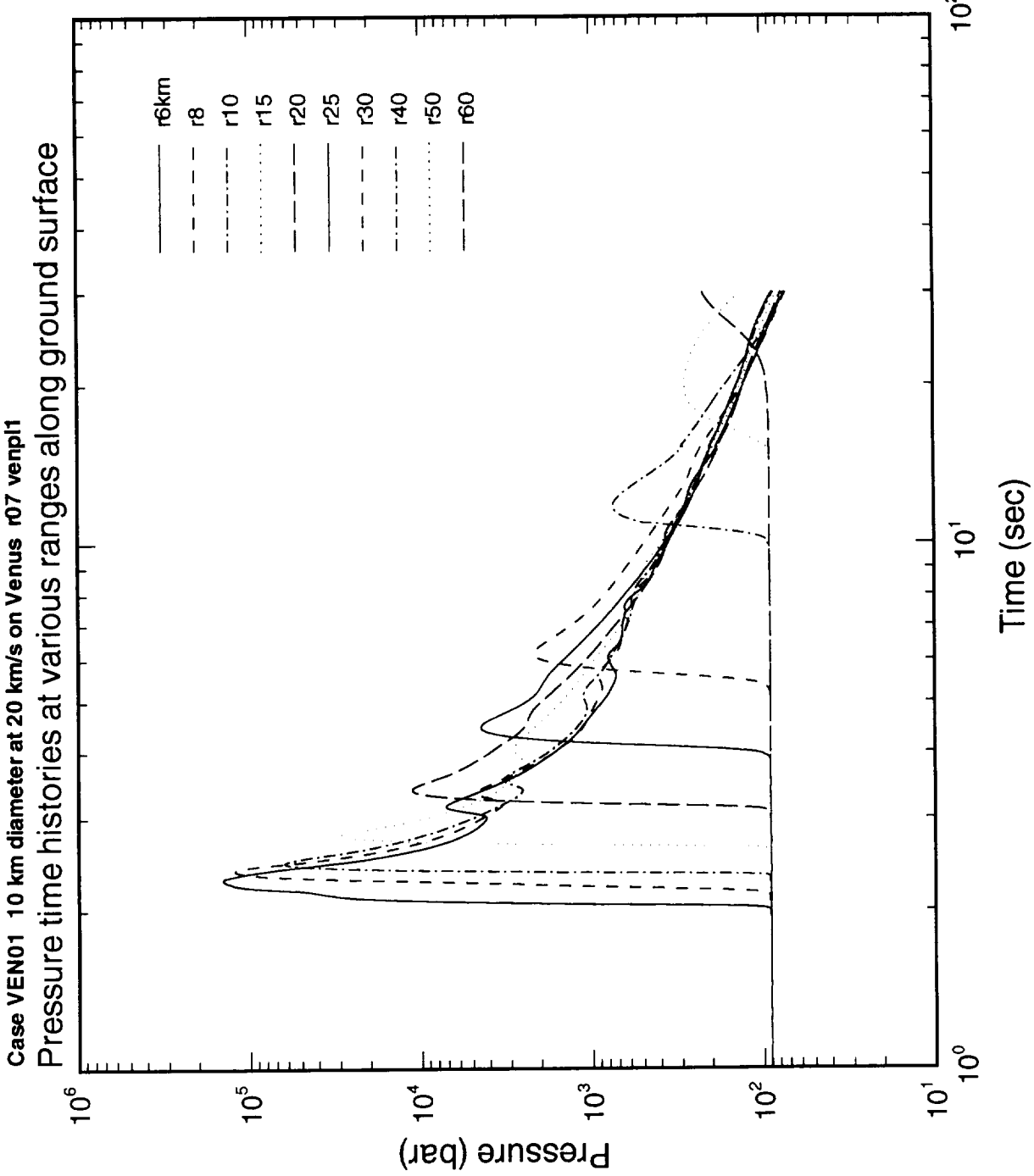
Case VEN01 10 km diameter at 20 km/s on Venus r07 venpl1
Pressure time histories at various ranges along ground surface
r6km
r8
r10
r15
r20
r25
r30
r40
r50
r60
Pressure (bar)
Time (sec)
10^6
10^5
10^4
10^3
10^2
10^1
10^0
10^1
10^2

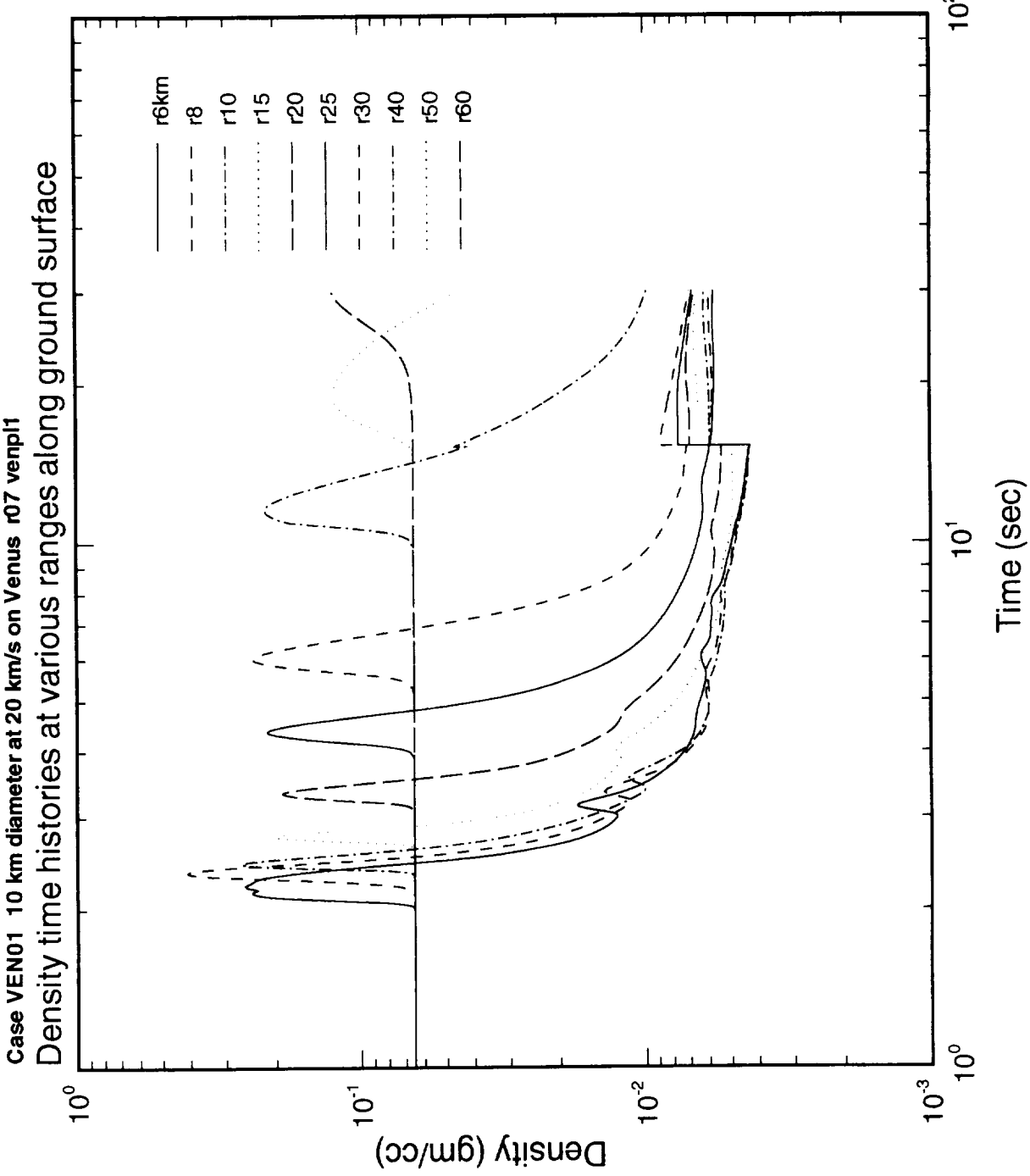
Case VEN01 10 km diameter at 20 km/s on Venus r07 venpl1
Density time histories at various ranges along ground surface
r6km
r8
r10
r15
r20
r25
r30
r40
r50
r60
Density (gm/cc)
Time (sec)
10^0
10^-1
10^-2
10^-3
10^1
10^2

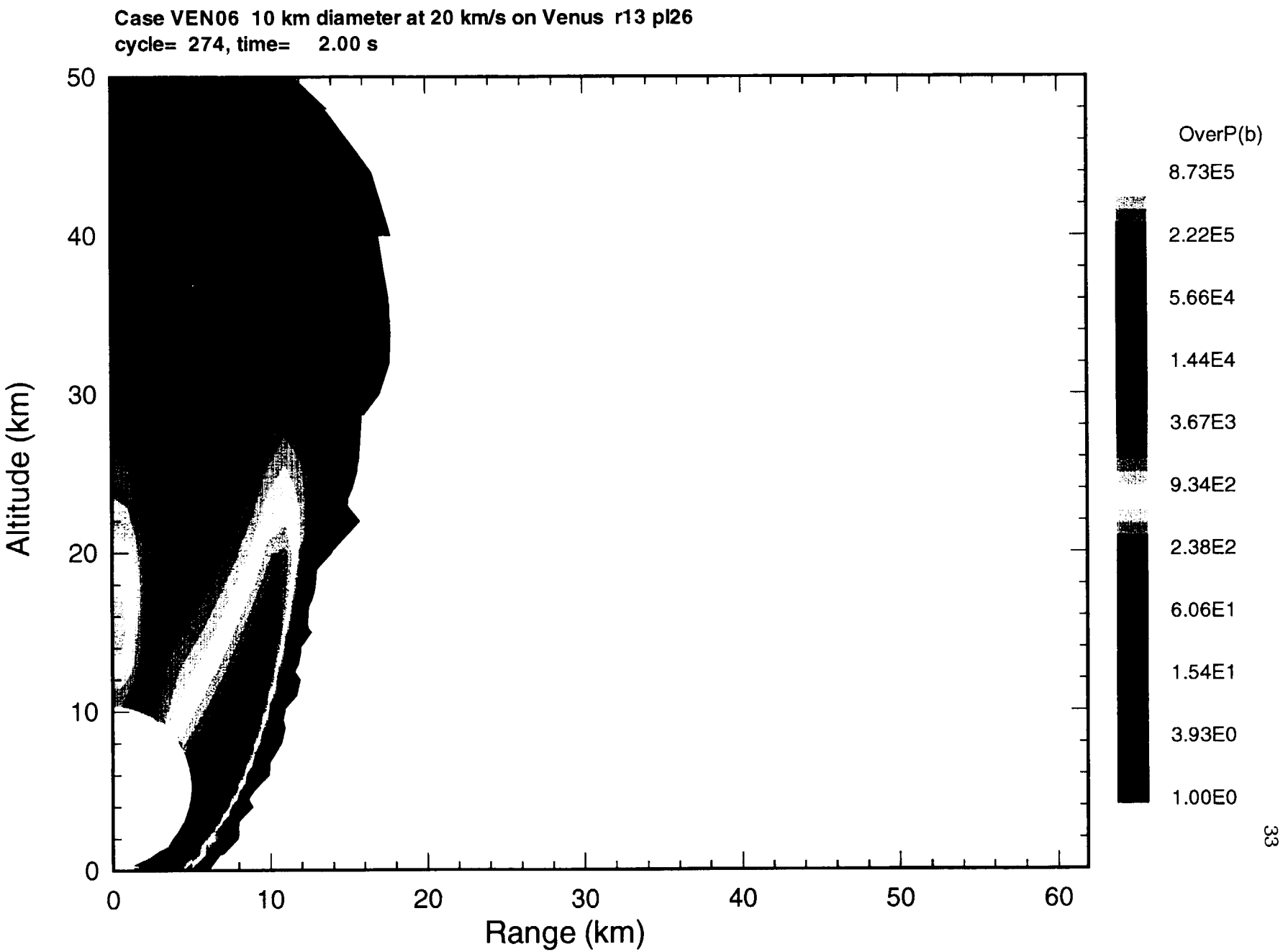
Case VEN06 10 km diameter at 20 km/s on Venus r13 pl26
cycle= 274, time= 2.00 s
Altitude (km)
Range (km)
0
10
20
30
40
50
60
OverP(b)
8.73E5
2.22E5
5.66E4
1.44E4
3.67E3
9.34E2
2.38E2
6.06E1
1.54E1
3.93E0
1.00E0

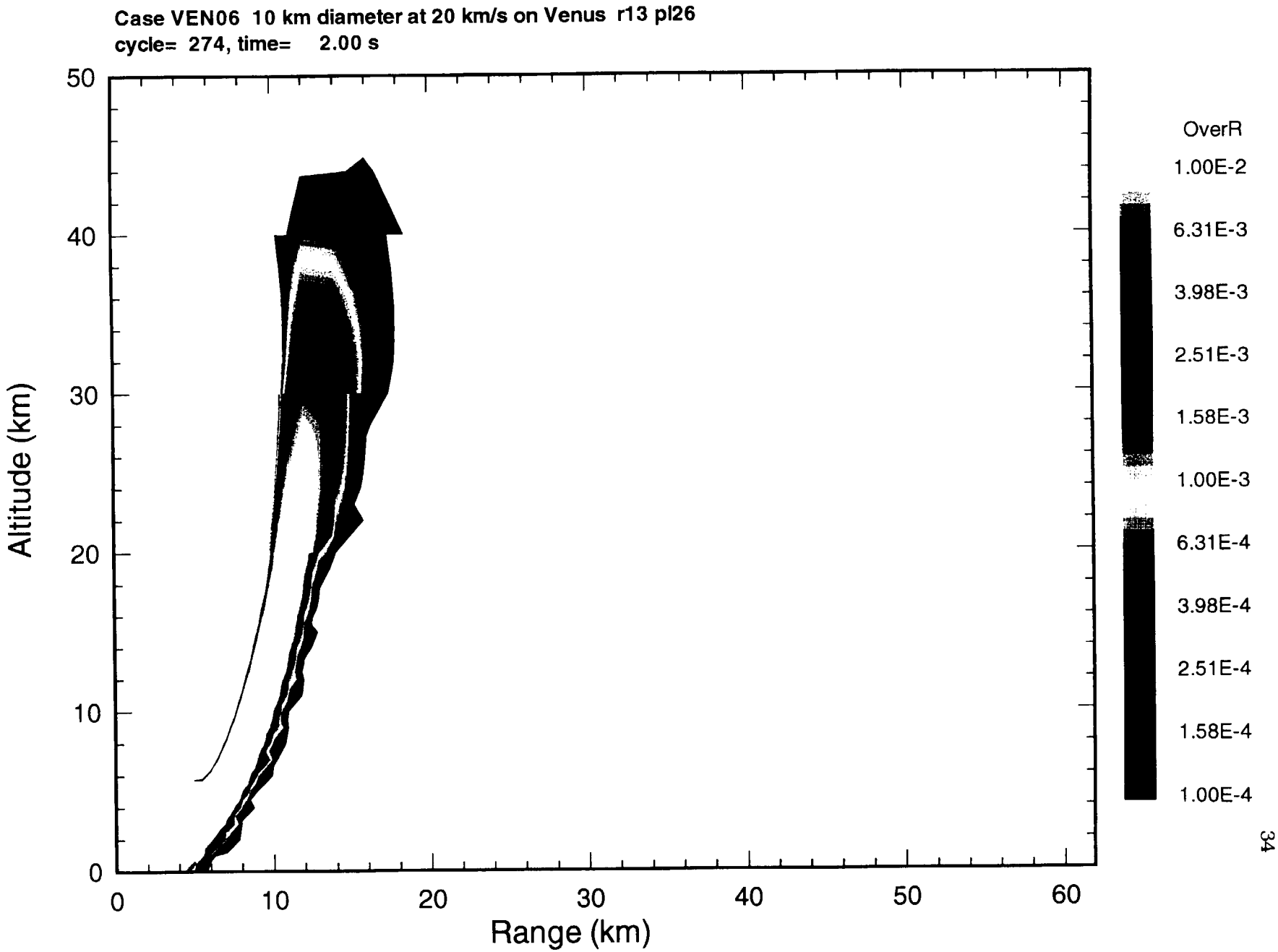
Case VEN06 10 km diameter at 20 km/s on Venus r13 pl26
cycle= 274, time= 2.00 s
Altitude (km)
Range (km)
0
10
20
30
40
50
60
OverR
1.00E-2
6.31E-3
3.98E-3
2.51E-3
1.58E-3
1.00E-3
6.31E-4
3.98E-4
2.51E-4
1.58E-4
1.00E-4

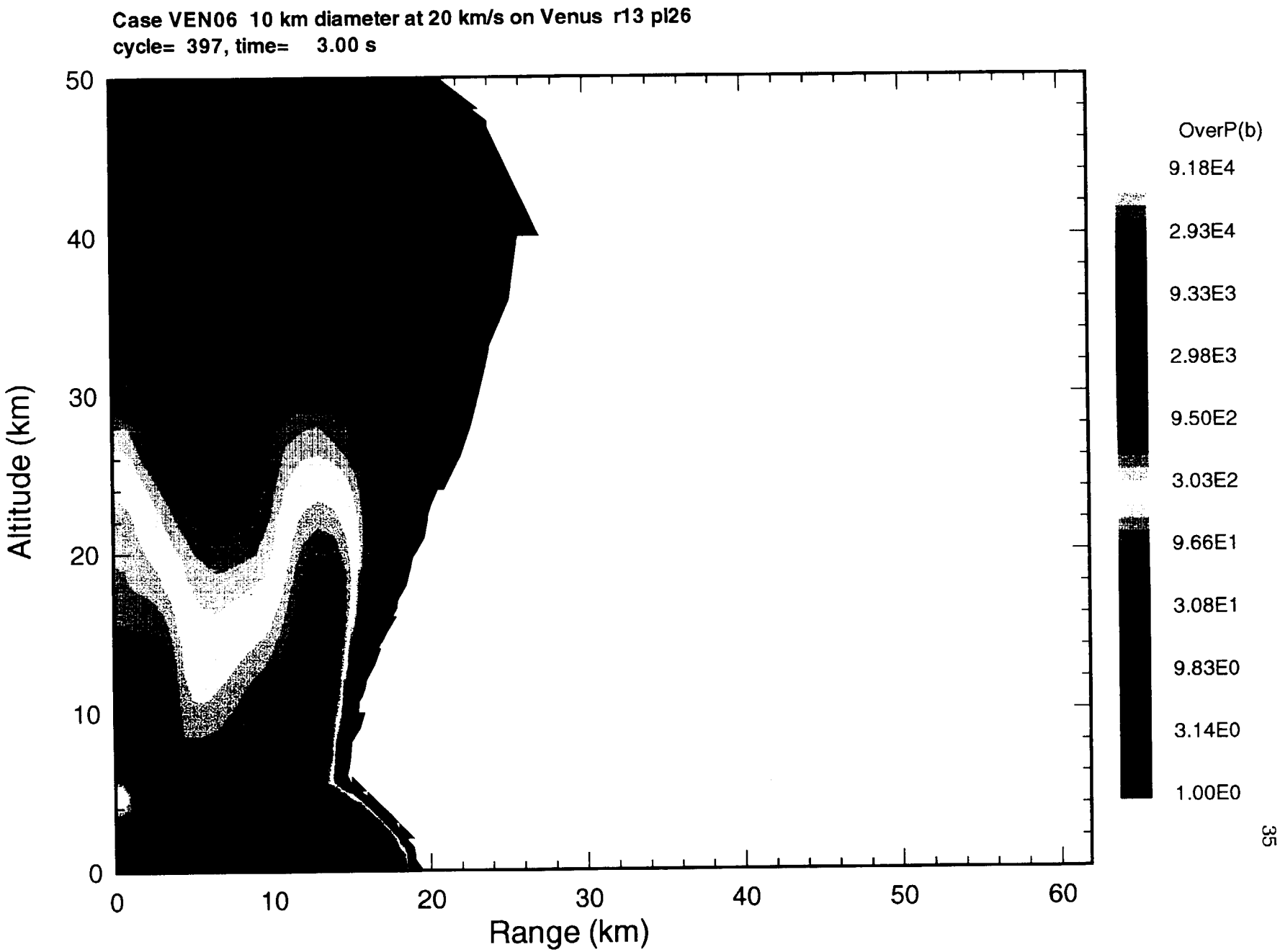
Case VEN06 10 km diameter at 20 km/s on Venus r13 pl26
cycle= 397, time= 3.00 s
Altitude (km)
Range (km)
0
10
20
30
40
50
60
OverP(b)
9.18E4
2.93E4
9.33E3
2.98E3
9.50E2
3.03E2
9.66E1
3.08E1
9.83E0
3.14E0
1.00E0

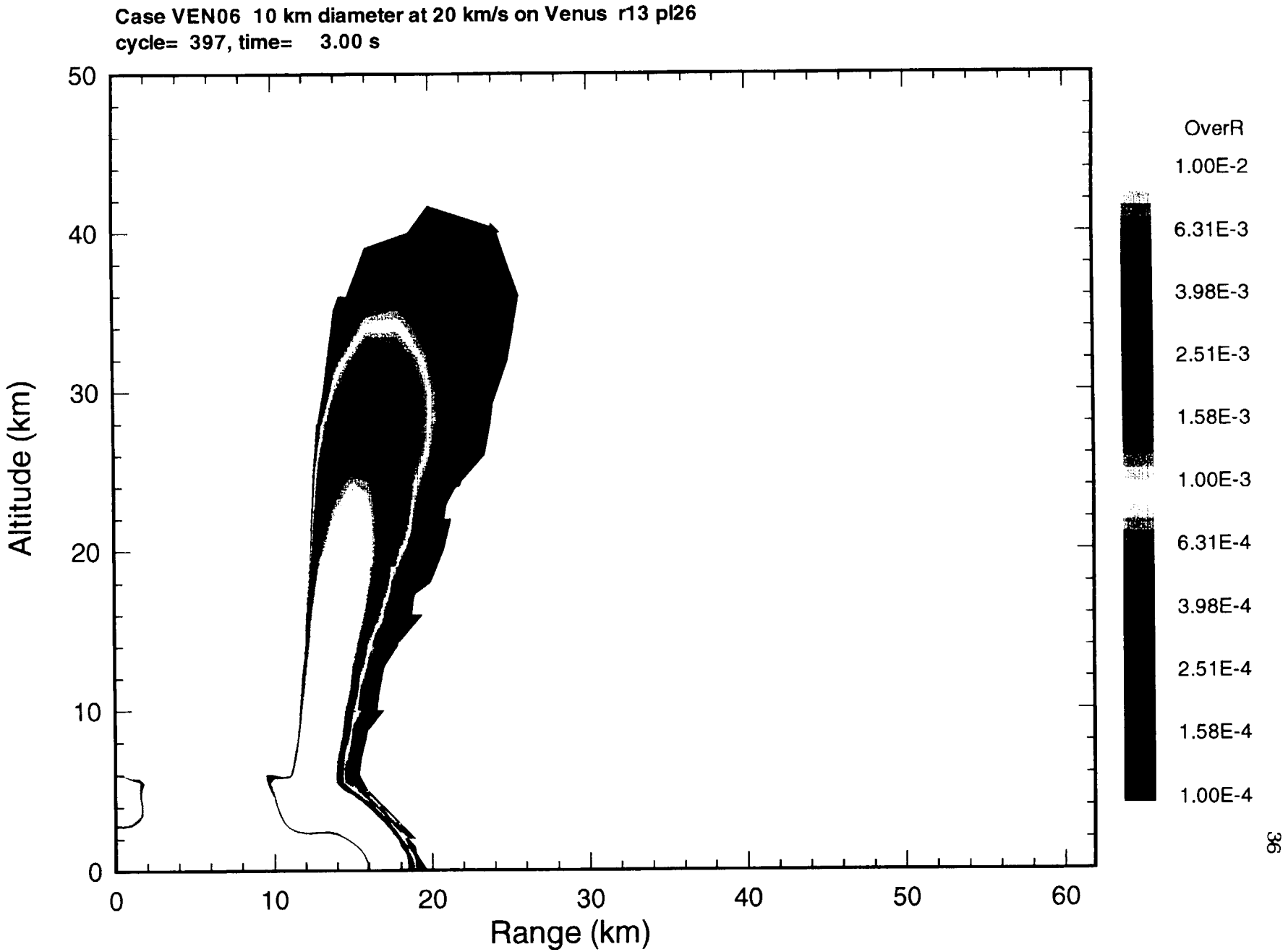
Case VEN06 10 km diameter at 20 km/s on Venus r13 pl26
cycle= 397, time= 3.00 s
Altitude (km)
Range (km)
0
10
20
30
40
50
60
OverR
1.00E-2
6.31E-3
3.98E-3
2.51E-3
1.58E-3
1.00E-3
6.31E-4
3.98E-4
2.51E-4
1.58E-4
1.00E-4

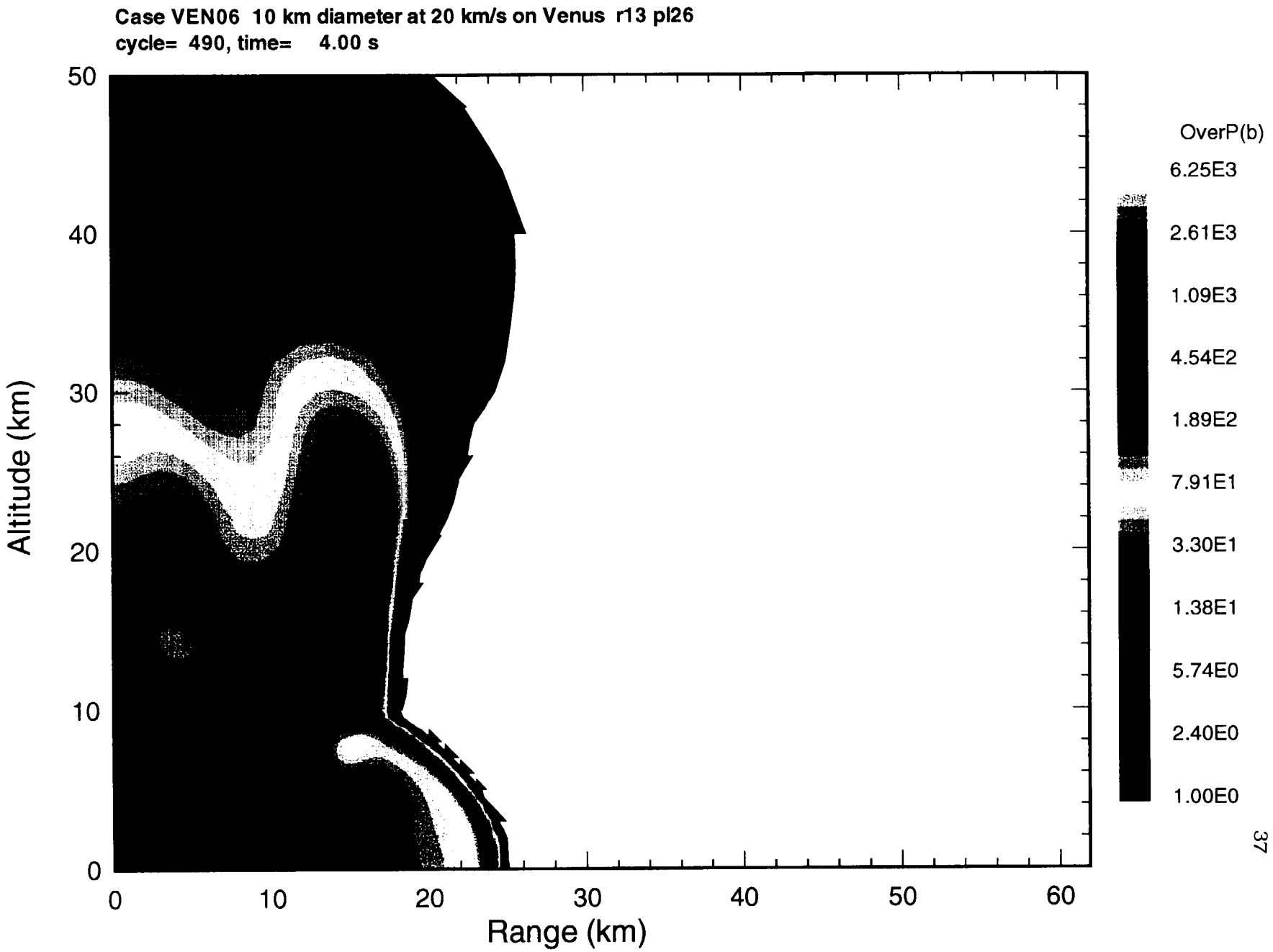
Case VEN06 10 km diameter at 20 km/s on Venus r13 pl26
cycle= 490, time= 4.00 s
Altitude (km)
Range (km)
0
10
20
30
40
50
60
OverP(b)
6.25E3
2.61E3
1.09E3
4.54E2
1.89E2
7.91E1
3.30E1
1.38E1
5.74E0
2.40E0
1.00E0

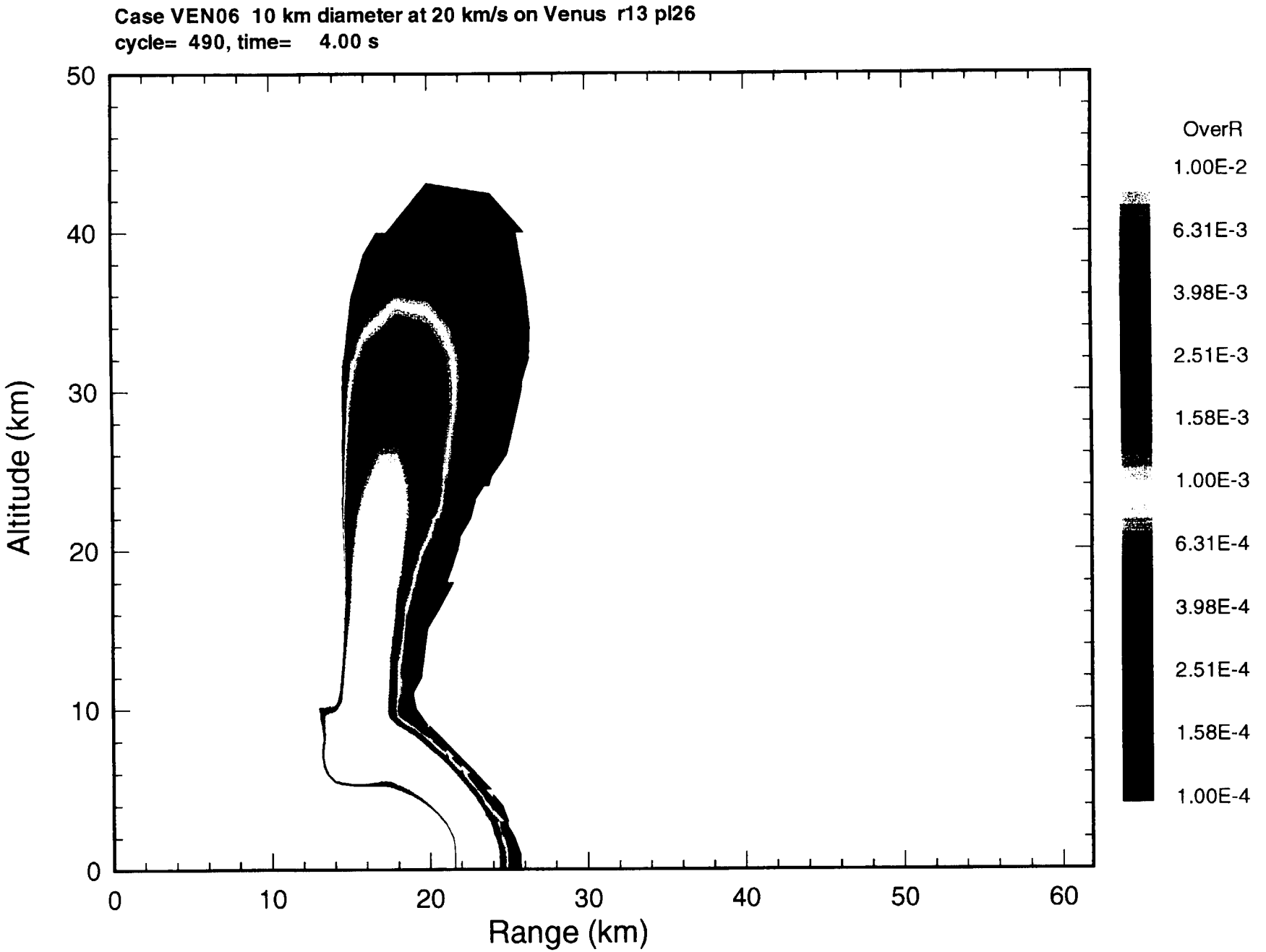
Case VEN06 10 km diameter at 20 km/s on Venus r13 pl26
cycle= 490, time= 4.00 s
Altitude (km)
Range (km)
0
10
20
30
40
50
60
OverR
1.00E-2
6.31E-3
3.98E-3
2.51E-3
1.58E-3
1.00E-3
6.31E-4
3.98E-4
2.51E-4
1.58E-4
1.00E-4

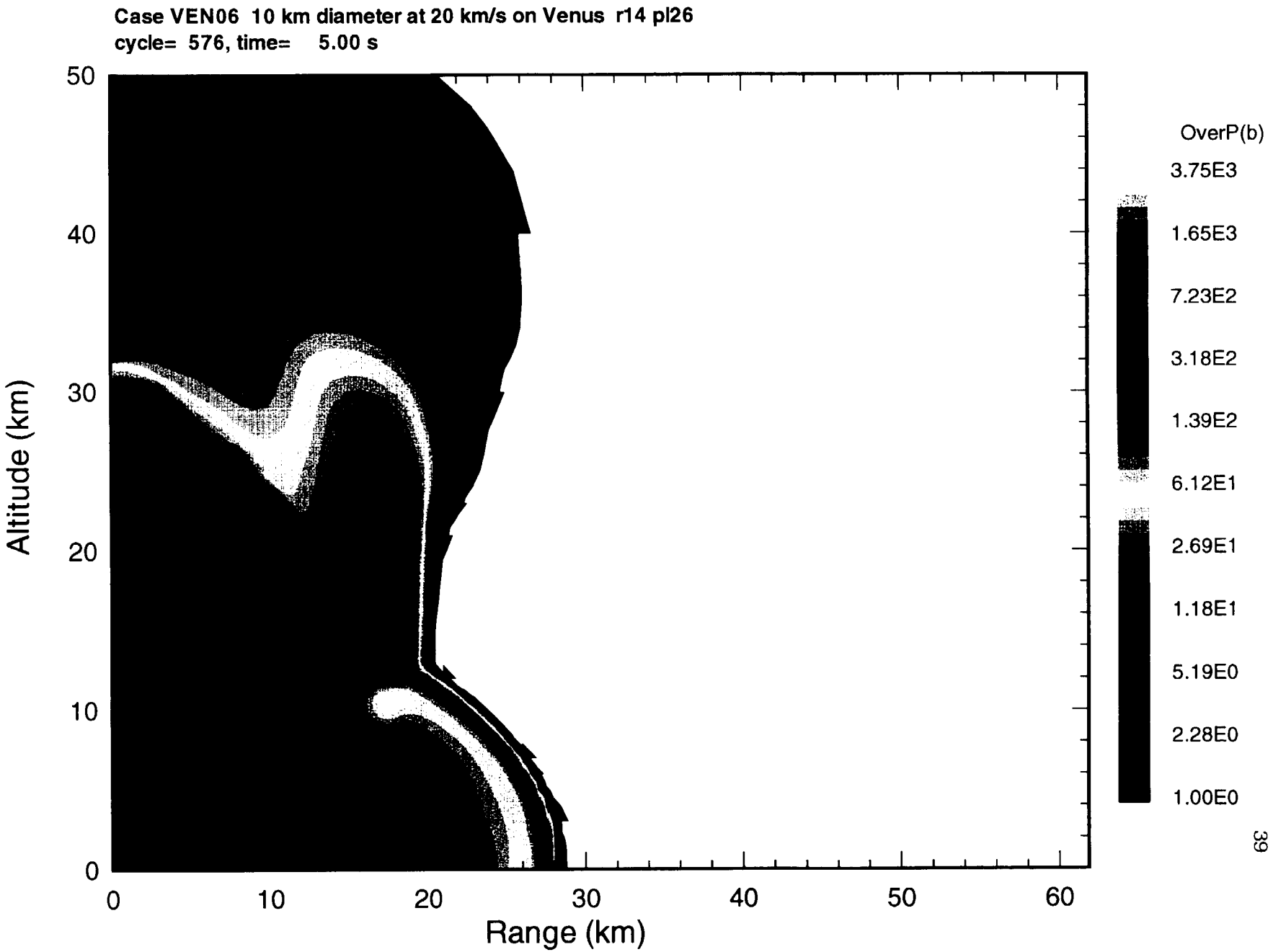
Case VEN06 10 km diameter at 20 km/s on Venus r14 pl26
cycle= 576, time= 5.00 s
Altitude (km)
Range (km)
0
10
20
30
40
50
60
OverP(b)
3.75E3
1.65E3
7.23E2
3.18E2
1.39E2
6.12E1
2.69E1
1.18E1
5.19E0
2.28E0
1.00E0

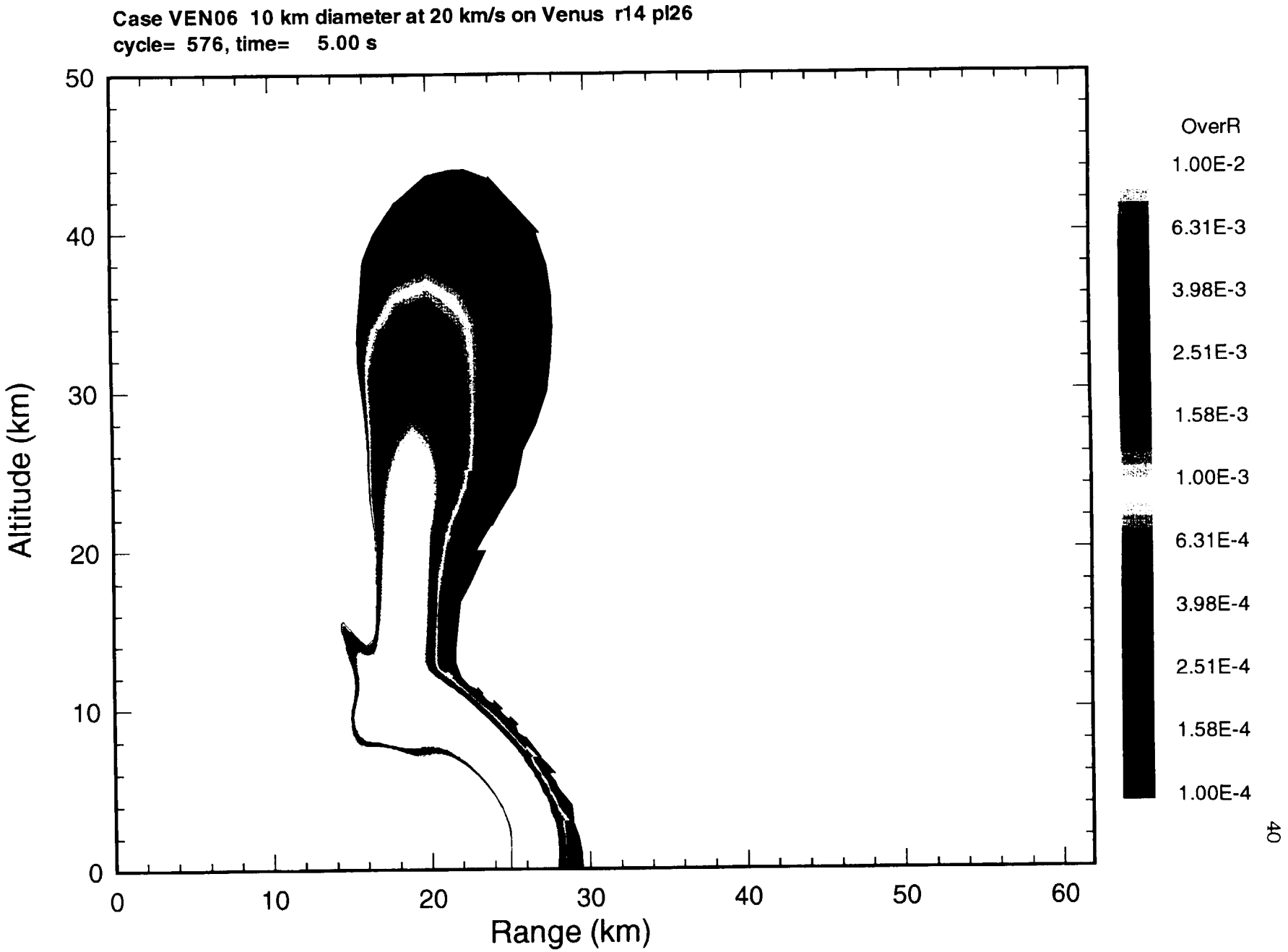
Case VEN06 10 km diameter at 20 km/s on Venus r14 pl26
cycle= 576, time= 5.00 s
Altitude (km)
Range (km)
0
10
20
30
40
50
60
OverR
1.00E-2
6.31E-3
3.98E-3
2.51E-3
1.58E-3
1.00E-3
6.31E-4
3.98E-4
2.51E-4
1.58E-4
1.00E-4

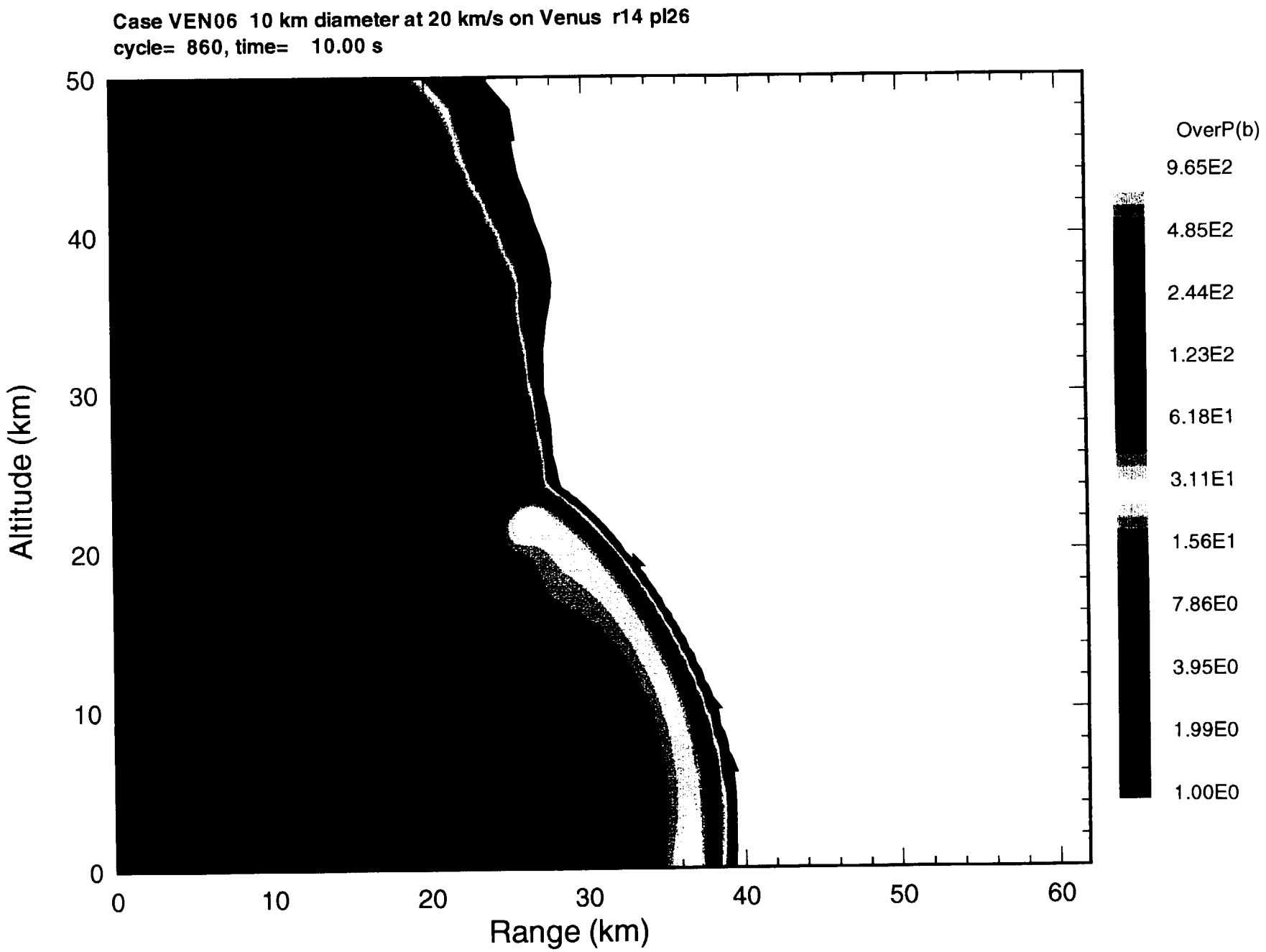
Case VEN06 10 km diameter at 20 km/s on Venus r14 pl26
cycle= 860, time= 10.00 s
Altitude (km)
Range (km)
0
10
20
30
40
50
60
OverP(b)
9.65E2
4.85E2
2.44E2
1.23E2
6.18E1
3.11E1
1.56E1
7.86E0
3.95E0
1.99E0
1.00E0

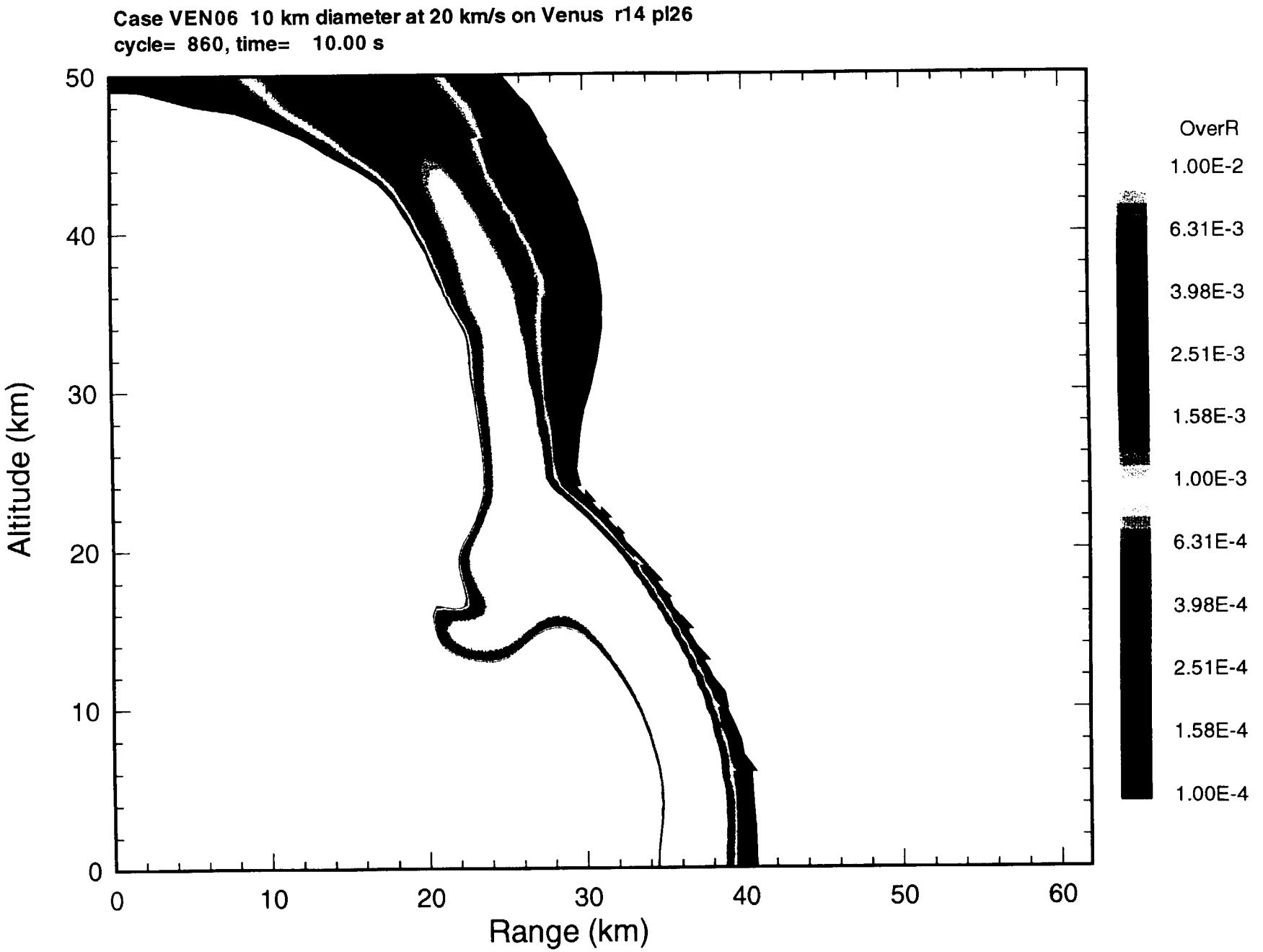
Case VEN06 10 km diameter at 20 km/s on Venus r14 pl26
cycle= 860, time= 10.00 s
Altitude (km)
Range (km)
0
10
20
30
40
50
60
OverR
1.00E-2
6.31E-3
3.98E-3
2.51E-3
1.58E-3
1.00E-3
6.31E-4
3.98E-4
2.51E-4
1.58E-4
1.00E-4

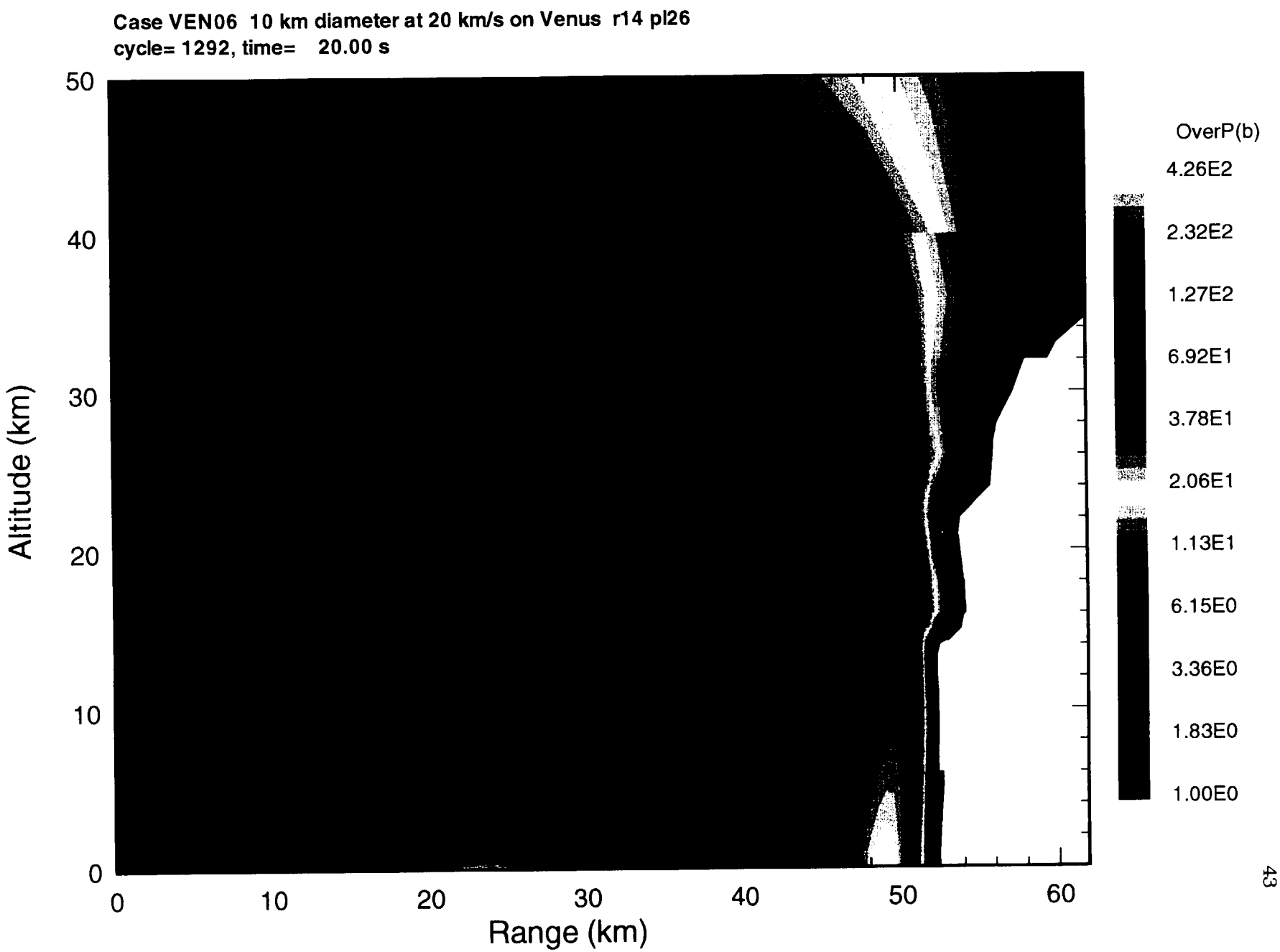
Case VEN06 10 km diameter at 20 km/s on Venus r14 pl26
cycle= 1292, time= 20.00 s
Altitude (km)
Range (km)
0
10
20
30
40
50
60
OverP(b)
4.26E2
2.32E2
1.27E2
6.92E1
3.78E1
2.06E1
1.13E1
6.15E0
3.36E0
1.83E0
1.00E0

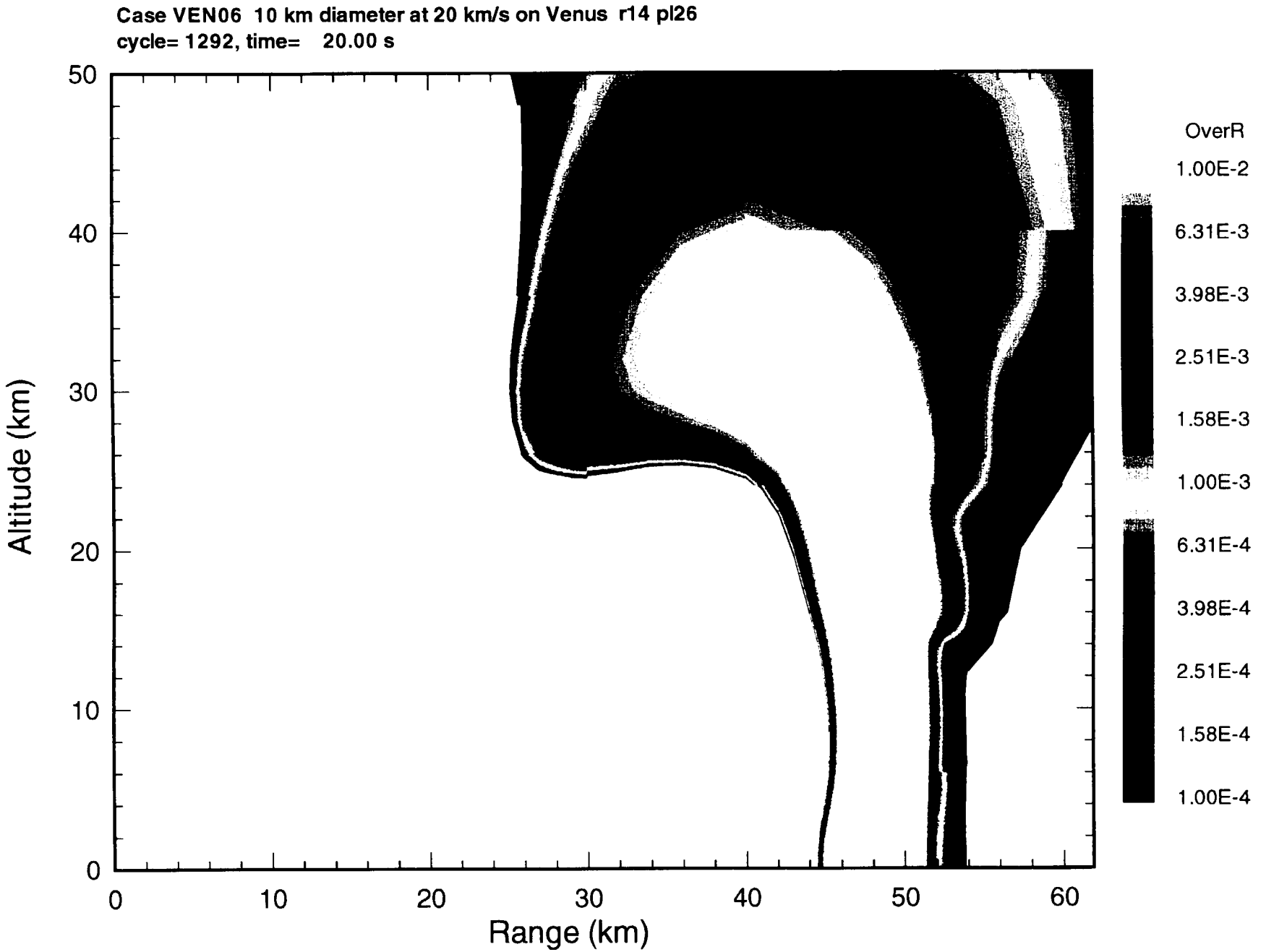
Case VEN06 10 km diameter at 20 km/s on Venus r14 pl26
cycle= 1292, time= 20.00 s
Altitude (km)
Range (km)
0
10
20
30
40
50
60
OverR
1.00E-2
6.31E-3
3.98E-3
2.51E-3
1.58E-3
1.00E-3
6.31E-4
3.98E-4
2.51E-4
1.58E-4
1.00E-4

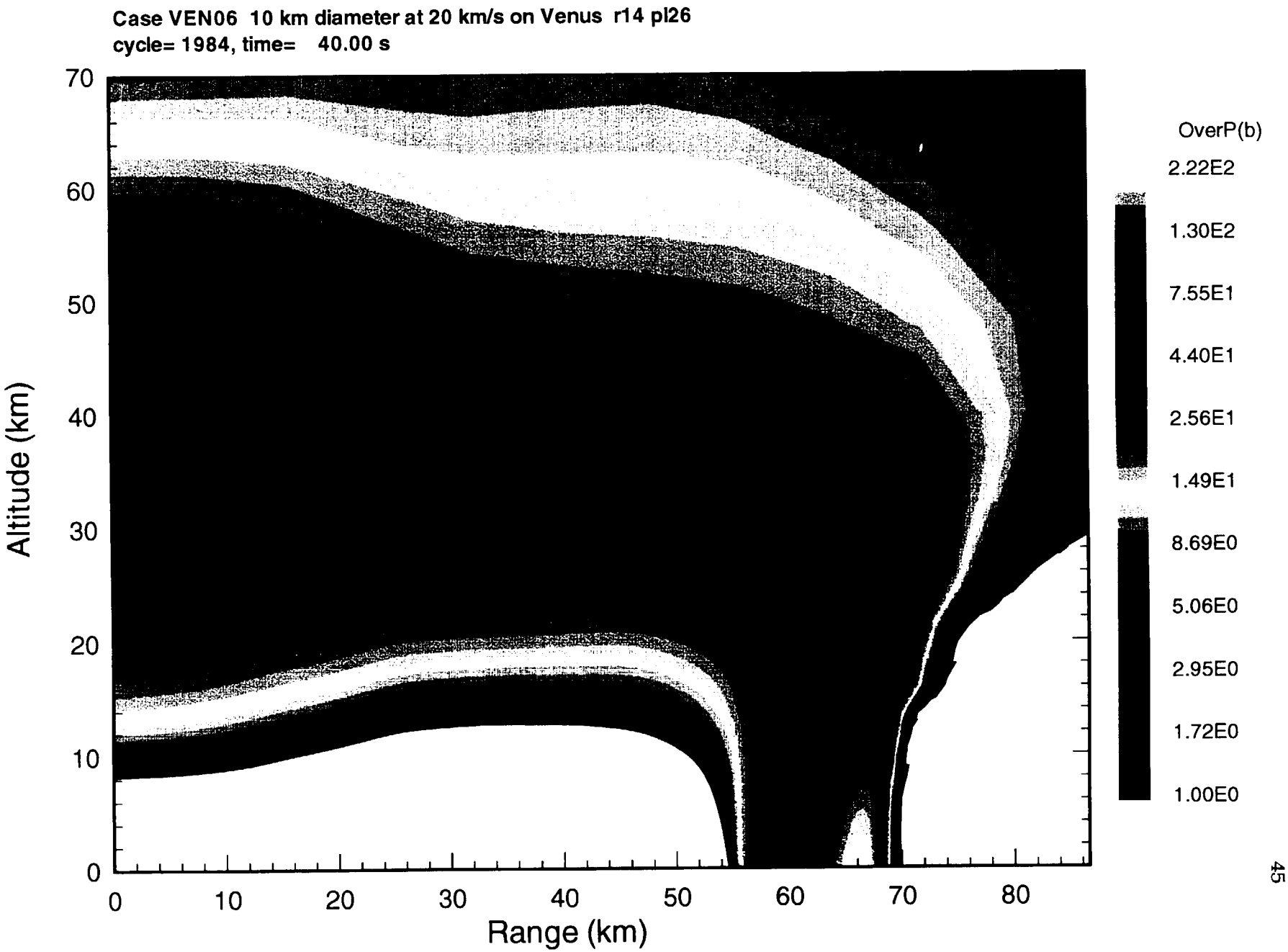
Case VEN06 10 km diameter at 20 km/s on Venus r14 pl26
cycle= 1984, time= 40.00 s
Altitude (km)
Range (km)
0
10
20
30
40
50
60
70
80
OverP(b)
2.22E2
1.30E2
7.55E1
4.40E1
2.56E1
1.49E1
8.69E0
5.06E0
2.95E0
1.72E0
1.00E0

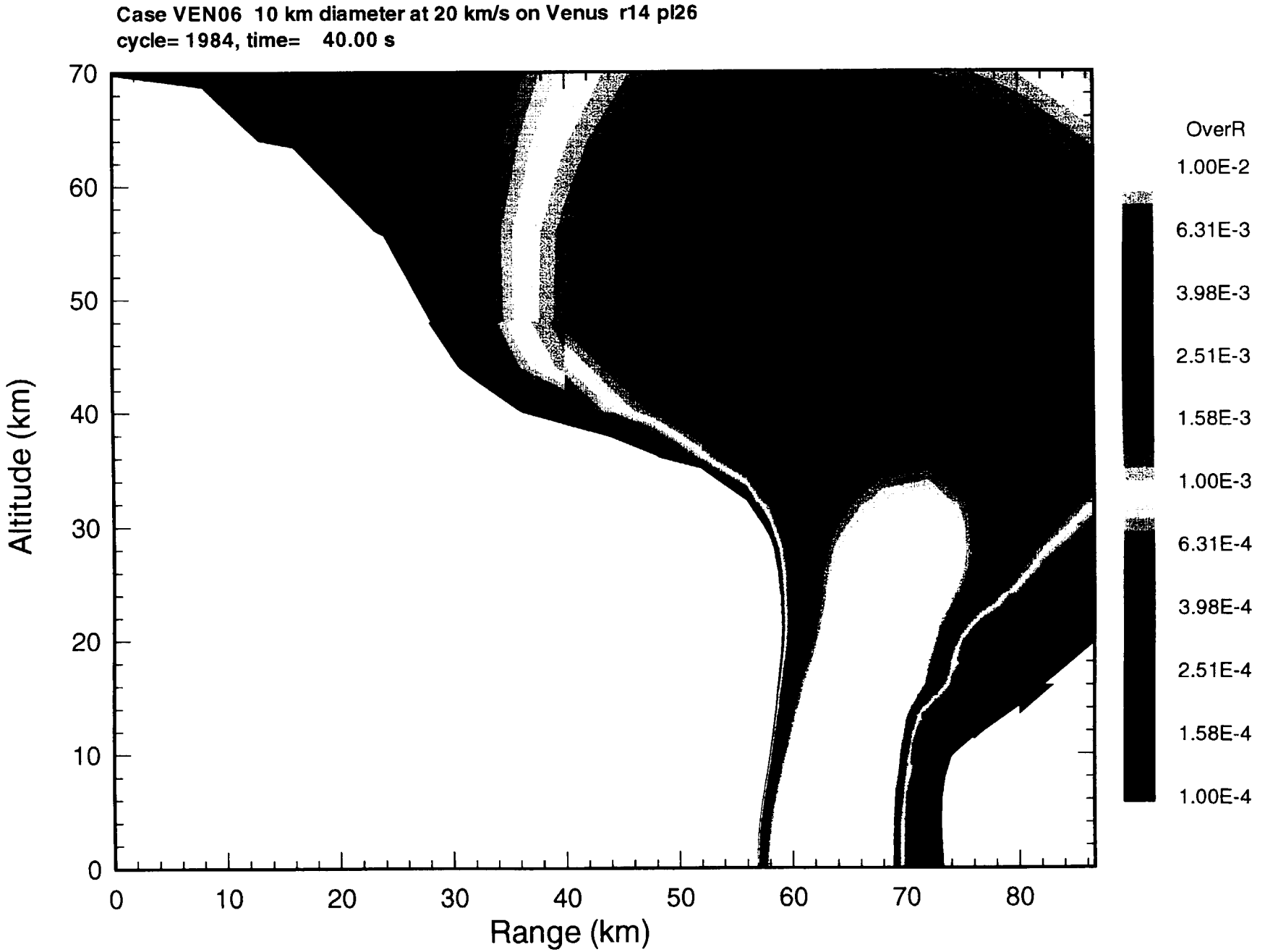
Case VEN06 10 km diameter at 20 km/s on Venus r14 pl26
cycle= 1984, time= 40.00 s
Altitude (km)
Range (km)
0
10
20
30
40
50
60
70
80
OverR
1.00E-2
6.31E-3
3.98E-3
2.51E-3
1.58E-3
1.00E-3
6.31E-4
3.98E-4
2.51E-4
1.58E-4
1.00E-4

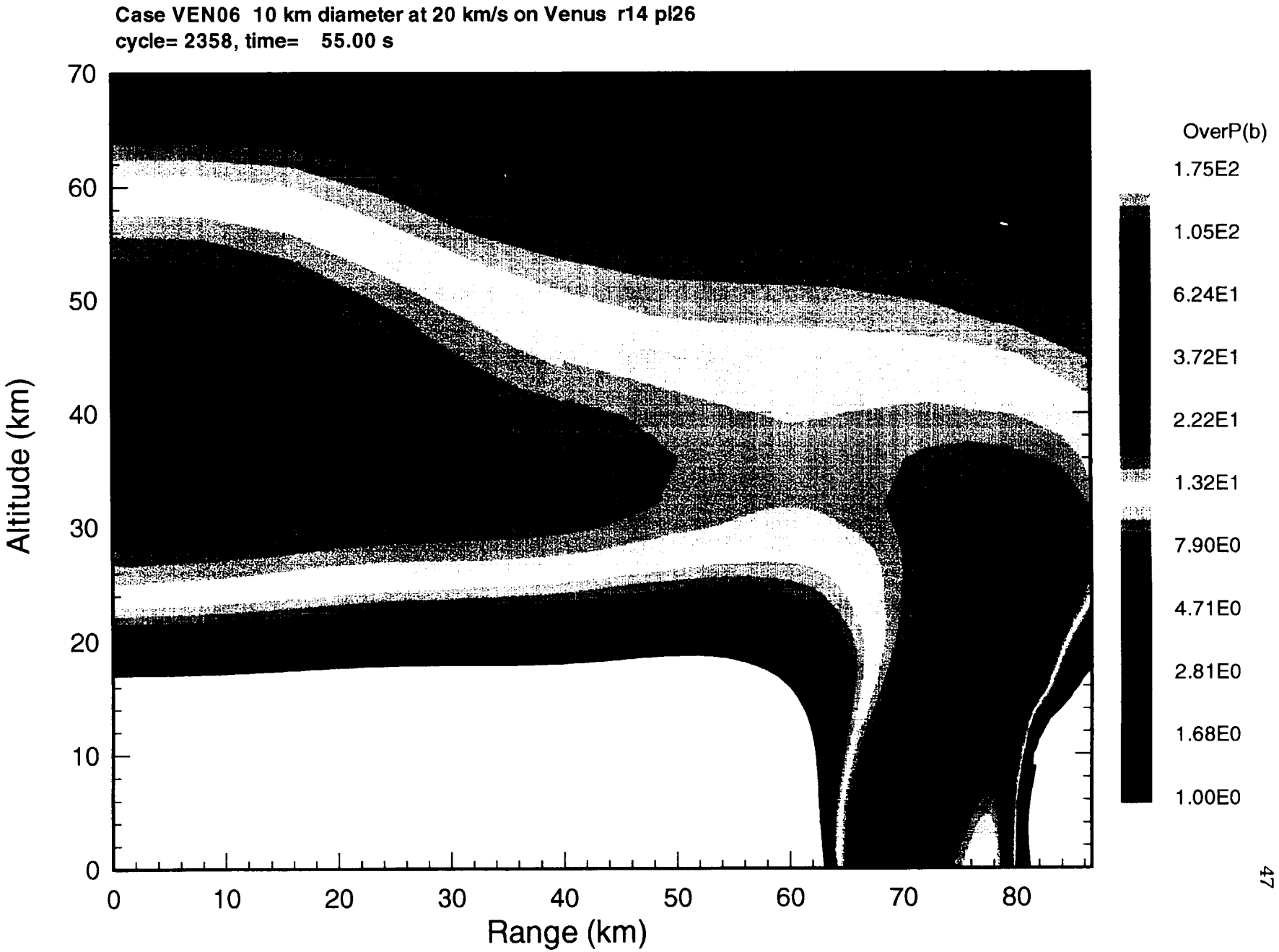
Case VEN06 10 km diameter at 20 km/s on Venus r14 pl26
cycle= 2358, time= 55.00 s
Altitude (km)
Range (km)
0
10
20
30
40
50
60
70
80
OverP(b)
1.75E2
1.05E2
6.24E1
3.72E1
2.22E1
1.32E1
7.90E0
4.71E0
2.81E0
1.68E0
1.00E0

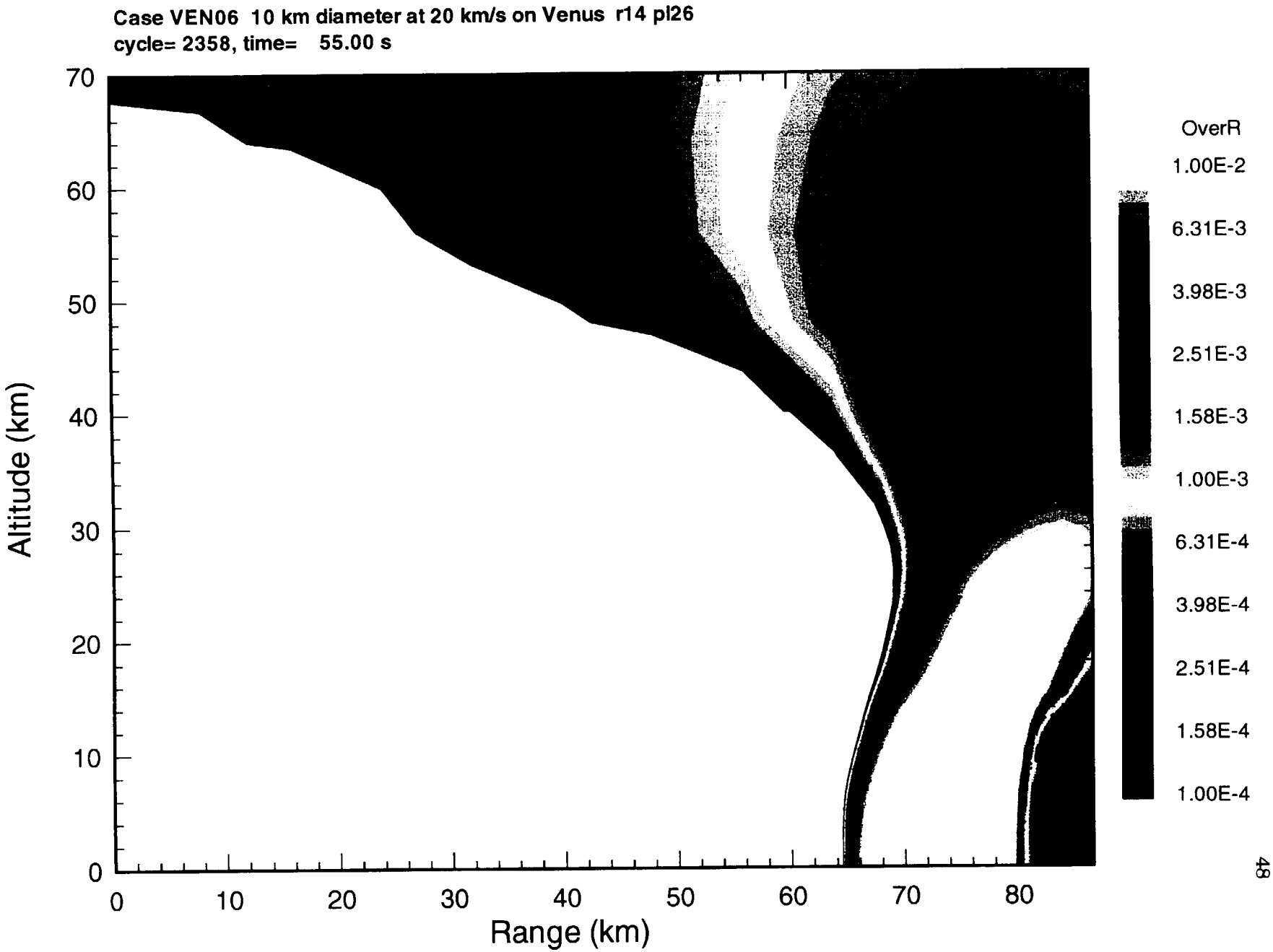
Case VEN06 10 km diameter at 20 km/s on Venus r14 pl26
cycle= 2358, time= 55.00 s
Altitude (km)
Range (km)
0
10
20
30
40
50
60
70
80
OverR
1.00E-2
6.31E-3
3.98E-3
2.51E-3
1.58E-3
1.00E-3
6.31E-4
3.98E-4
2.51E-4
1.58E-4
1.00E-4

20 km/s Asteroid into Venus

Scaled Time = 0.367 when Crater Radius 0.75

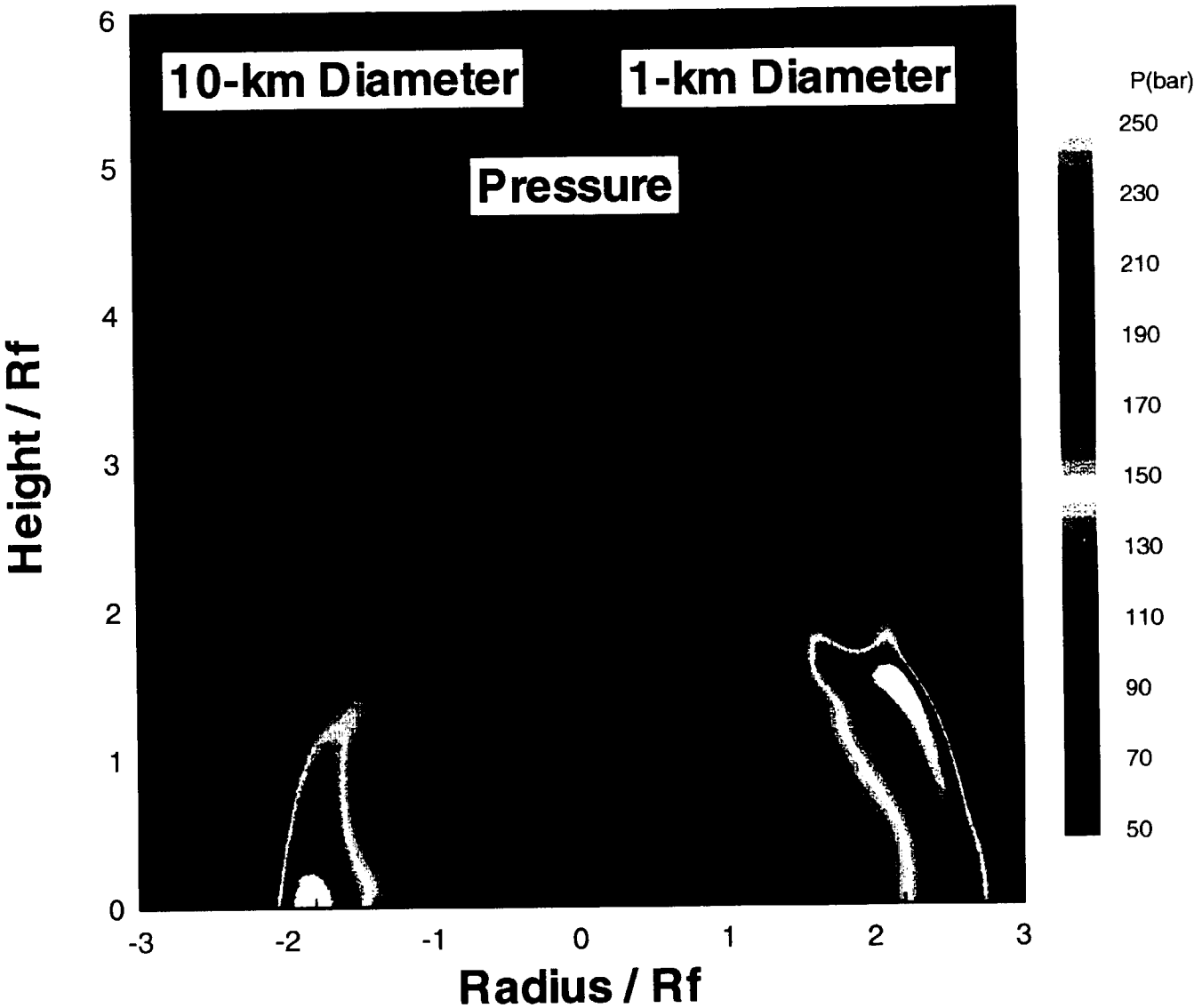

20 km/s Asteroid into Venus

Scaled Time = 0.367 when Crater Radius 0.75

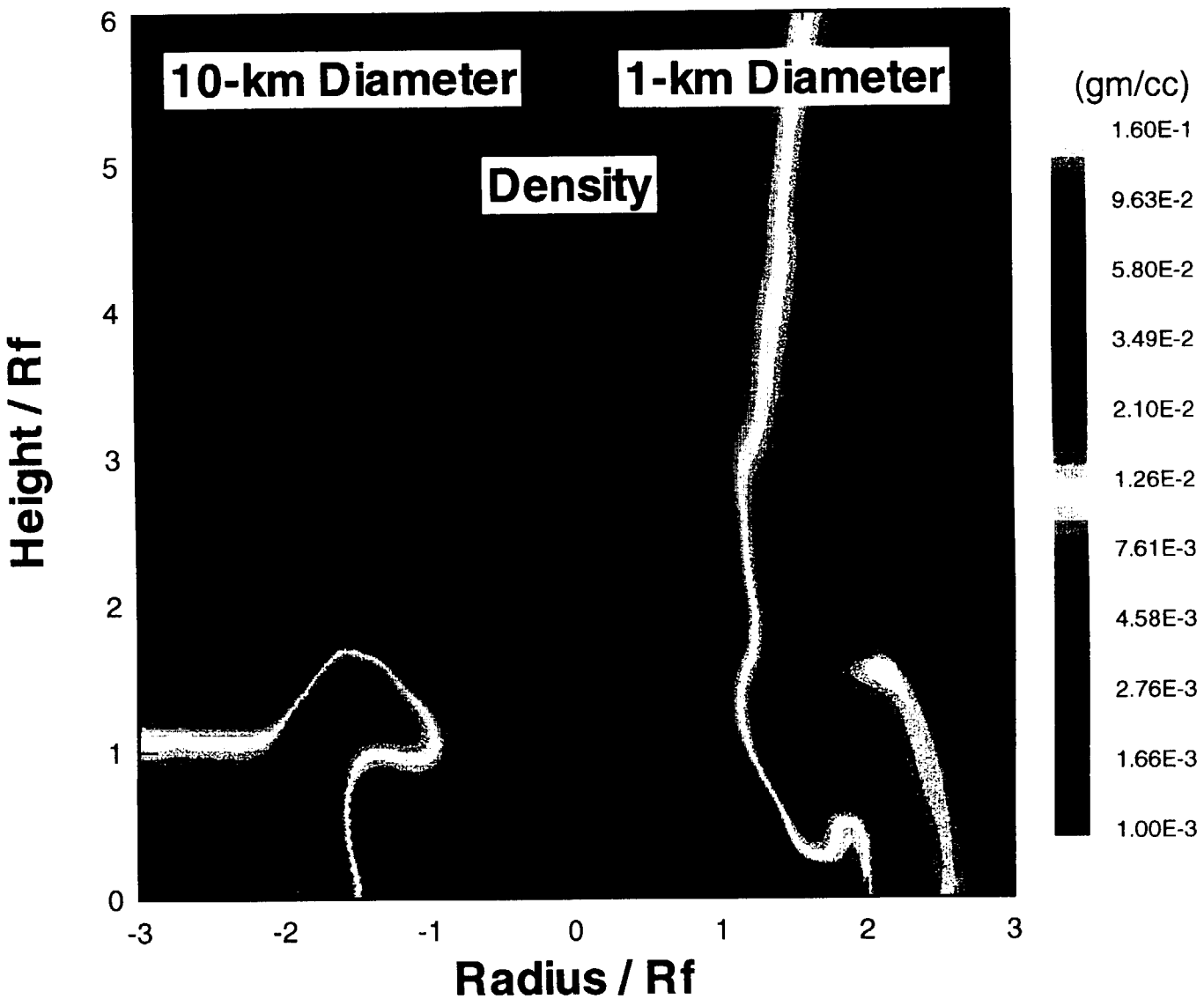

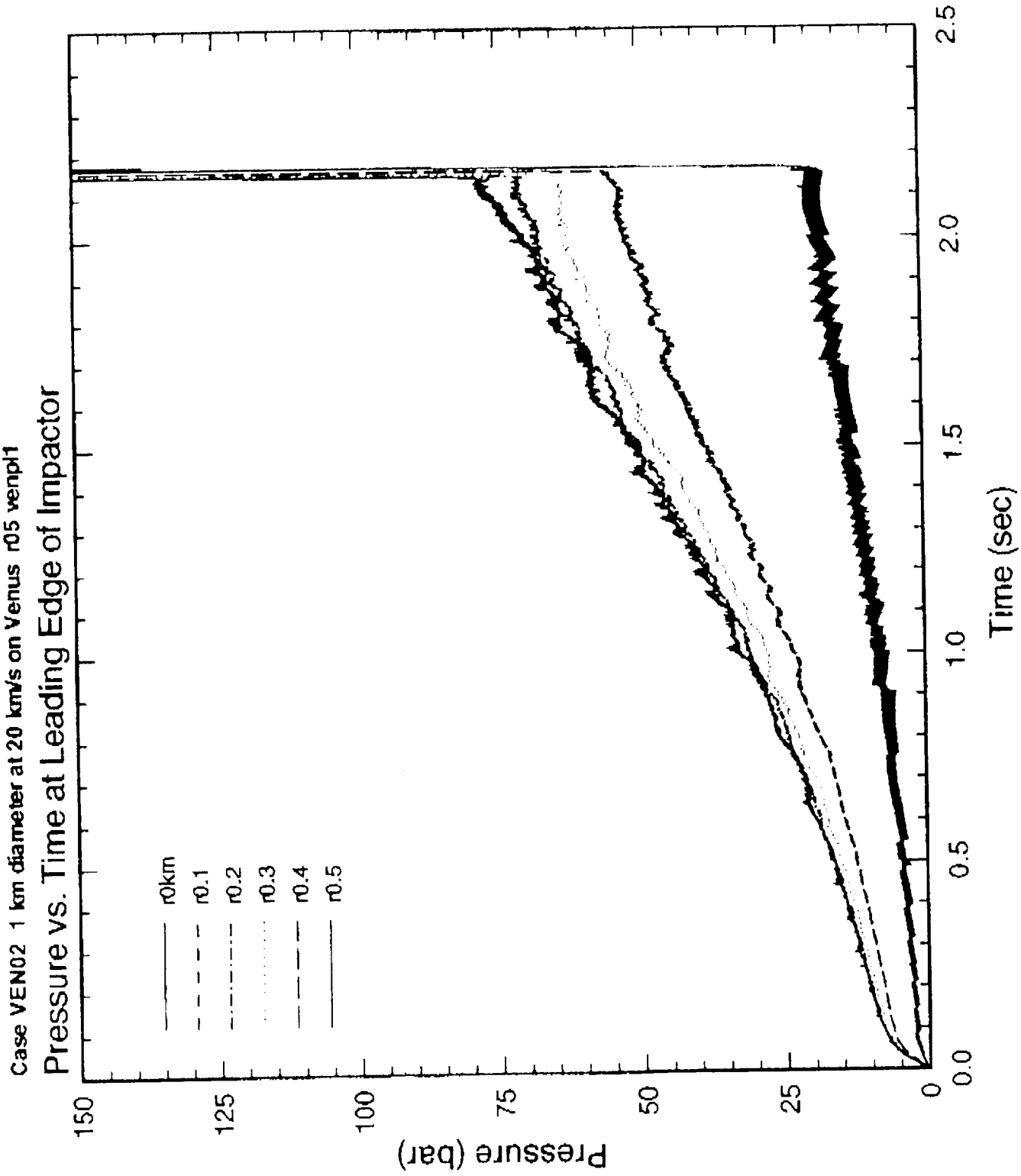
Case VEN02 1 km diameter at 20 km/s on Venus r05 venpl1
Pressure vs. Time at Leading Edge of Impactor
r0km
r0.1
r0.2
r0.3
r0.4
r0.5
Pressure (bar)
Time (sec)
0
25
50
75
100
125
150
0.0
0.5
1.0
1.5
2.0
2.5

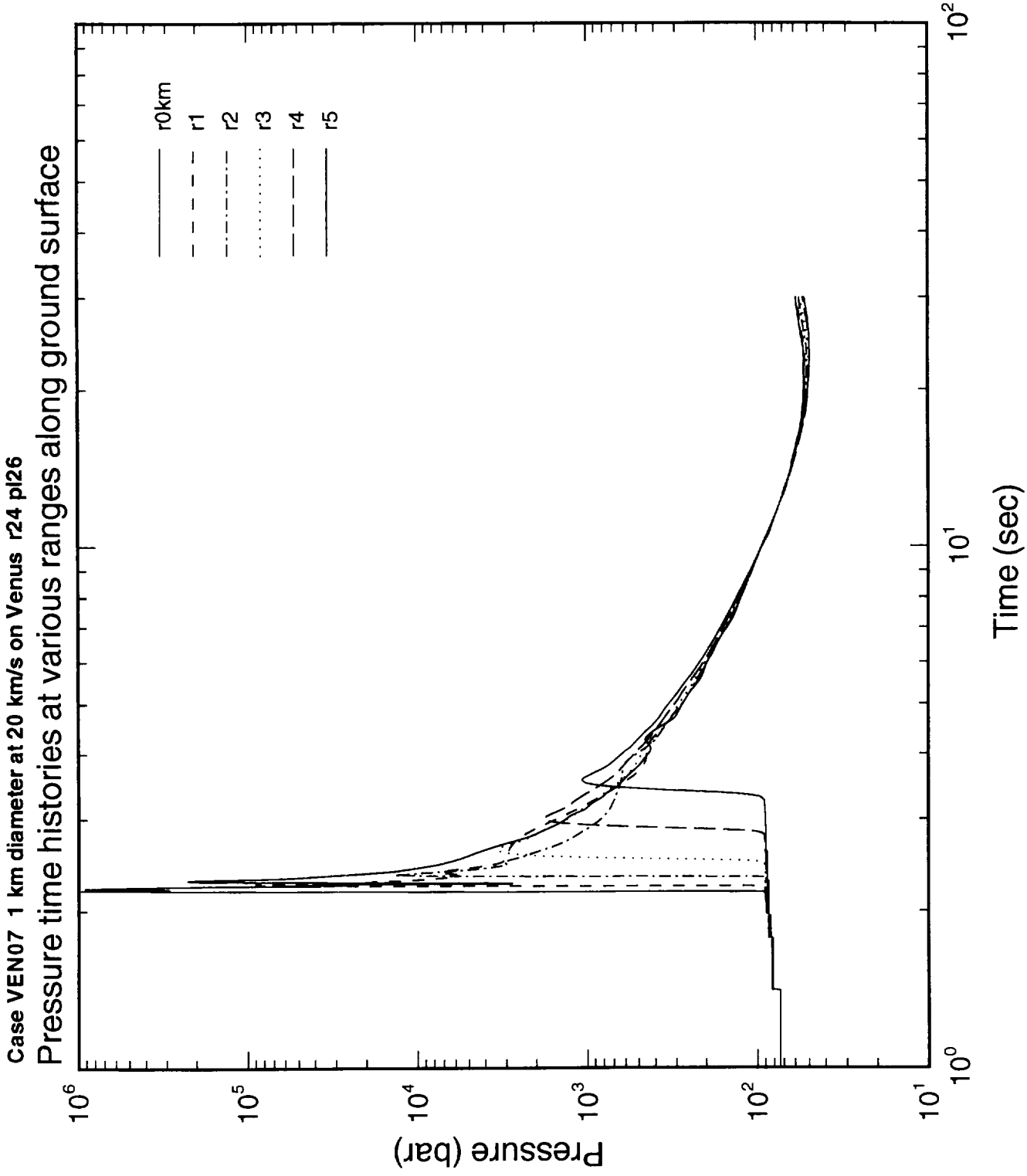
Case VEN07 1 km diameter at 20 km/s on Venus r24 pl26
Pressure time histories at various ranges along ground surface
r0km
r1
r2
r3
r4
r5
Pressure (bar)
Time (sec)
10^6
10^5
10^4
10^3
10^2
10^1
10^0
10^1
10^2

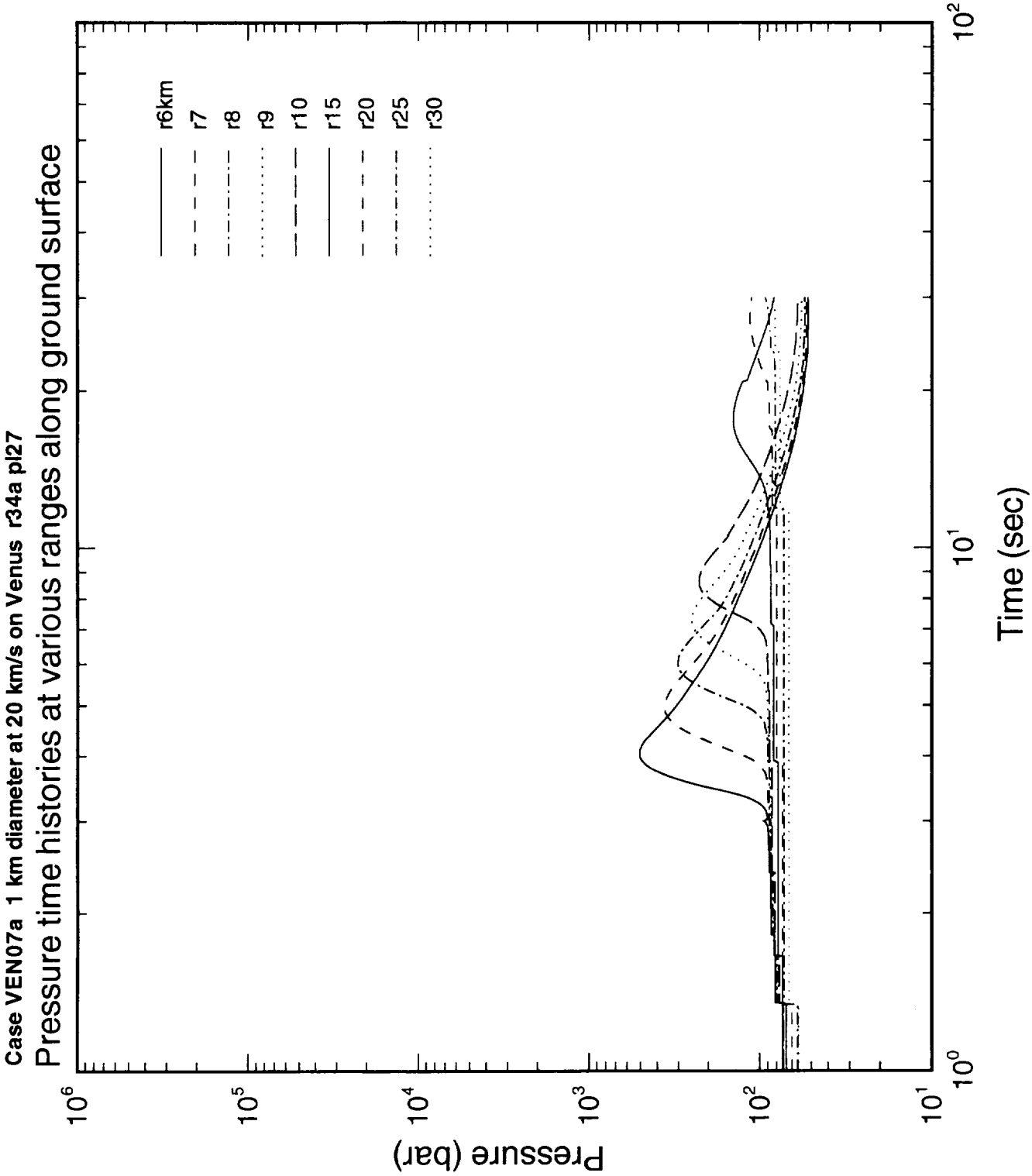
Case VEN07a 1 km diameter at 20 km/s on Venus r34a pl27
Pressure time histories at various ranges along ground surface
r6km
r7
r8
r9
r10
r15
r20
r25
r30
Pressure (bar)
Time (sec)
10^6
10^5
10^4
10^3
10^2
10^1
10^0
10^1
10^2

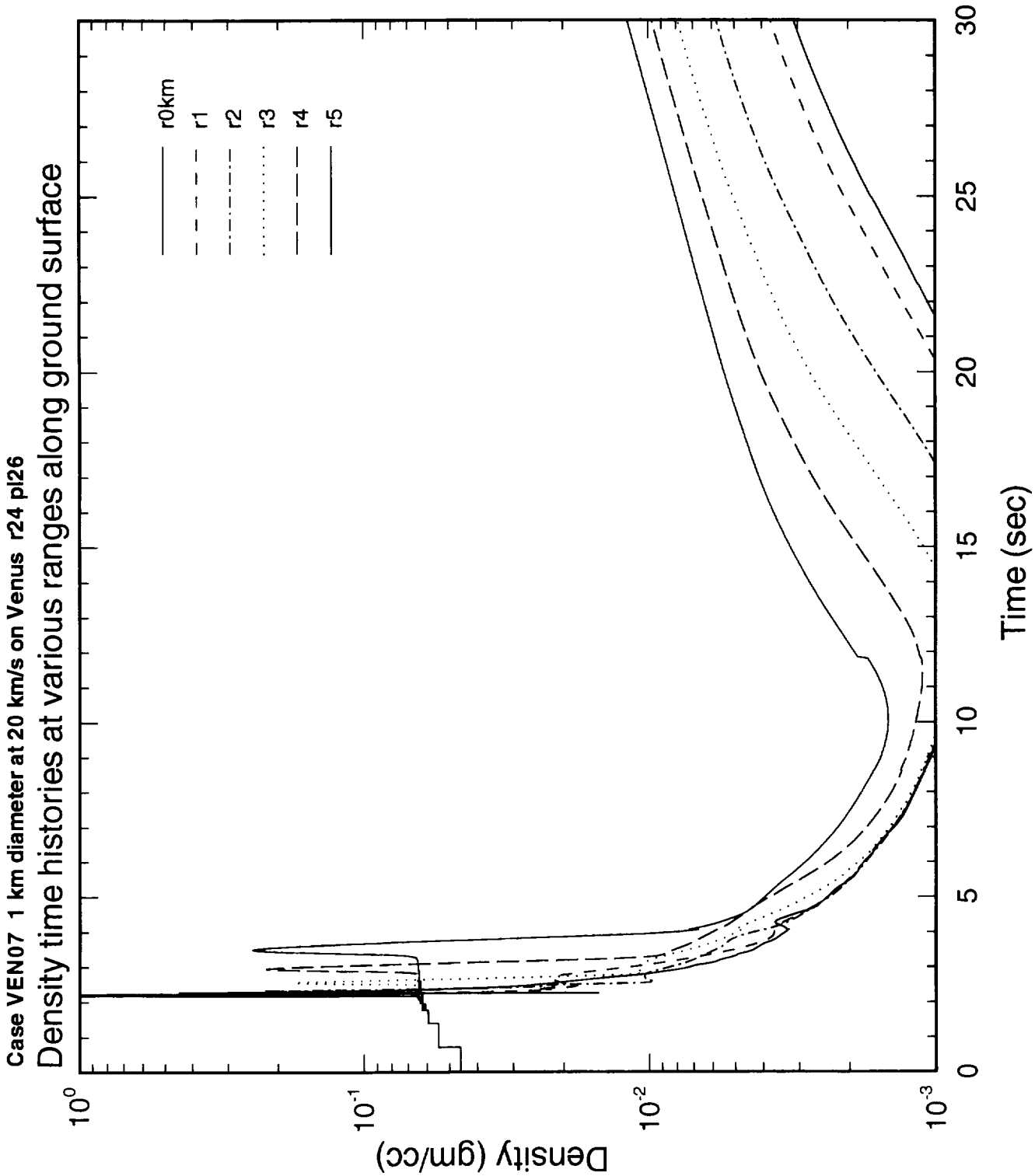
Case VEN07 1 km diameter at 20 km/s on Venus r24 pl26
Density time histories at various ranges along ground surface
r0km
r1
r2
r3
r4
r5
Density (gm/cc)
10^{0}
10^{-1}
10^{-2}
10^{-3}
0
5
10
15
20
25
30
Time (sec)

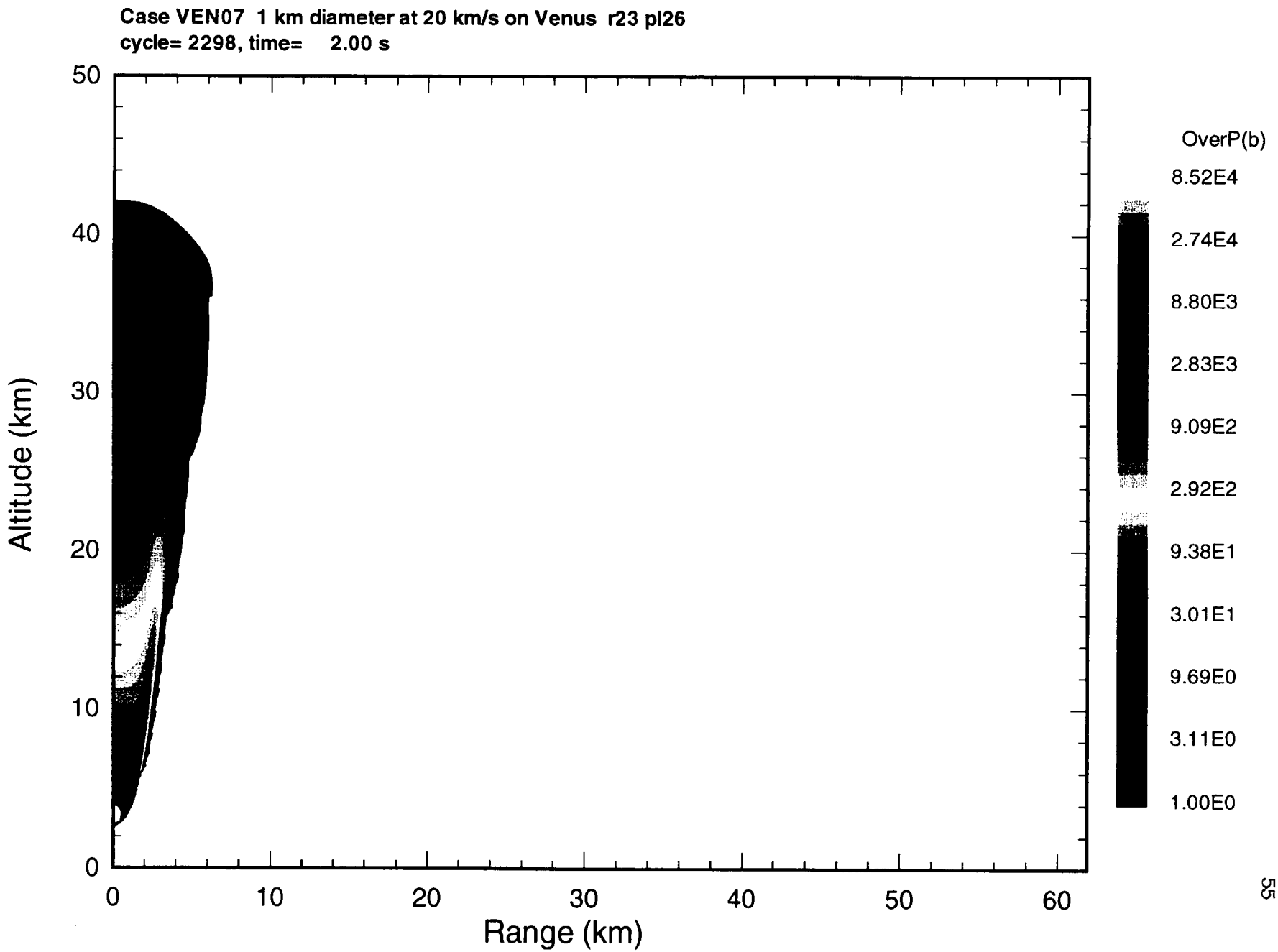
Case VEN07 1 km diameter at 20 km/s on Venus r23 pl26
cycle= 2298, time= 2.00 s
Altitude (km)
Range (km)
0
10
20
30
40
50
60
OverP(b)
8.52E4
2.74E4
8.80E3
2.83E3
9.09E2
2.92E2
9.38E1
3.01E1
9.69E0
3.11E0
1.00E0

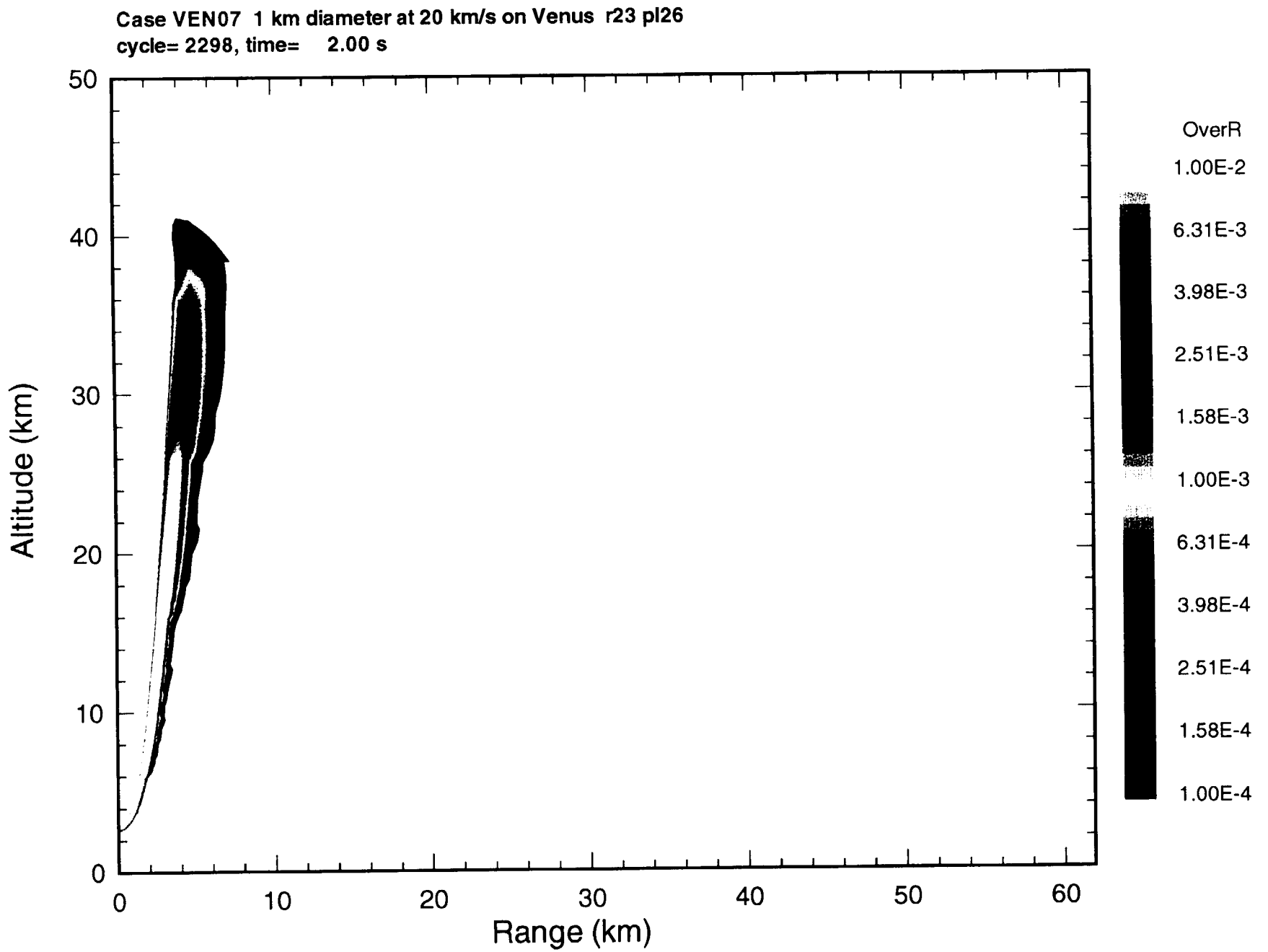
Case VEN07 1 km diameter at 20 km/s on Venus r23 pl26
cycle= 2298, time= 2.00 s
Altitude (km)
Range (km)
0
10
20
30
40
50
60
OverR
1.00E-2
6.31E-3
3.98E-3
2.51E-3
1.58E-3
1.00E-3
6.31E-4
3.98E-4
2.51E-4
1.58E-4
1.00E-4

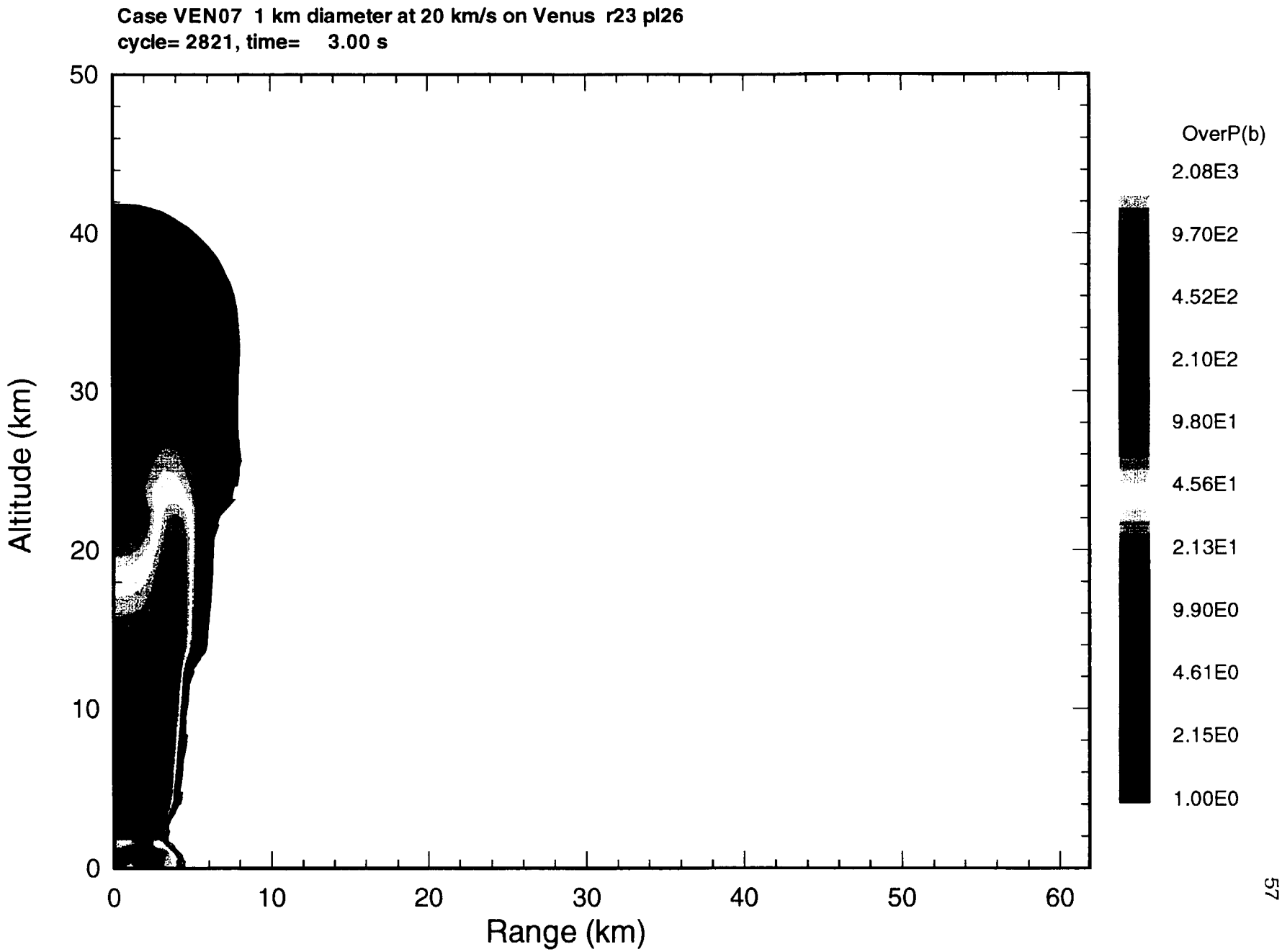
Case VEN07 1 km diameter at 20 km/s on Venus r23 pl26
cycle= 2821, time= 3.00 s
Altitude (km)
Range (km)
0
10
20
30
40
50
60
OverP(b)
2.08E3
9.70E2
4.52E2
2.10E2
9.80E1
4.56E1
2.13E1
9.90E0
4.61E0
2.15E0
1.00E0

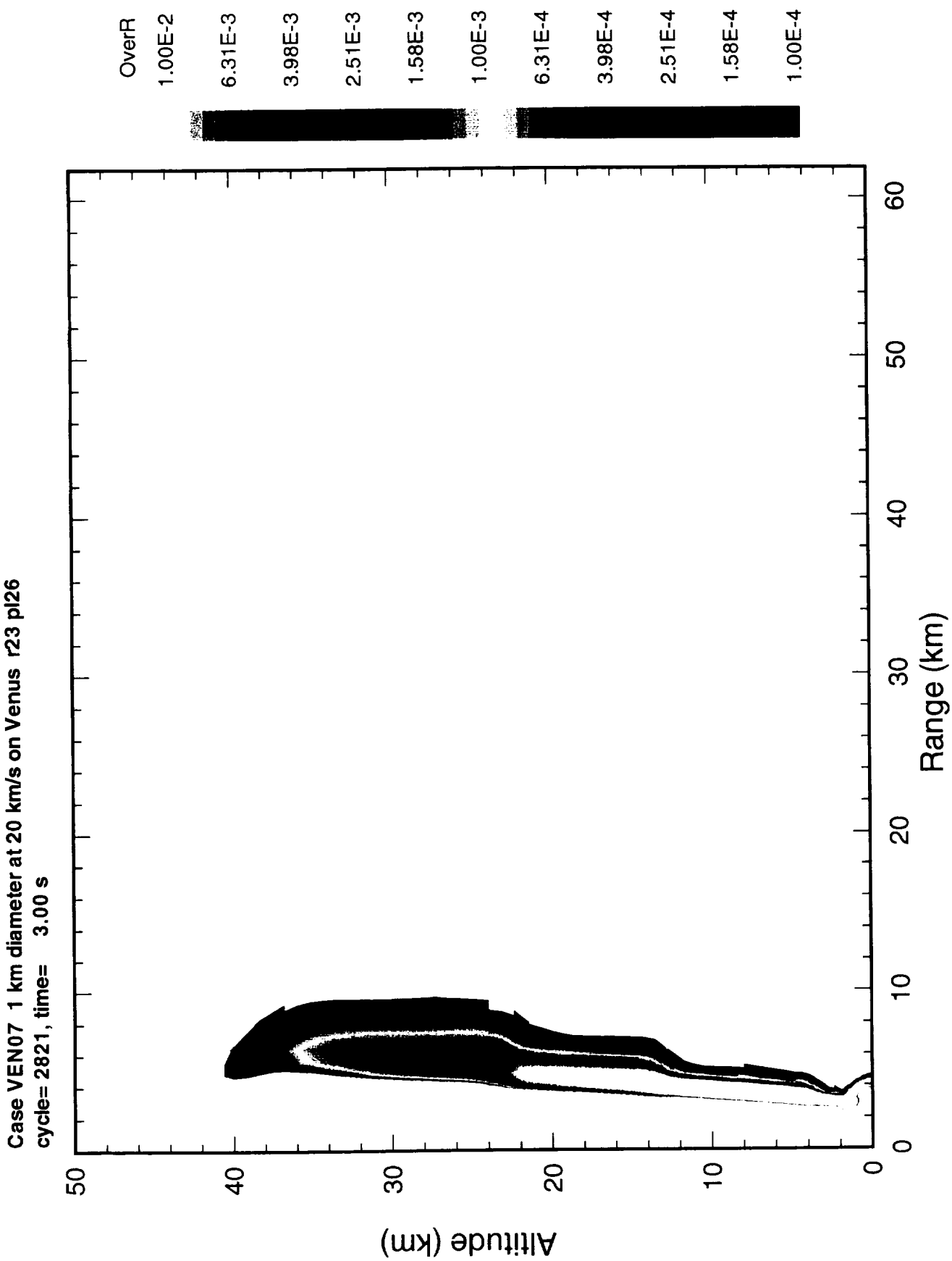
Case VEN07 1 km diameter at 20 km/s on Venus r23 pl26
cycle= 2821, time= 3.00 s
OverR
1.00E-2
6.31E-3
3.98E-3
2.51E-3
1.58E-3
1.00E-3
6.31E-4
3.98E-4
2.51E-4
1.58E-4
1.00E-4
Altitude (km)
Range (km)
0
10
20
30
40
50
60

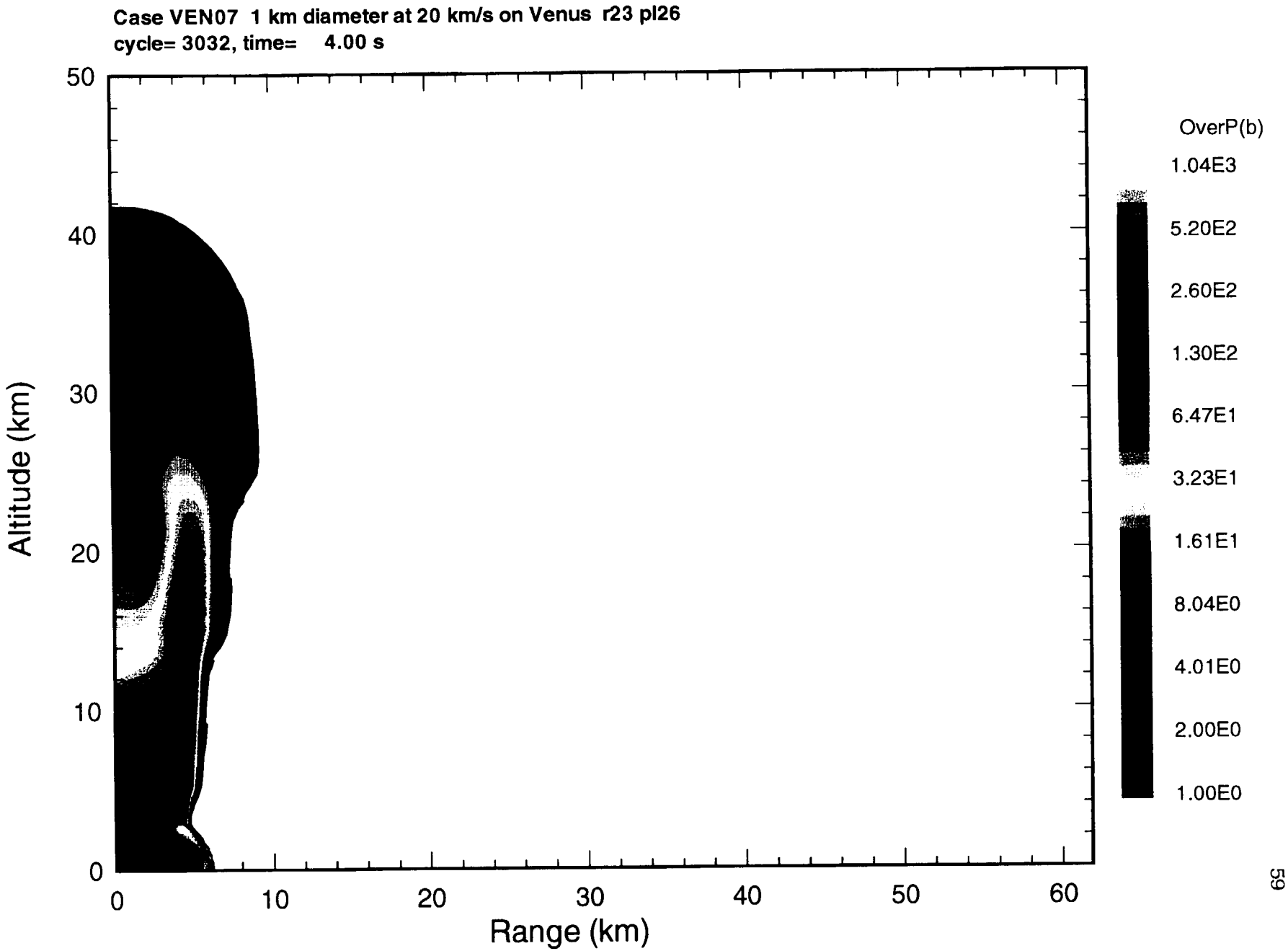
Case VEN07 1 km diameter at 20 km/s on Venus r23 pl26
cycle= 3032, time= 4.00 s
Altitude (km)
Range (km)
0
10
20
30
40
50
60
OverP(b)
1.04E3
5.20E2
2.60E2
1.30E2
6.47E1
3.23E1
1.61E1
8.04E0
4.01E0
2.00E0
1.00E0

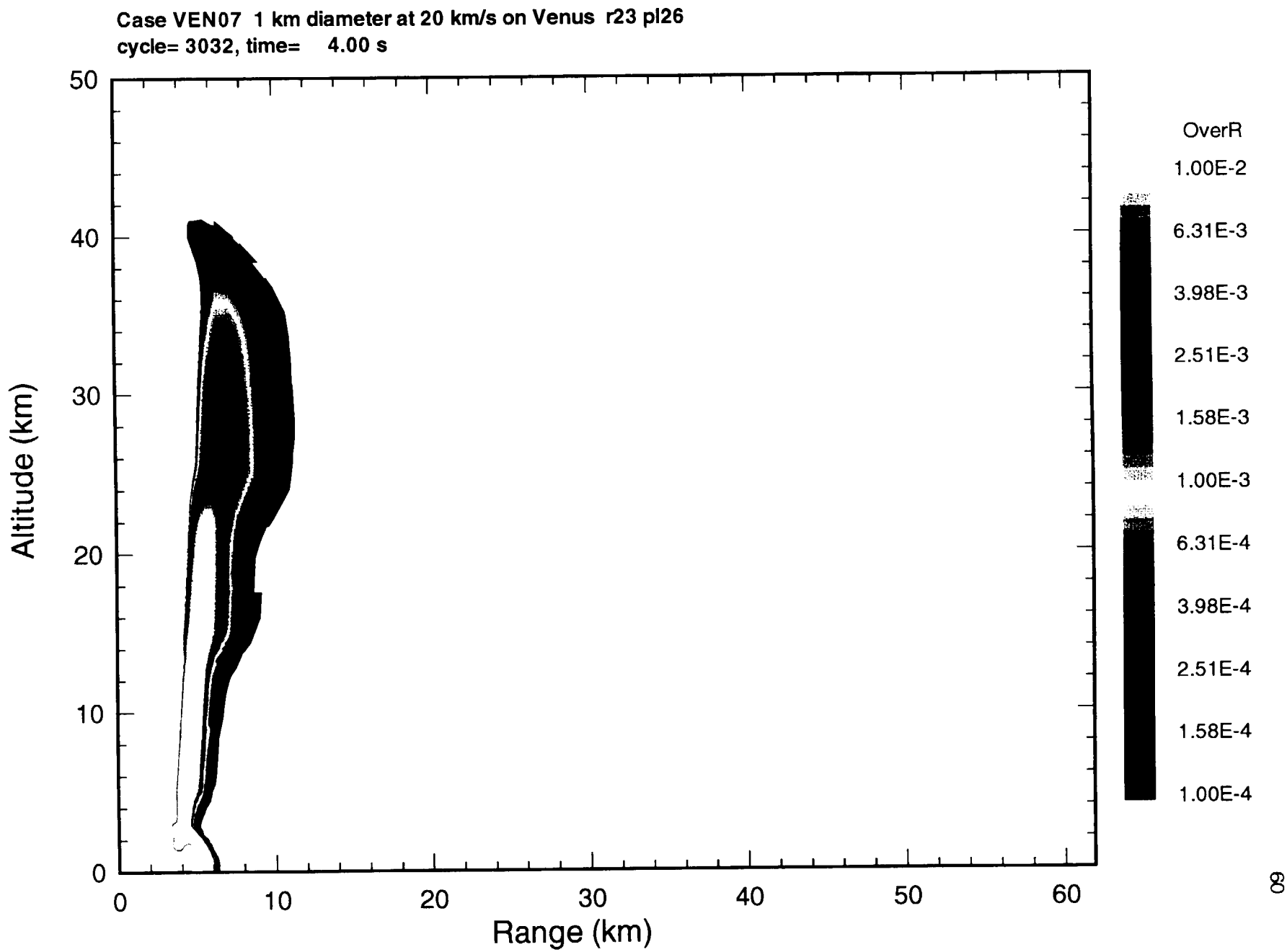
Case VEN07 1 km diameter at 20 km/s on Venus r23 pl26
cycle= 3032, time= 4.00 s
Altitude (km)
Range (km)
0
10
20
30
40
50
60
OverR
1.00E-2
6.31E-3
3.98E-3
2.51E-3
1.58E-3
1.00E-3
6.31E-4
3.98E-4
2.51E-4
1.58E-4
1.00E-4

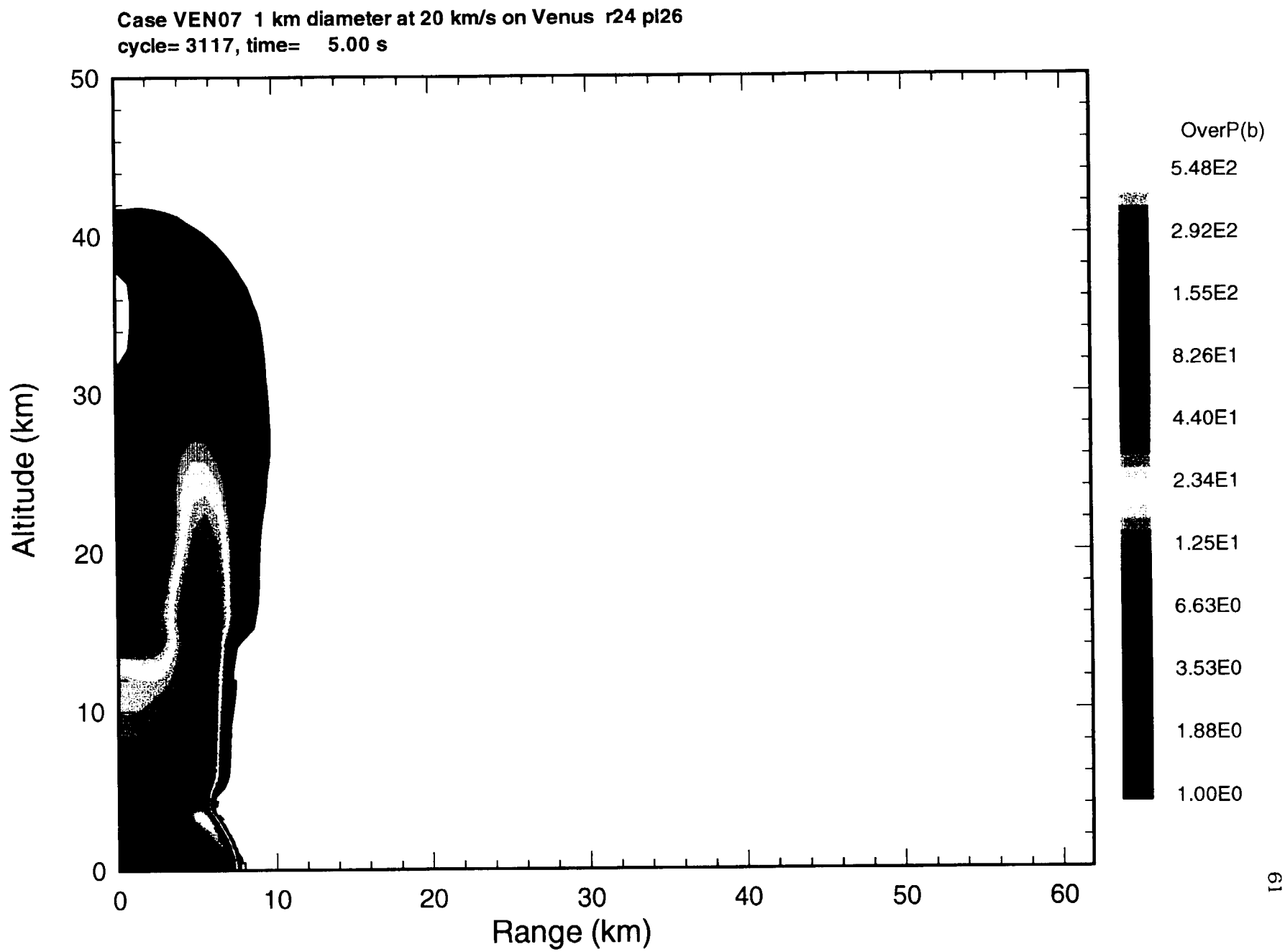
Case VEN07 1 km diameter at 20 km/s on Venus r24 pl26
cycle= 3117, time= 5.00 s
Altitude (km)
Range (km)
0
10
20
30
40
50
60
OverP(b)
5.48E2
2.92E2
1.55E2
8.26E1
4.40E1
2.34E1
1.25E1
6.63E0
3.53E0
1.88E0
1.00E0

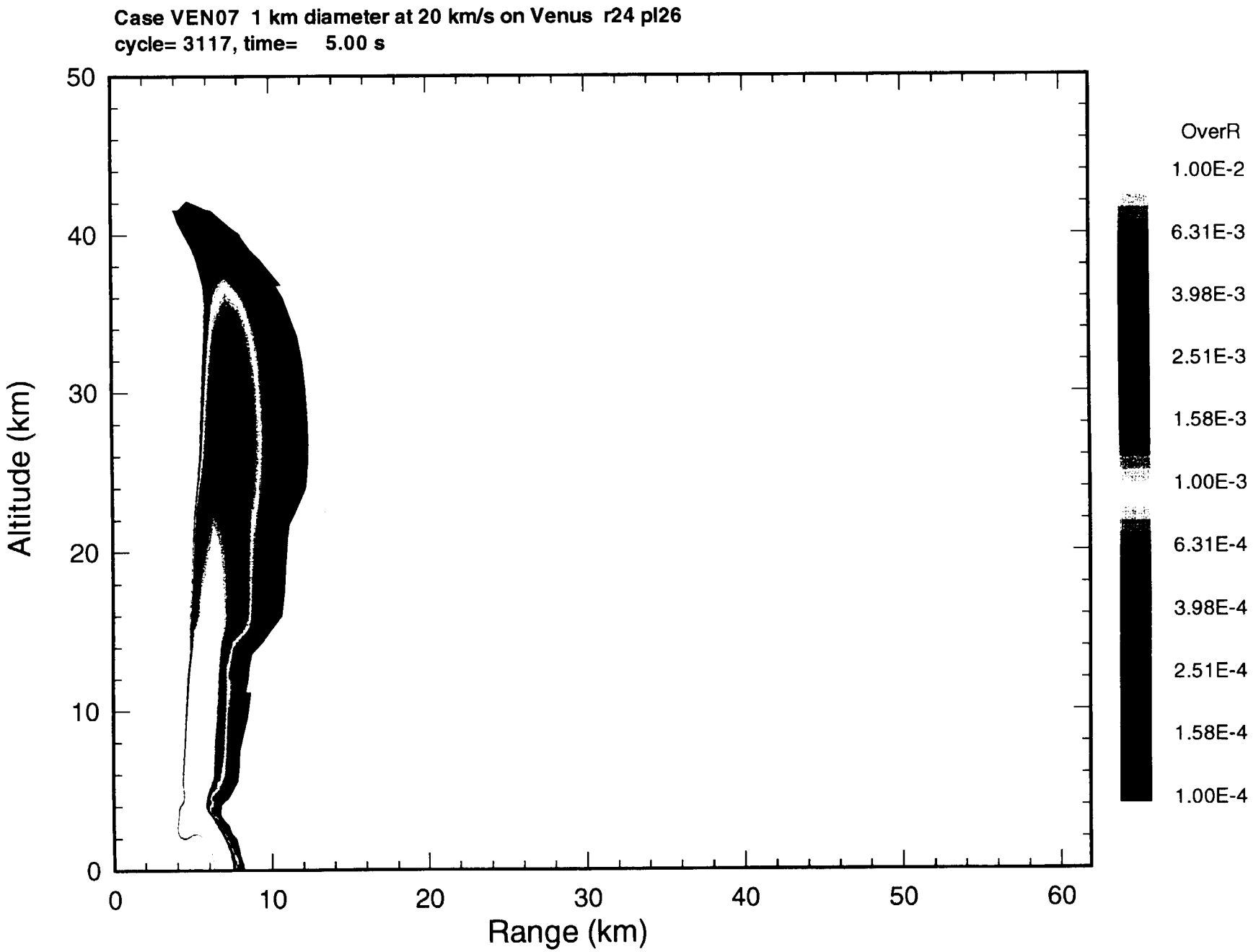
Case VEN07 1 km diameter at 20 km/s on Venus r24 pl26
cycle= 3117, time= 5.00 s
Altitude (km)
Range (km)
0
10
20
30
40
50
60
OverR
1.00E-2
6.31E-3
3.98E-3
2.51E-3
1.58E-3
1.00E-3
6.31E-4
3.98E-4
2.51E-4
1.58E-4
1.00E-4

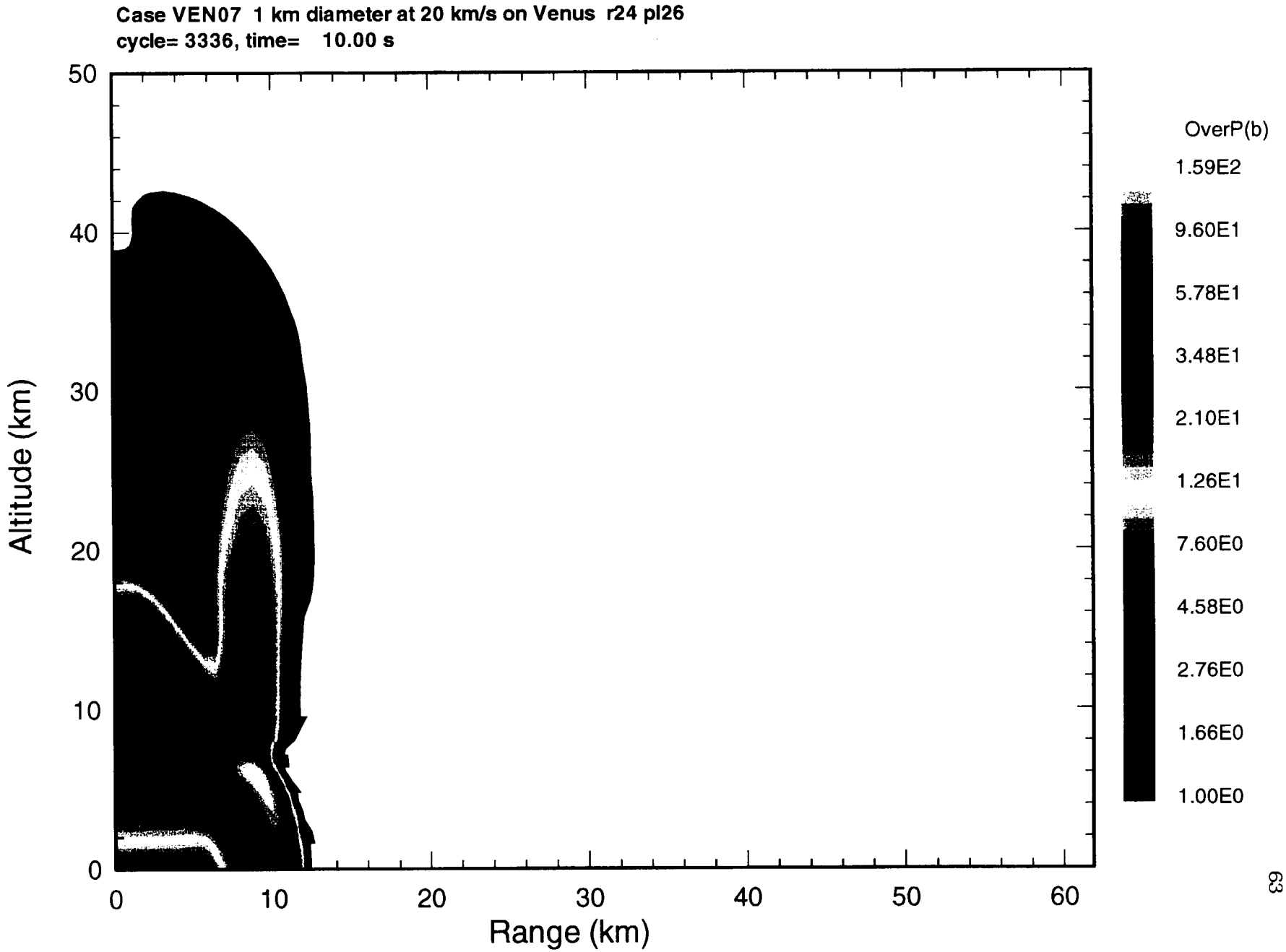
Case VEN07 1 km diameter at 20 km/s on Venus r24 pl26
cycle= 3336, time= 10.00 s
Altitude (km)
Range (km)
0
10
20
30
40
50
60
OverP(b)
1.59E2
9.60E1
5.78E1
3.48E1
2.10E1
1.26E1
7.60E0
4.58E0
2.76E0
1.66E0
1.00E0

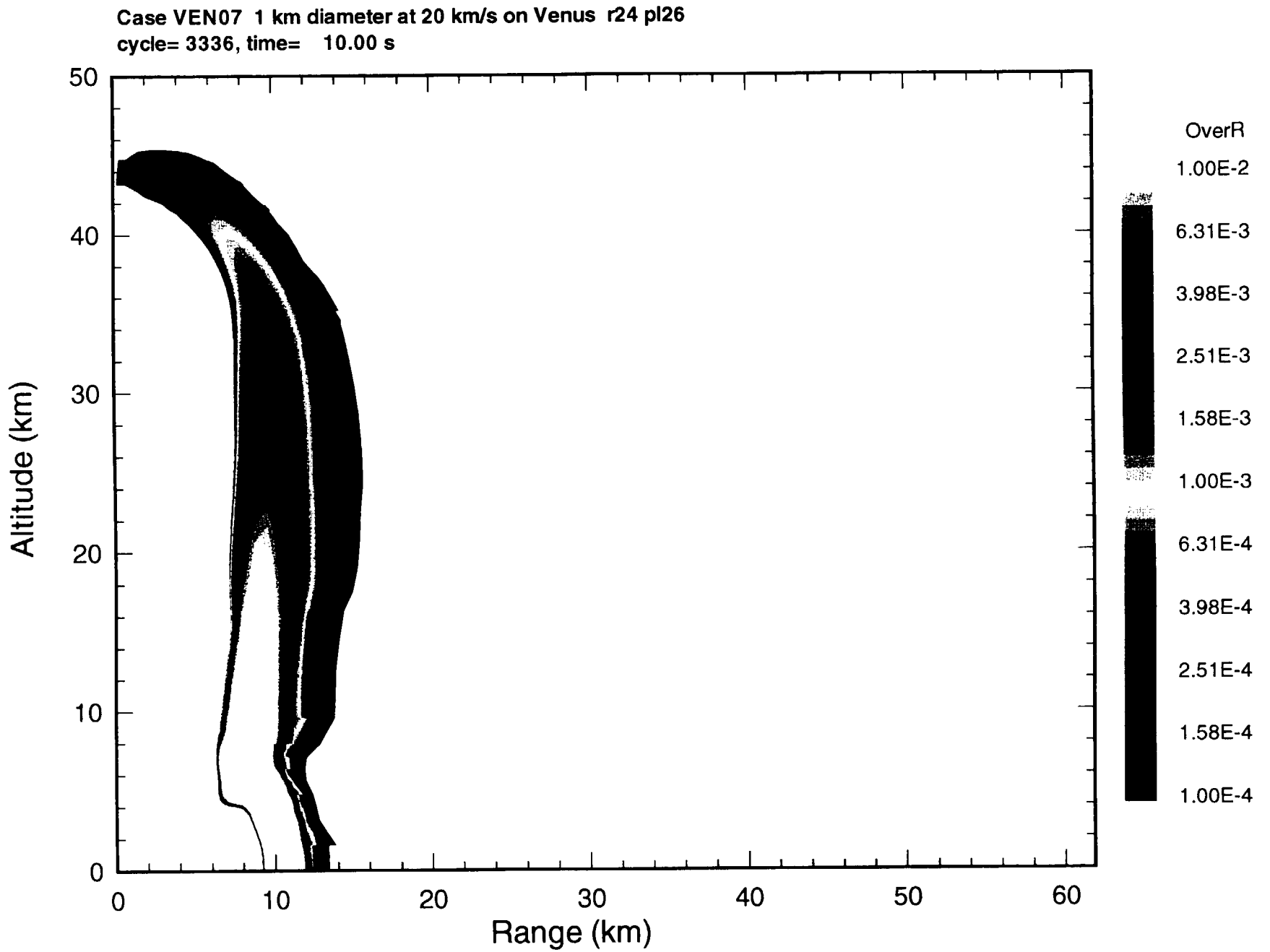
Case VEN07 1 km diameter at 20 km/s on Venus r24 pl26
cycle= 3336, time= 10.00 s
Altitude (km)
Range (km)
0
10
20
30
40
50
60
OverR
1.00E-2
6.31E-3
3.98E-3
2.51E-3
1.58E-3
1.00E-3
6.31E-4
3.98E-4
2.51E-4
1.58E-4
1.00E-4

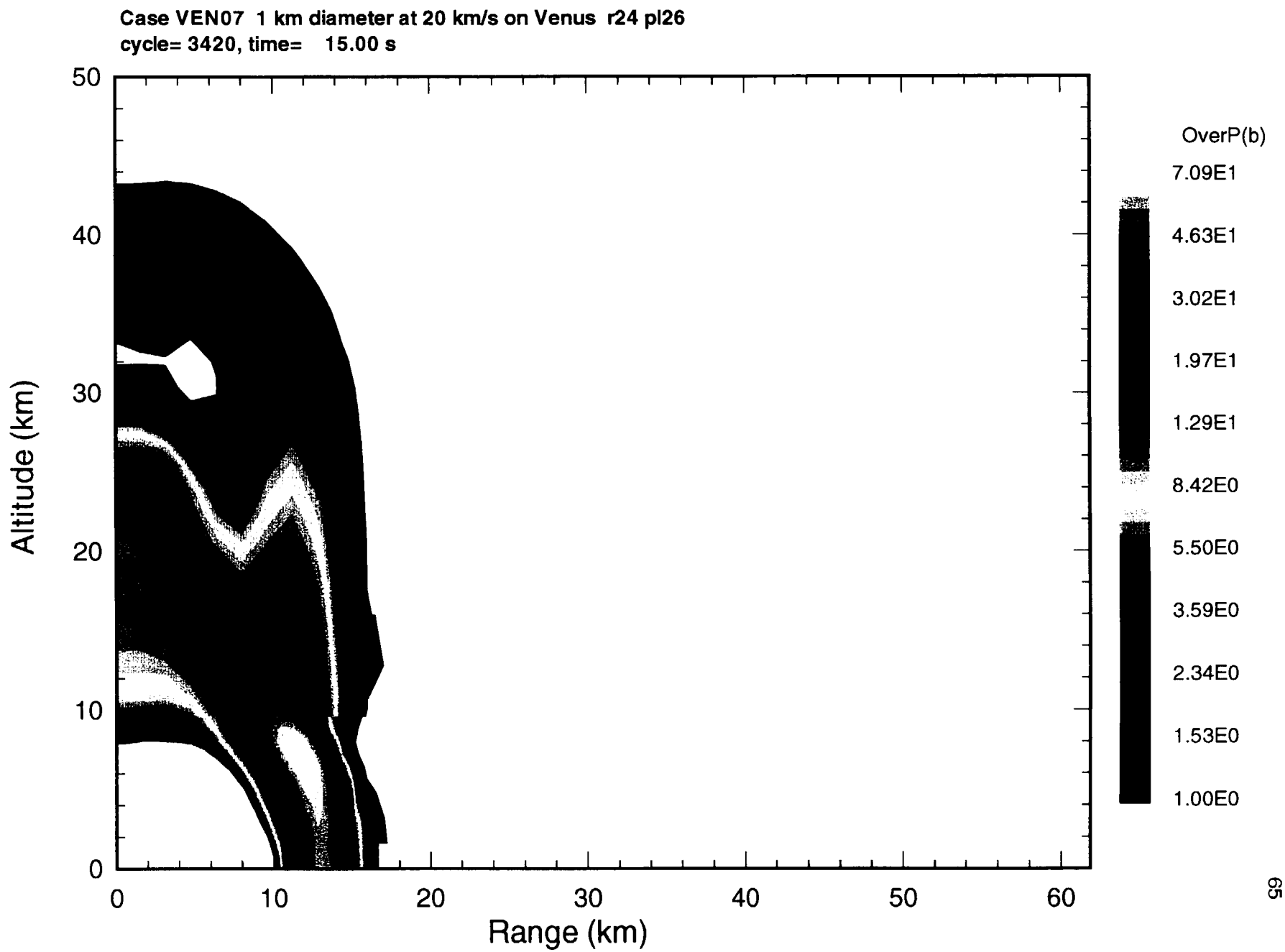
Case VEN07 1 km diameter at 20 km/s on Venus r24 pl26
cycle= 3420, time= 15.00 s
Altitude (km)
Range (km)
0
10
20
30
40
50
60
OverP(b)
7.09E1
4.63E1
3.02E1
1.97E1
1.29E1
8.42E0
5.50E0
3.59E0
2.34E0
1.53E0
1.00E0

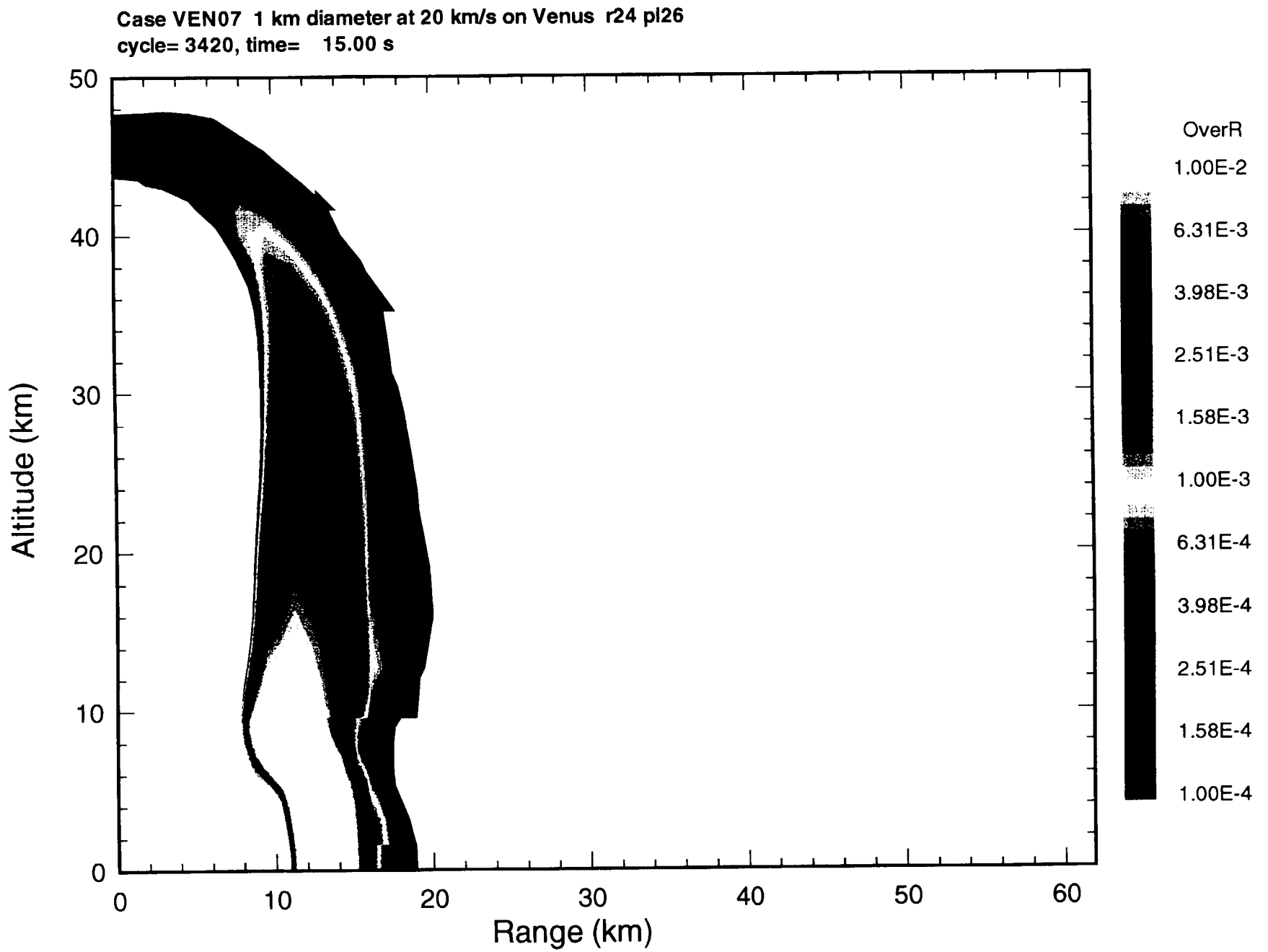
Case VEN07 1 km diameter at 20 km/s on Venus r24 pl26
cycle= 3420, time= 15.00 s
Altitude (km)
Range (km)
0
10
20
30
40
50
60
OverR
1.00E-2
6.31E-3
3.98E-3
2.51E-3
1.58E-3
1.00E-3
6.31E-4
3.98E-4
2.51E-4
1.58E-4
1.00E-4

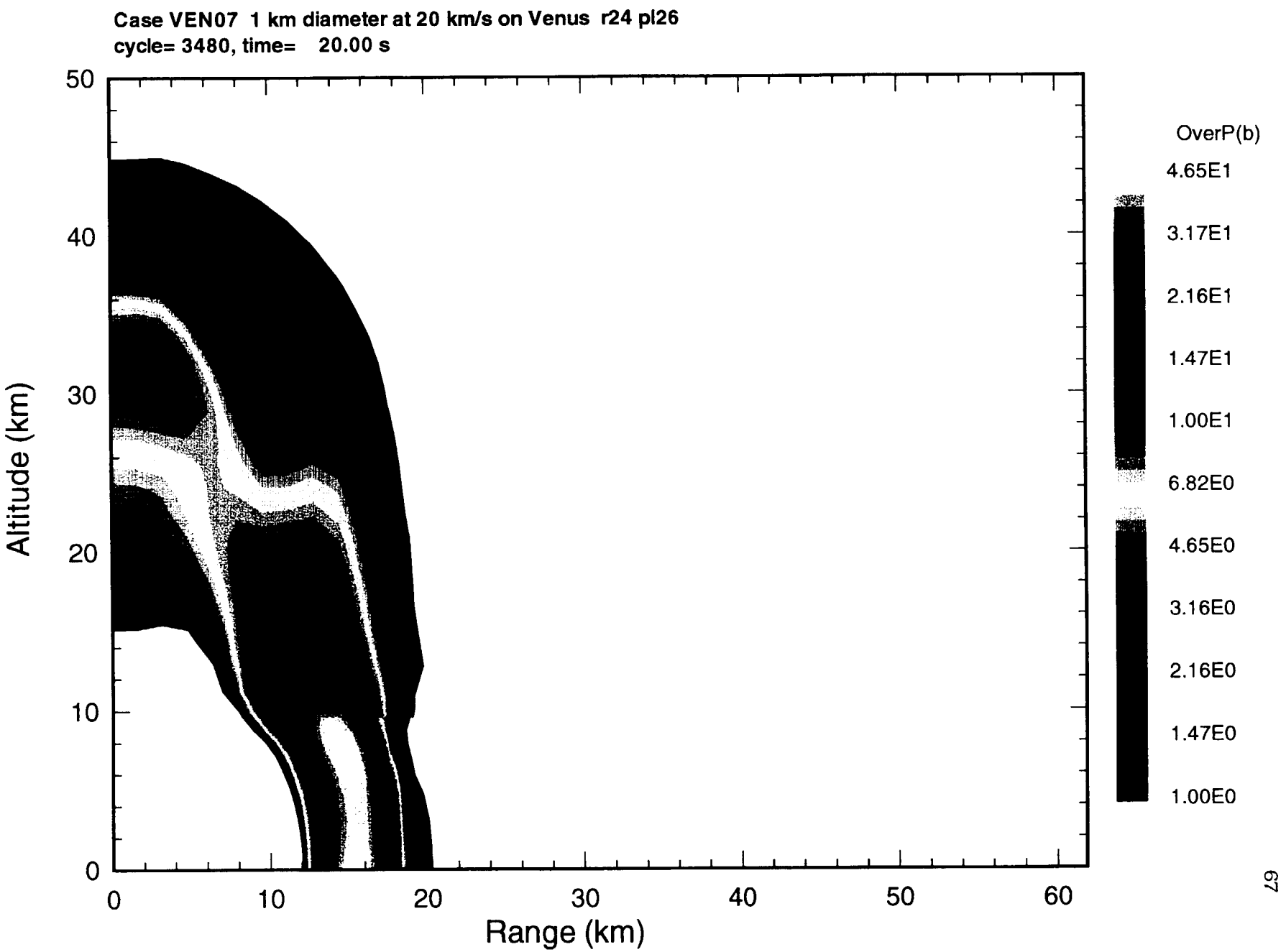
Case VEN07 1 km diameter at 20 km/s on Venus r24 pl26
cycle= 3480, time= 20.00 s
Altitude (km)
Range (km)
0
10
20
30
40
50
60
OverP(b)
4.65E1
3.17E1
2.16E1
1.47E1
1.00E1
6.82E0
4.65E0
3.16E0
2.16E0
1.47E0
1.00E0

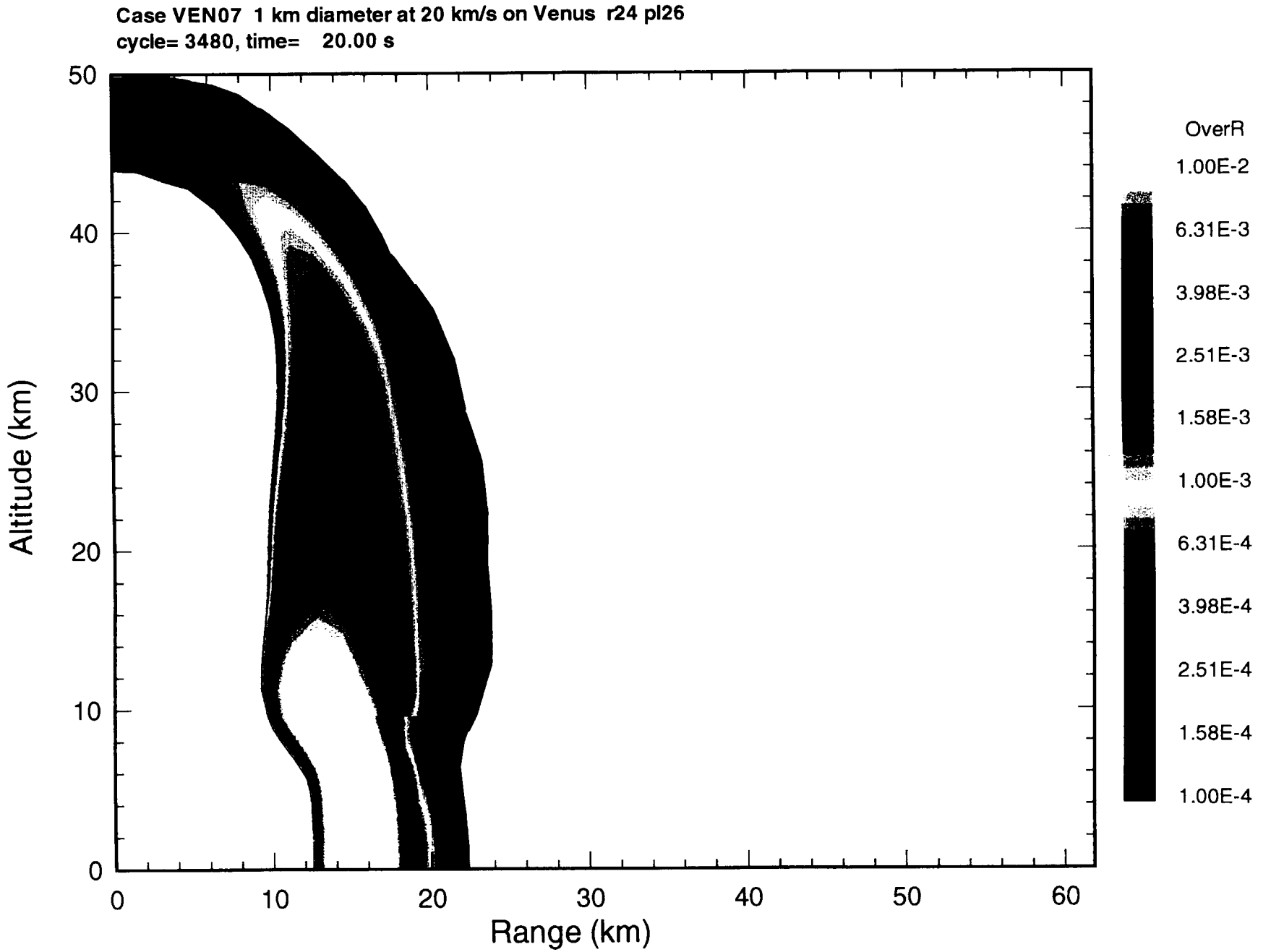
Case VEN07 1 km diameter at 20 km/s on Venus r24 pl26
cycle= 3480, time= 20.00 s
Altitude (km)
Range (km)
0
10
20
30
40
50
60
OverR
1.00E-2
6.31E-3
3.98E-3
2.51E-3
1.58E-3
1.00E-3
6.31E-4
3.98E-4
2.51E-4
1.58E-4
1.00E-4

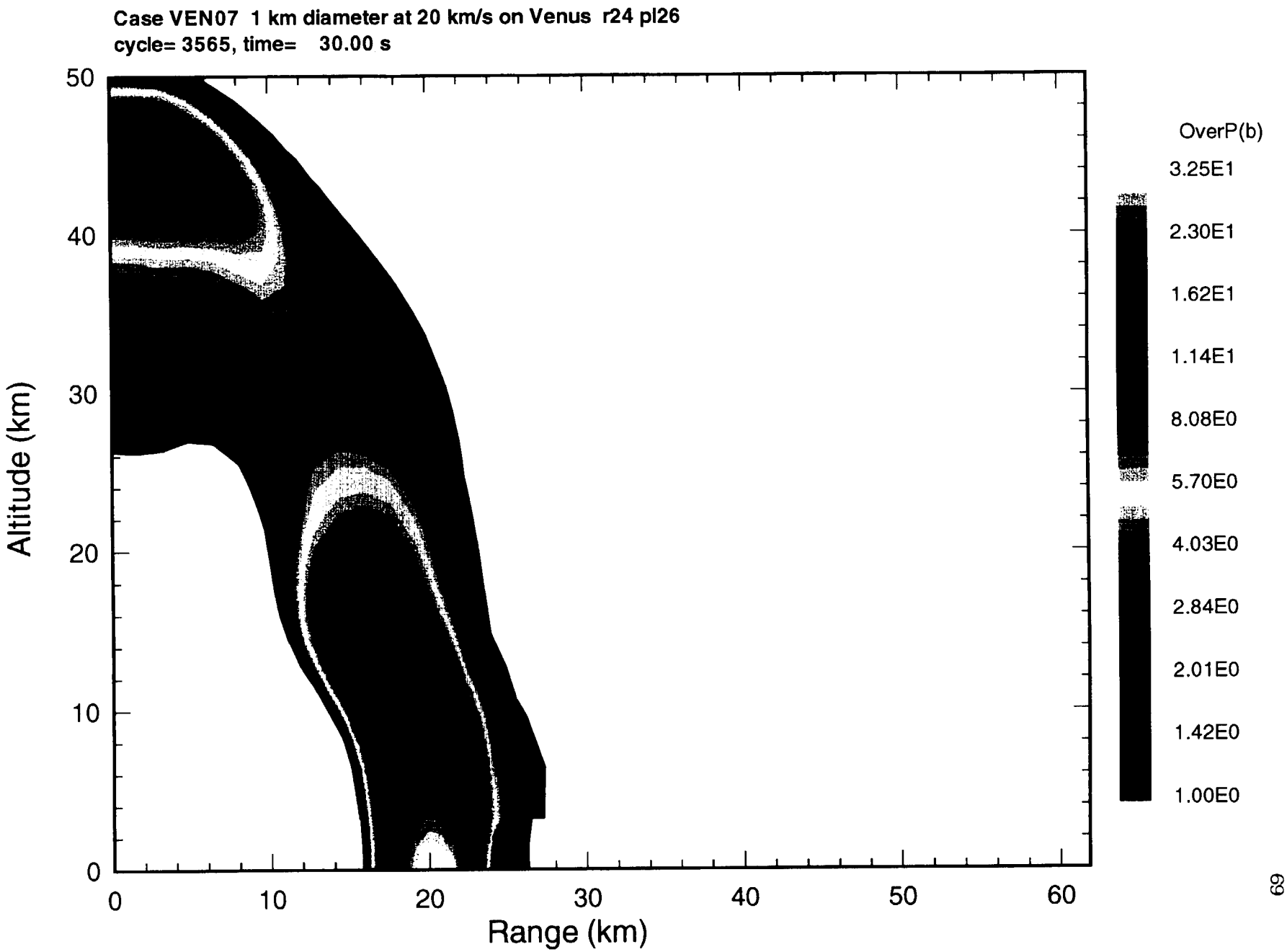
Case VEN07 1 km diameter at 20 km/s on Venus r24 pl26
cycle= 3565, time= 30.00 s
Altitude (km)
Range (km)
0
10
20
30
40
50
60
OverP(b)
3.25E1
2.30E1
1.62E1
1.14E1
8.08E0
5.70E0
4.03E0
2.84E0
2.01E0
1.42E0
1.00E0

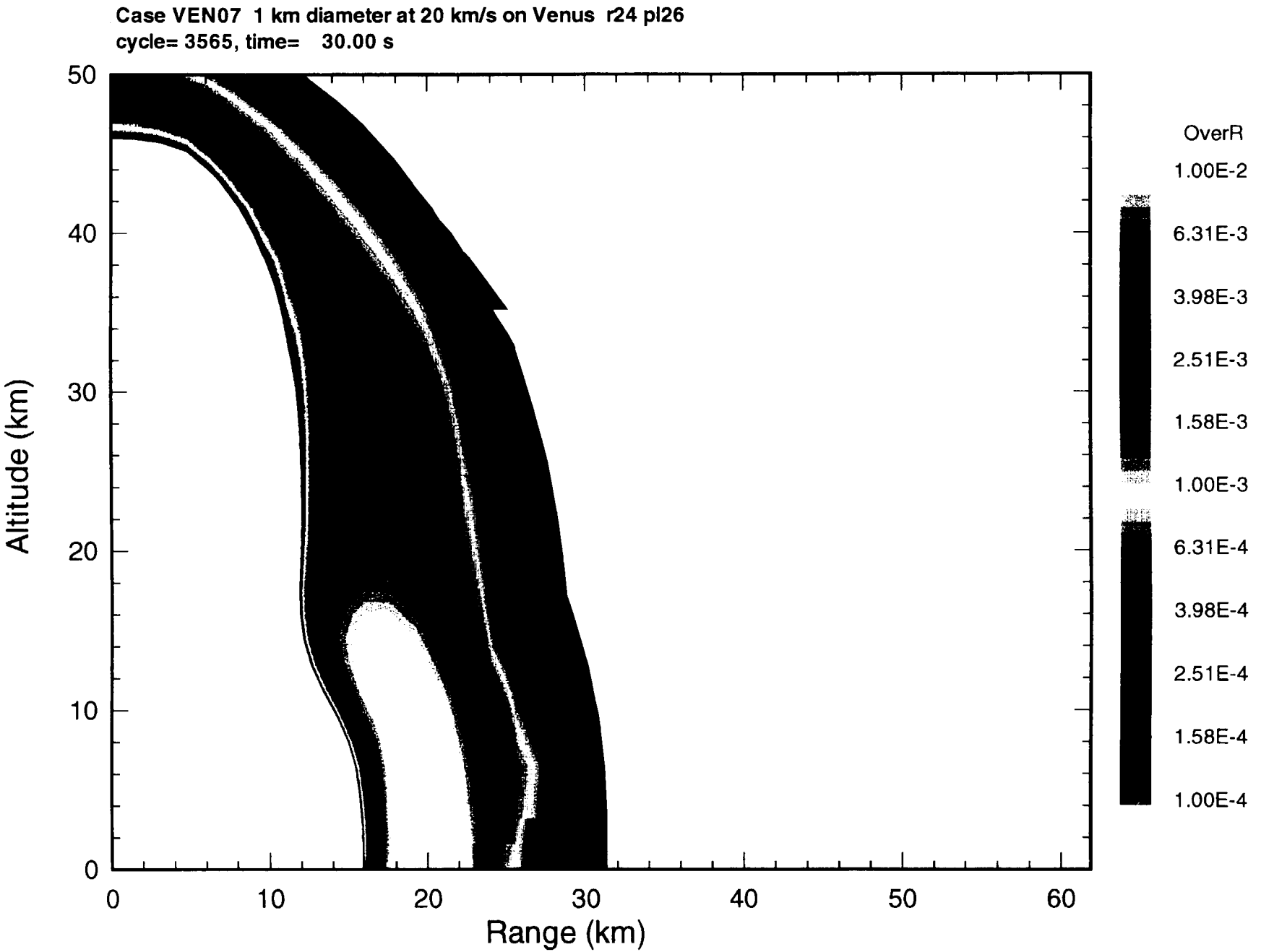
Case VEN07 1 km diameter at 20 km/s on Venus r24 pl26
cycle= 3565, time= 30.00 s
Altitude (km)
Range (km)
0
10
20
30
40
50
60
OverR
1.00E-2
6.31E-3
3.98E-3
2.51E-3
1.58E-3
1.00E-3
6.31E-4
3.98E-4
2.51E-4
1.58E-4
1.00E-4

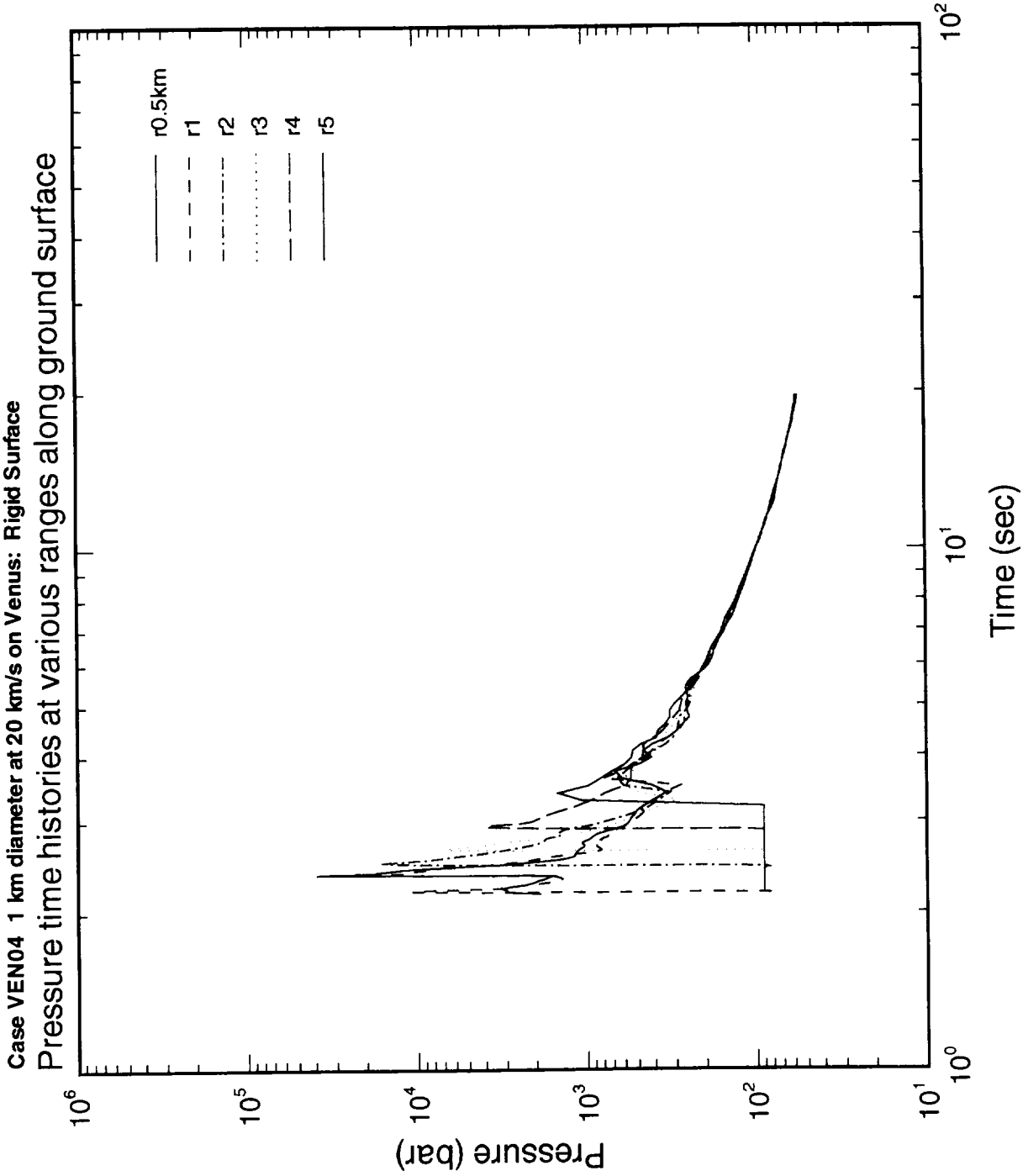
Case VEN04 1 km diameter at 20 km/s on Venus: Rigid Surface
Pressure time histories at various ranges along ground surface
r0.5km
r1
r2
r3
r4
r5
Pressure (bar)
Time (sec)
10^6
10^5
10^4
10^3
10^2
10^1
10^0
10^1
10^2

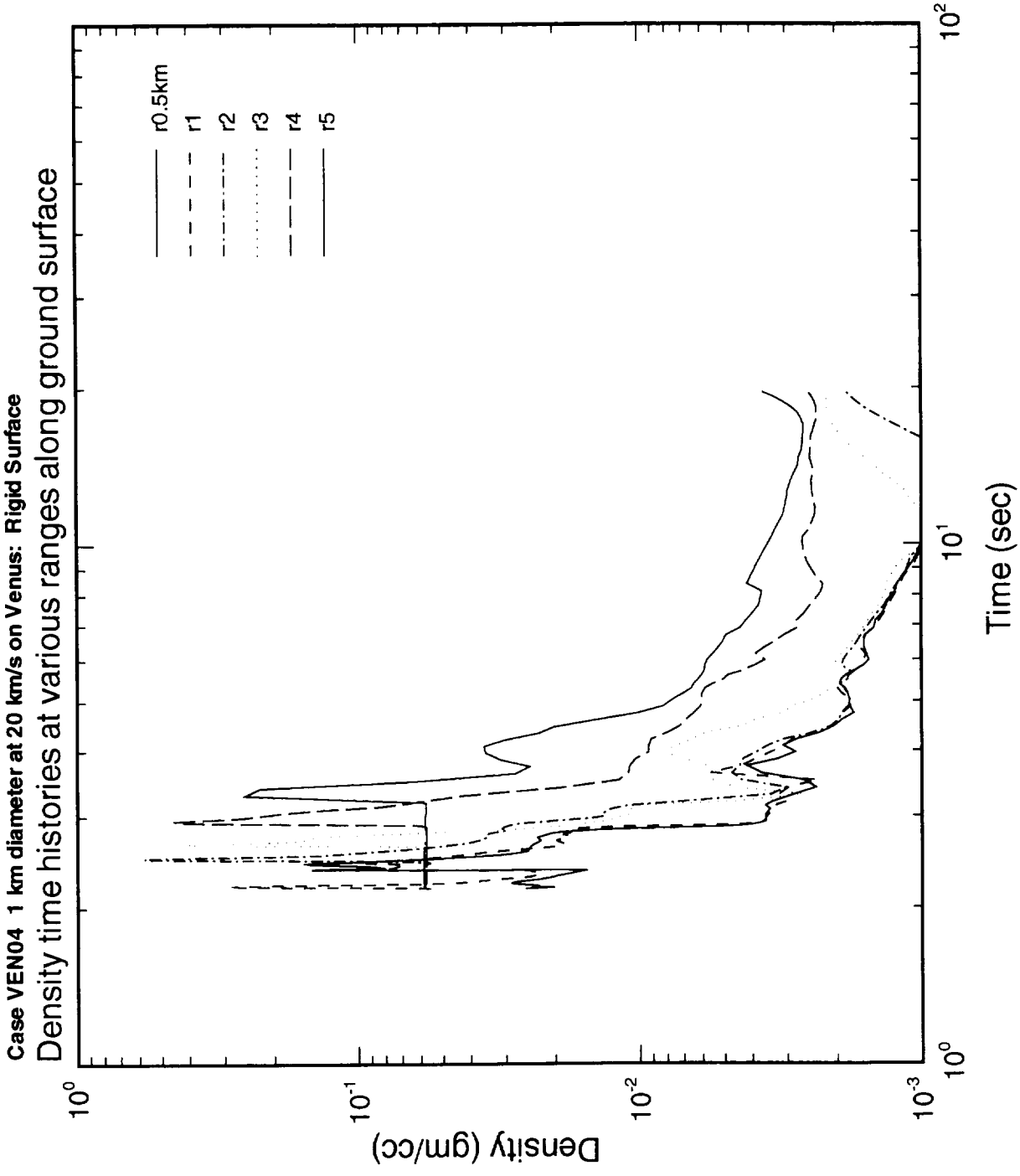
Case VEN04 1 km diameter at 20 km/s on Venus: Rigid Surface
Density time histories at various ranges along ground surface
r0.5km
r1
r2
r3
r4
r5
Density (gm/cc)
Time (sec)
10^0
10^-1
10^-2
10^-3
10^0
10^1
10^2

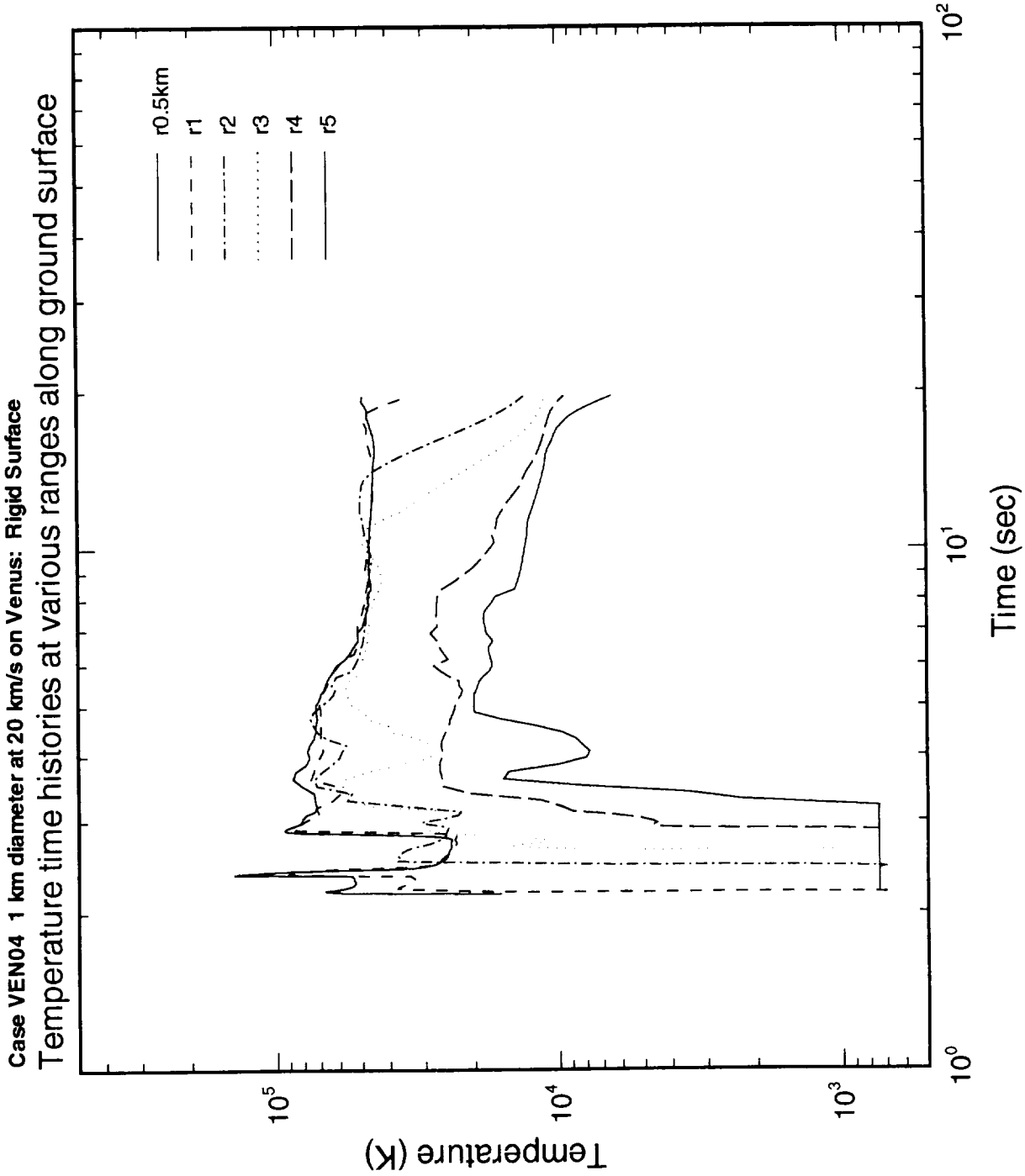
Case VEN04 1 km diameter at 20 km/s on Venus: Rigid Surface
Temperature time histories at various ranges along ground surface
r0.5km
r1
r2
r3
r4
r5
Temperature (K)
10^5
10^4
10^3
10^0
10^1
10^2
Time (sec)

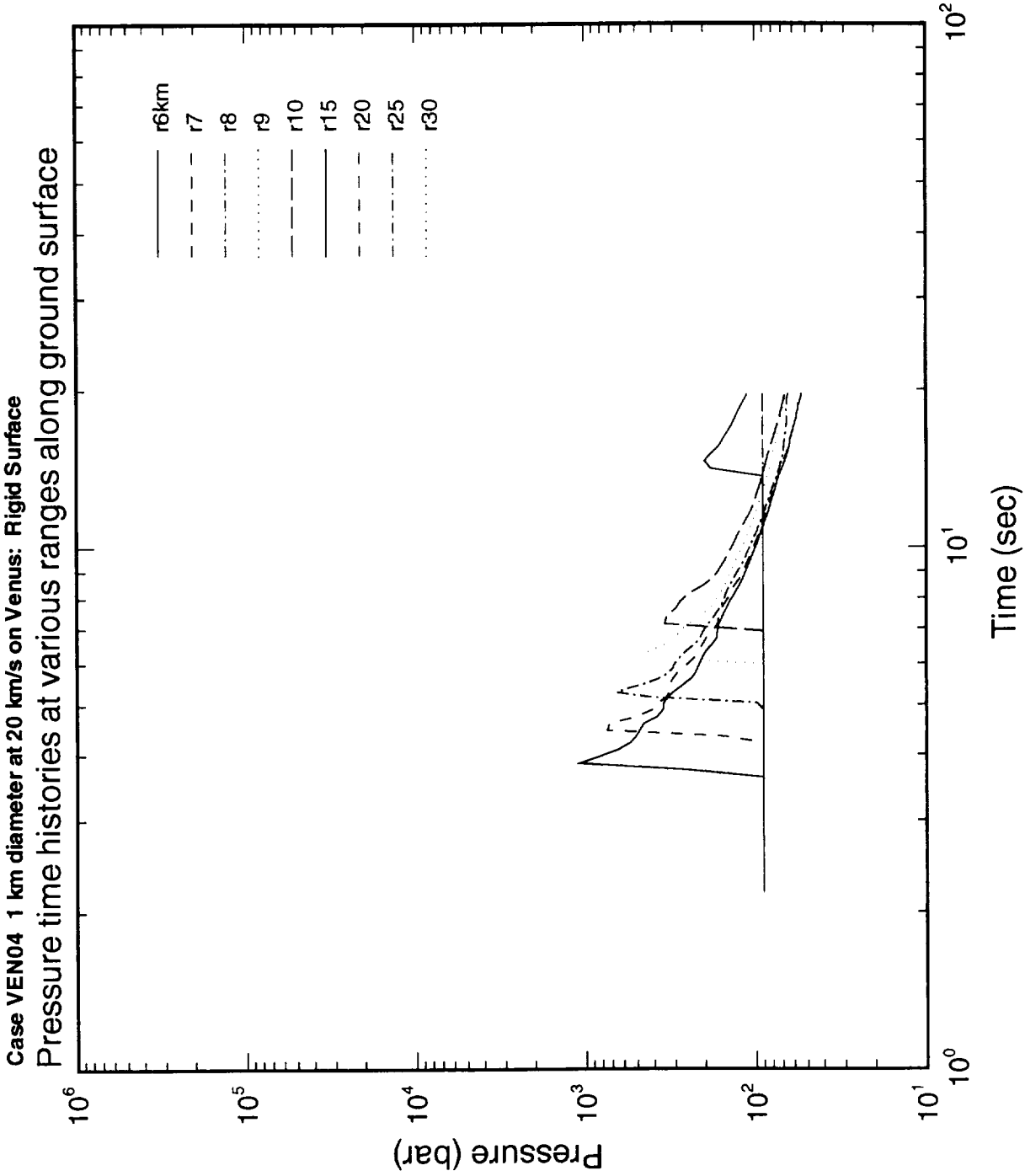
Case VEN04 1 km diameter at 20 km/s on Venus: Rigid Surface
Pressure time histories at various ranges along ground surface
r6km
r7
r8
r9
r10
r15
r20
r25
r30
Pressure (bar)
Time (sec)
10^6
10^5
10^4
10^3
10^2
10^1
10^0
10^1
10^2

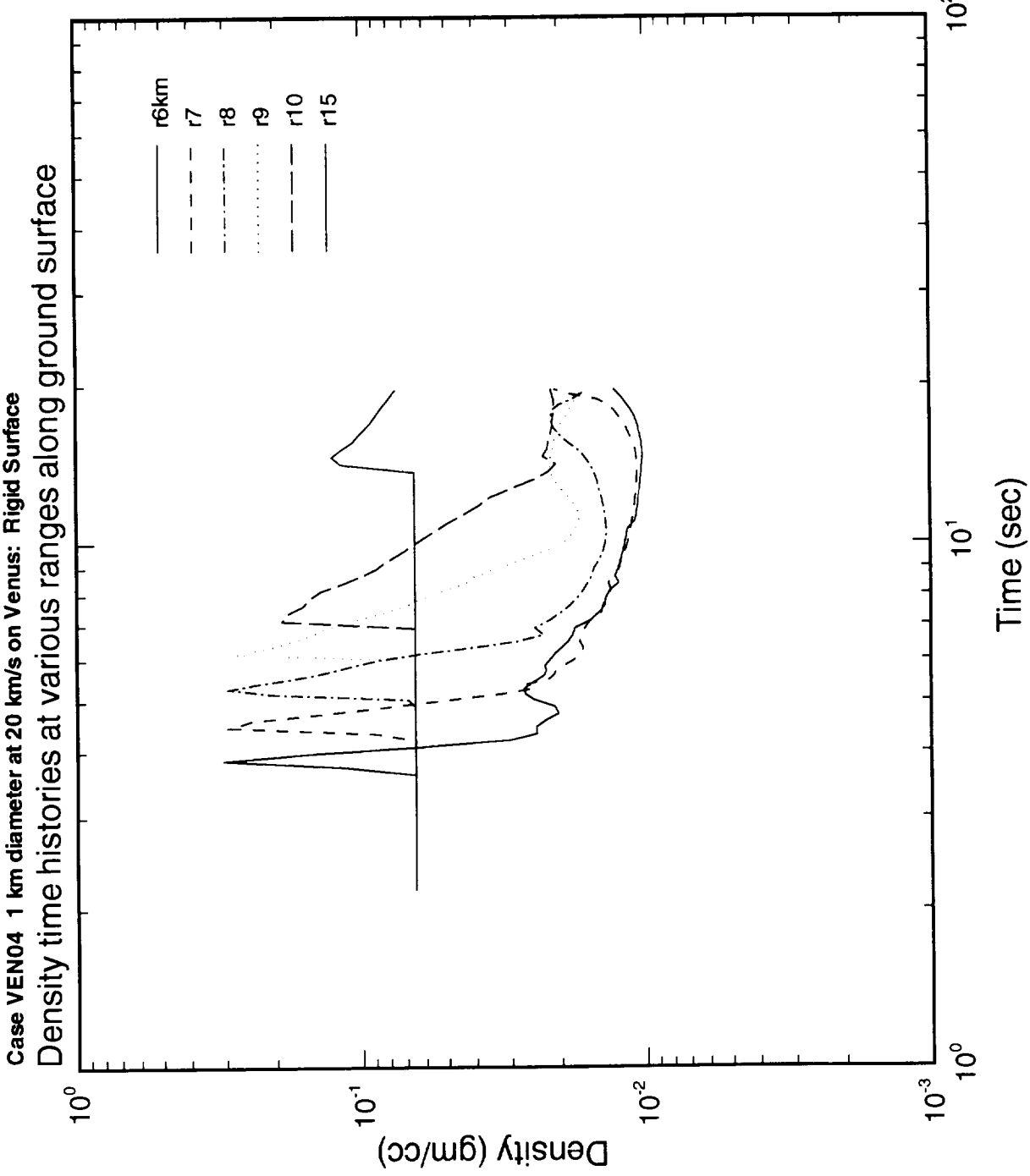
Case VEN04 1 km diameter at 20 km/s on Venus: Rigid Surface
Density time histories at various ranges along ground surface
r6km
r7
r8
r9
r10
r15
Density (gm/cc)
Time (sec)
10^0
10^-1
10^-2
10^-3
10^1
10^2

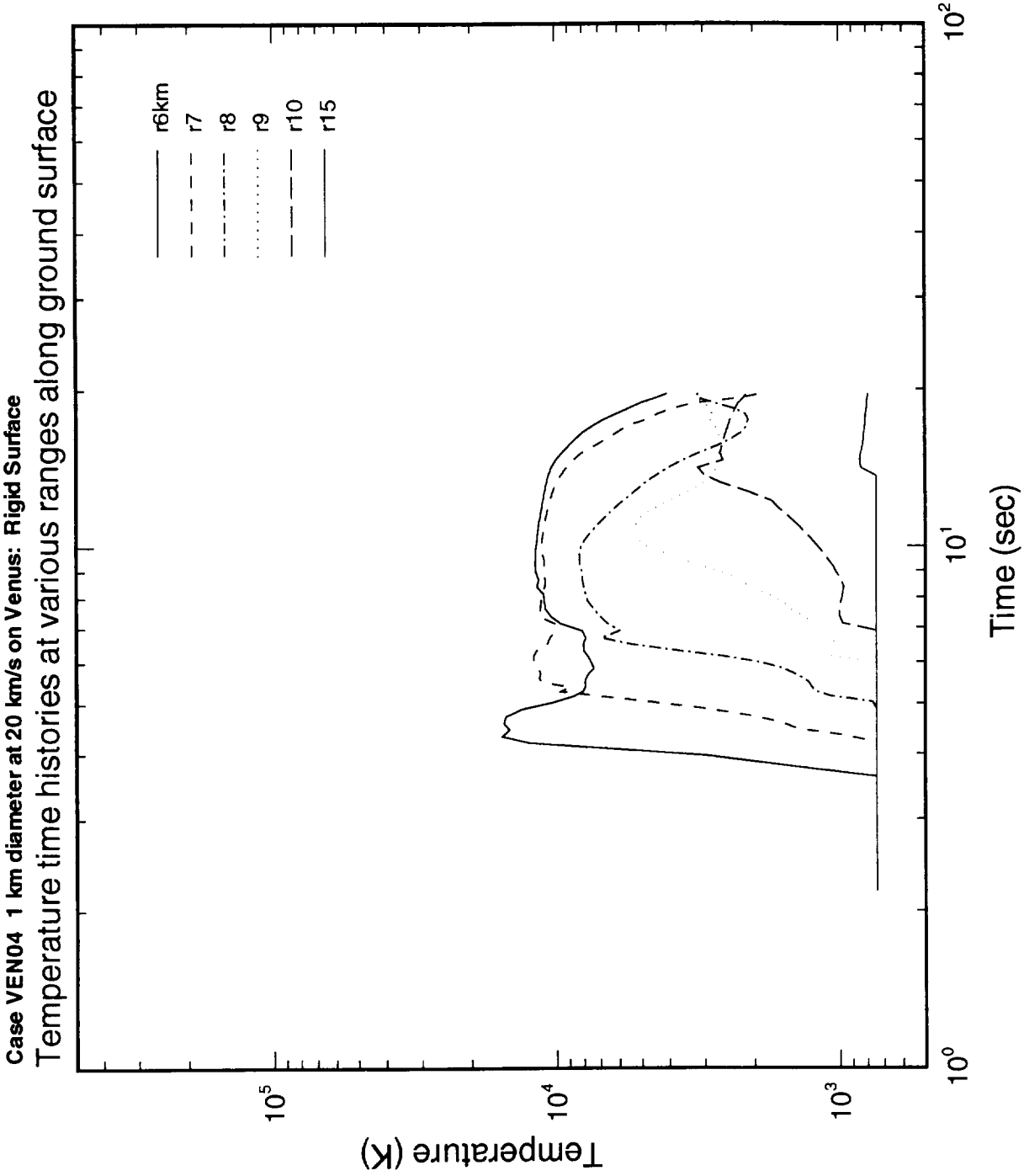
Case VEN04 1 km diameter at 20 km/s on Venus: Rigid Surface
Temperature time histories at various ranges along ground surface
r6km
r7
r8
r9
r10
r15
Temperature (K)
Time (sec)
10^3
10^4
10^5
10^0
10^1
10^2

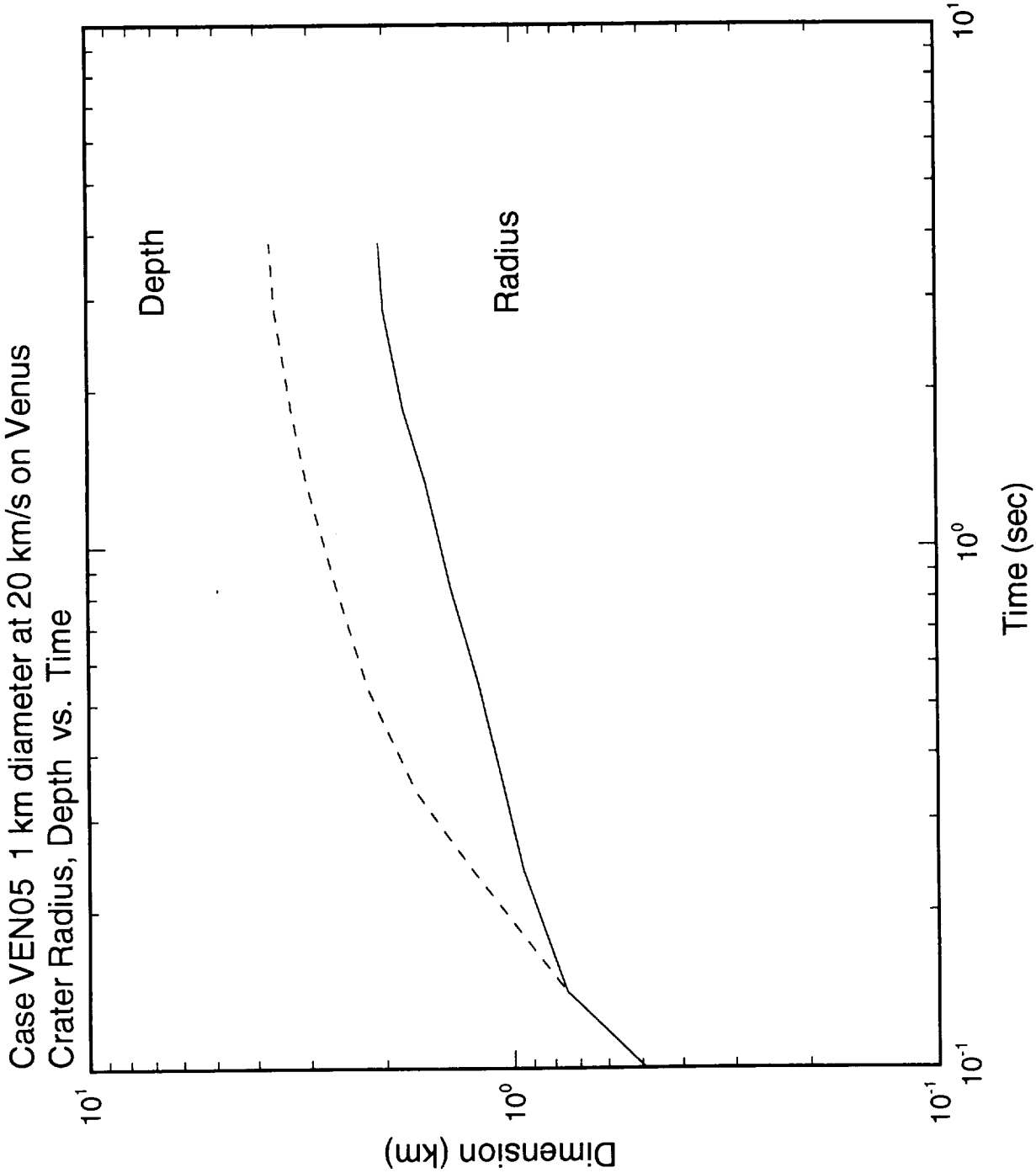
Case VEN05 1 km diameter at 20 km/s on Venus
Crater Radius, Depth vs. Time
Depth
Radius
Dimension (km)
Time (sec)
10^{1}
10^{0}
10^{-1}
10^{-1}
10^{0}
10^{1}

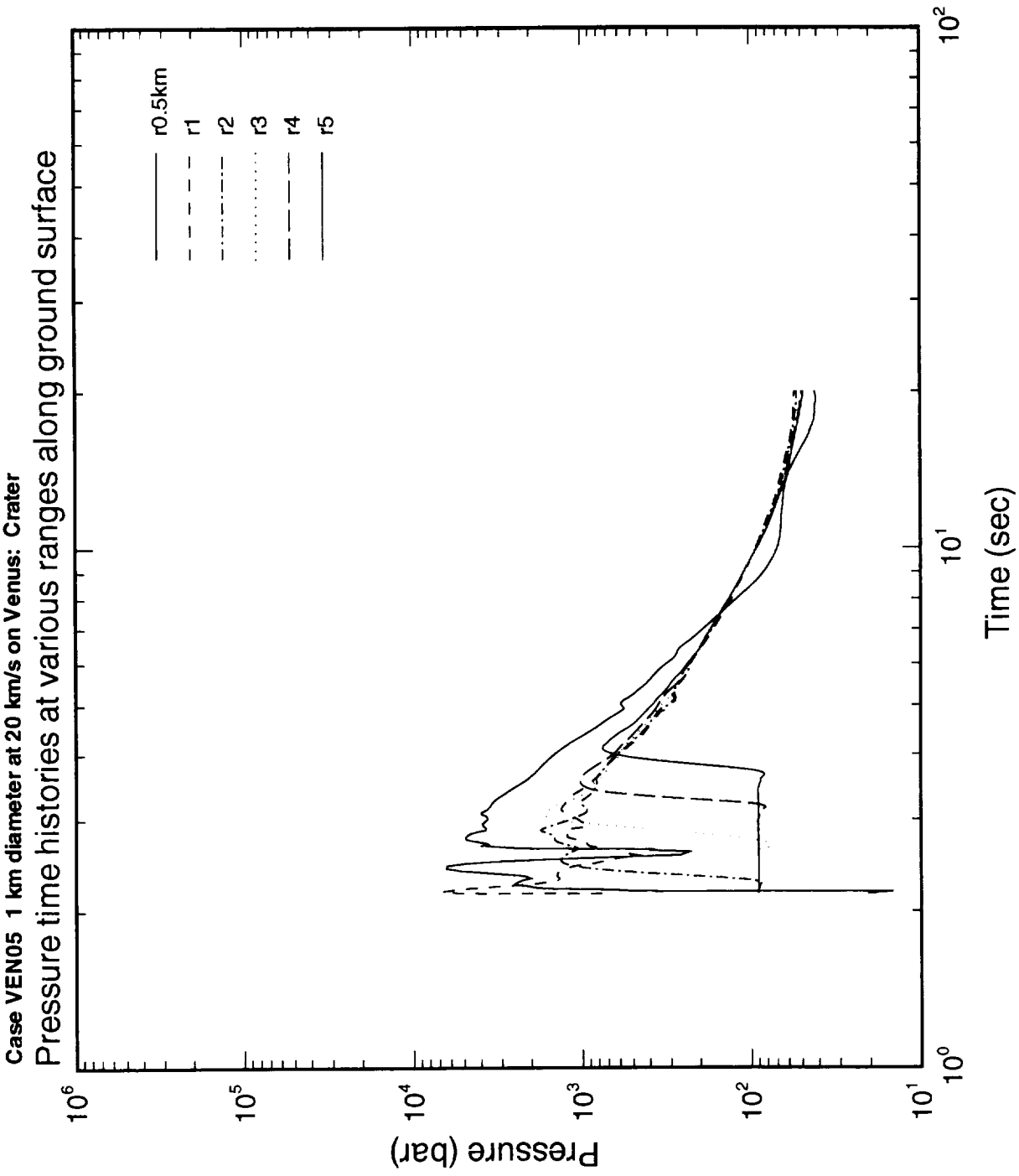
Case VEN05 1 km diameter at 20 km/s on Venus: Crater
Pressure time histories at various ranges along ground surface
r0.5km
r1
r2
r3
r4
r5
Pressure (bar)
Time (sec)
10^6
10^5
10^4
10^3
10^2
10^1
10^0
10^1
10^2

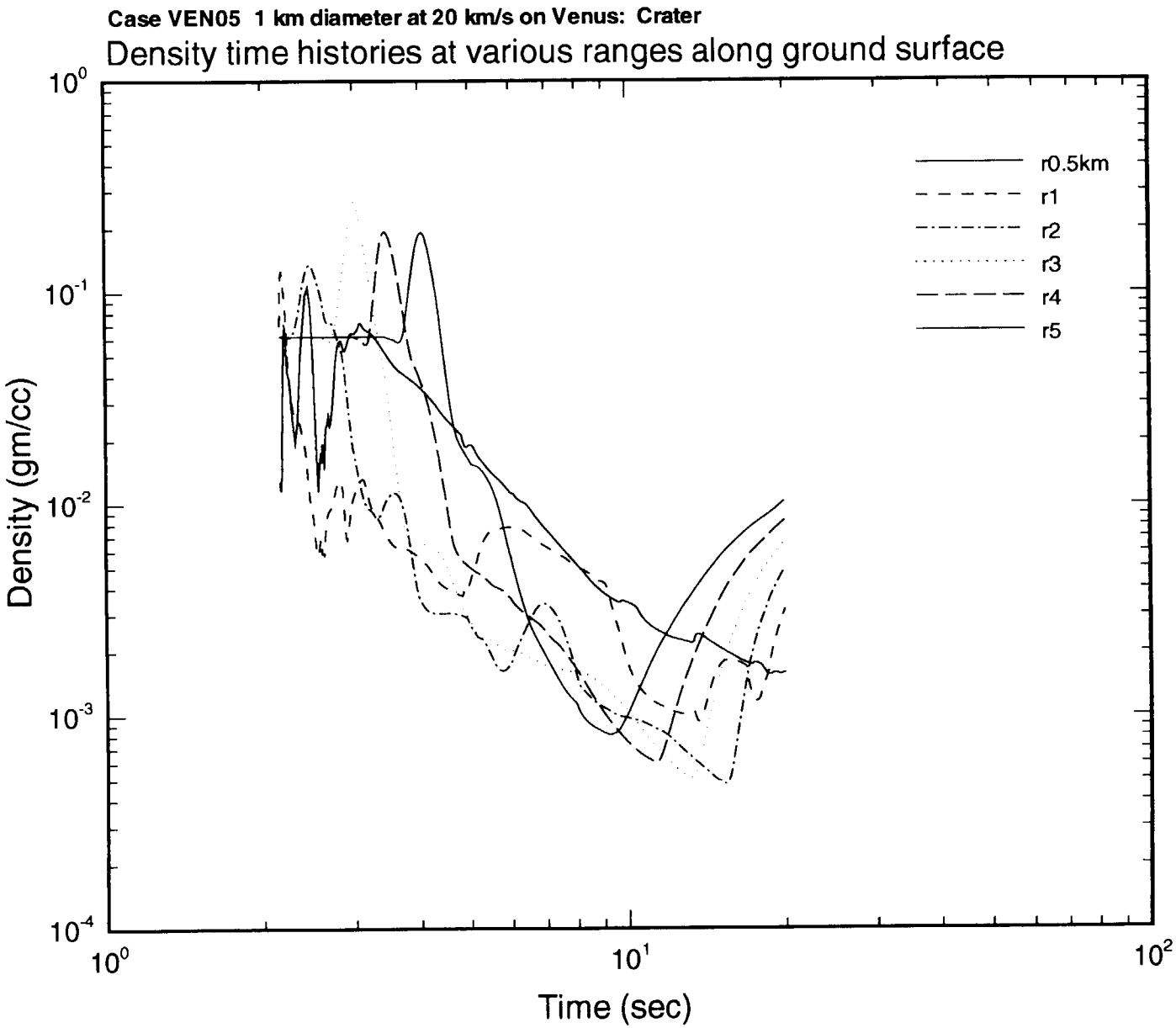
Case VEN05 1 km diameter at 20 km/s on Venus: Crater
Density time histories at various ranges along ground surface
Density (gm/cc)
Time (sec)
r0.5km
r1
r2
r3
r4
r5

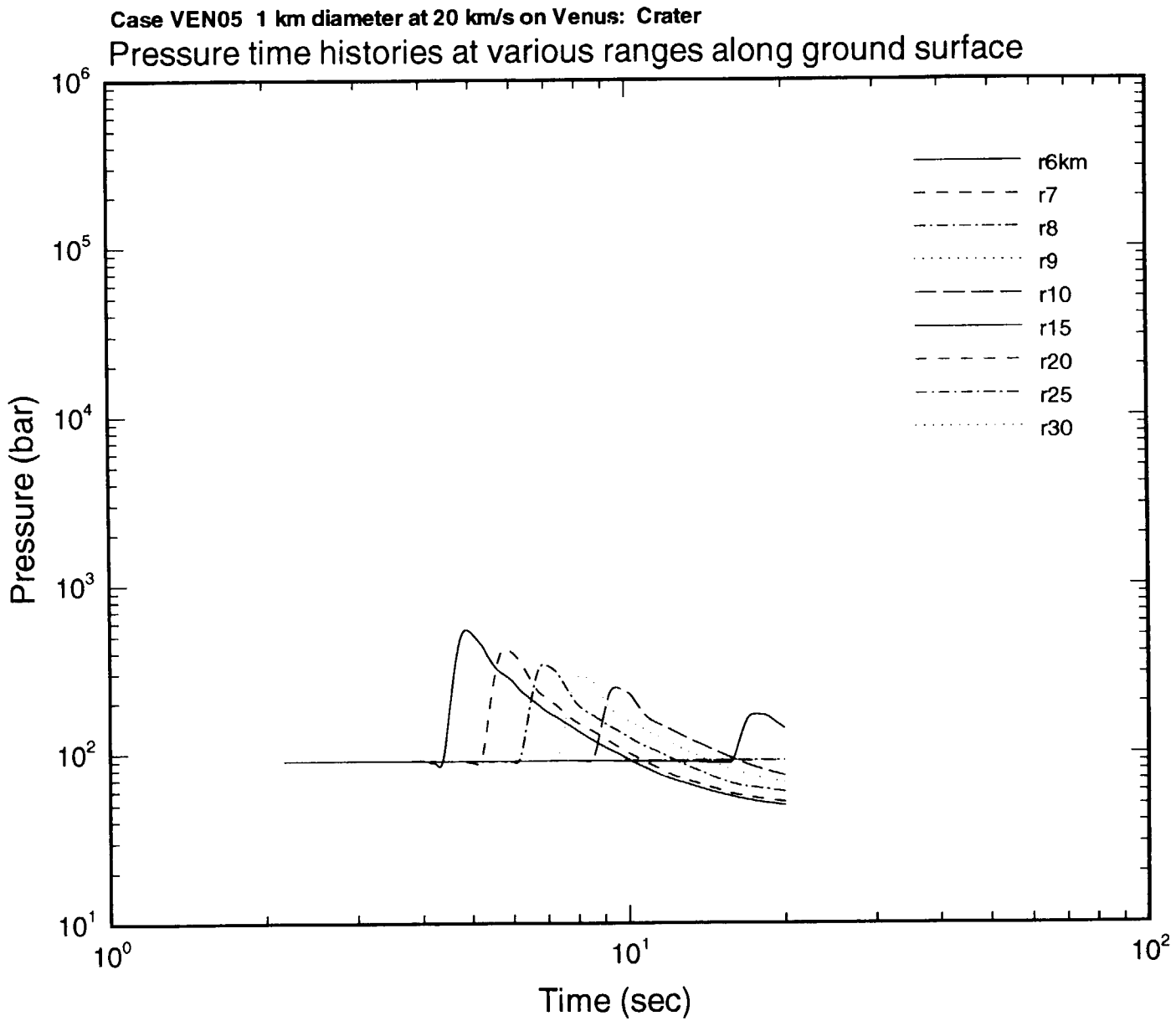
Case VEN05 1 km diameter at 20 km/s on Venus: Crater
Pressure time histories at various ranges along ground surface
Pressure (bar)
Time (sec)
10^6
10^5
10^4
10^3
10^2
10^1
10^0
10^1
10^2
r6km
r7
r8
r9
r10
r15
r20
r25
r30

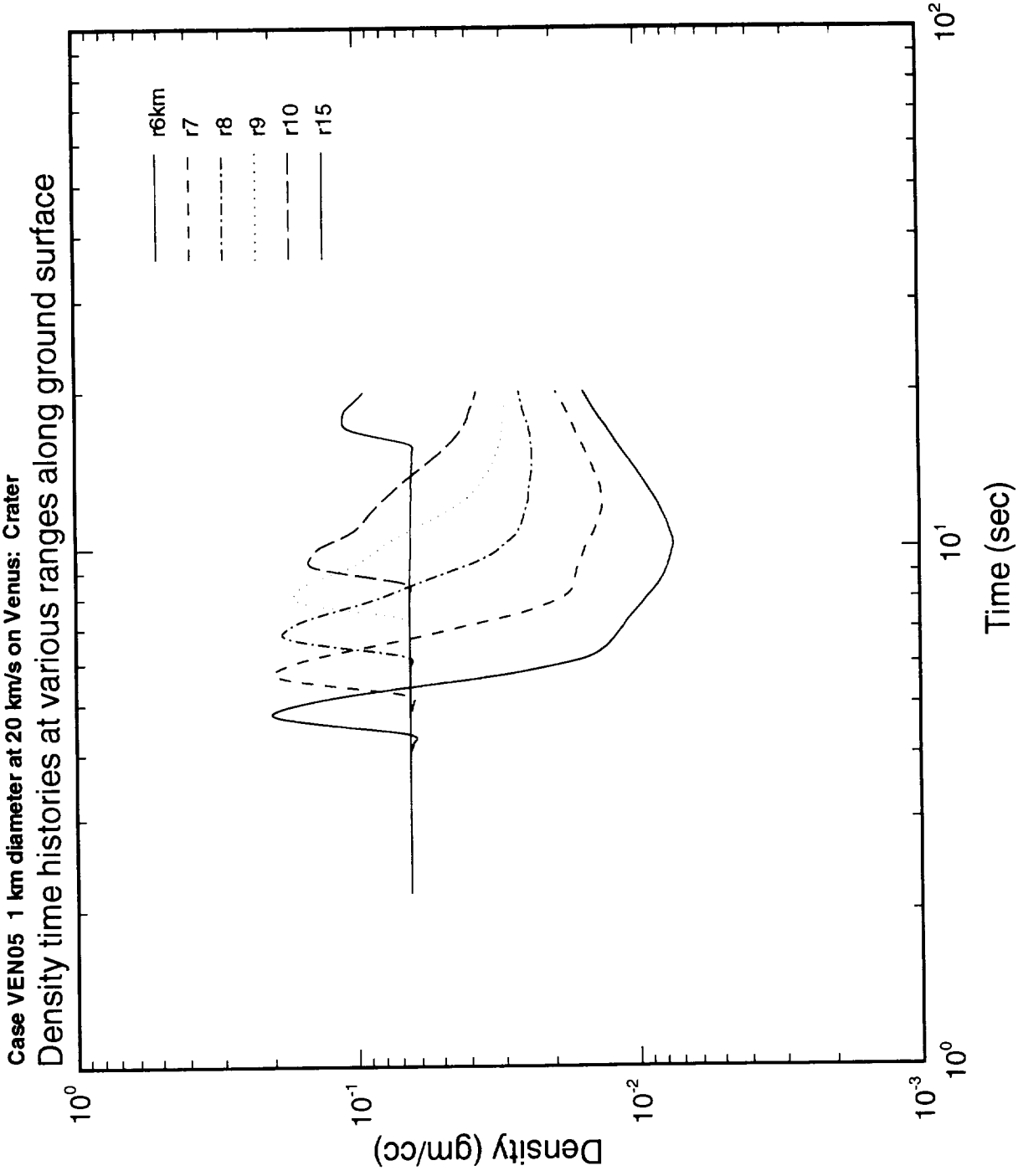
Case VEN05 1 km diameter at 20 km/s on Venus: Crater
Density time histories at various ranges along ground surface
r6km
r7
r8
r9
r10
r15
Density (gm/cc)
Time (sec)
10^0
10^-1
10^-2
10^-3
10^1
10^2

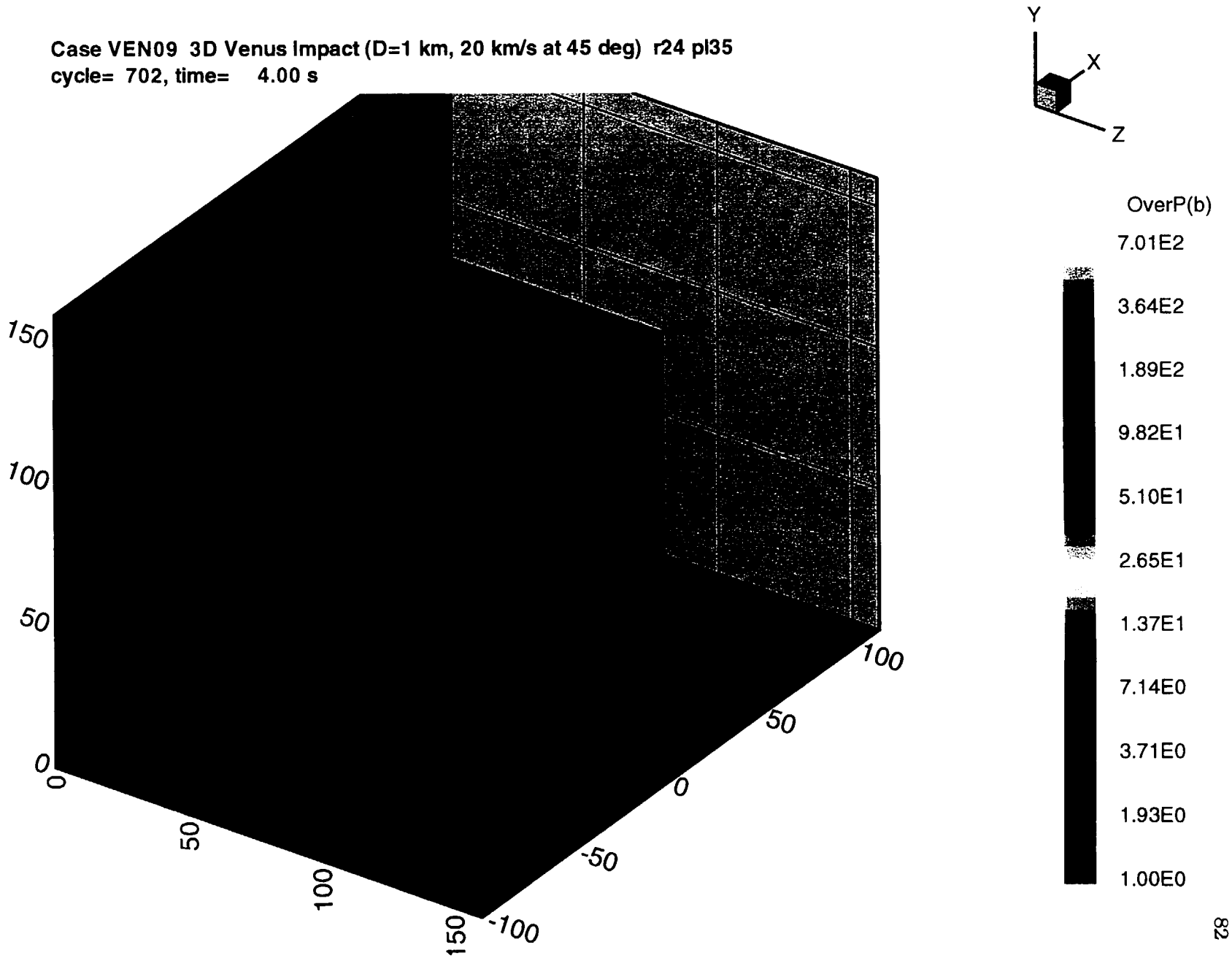
Case VEN09 3D Venus Impact (D=1 km, 20 km/s at 45 deg) r24 pl35
cycle= 702, time= 4.00 s
Y
X
Z
OverP(b)
7.01E2
3.64E2
1.89E2
9.82E1
5.10E1
2.65E1
1.37E1
7.14E0
3.71E0
1.93E0
1.00E0
150
100
50
0
0
50
100
150
-100
-50
0
50
100

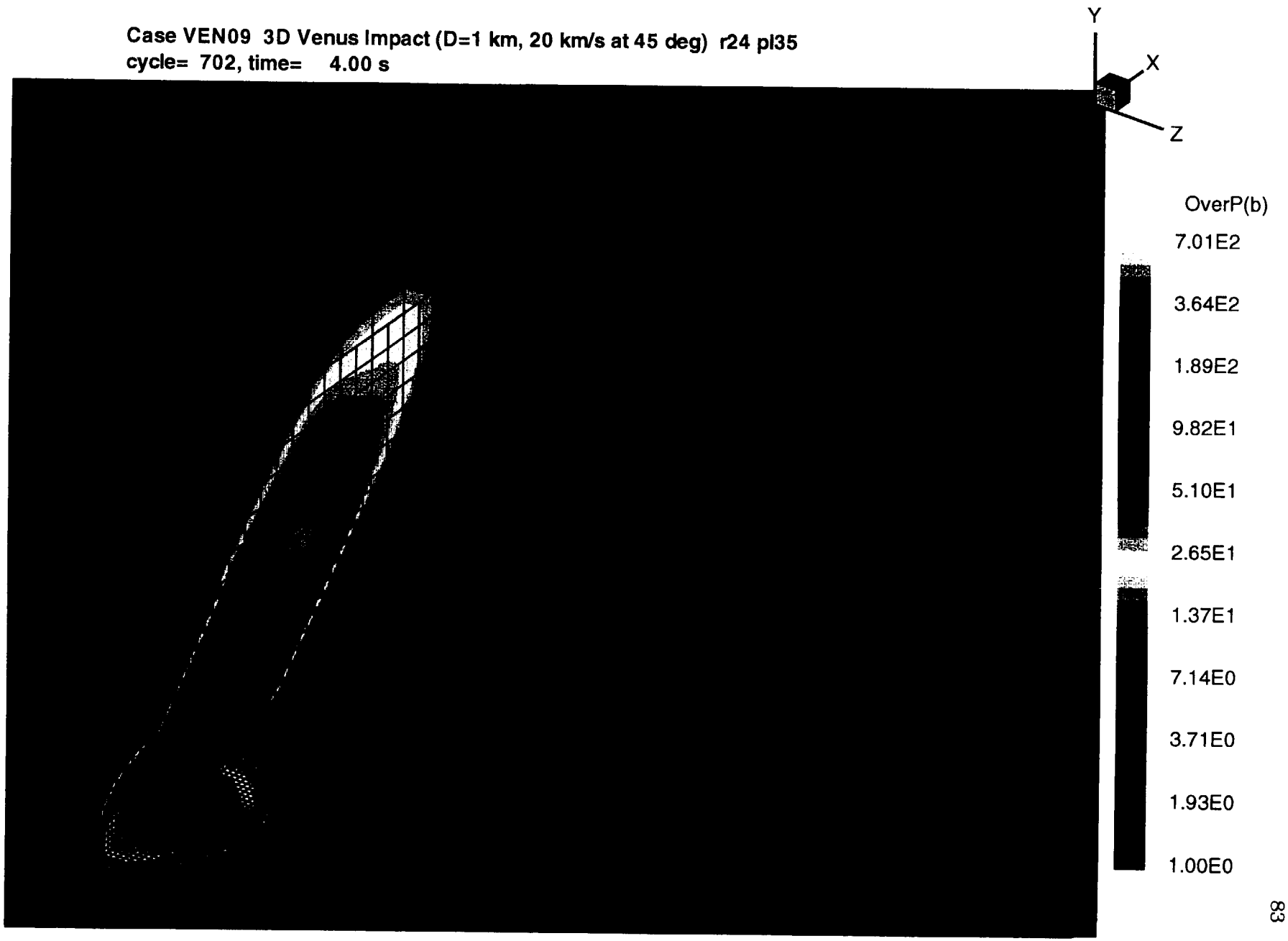
Case VEN09 3D Venus Impact (D=1 km, 20 km/s at 45 deg) r24 pl35
cycle= 702, time= 4.00 s
Y
X
Z
OverP(b)
7.01E2
3.64E2
1.89E2
9.82E1
5.10E1
2.65E1
1.37E1
7.14E0
3.71E0
1.93E0
1.00E0

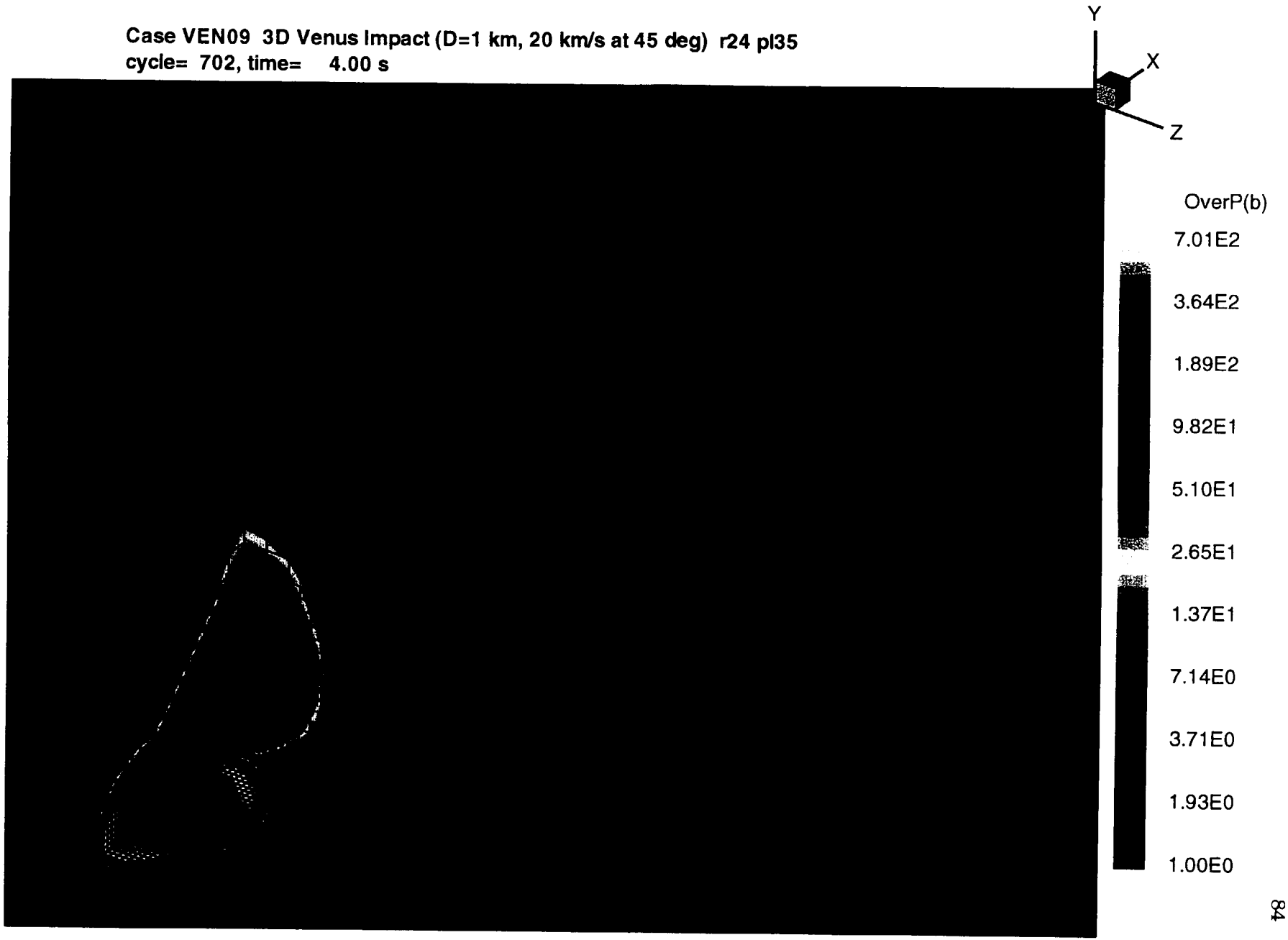
Case VEN09 3D Venus Impact (D=1 km, 20 km/s at 45 deg) r24 pl35
cycle= 702, time= 4.00 s
Y
X
Z
OverP(b)
7.01E2
3.64E2
1.89E2
9.82E1
5.10E1
2.65E1
1.37E1
7.14E0
3.71E0
1.93E0
1.00E0

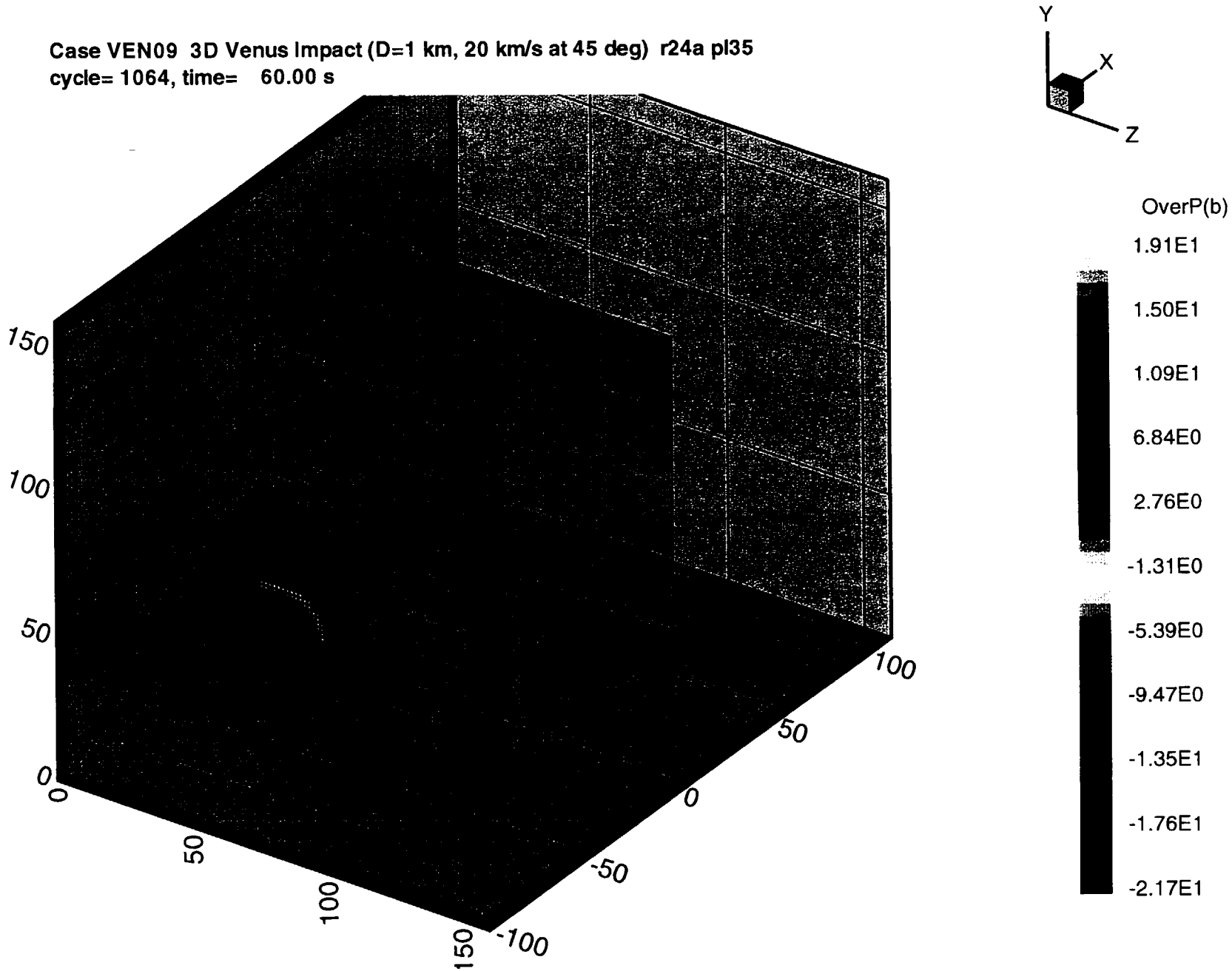
Case VEN09 3D Venus Impact (D=1 km, 20 km/s at 45 deg) r24a pl35
cycle= 1064, time= 60.00 s
Y
X
Z
OverP(b)
1.91E1
1.50E1
1.09E1
6.84E0
2.76E0
-1.31E0
-5.39E0
-9.47E0
-1.35E1
-1.76E1
-2.17E1
150
100
50
0
0
50
100
150
-100
-50
0
50
100

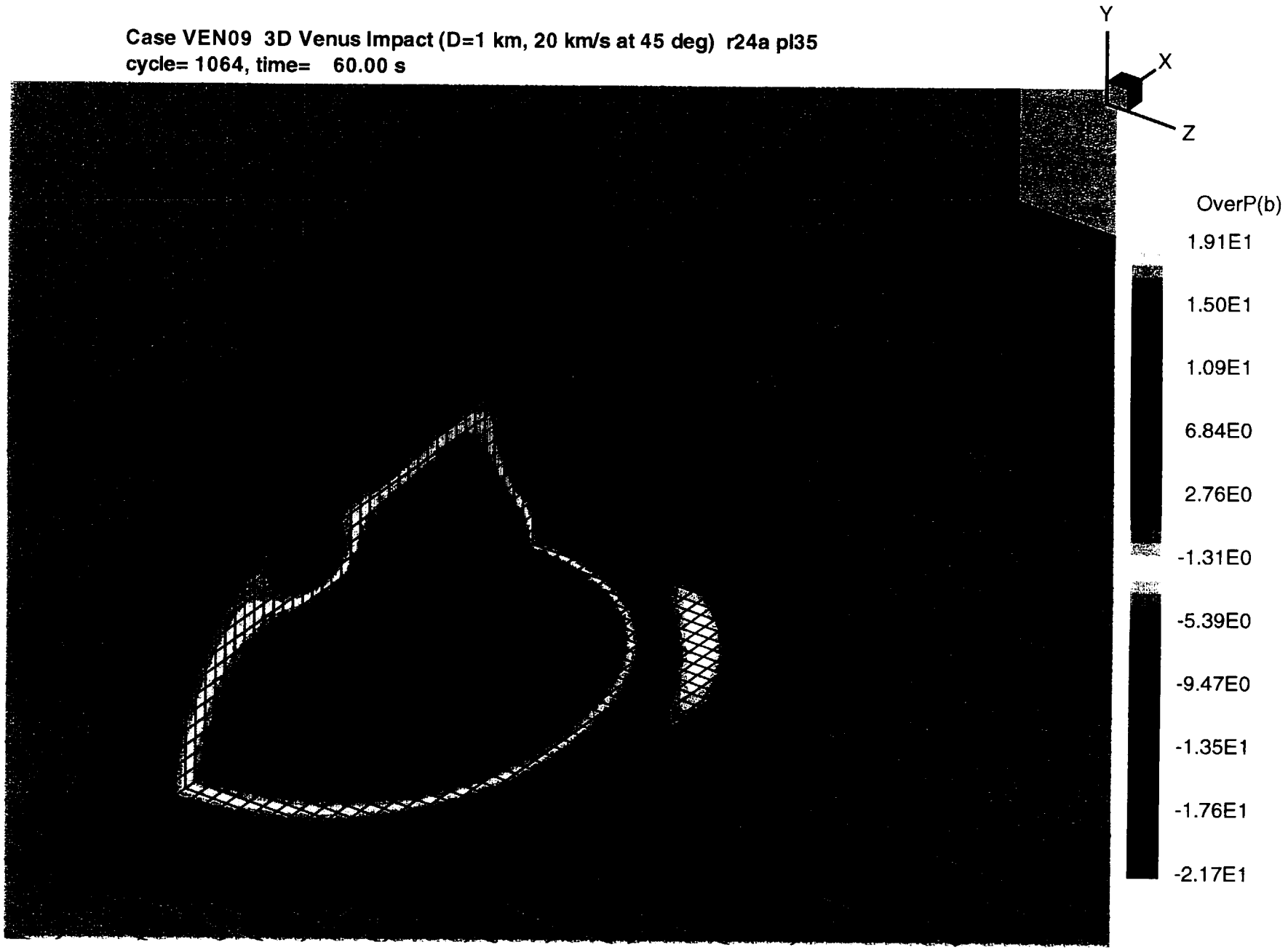
Case VEN09 3D Venus Impact (D=1 km, 20 km/s at 45 deg) r24a pl35
cycle= 1064, time= 60.00 s
Y
X
Z
OverP(b)
1.91E1
1.50E1
1.09E1
6.84E0
2.76E0
-1.31E0
-5.39E0
-9.47E0
-1.35E1
-1.76E1
-2.17E1

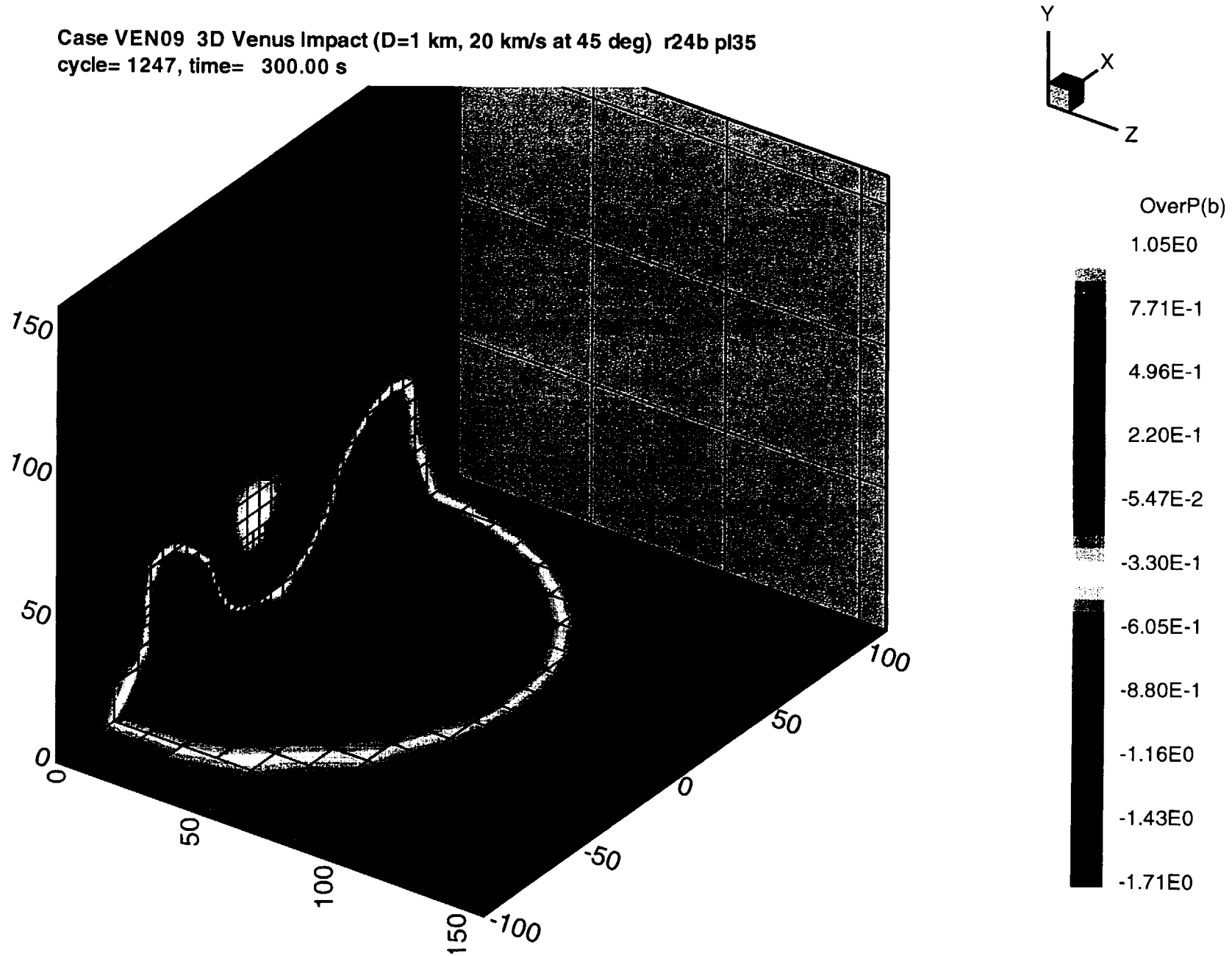
Case VEN09 3D Venus Impact (D=1 km, 20 km/s at 45 deg) r24b pl35
cycle= 1247, time= 300.00 s
Y
X
Z
OverP(b)
1.05E0
7.71E-1
4.96E-1
2.20E-1
-5.47E-2
-3.30E-1
-6.05E-1
-8.80E-1
-1.16E0
-1.43E0
-1.71E0
150
100
50
0
0
50
100
150
-100
-50
0
50
100

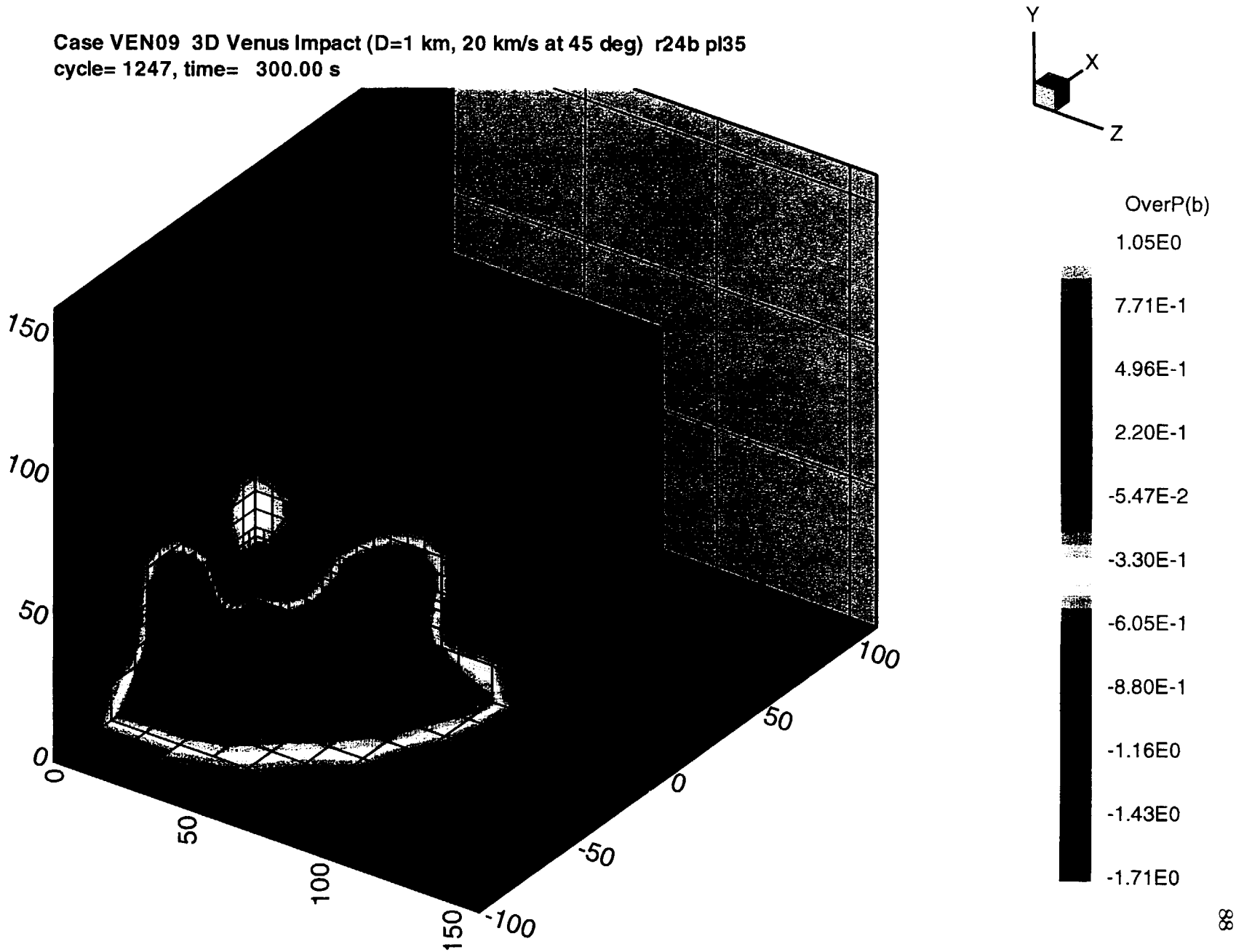
Case VEN09 3D Venus Impact (D=1 km, 20 km/s at 45 deg) r24b pl35
cycle= 1247, time= 300.00 s
Y
X
Z
OverP(b)
1.05E0
7.71E-1
4.96E-1
2.20E-1
-5.47E-2
-3.30E-1
-6.05E-1
-8.80E-1
-1.16E0
-1.43E0
-1.71E0
150
100
50
0
0
50
100
150
-100
-50
0
50
100

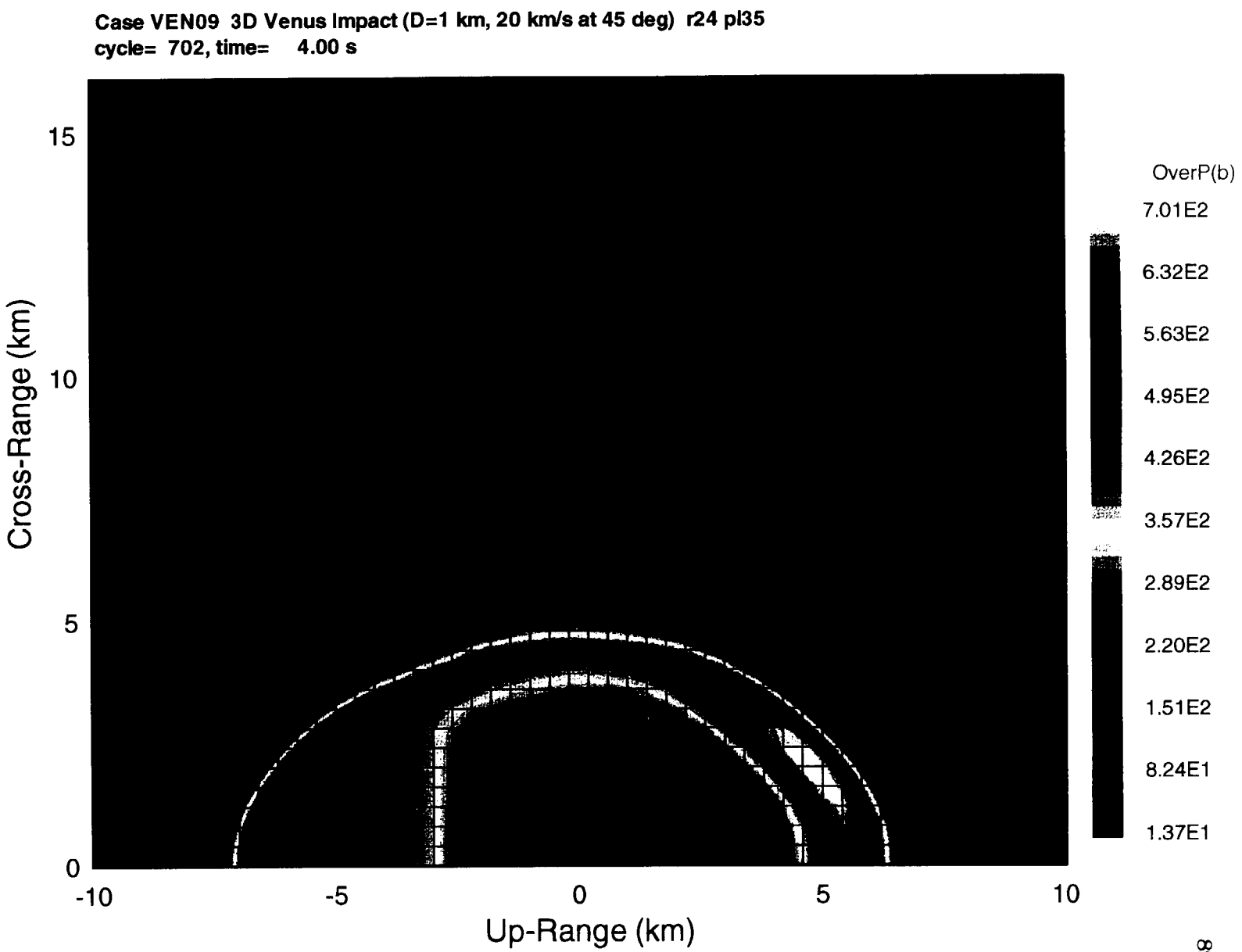
Case VEN09 3D Venus Impact (D=1 km, 20 km/s at 45 deg) r24 pl35
cycle= 702, time= 4.00 s
Cross-Range (km)
15
10
5
0
-10
-5
0
5
10
Up-Range (km)
OverP(b)
7.01E2
6.32E2
5.63E2
4.95E2
4.26E2
3.57E2
2.89E2
2.20E2
1.51E2
8.24E1
1.37E1

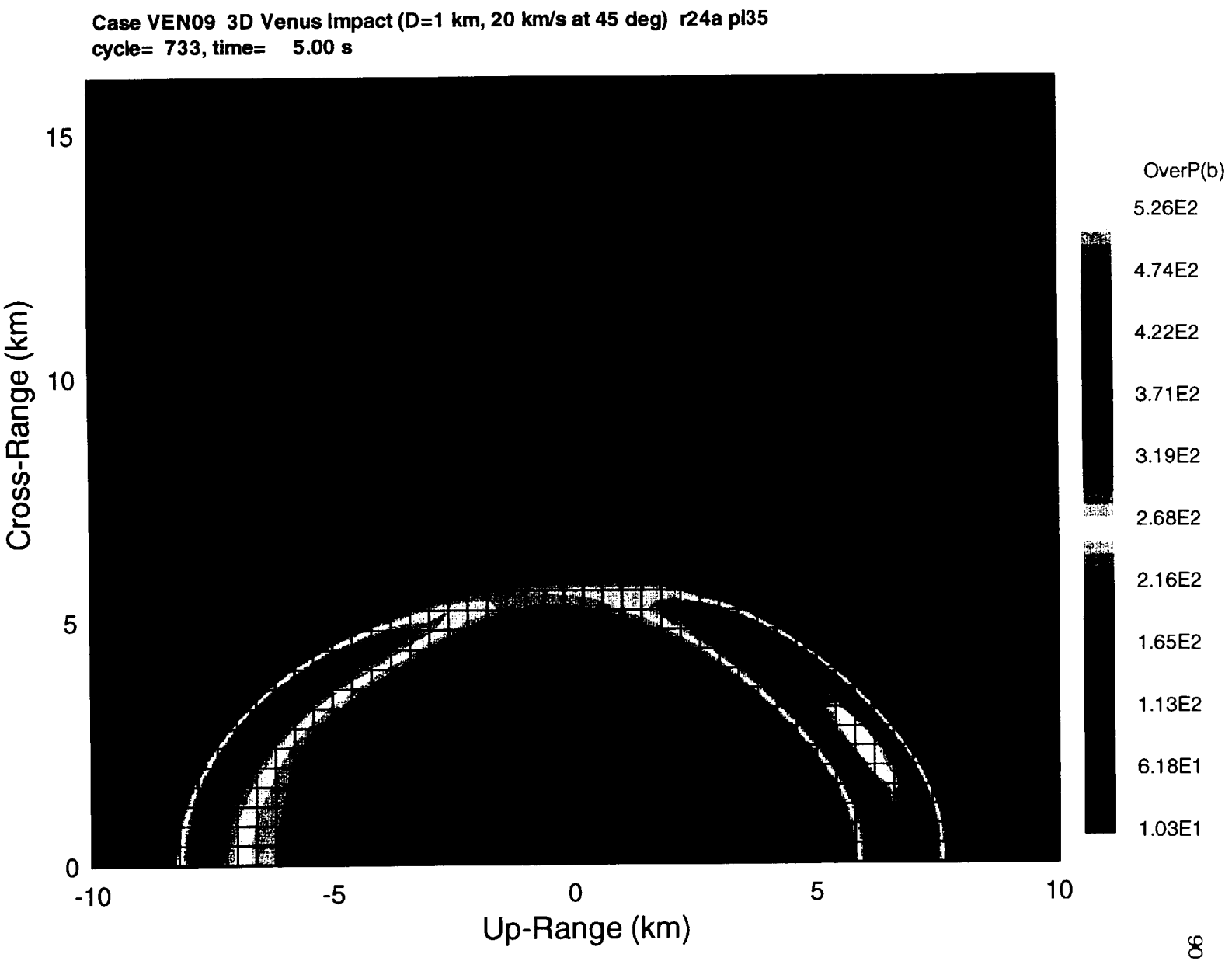
Case VEN09 3D Venus Impact (D=1 km, 20 km/s at 45 deg) r24a pl35
cycle= 733, time= 5.00 s
Cross-Range (km)
15
10
5
0
-10
-5
0
5
10
Up-Range (km)
OverP(b)
5.26E2
4.74E2
4.22E2
3.71E2
3.19E2
2.68E2
2.16E2
1.65E2
1.13E2
6.18E1
1.03E1

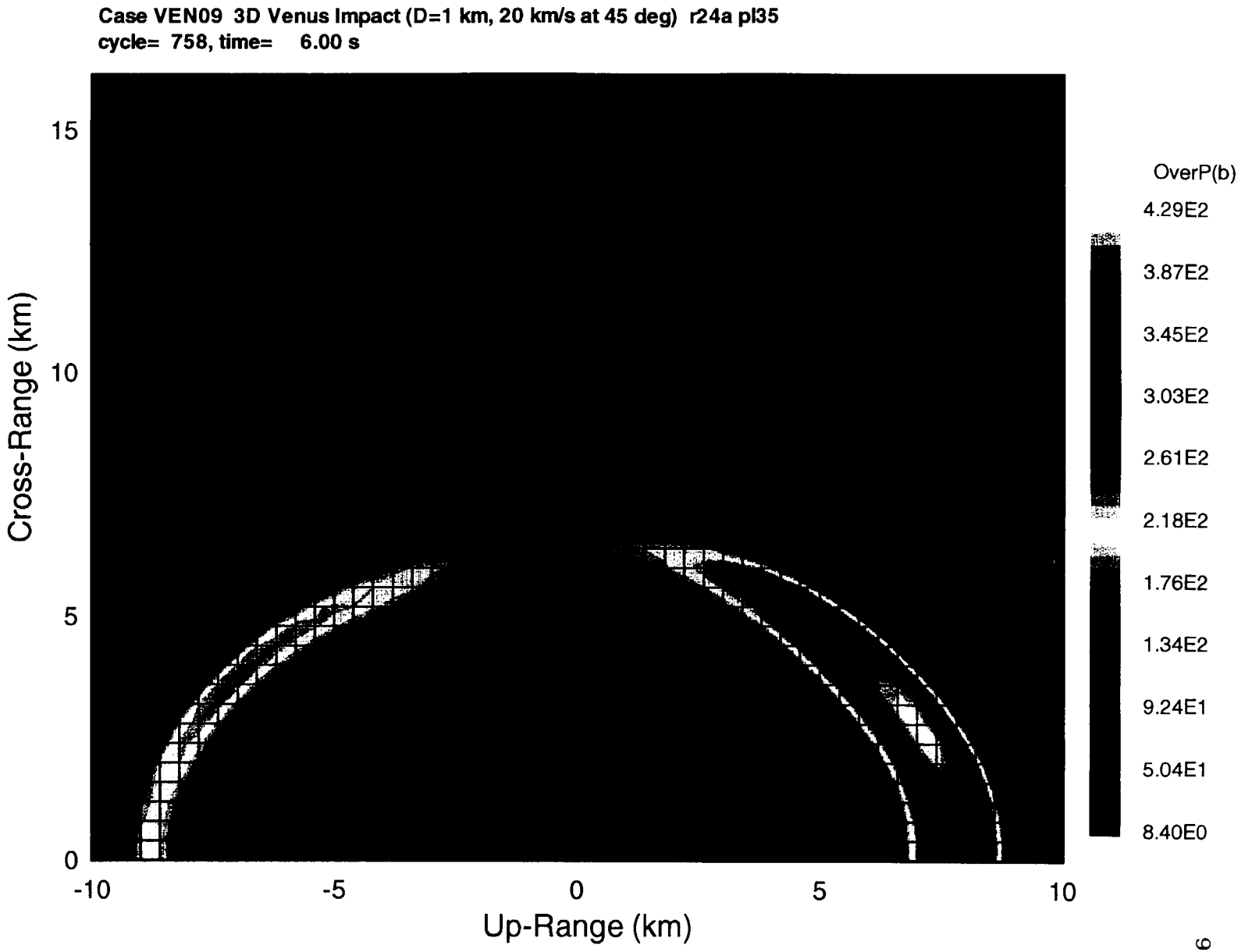
Case VEN09 3D Venus Impact (D=1 km, 20 km/s at 45 deg) r24a pl35
cycle= 758, time= 6.00 s
Cross-Range (km)
15
10
5
0
-10
-5
0
5
10
Up-Range (km)
OverP(b)
4.29E2
3.87E2
3.45E2
3.03E2
2.61E2
2.18E2
1.76E2
1.34E2
9.24E1
5.04E1
8.40E0

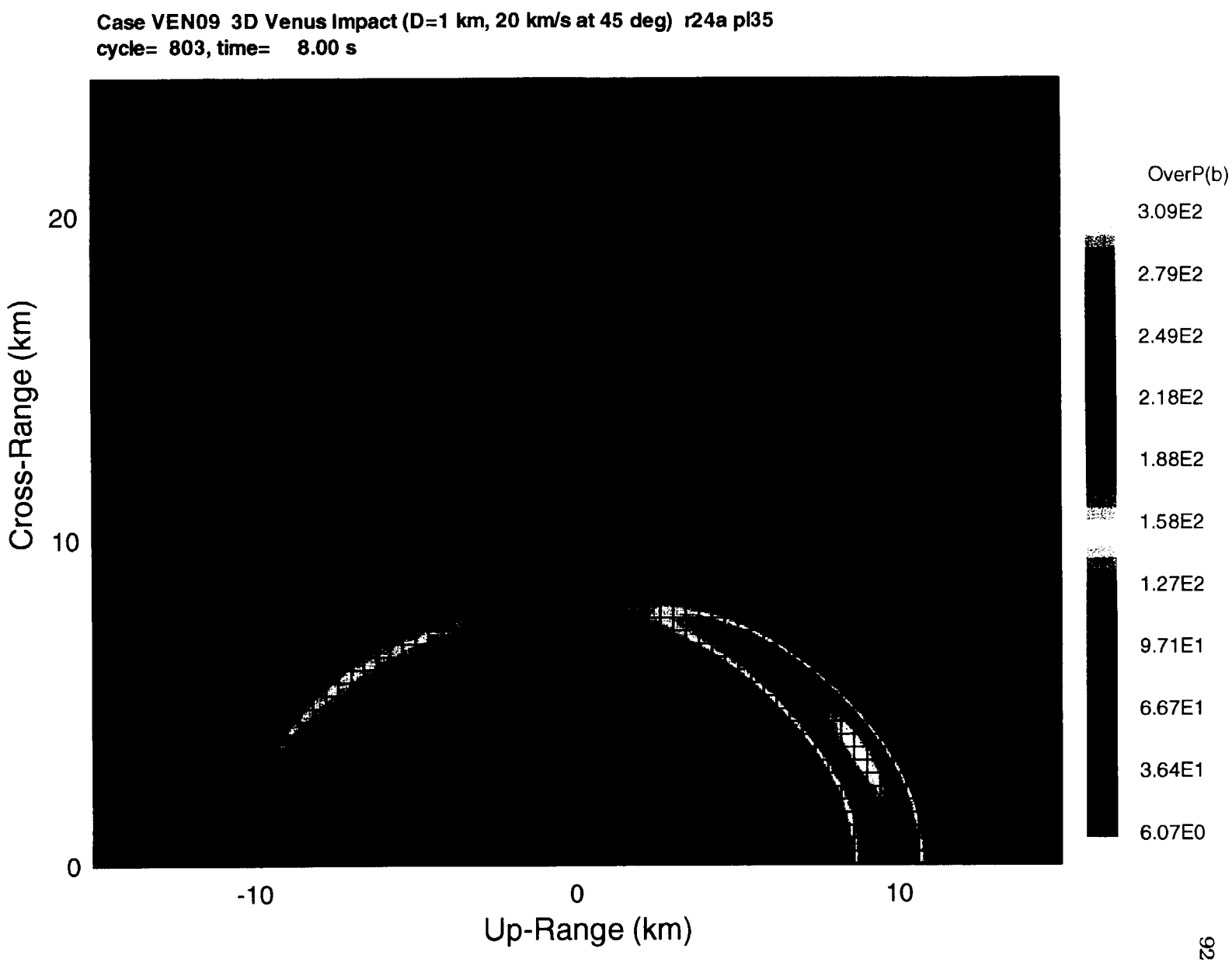
Case VEN09 3D Venus Impact (D=1 km, 20 km/s at 45 deg) r24a pl35
cycle= 803, time= 8.00 s
Cross-Range (km)
20
10
0
-10
0
10
Up-Range (km)
OverP(b)
3.09E2
2.79E2
2.49E2
2.18E2
1.88E2
1.58E2
1.27E2
9.71E1
6.67E1
3.64E1
6.07E0

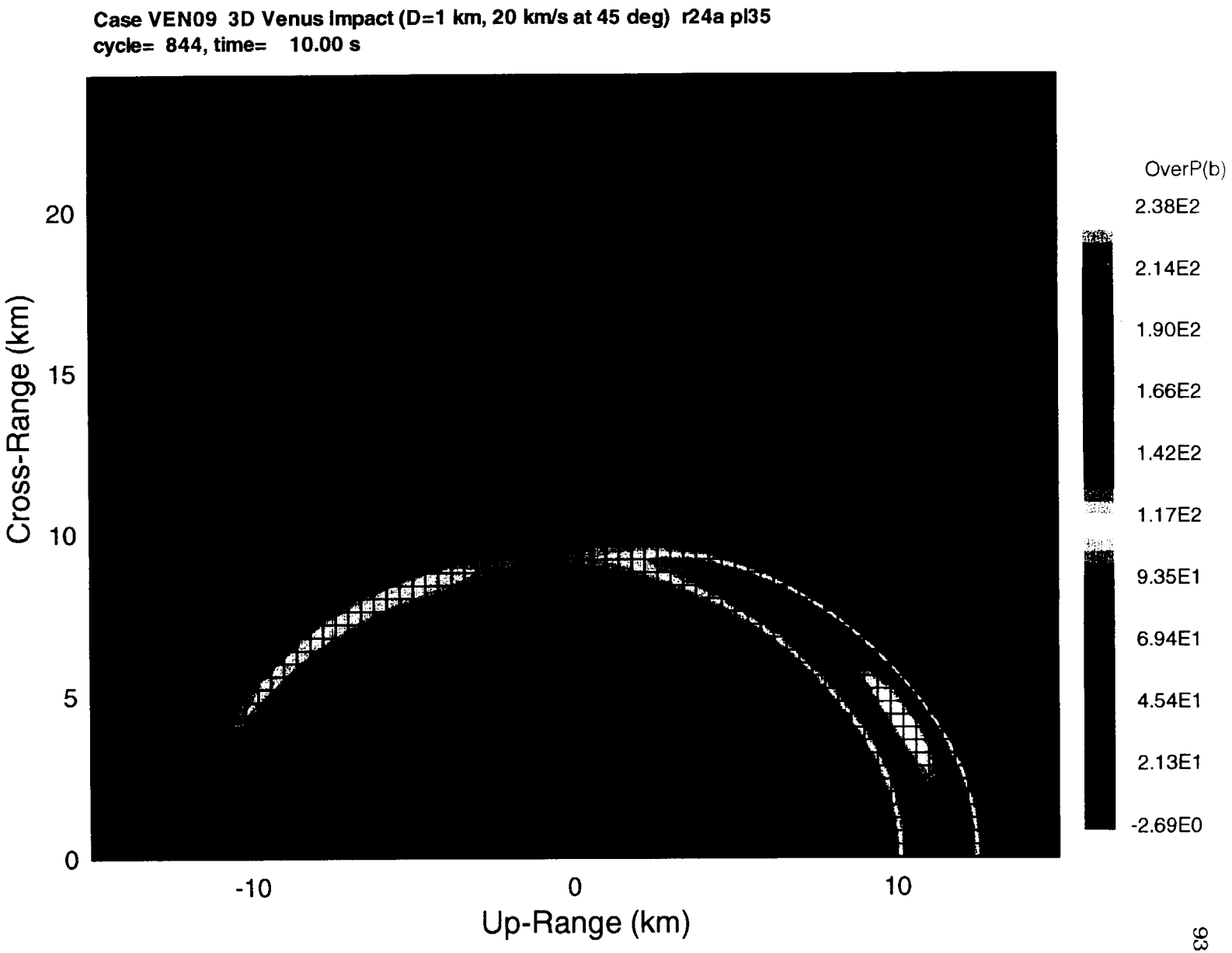
Case VEN09 3D Venus Impact (D=1 km, 20 km/s at 45 deg) r24a pl35
cycle= 844, time= 10.00 s
Cross-Range (km)
0
5
10
15
20
-10
0
10
Up-Range (km)
OverP(b)
2.38E2
2.14E2
1.90E2
1.66E2
1.42E2
1.17E2
9.35E1
6.94E1
4.54E1
2.13E1
-2.69E0

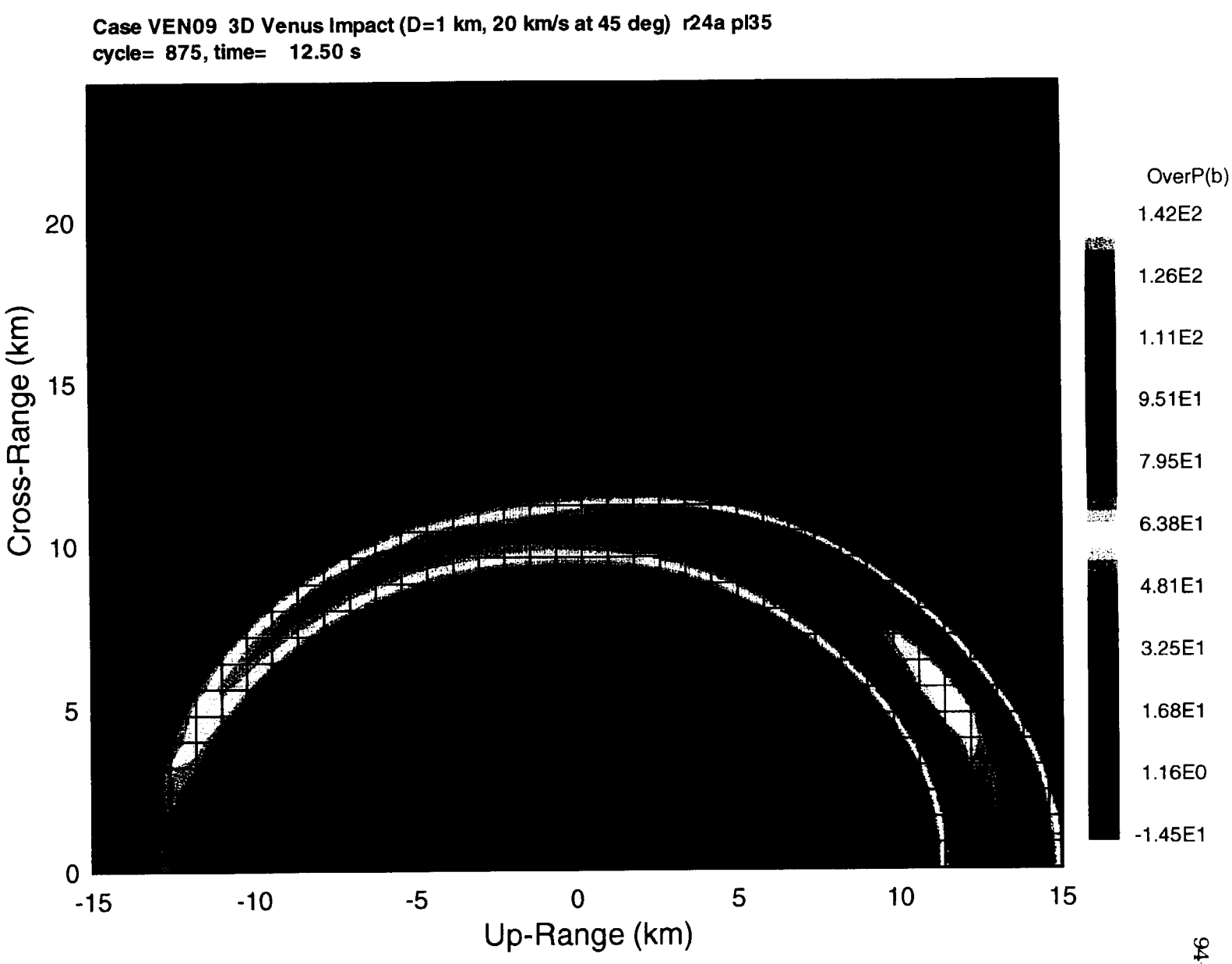
Case VEN09 3D Venus Impact (D=1 km, 20 km/s at 45 deg) r24a pl35
cycle= 875, time= 12.50 s
Cross-Range (km)
20
15
10
5
0
-15
-10
-5
0
5
10
15
Up-Range (km)
OverP(b)
1.42E2
1.26E2
1.11E2
9.51E1
7.95E1
6.38E1
4.81E1
3.25E1
1.68E1
1.16E0
-1.45E1

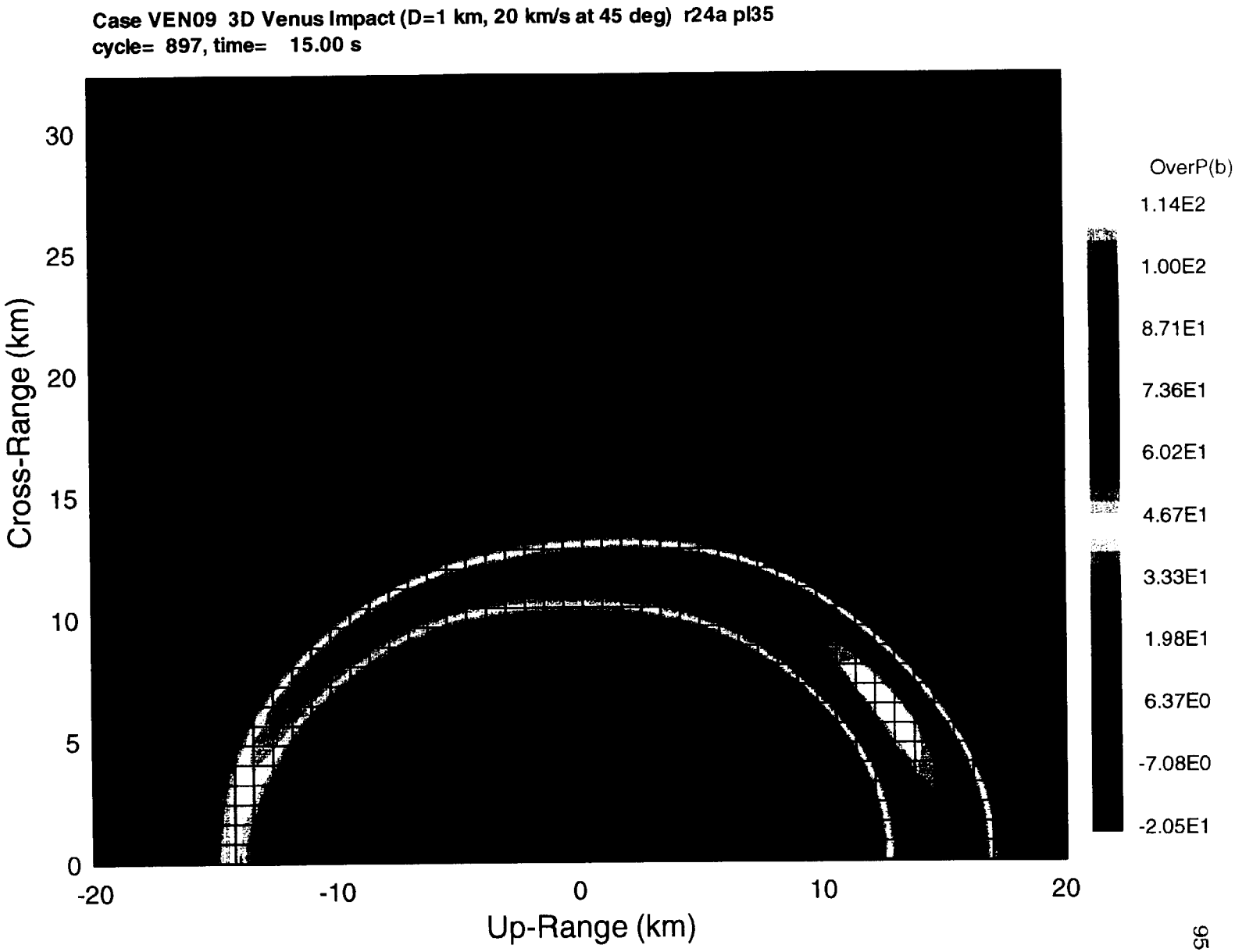
Case VEN09 3D Venus Impact (D=1 km, 20 km/s at 45 deg) r24a pl35
cycle= 897, time= 15.00 s
Cross-Range (km)
30
25
20
15
10
5
0
-20
-10
0
10
20
Up-Range (km)
OverP(b)
1.14E2
1.00E2
8.71E1
7.36E1
6.02E1
4.67E1
3.33E1
1.98E1
6.37E0
-7.08E0
-2.05E1

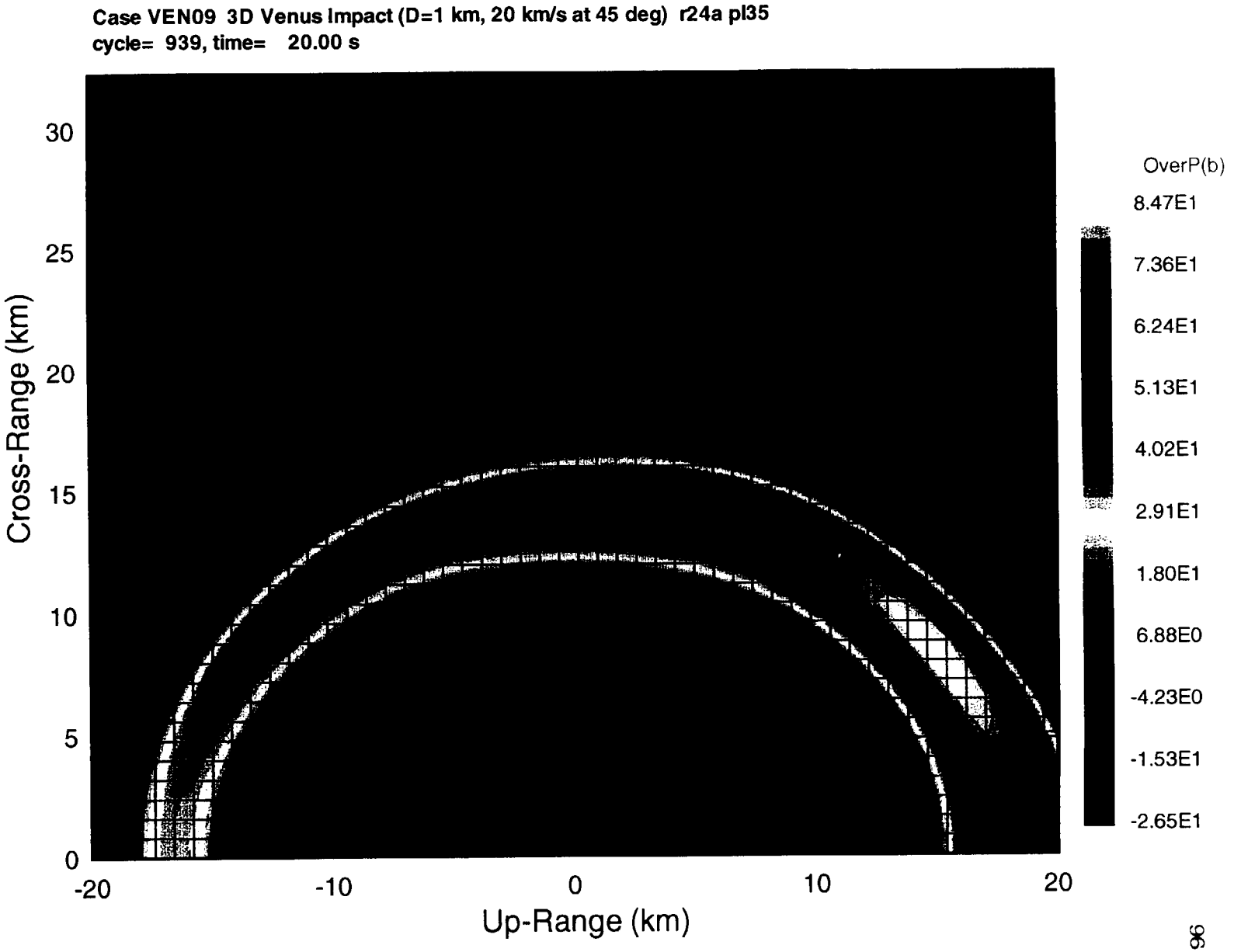
Case VEN09 3D Venus Impact (D=1 km, 20 km/s at 45 deg) r24a pl35
cycle= 939, time= 20.00 s
Cross-Range (km)
30
25
20
15
10
5
0
-20
-10
0
10
20
Up-Range (km)
OverP(b)
8.47E1
7.36E1
6.24E1
5.13E1
4.02E1
2.91E1
1.80E1
6.88E0
-4.23E0
-1.53E1
-2.65E1

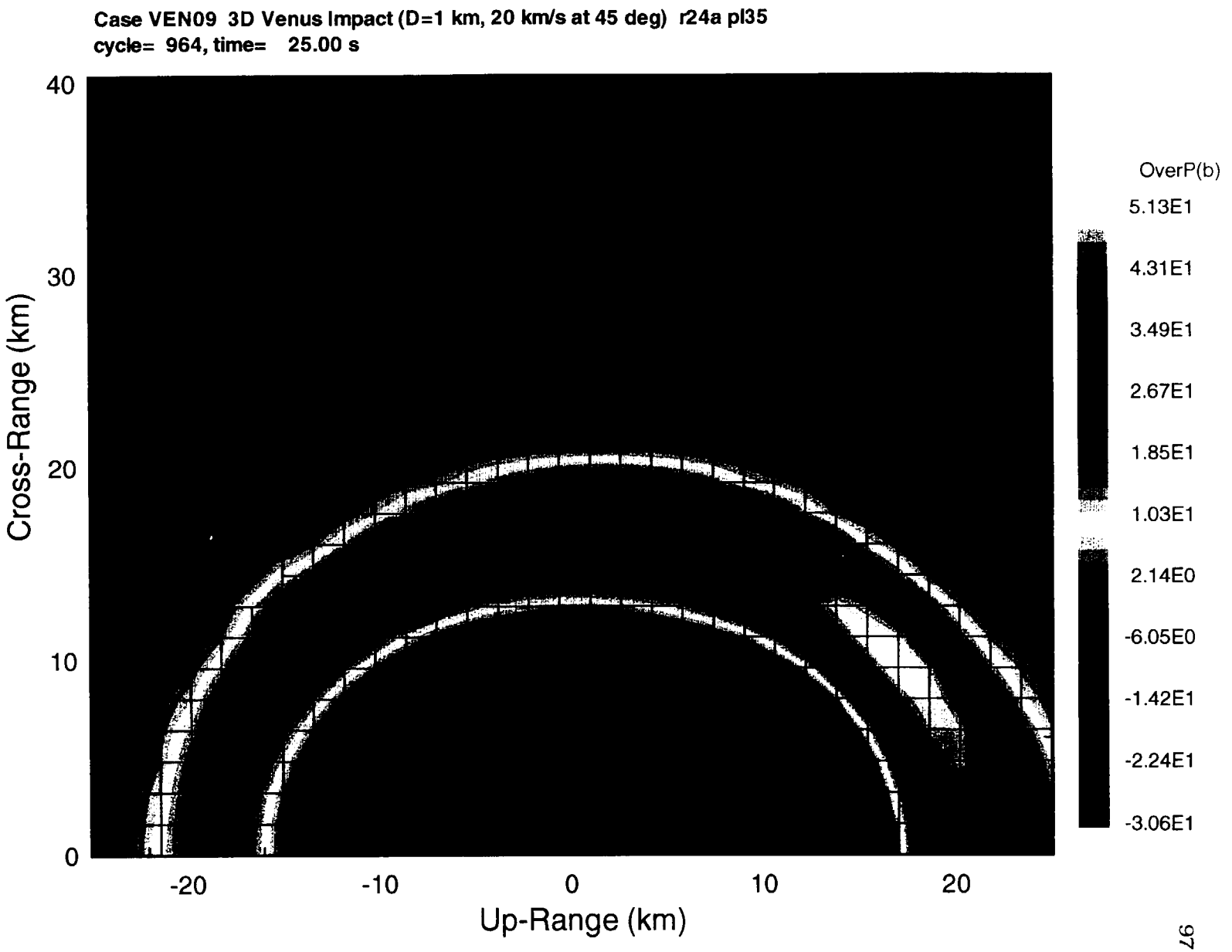
Case VEN09 3D Venus Impact (D=1 km, 20 km/s at 45 deg) r24a pl35
cycle= 964, time= 25.00 s
Cross-Range (km)
40
30
20
10
0
-20
-10
0
10
20
Up-Range (km)
OverP(b)
5.13E1
4.31E1
3.49E1
2.67E1
1.85E1
1.03E1
2.14E0
-6.05E0
-1.42E1
-2.24E1
-3.06E1

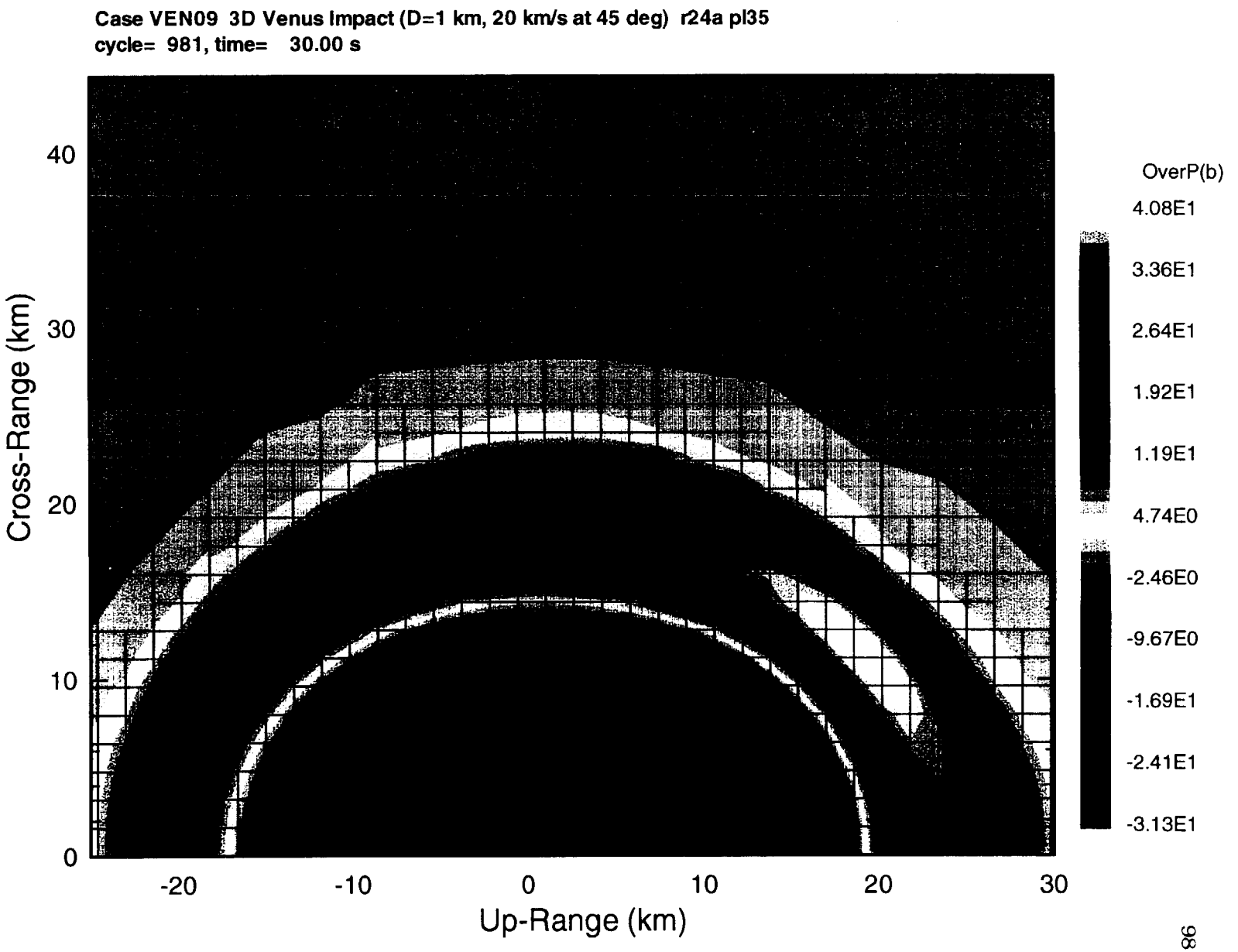
Case VEN09 3D Venus Impact (D=1 km, 20 km/s at 45 deg) r24a pl35
cycle= 981, time= 30.00 s
Cross-Range (km)
40
30
20
10
0
-20
-10
0
10
20
30
Up-Range (km)
OverP(b)
4.08E1
3.36E1
2.64E1
1.92E1
1.19E1
4.74E0
-2.46E0
-9.67E0
-1.69E1
-2.41E1
-3.13E1

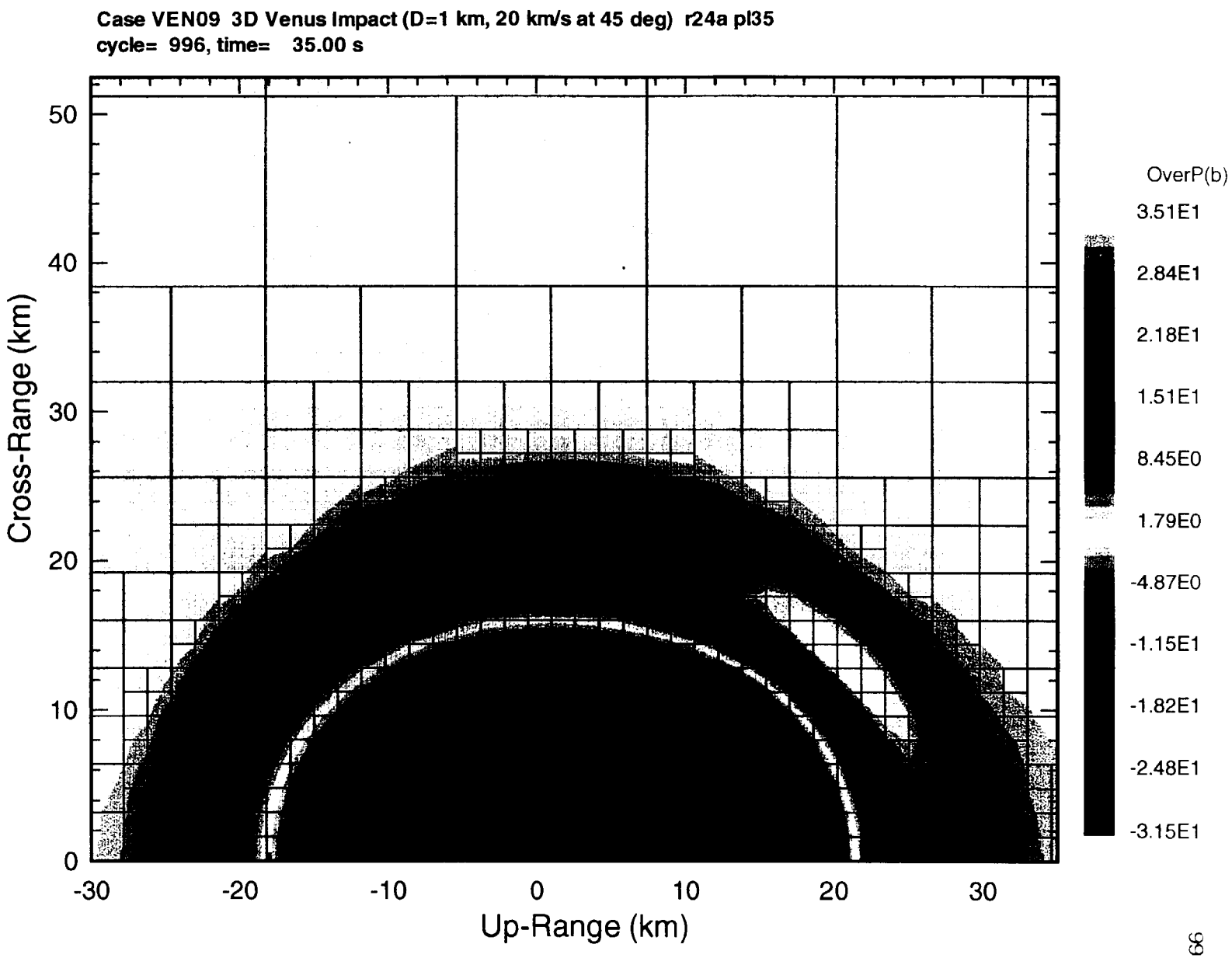
Case VEN09 3D Venus Impact (D=1 km, 20 km/s at 45 deg) r24a pl35
cycle= 996, time= 35.00 s
Cross-Range (km)
Up-Range (km)
50
40
30
20
10
0
-30
-20
-10
0
10
20
30
OverP(b)
3.51E1
2.84E1
2.18E1
1.51E1
8.45E0
1.79E0
-4.87E0
-1.15E1
-1.82E1
-2.48E1
-3.15E1

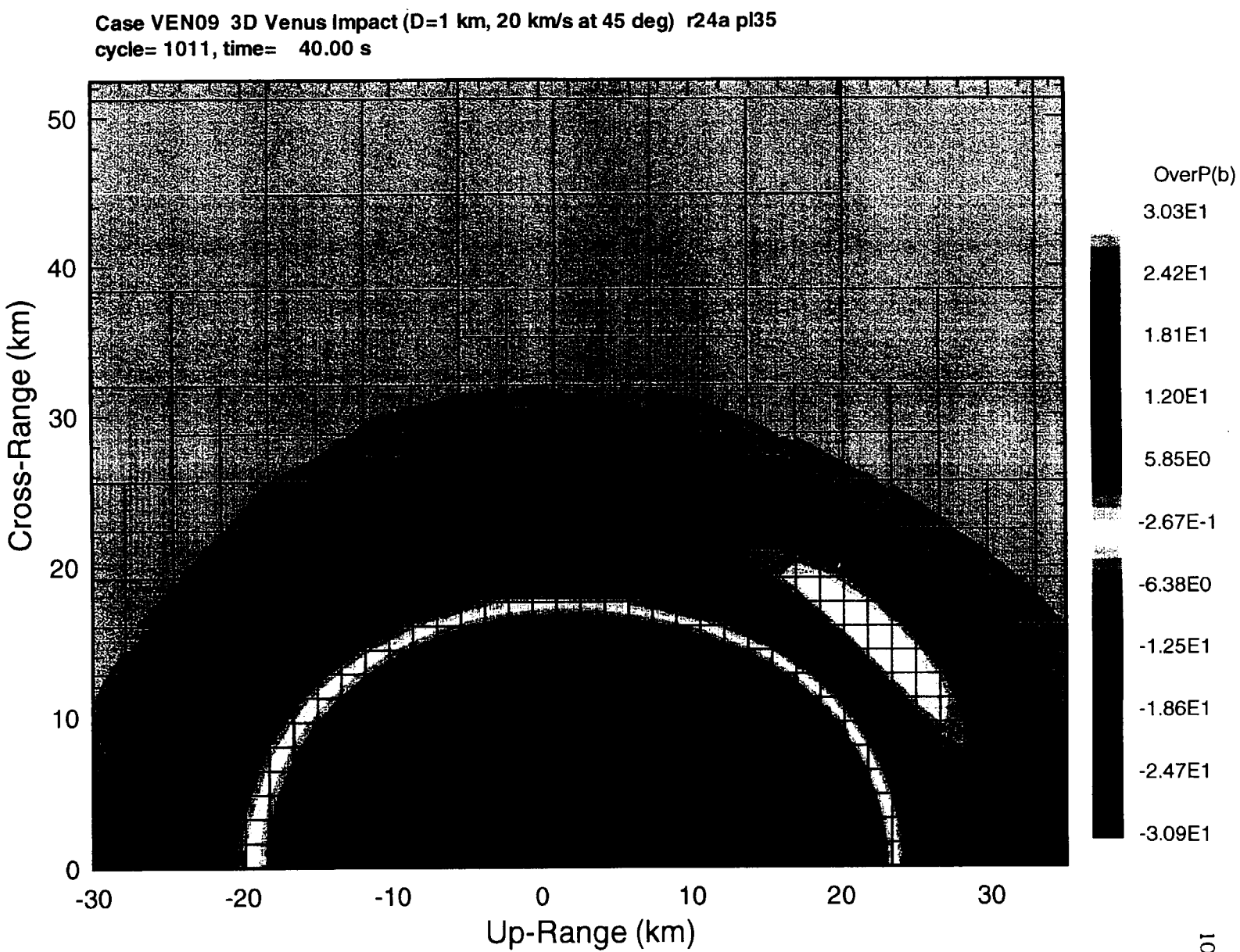
Case VEN09 3D Venus Impact (D=1 km, 20 km/s at 45 deg) r24a pl35
cycle= 1011, time= 40.00 s
Cross-Range (km)
50
40
30
20
10
0
-30
-20
-10
0
10
20
30
Up-Range (km)
OverP(b)
3.03E1
2.42E1
1.81E1
1.20E1
5.85E0
-2.67E-1
-6.38E0
-1.25E1
-1.86E1
-2.47E1
-3.09E1

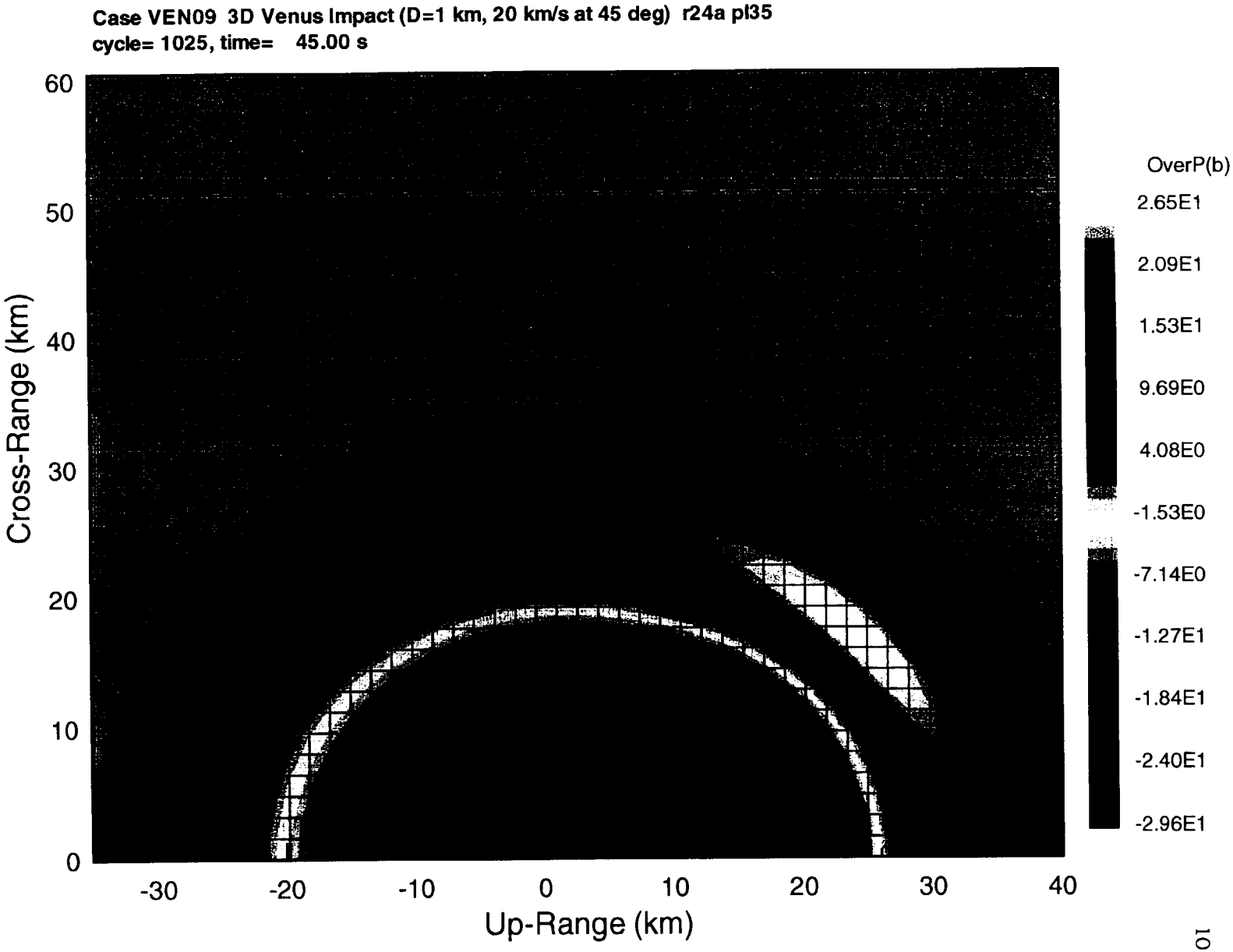
Case VEN09 3D Venus Impact (D=1 km, 20 km/s at 45 deg) r24a pl35
cycle= 1025, time= 45.00 s
Cross-Range (km)
Up-Range (km)
60
50
40
30
20
10
0
-30
-20
-10
0
10
20
30
40
OverP(b)
2.65E1
2.09E1
1.53E1
9.69E0
4.08E0
-1.53E0
-7.14E0
-1.27E1
-1.84E1
-2.40E1
-2.96E1

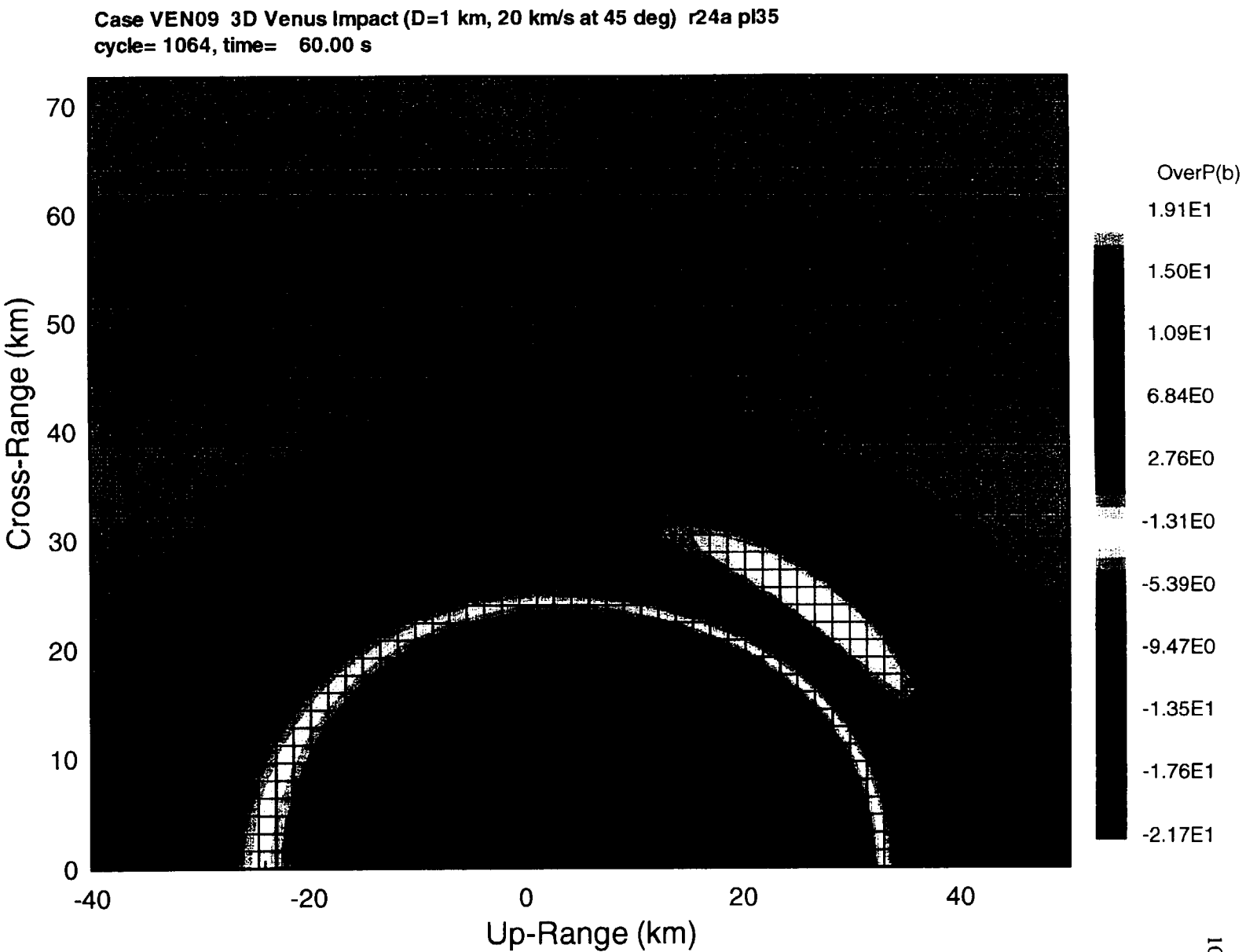
Case VEN09 3D Venus Impact (D=1 km, 20 km/s at 45 deg) r24a pl35
cycle= 1064, time= 60.00 s
Cross-Range (km)
70
60
50
40
30
20
10
0
-40
-20
0
20
40
Up-Range (km)
OverP(b)
1.91E1
1.50E1
1.09E1
6.84E0
2.76E0
-1.31E0
-5.39E0
-9.47E0
-1.35E1
-1.76E1
-2.17E1

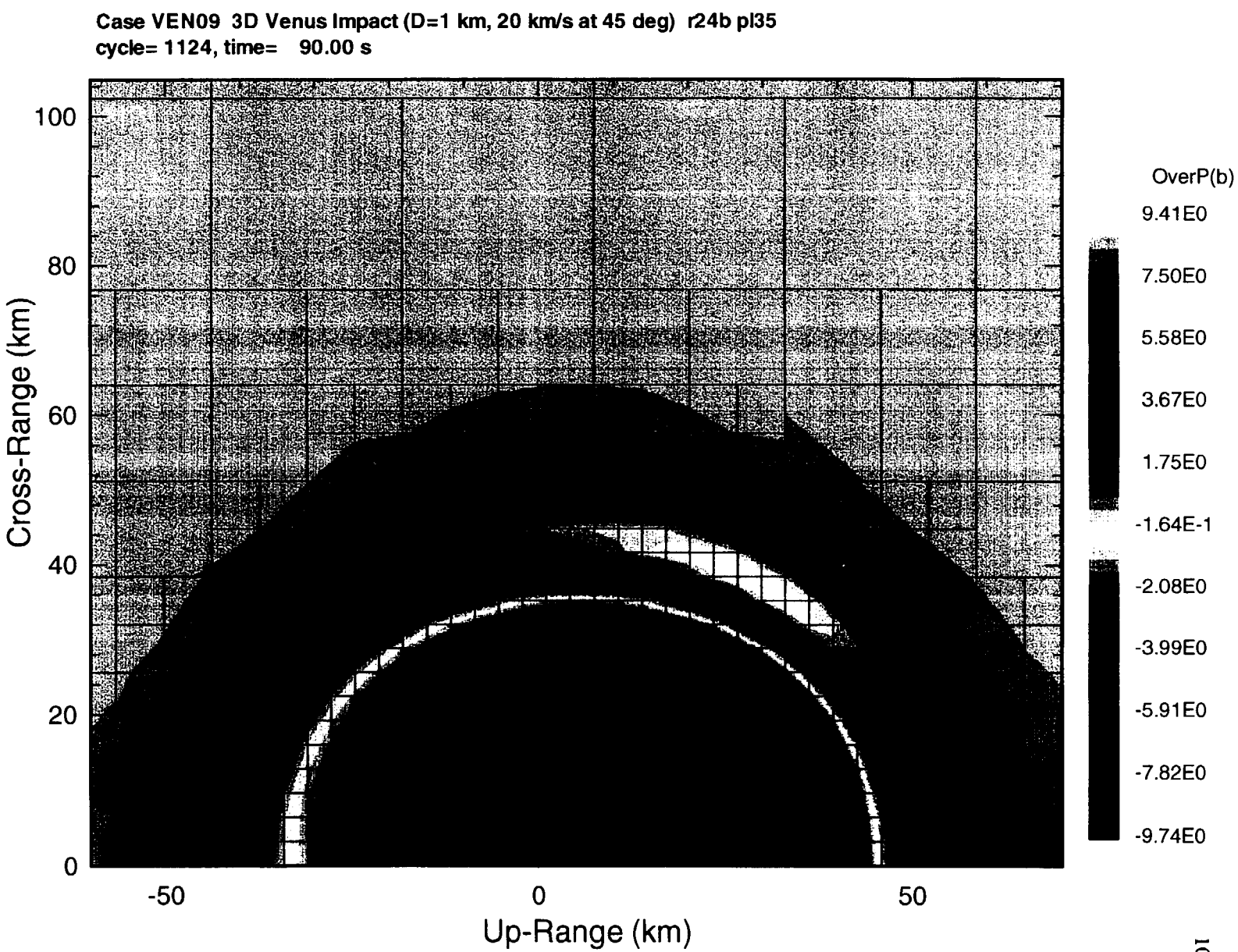
Case VEN09 3D Venus Impact (D=1 km, 20 km/s at 45 deg) r24b pl35
cycle= 1124, time= 90.00 s
Cross-Range (km)
100
80
60
40
20
0
-50
0
50
Up-Range (km)
OverP(b)
9.41E0
7.50E0
5.58E0
3.67E0
1.75E0
-1.64E-1
-2.08E0
-3.99E0
-5.91E0
-7.82E0
-9.74E0

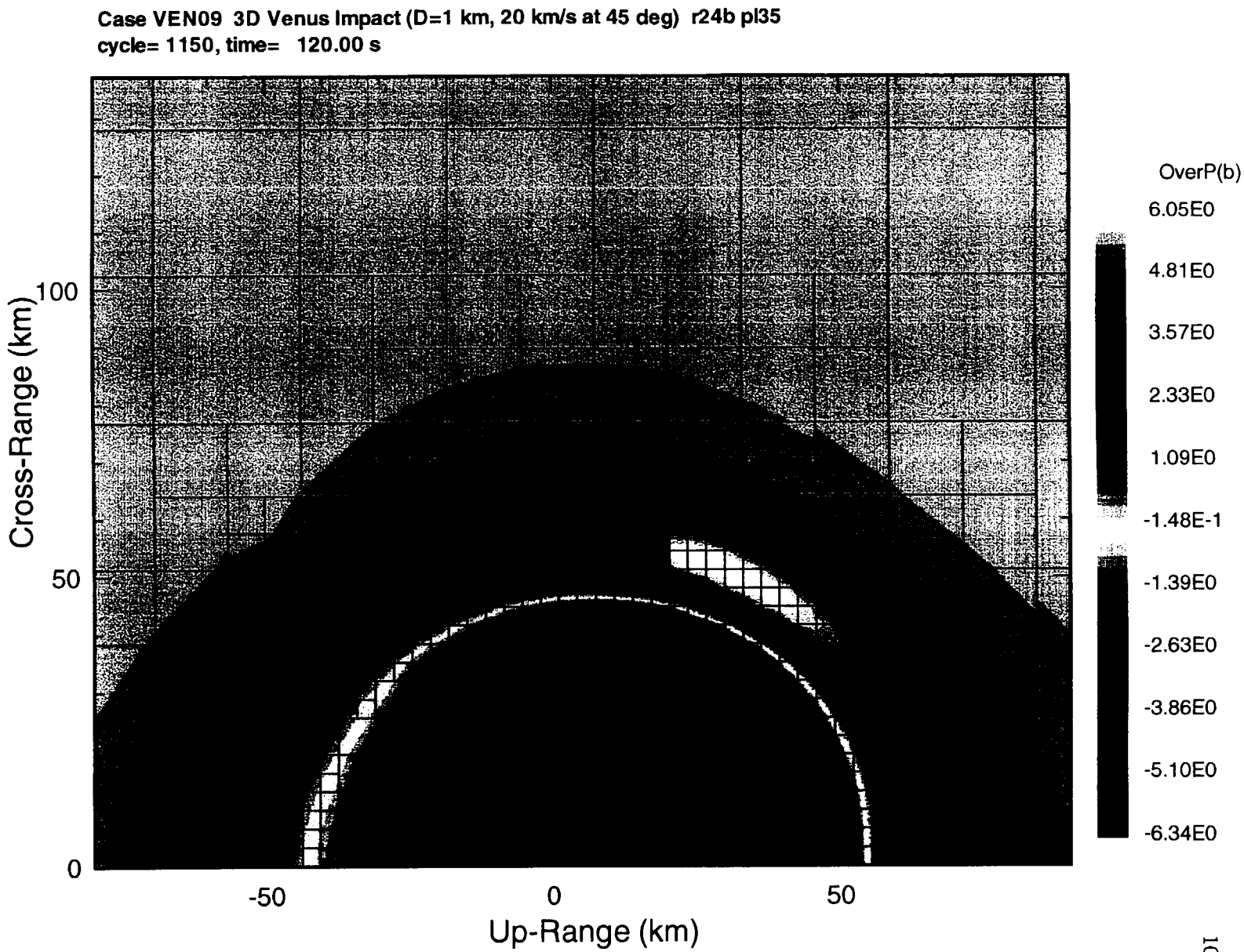
Case VEN09 3D Venus Impact (D=1 km, 20 km/s at 45 deg) r24b pl35
cycle= 1150, time= 120.00 s
Cross-Range (km)
100
50
0
-50
0
50
Up-Range (km)
OverP(b)
6.05E0
4.81E0
3.57E0
2.33E0
1.09E0
-1.48E-1
-1.39E0
-2.63E0
-3.86E0
-5.10E0
-6.34E0

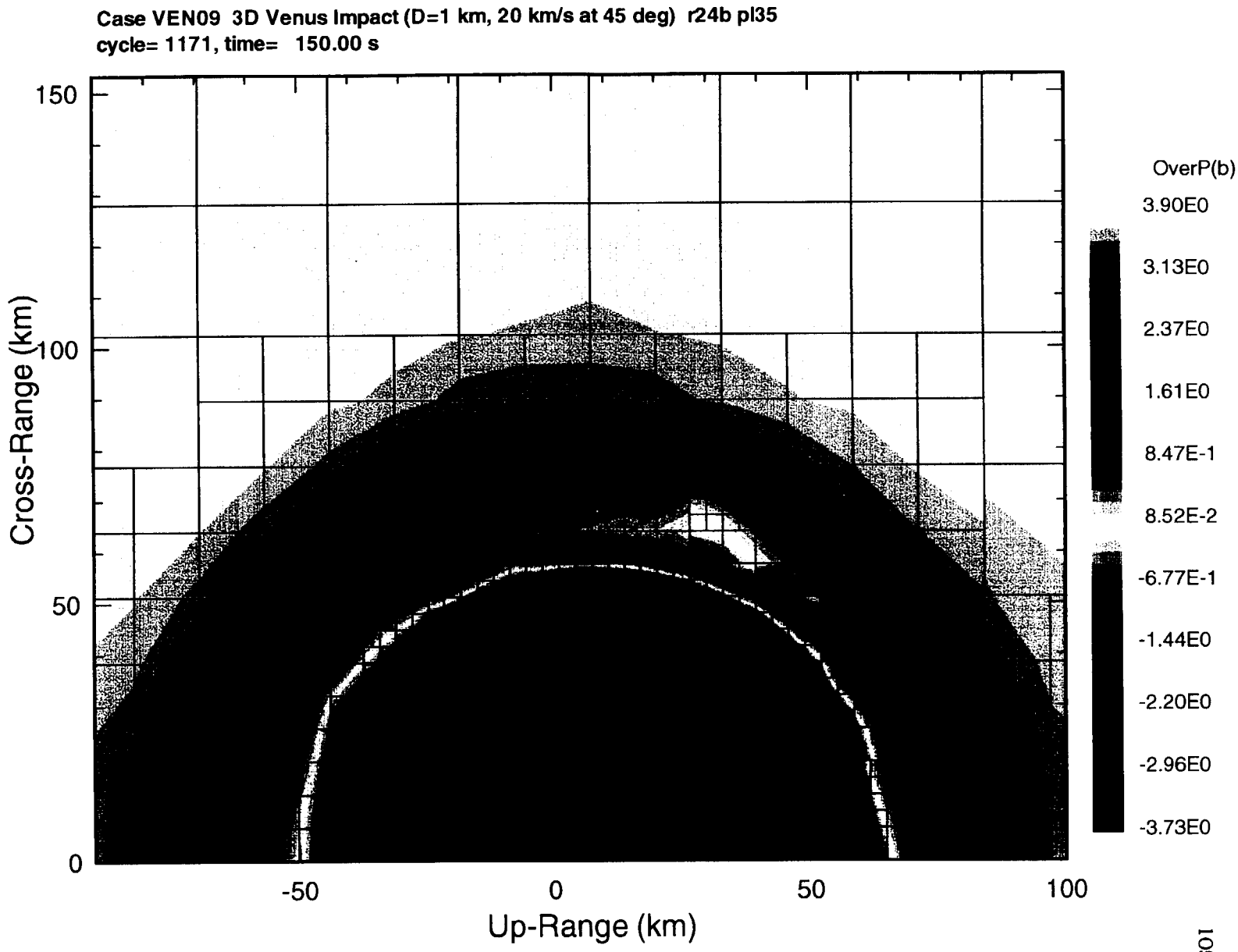
Case VEN09 3D Venus Impact (D=1 km, 20 km/s at 45 deg) r24b pl35
cycle= 1171, time= 150.00 s
150
100
50
0
Cross-Range (km)
-50
0
50
100
Up-Range (km)
OverP(b)
3.90E0
3.13E0
2.37E0
1.61E0
8.47E-1
8.52E-2
-6.77E-1
-1.44E0
-2.20E0
-2.96E0
-3.73E0

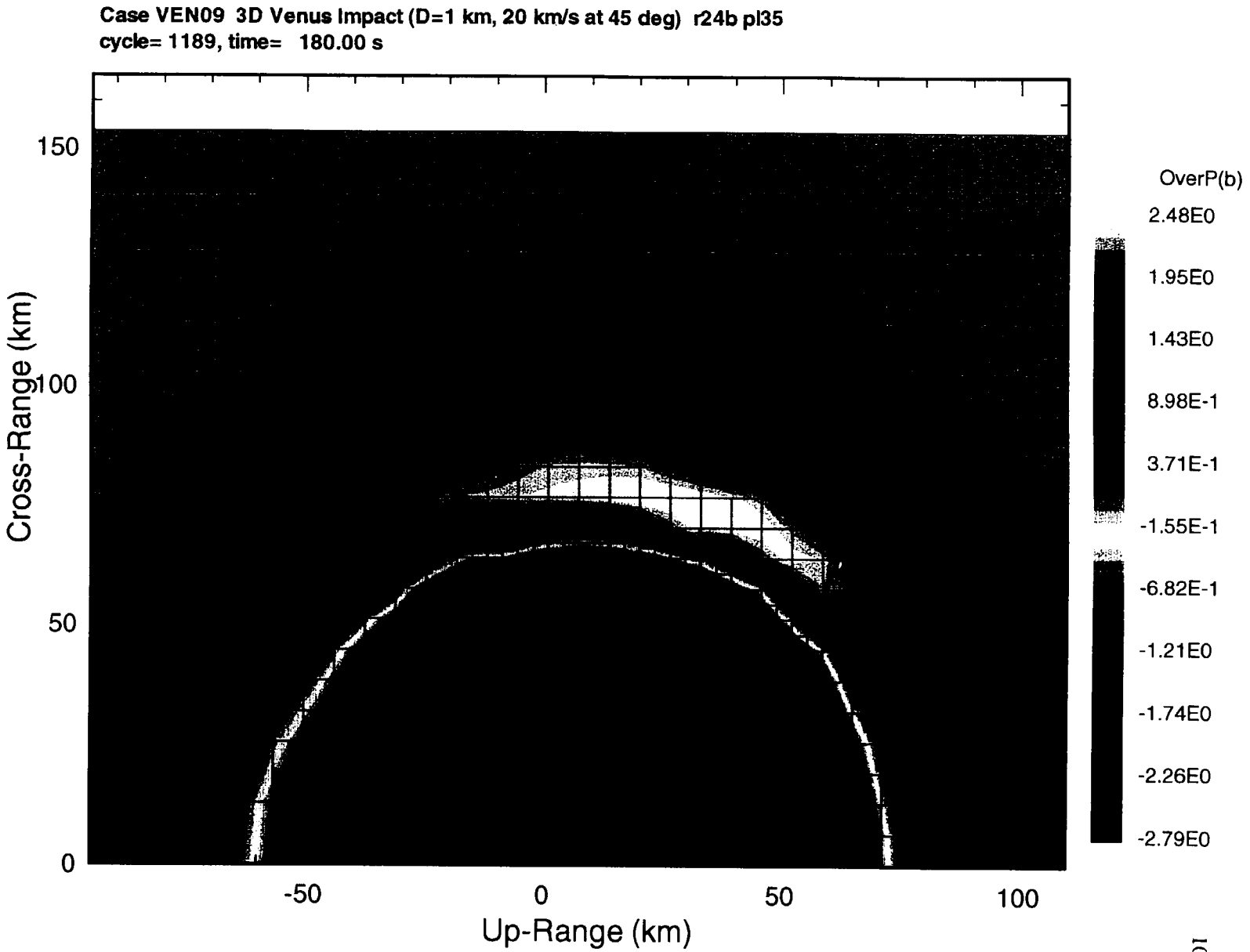
Case VEN09 3D Venus Impact (D=1 km, 20 km/s at 45 deg) r24b pl35
cycle= 1189, time= 180.00 s
150
100
50
0
Cross-Range (km)
-50
0
50
100
Up-Range (km)
OverP(b)
2.48E0
1.95E0
1.43E0
8.98E-1
3.71E-1
-1.55E-1
-6.82E-1
-1.21E0
-1.74E0
-2.26E0
-2.79E0

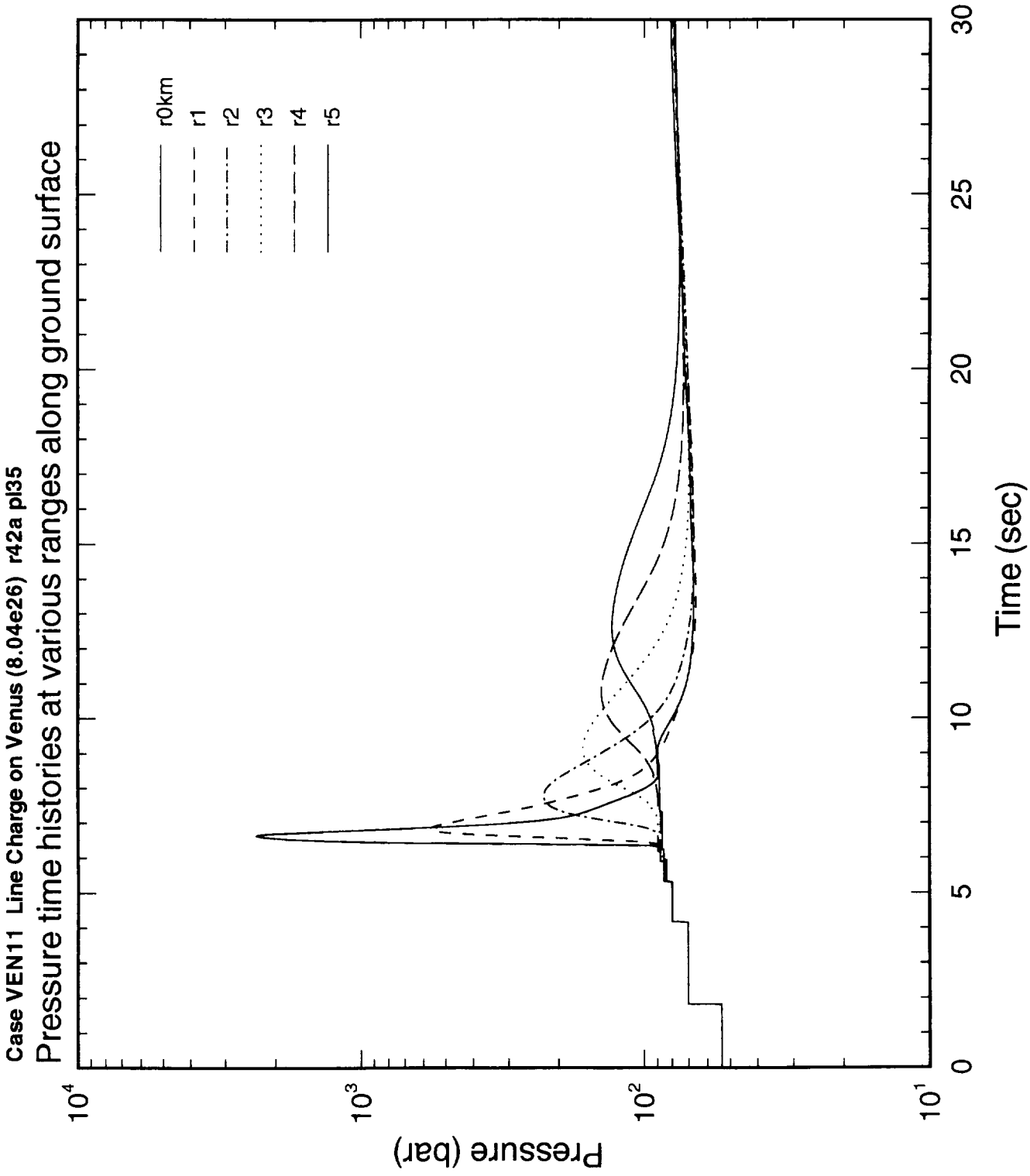
Case VEN11 Line Charge on Venus (8.04e26) r42a pl35
Pressure time histories at various ranges along ground surface
r0km
r1
r2
r3
r4
r5
Pressure (bar)
Time (sec)
10^4
10^3
10^2
10^1
0
5
10
15
20
25
30

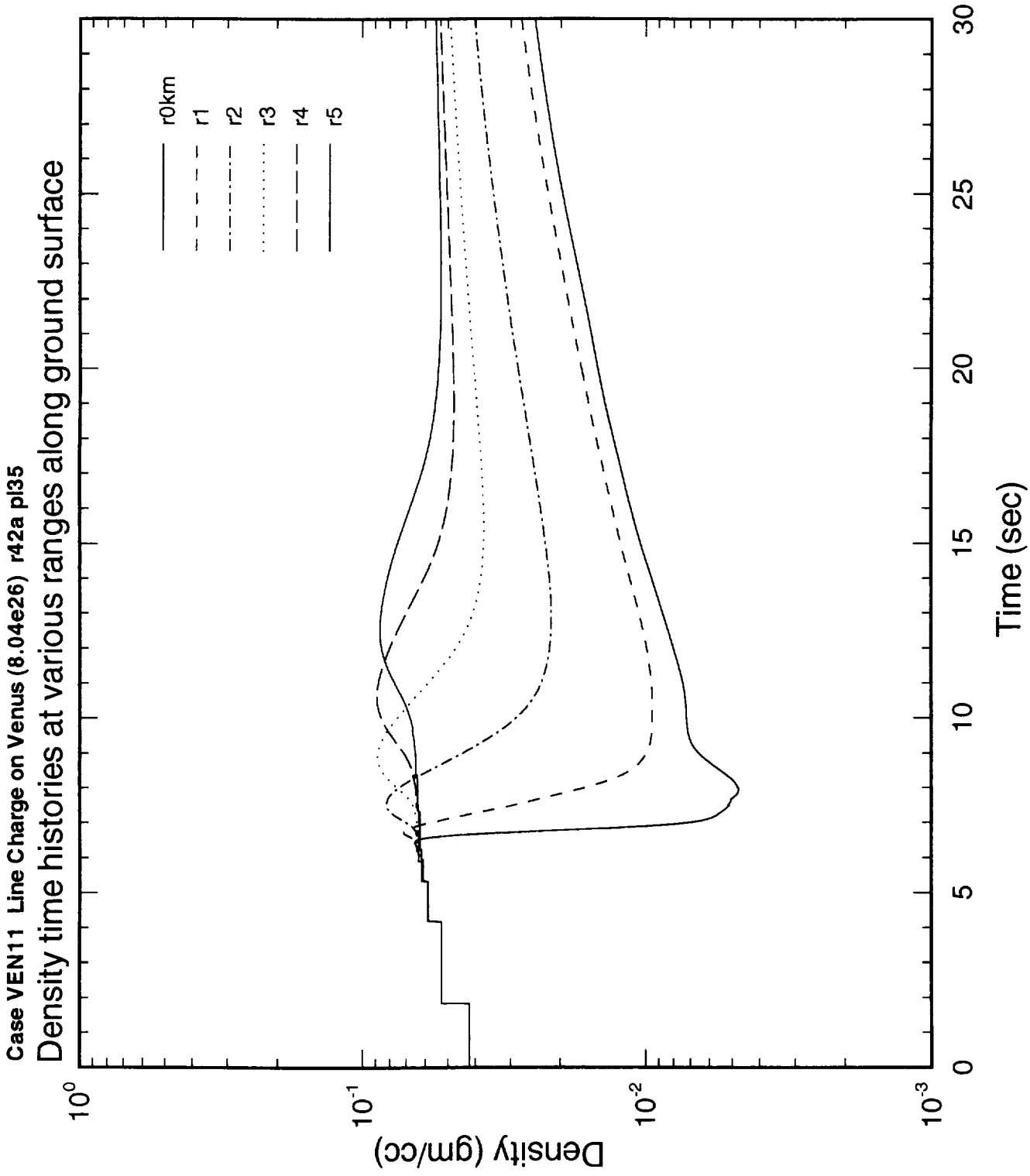
Case VEN11 Line Charge on Venus (8.04e26) r42a pl35
Density time histories at various ranges along ground surface
r0km
r1
r2
r3
r4
r5
Density (gm/cc)
Time (sec)
10^0
10^-1
10^-2
10^-3
0
5
10
15
20
25
30

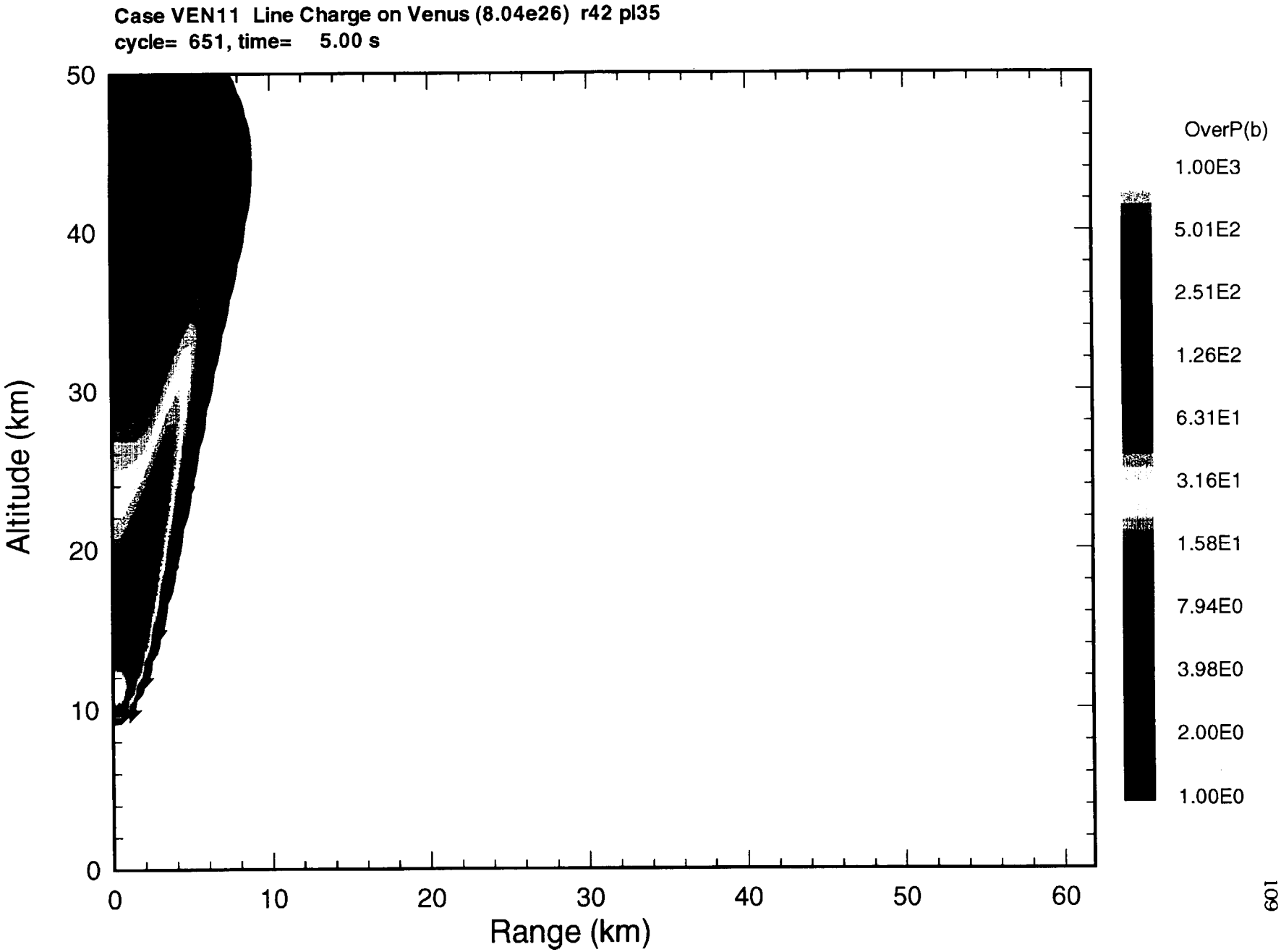
Case VEN11 Line Charge on Venus (8.04e26) r42 pl35
cycle= 651, time= 5.00 s
Altitude (km)
Range (km)
0
10
20
30
40
50
60
OverP(b)
1.00E3
5.01E2
2.51E2
1.26E2
6.31E1
3.16E1
1.58E1
7.94E0
3.98E0
2.00E0
1.00E0

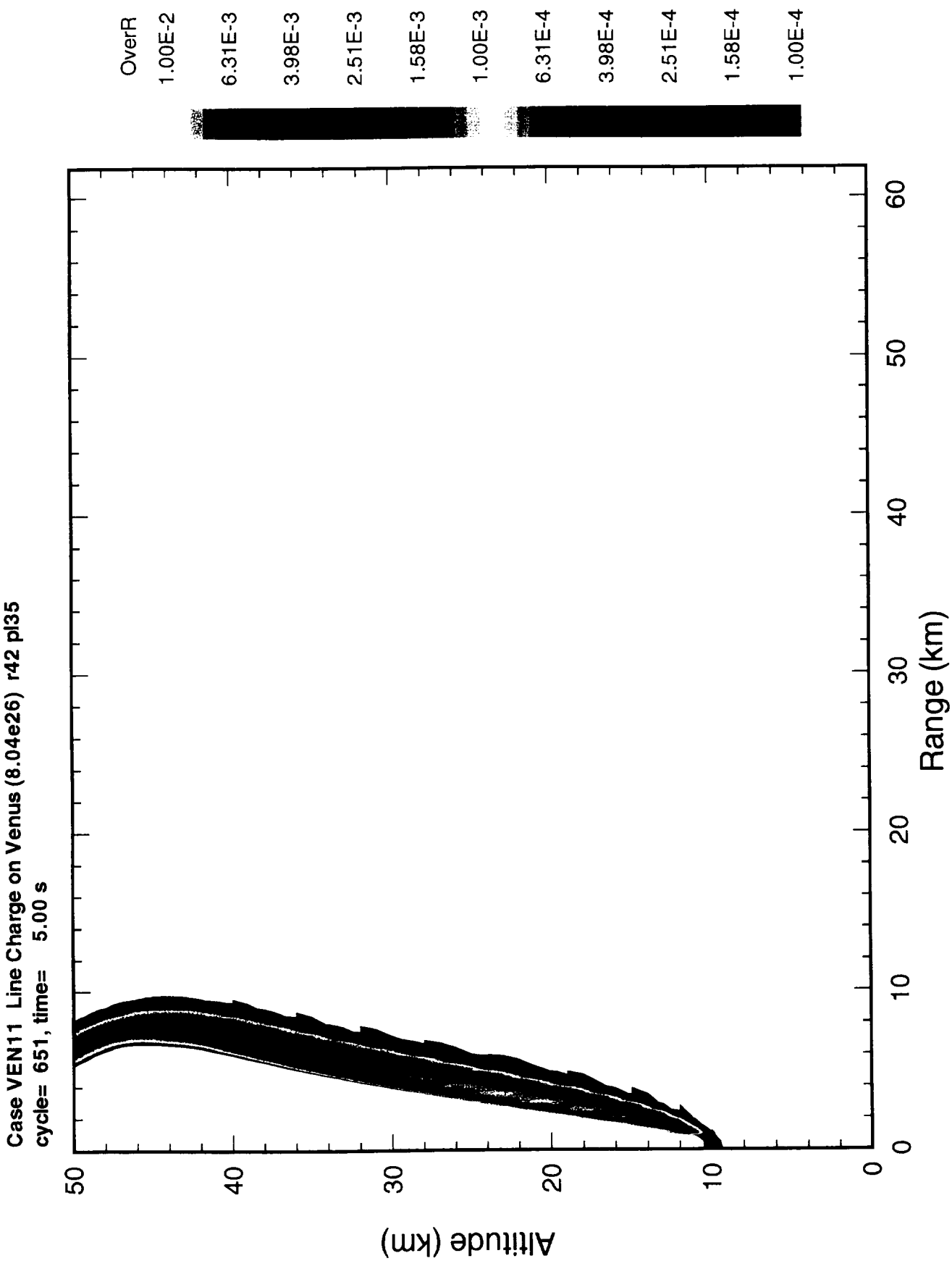
Case VEN11 Line Charge on Venus (8.04e26) r42 pl35
cycle= 651, time= 5.00 s
OverR
1.00E-2
6.31E-3
3.98E-3
2.51E-3
1.58E-3
1.00E-3
6.31E-4
3.98E-4
2.51E-4
1.58E-4
1.00E-4
Altitude (km)
Range (km)
0
10
20
30
40
50
60

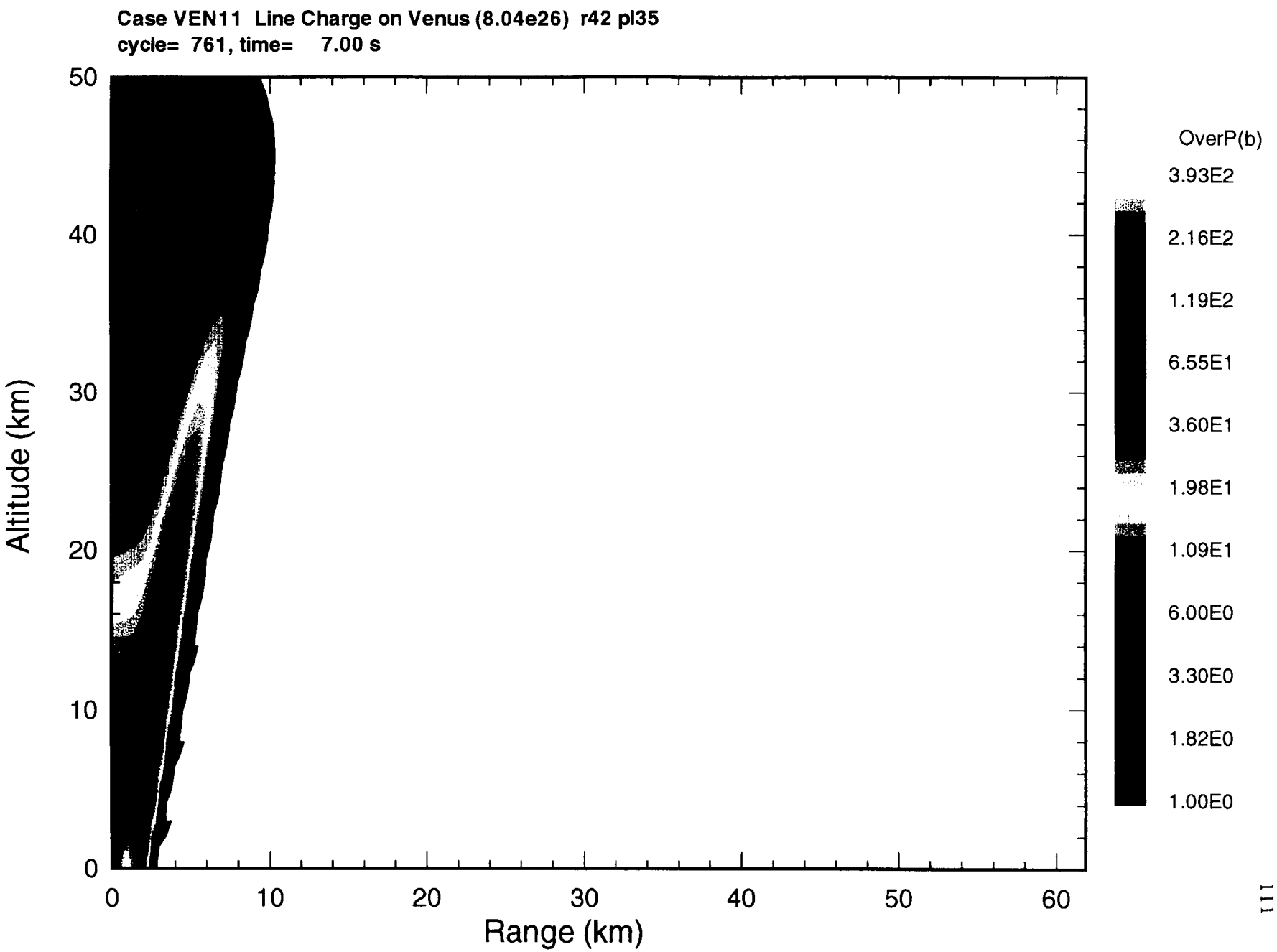
Case VEN11 Line Charge on Venus (8.04e26) r42 pl35
cycle= 761, time= 7.00 s
Altitude (km)
0
10
20
30
40
50
Range (km)
0
10
20
30
40
50
60
OverP(b)
3.93E2
2.16E2
1.19E2
6.55E1
3.60E1
1.98E1
1.09E1
6.00E0
3.30E0
1.82E0
1.00E0

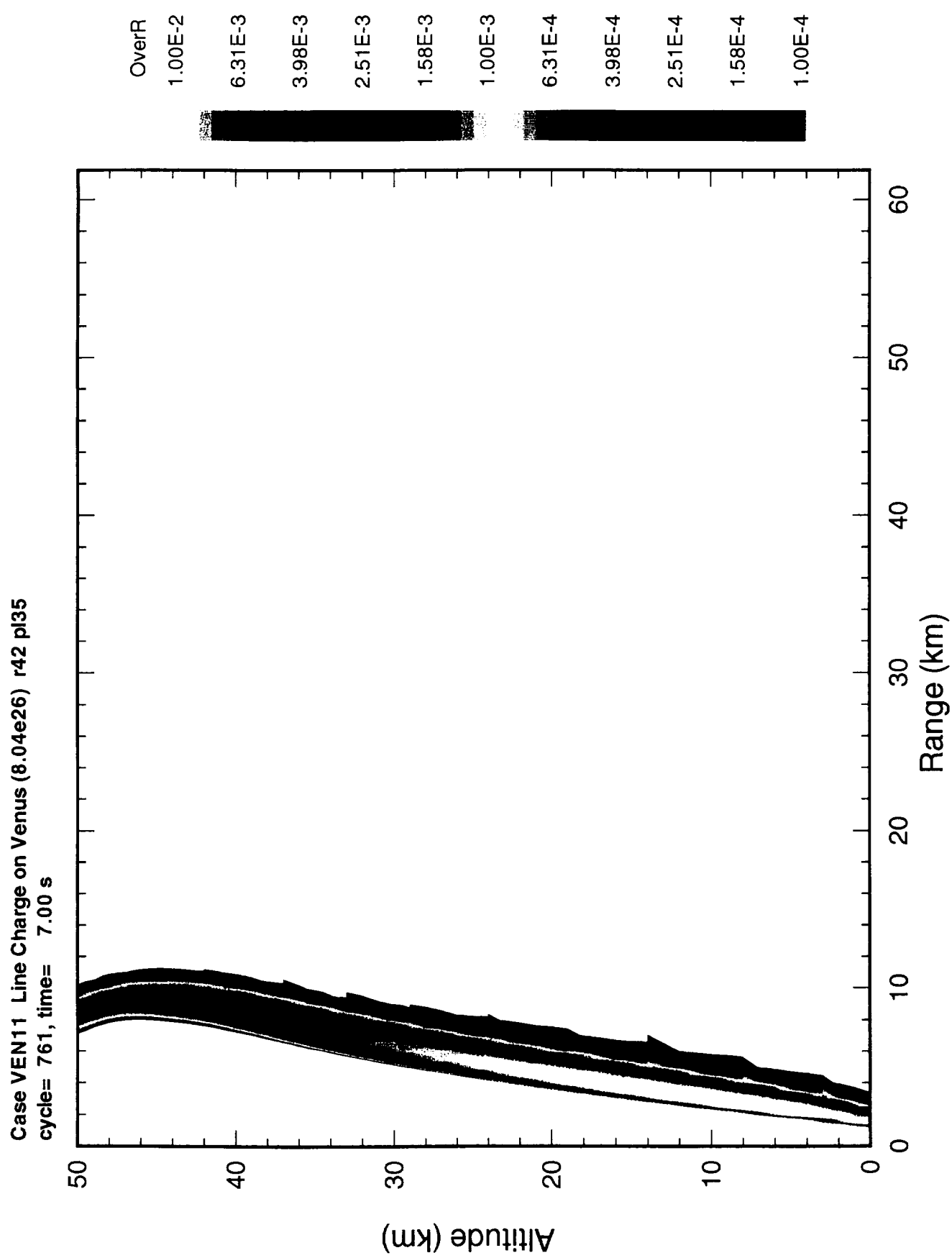
Case VEN11 Line Charge on Venus (8.04e26) r42 pl35
cycle= 761, time= 7.00 s
OverR
1.00E-2
6.31E-3
3.98E-3
2.51E-3
1.58E-3
1.00E-3
6.31E-4
3.98E-4
2.51E-4
1.58E-4
1.00E-4
Altitude (km)
0
10
20
30
40
50
Range (km)
0
10
20
30
40
50
60

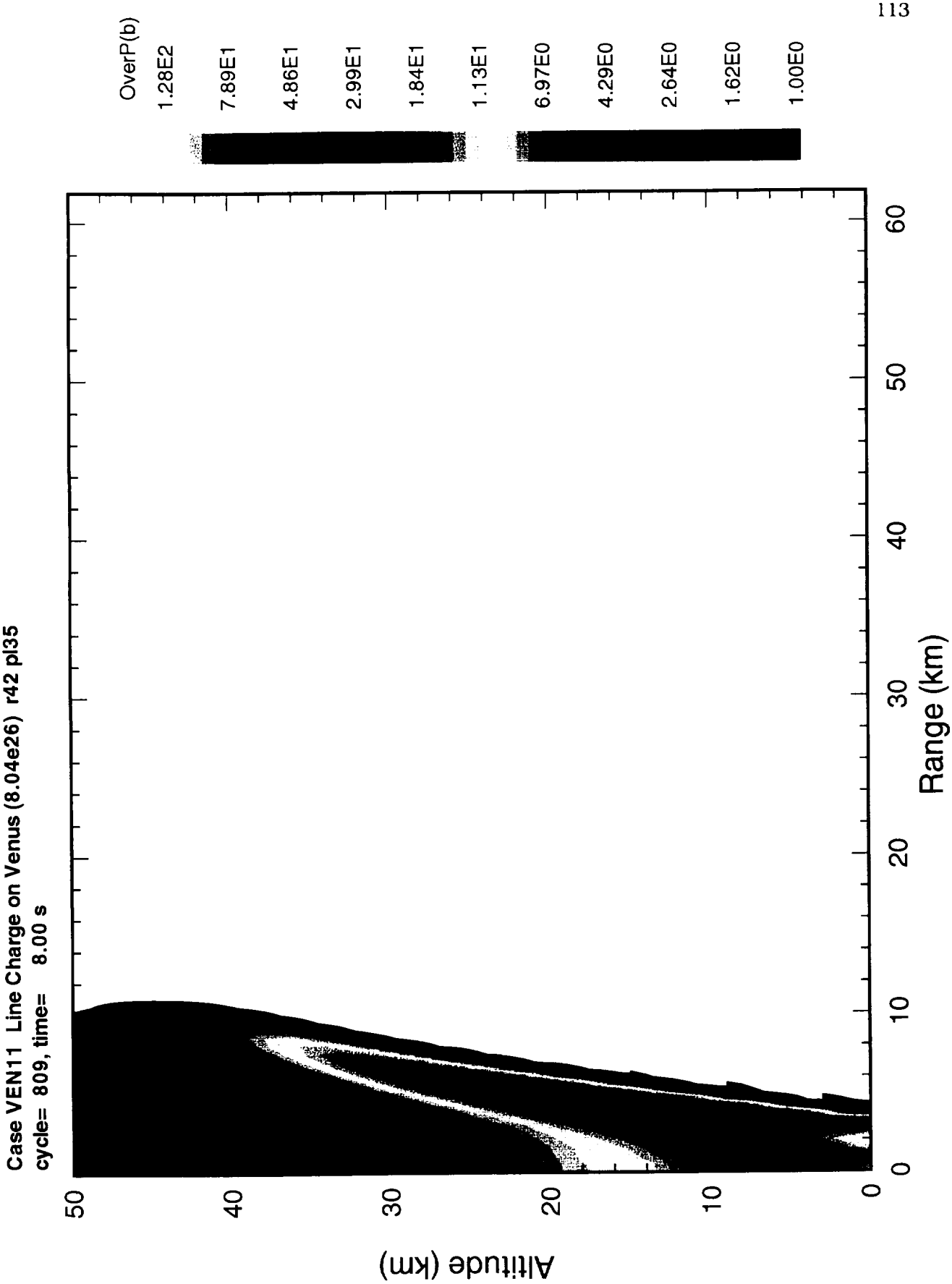
Case VEN11 Line Charge on Venus (8.04e26) r42 pl35
cycle= 809, time= 8.00 s
OverP(b)
1.28E2
7.89E1
4.86E1
2.99E1
1.84E1
1.13E1
6.97E0
4.29E0
2.64E0
1.62E0
1.00E0
Altitude (km)
0
10
20
30
40
50
Range (km)
0
10
20
30
40
50
60

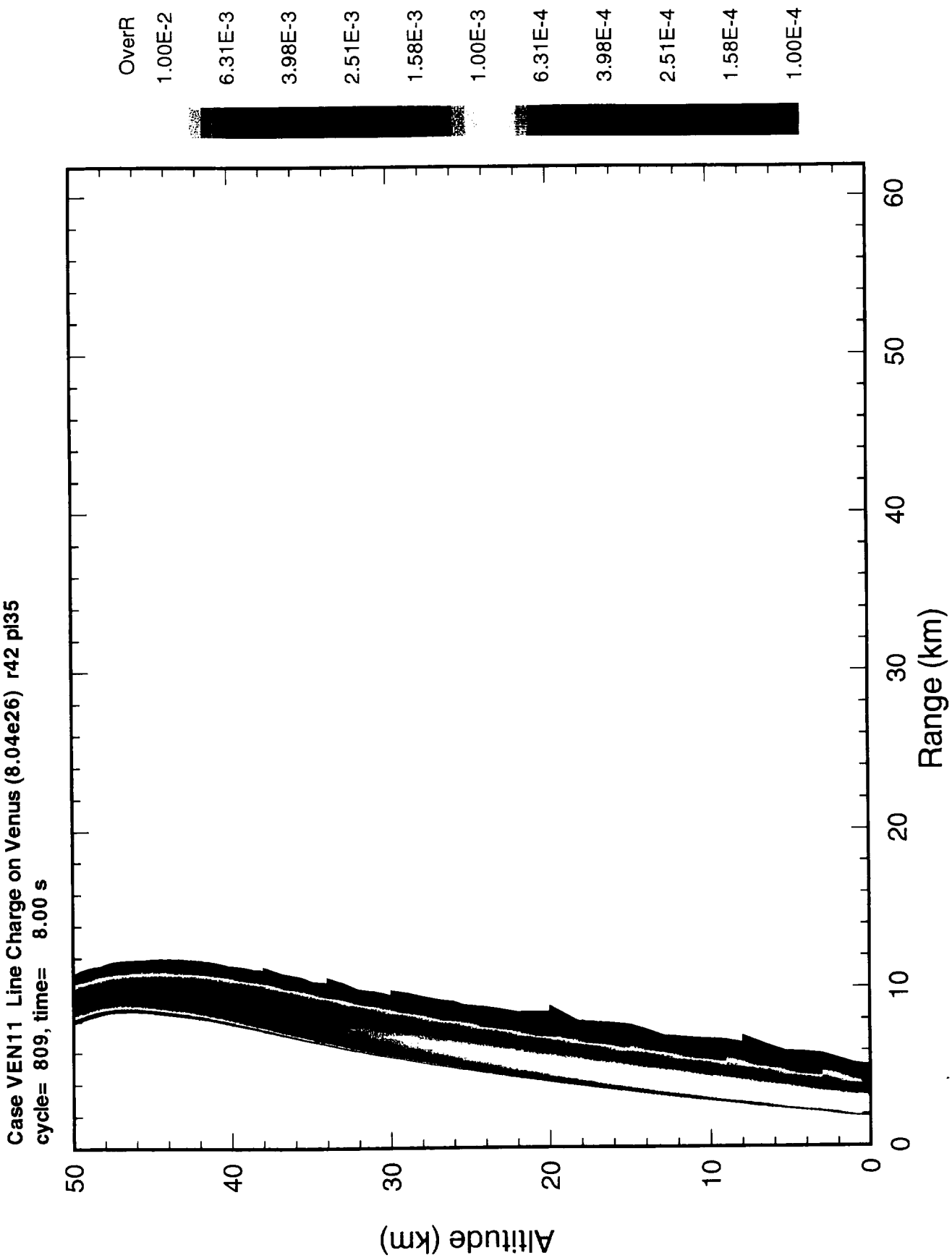
Case VEN11 Line Charge on Venus (8.04e26) r42 pl35
cycle= 809, time= 8.00 s
OverR
1.00E-2
6.31E-3
3.98E-3
2.51E-3
1.58E-3
1.00E-3
6.31E-4
3.98E-4
2.51E-4
1.58E-4
1.00E-4
Altitude (km)
0
10
20
30
40
50
Range (km)
0
10
20
30
40
50
60

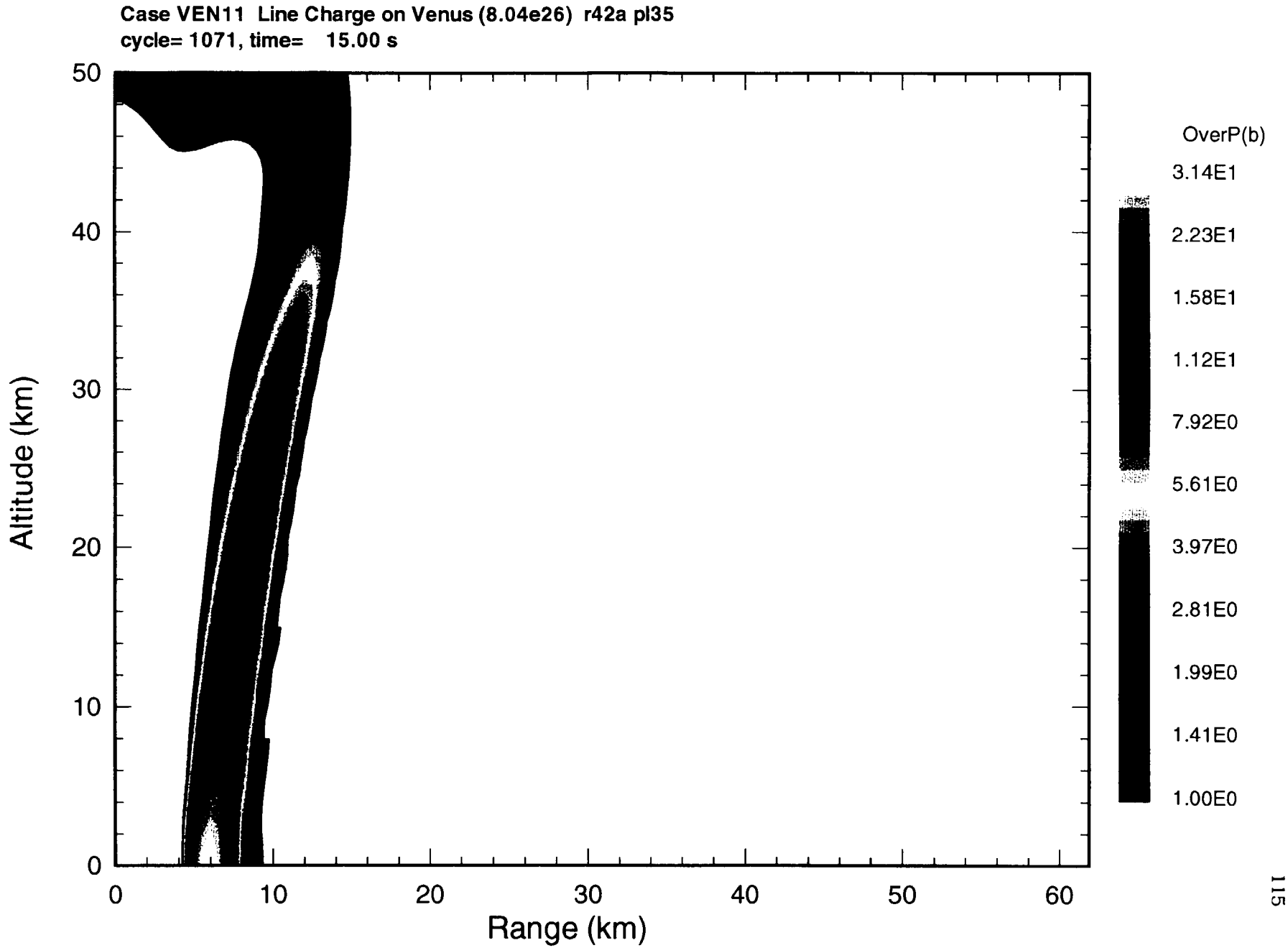
Case VEN11 Line Charge on Venus (8.04e26) r42a pl35
cycle= 1071, time= 15.00 s
Altitude (km)
Range (km)
0
10
20
30
40
50
60
OverP(b)
3.14E1
2.23E1
1.58E1
1.12E1
7.92E0
5.61E0
3.97E0
2.81E0
1.99E0
1.41E0
1.00E0

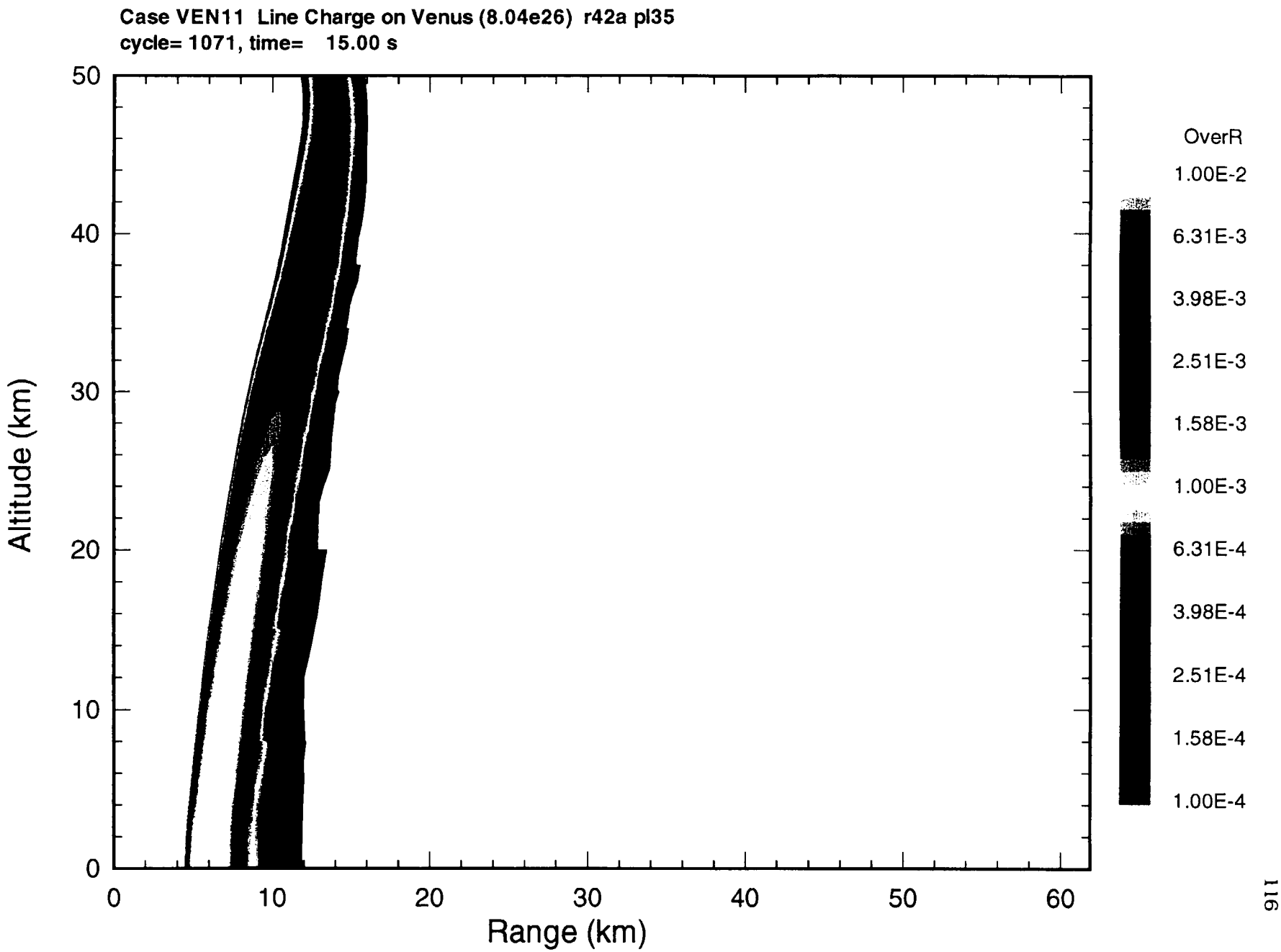
Case VEN11 Line Charge on Venus (8.04e26) r42a pl35
cycle= 1071, time= 15.00 s
Altitude (km)
0
10
20
30
40
50
Range (km)
0
10
20
30
40
50
60
OverR
1.00E-2
6.31E-3
3.98E-3
2.51E-3
1.58E-3
1.00E-3
6.31E-4
3.98E-4
2.51E-4
1.58E-4
1.00E-4

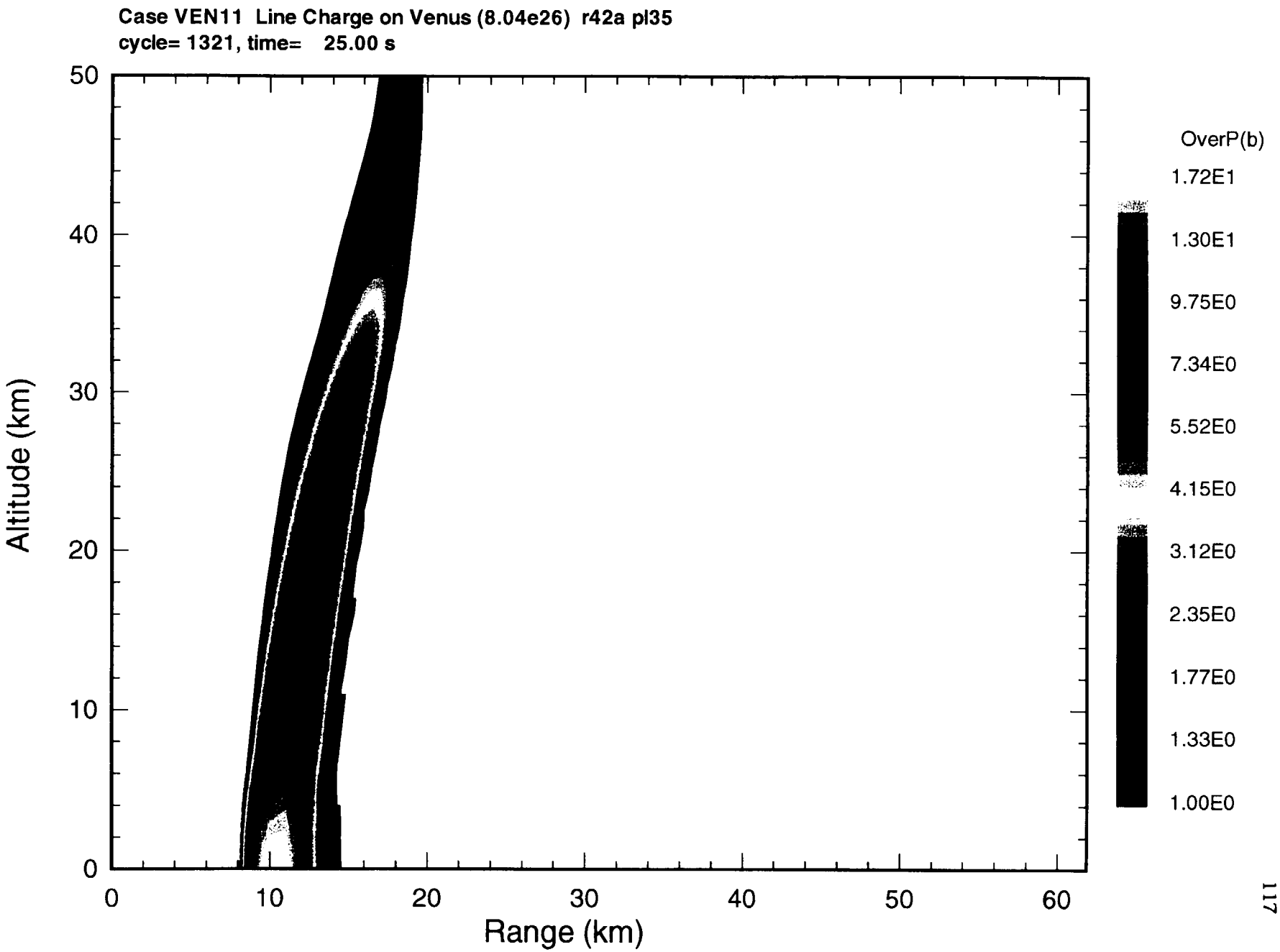
Case VEN11 Line Charge on Venus (8.04e26) r42a pl35
cycle= 1321, time= 25.00 s
Altitude (km)
Range (km)
0
10
20
30
40
50
60
OverP(b)
1.72E1
1.30E1
9.75E0
7.34E0
5.52E0
4.15E0
3.12E0
2.35E0
1.77E0
1.33E0
1.00E0

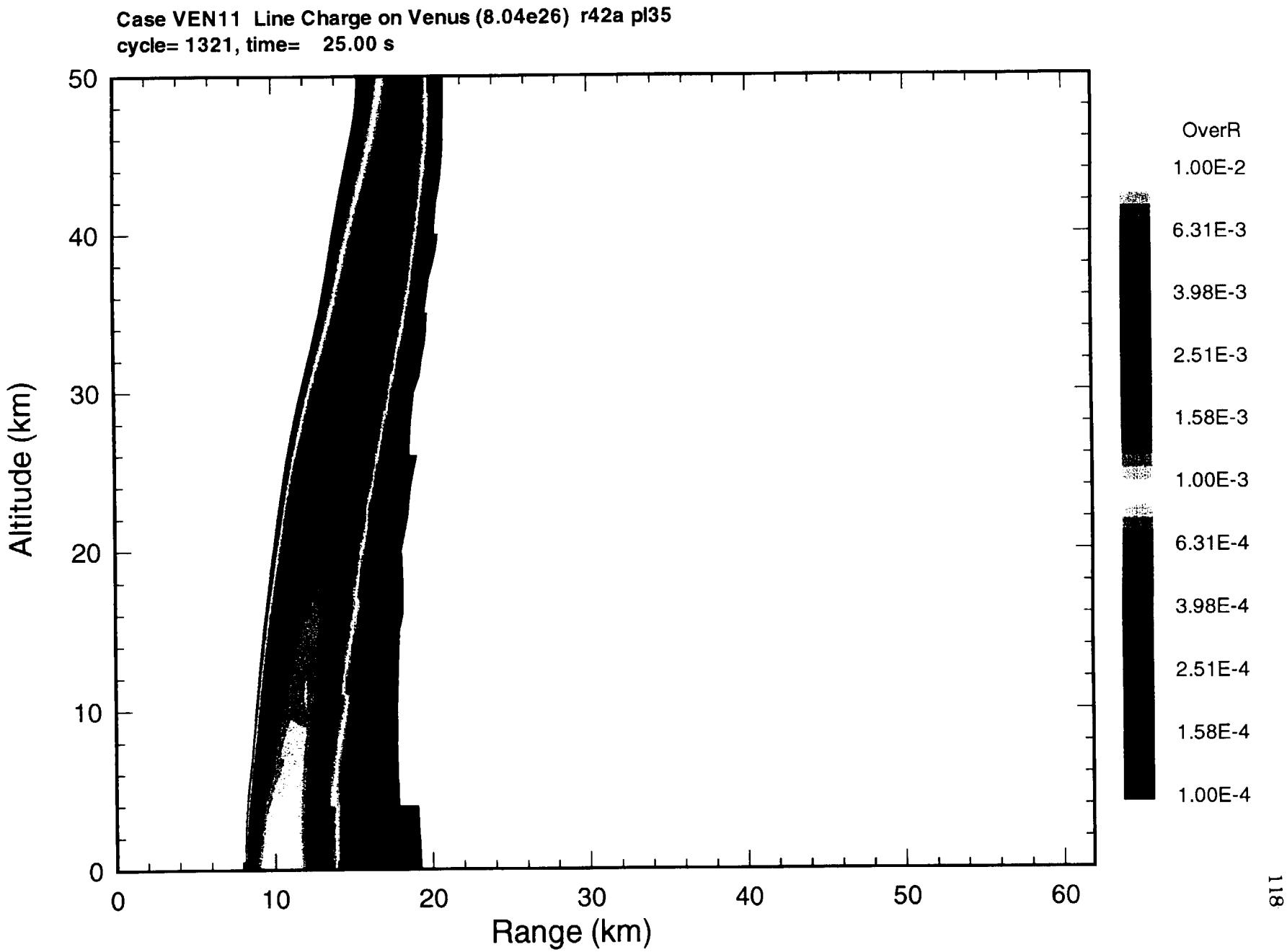
Case VEN11 Line Charge on Venus (8.04e26) r42a pl35
cycle= 1321, time= 25.00 s
Altitude (km)
Range (km)
0
10
20
30
40
50
60
OverR
1.00E-2
6.31E-3
3.98E-3
2.51E-3
1.58E-3
1.00E-3
6.31E-4
3.98E-4
2.51E-4
1.58E-4
1.00E-4

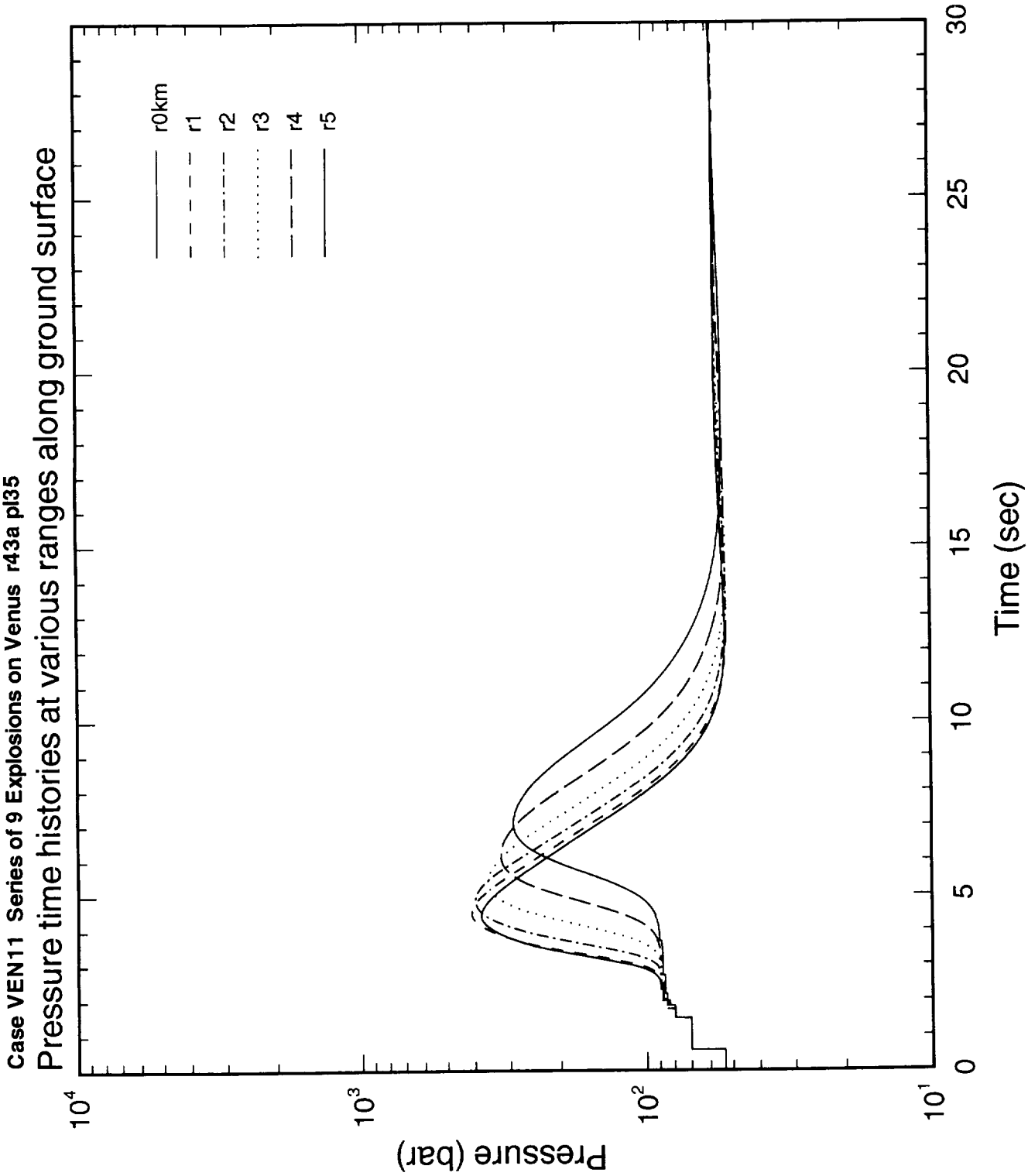
Case VEN11 Series of 9 Explosions on Venus r43a pl35
Pressure time histories at various ranges along ground surface
r0km
r1
r2
r3
r4
r5
Pressure (bar)
Time (sec)
10^4
10^3
10^2
10^1
0
5
10
15
20
25
30

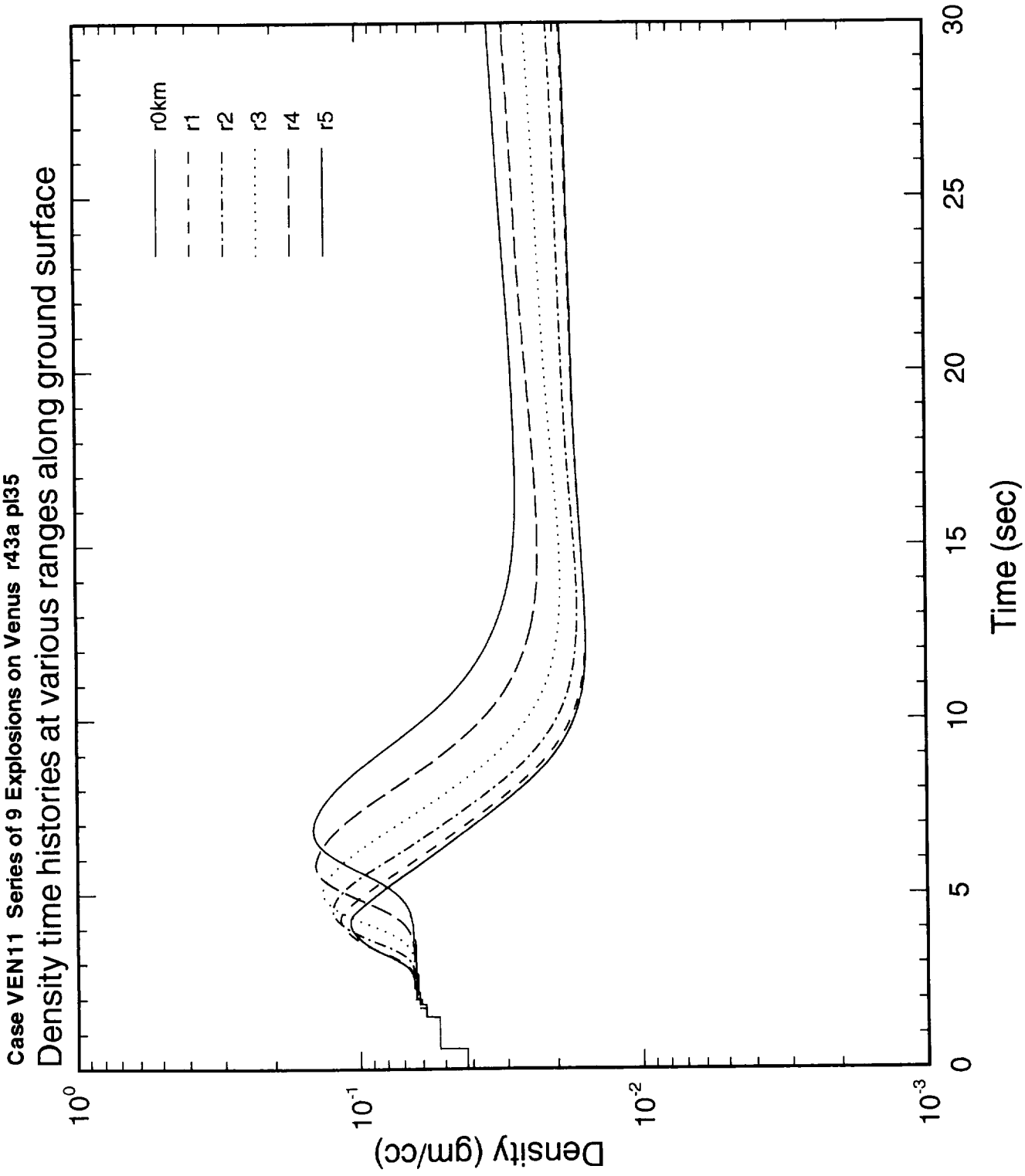
Case VEN11 Series of 9 Explosions on Venus r43a pl35
Density time histories at various ranges along ground surface
r0km
r1
r2
r3
r4
r5
Density (gm/cc)
Time (sec)
10^0
10^-1
10^-2
10^-3
0
5
10
15
20
25
30

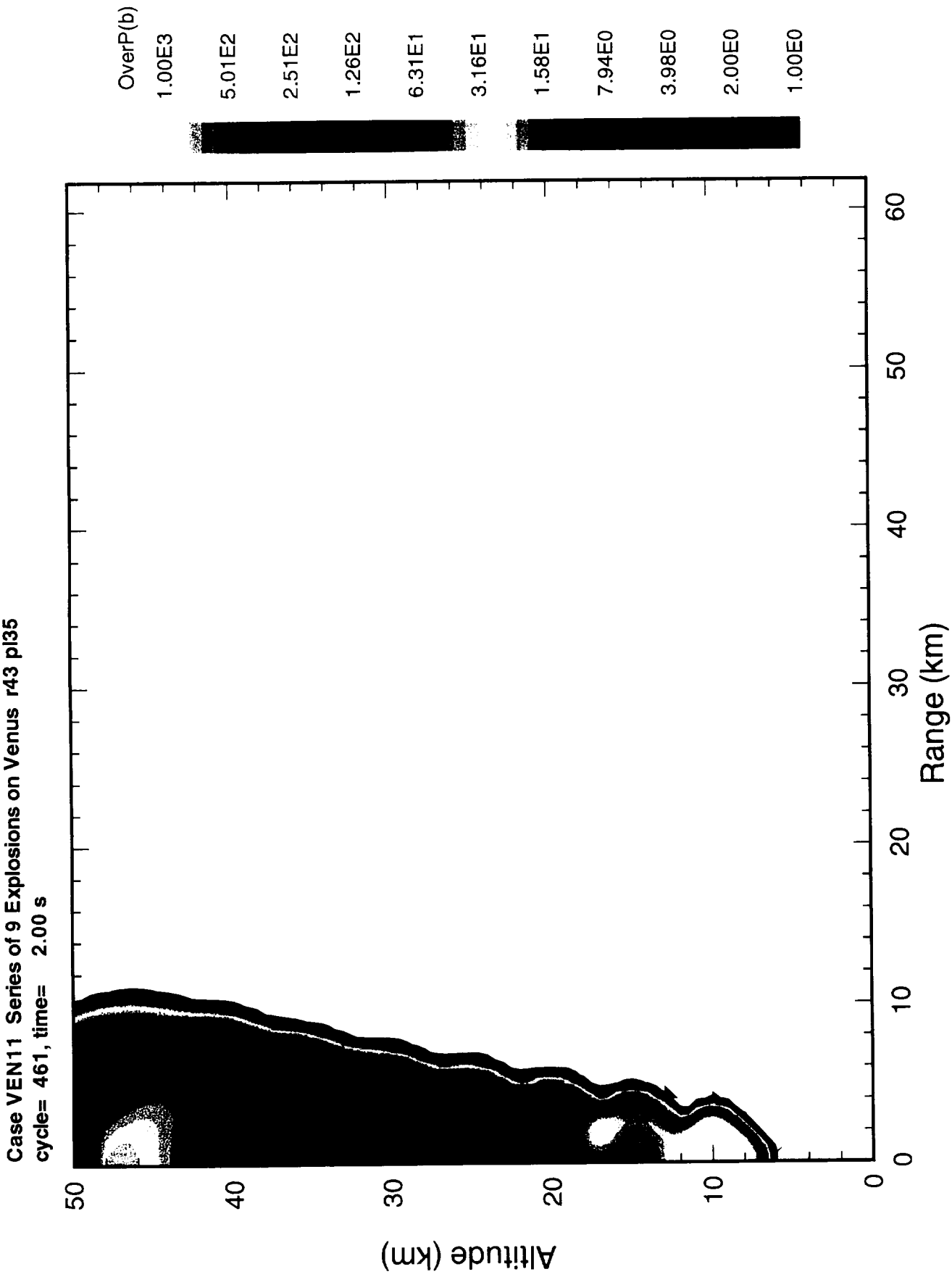
Case VEN11 Series of 9 Explosions on Venus r43 pl35
cycle= 461, time= 2.00 s
OverP(b)
1.00E3
5.01E2
2.51E2
1.26E2
6.31E1
3.16E1
1.58E1
7.94E0
3.98E0
2.00E0
1.00E0
Altitude (km)
0
10
20
30
40
50
Range (km)
0
10
20
30
40
50
60

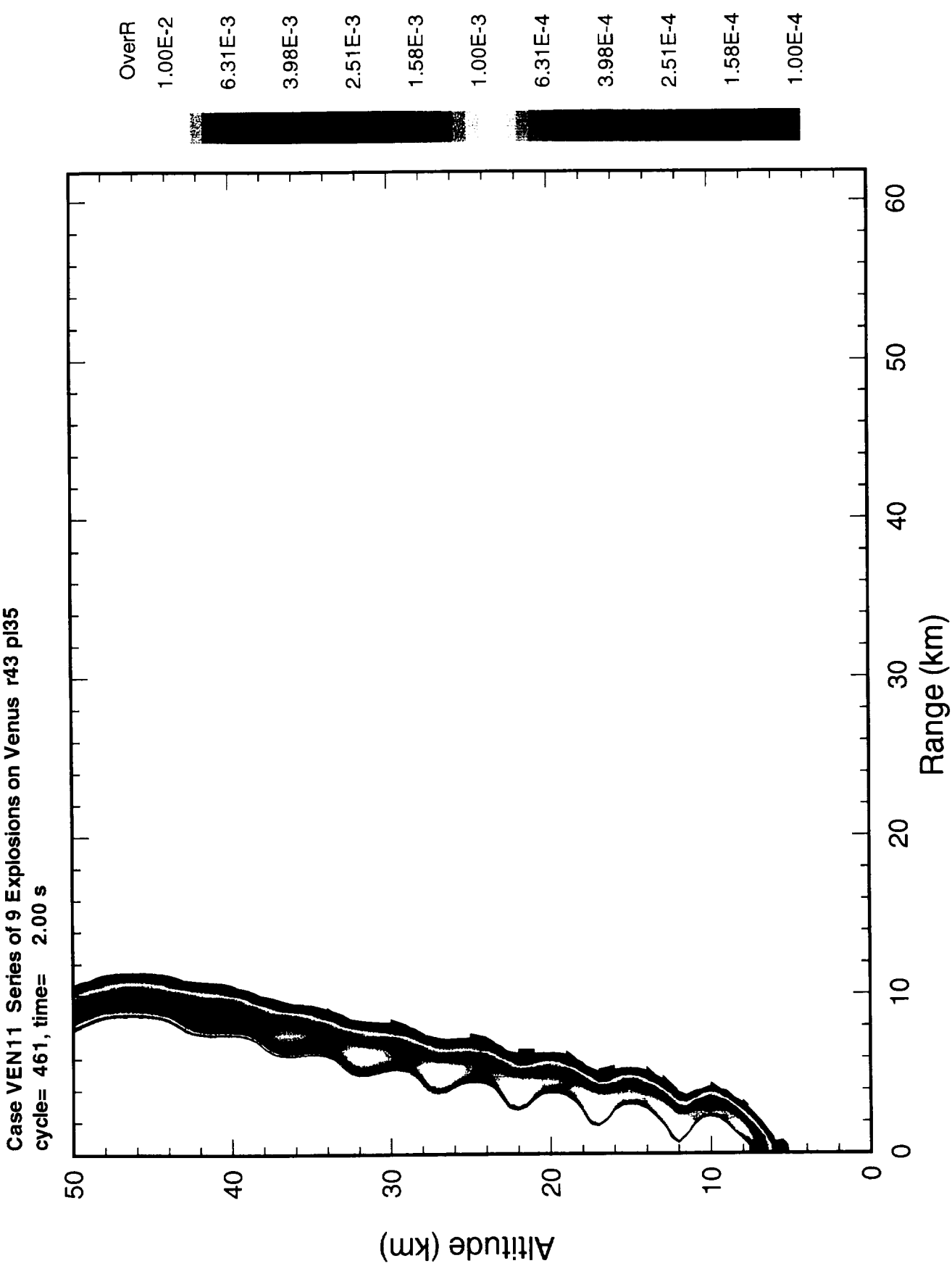
Case VEN11 Series of 9 Explosions on Venus r43 pl35
cycle= 461, time= 2.00 s
OverR
1.00E-2
6.31E-3
3.98E-3
2.51E-3
1.58E-3
1.00E-3
6.31E-4
3.98E-4
2.51E-4
1.58E-4
1.00E-4
Altitude (km)
0
10
20
30
40
50
Range (km)
0
10
20
30
40
50
60

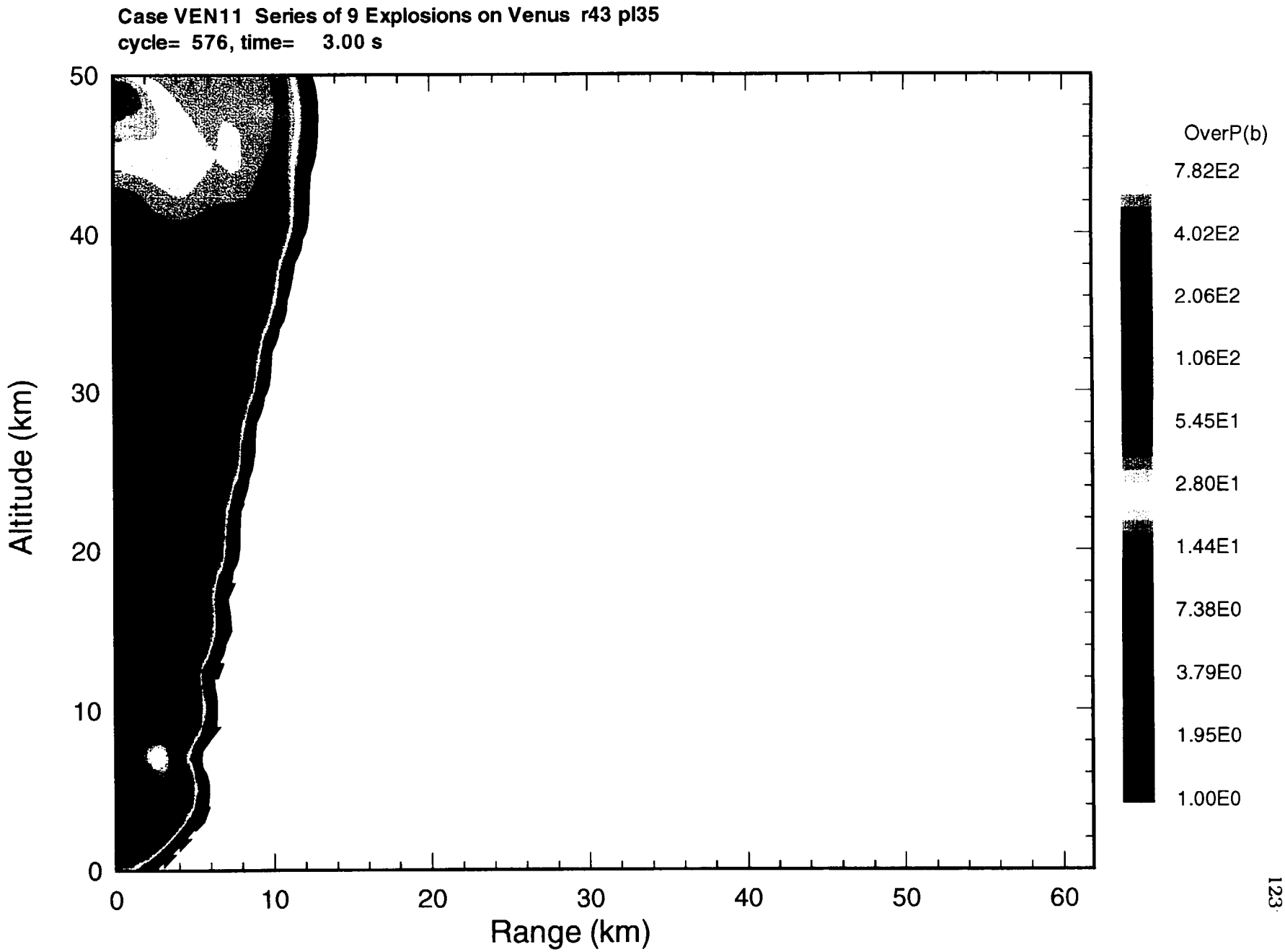
Case VEN11 Series of 9 Explosions on Venus r43 pl35
cycle= 576, time= 3.00 s
Altitude (km)
Range (km)
0
10
20
30
40
50
60
OverP(b)
7.82E2
4.02E2
2.06E2
1.06E2
5.45E1
2.80E1
1.44E1
7.38E0
3.79E0
1.95E0
1.00E0

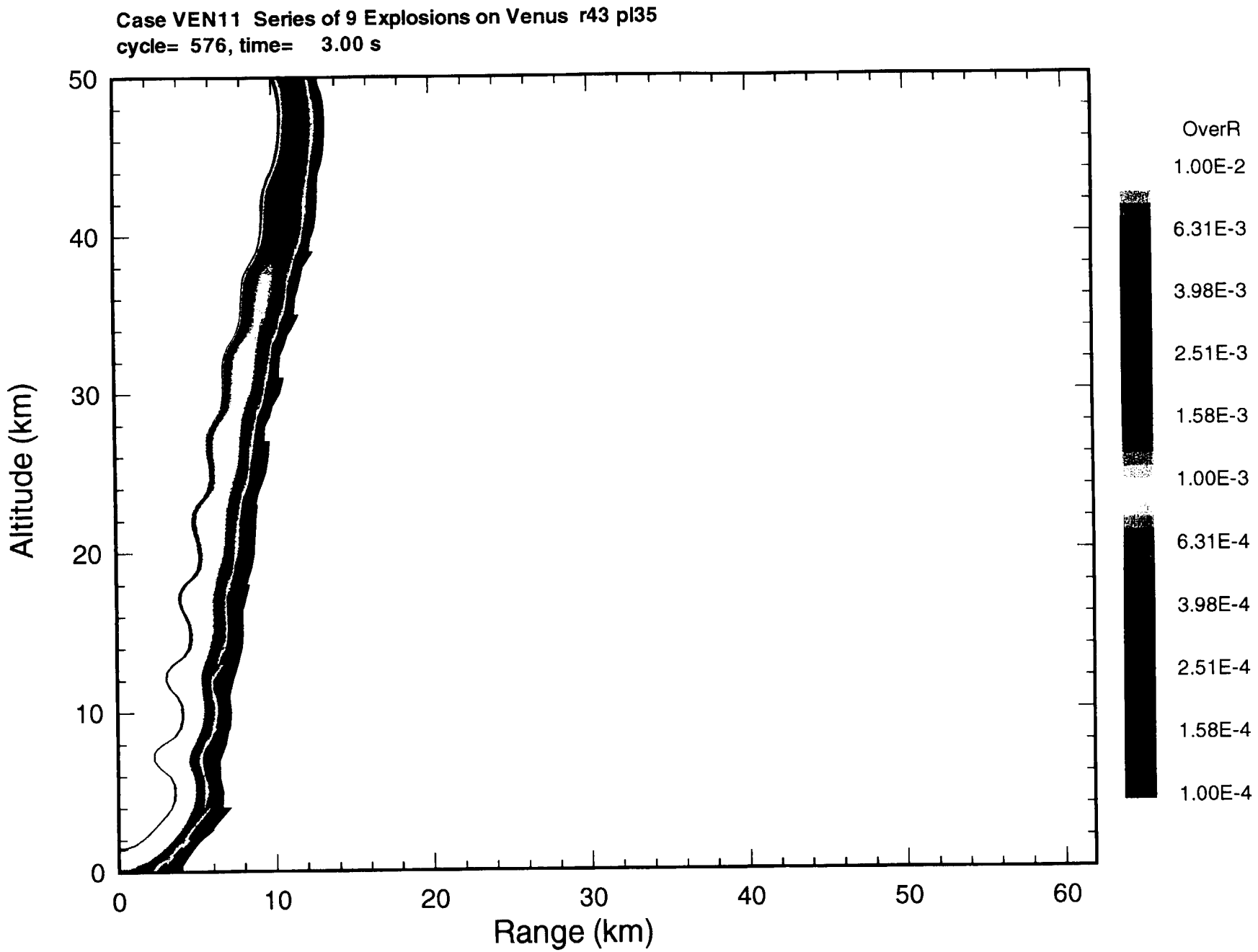
Case VEN11 Series of 9 Explosions on Venus r43 pl35
cycle= 576, time= 3.00 s
Altitude (km)
Range (km)
0
10
20
30
40
50
60
OverR
1.00E-2
6.31E-3
3.98E-3
2.51E-3
1.58E-3
1.00E-3
6.31E-4
3.98E-4
2.51E-4
1.58E-4
1.00E-4

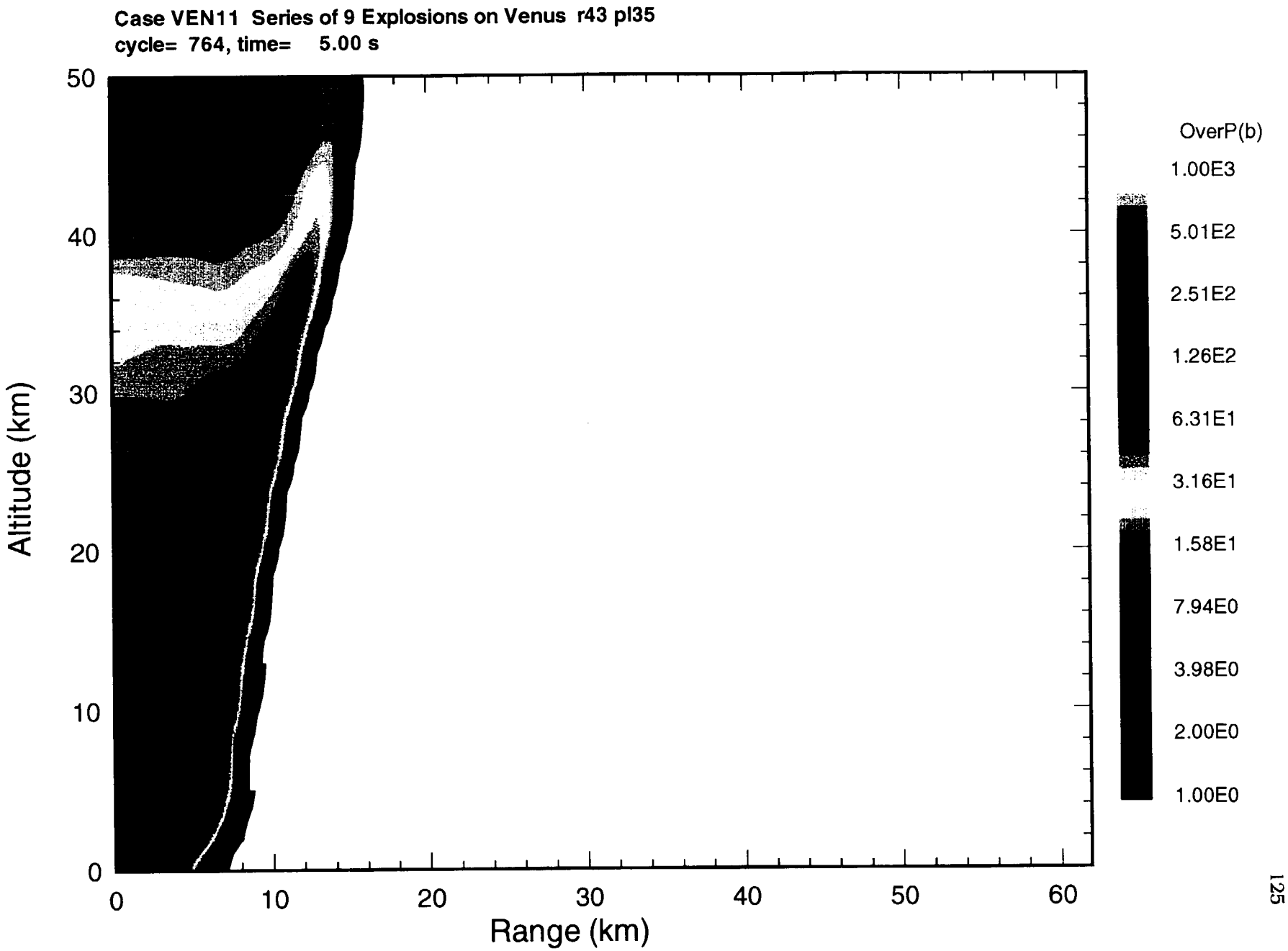
Case VEN11 Series of 9 Explosions on Venus r43 pl35
cycle= 764, time= 5.00 s
Altitude (km)
0
10
20
30
40
50
Range (km)
0
10
20
30
40
50
60
OverP(b)
1.00E3
5.01E2
2.51E2
1.26E2
6.31E1
3.16E1
1.58E1
7.94E0
3.98E0
2.00E0
1.00E0

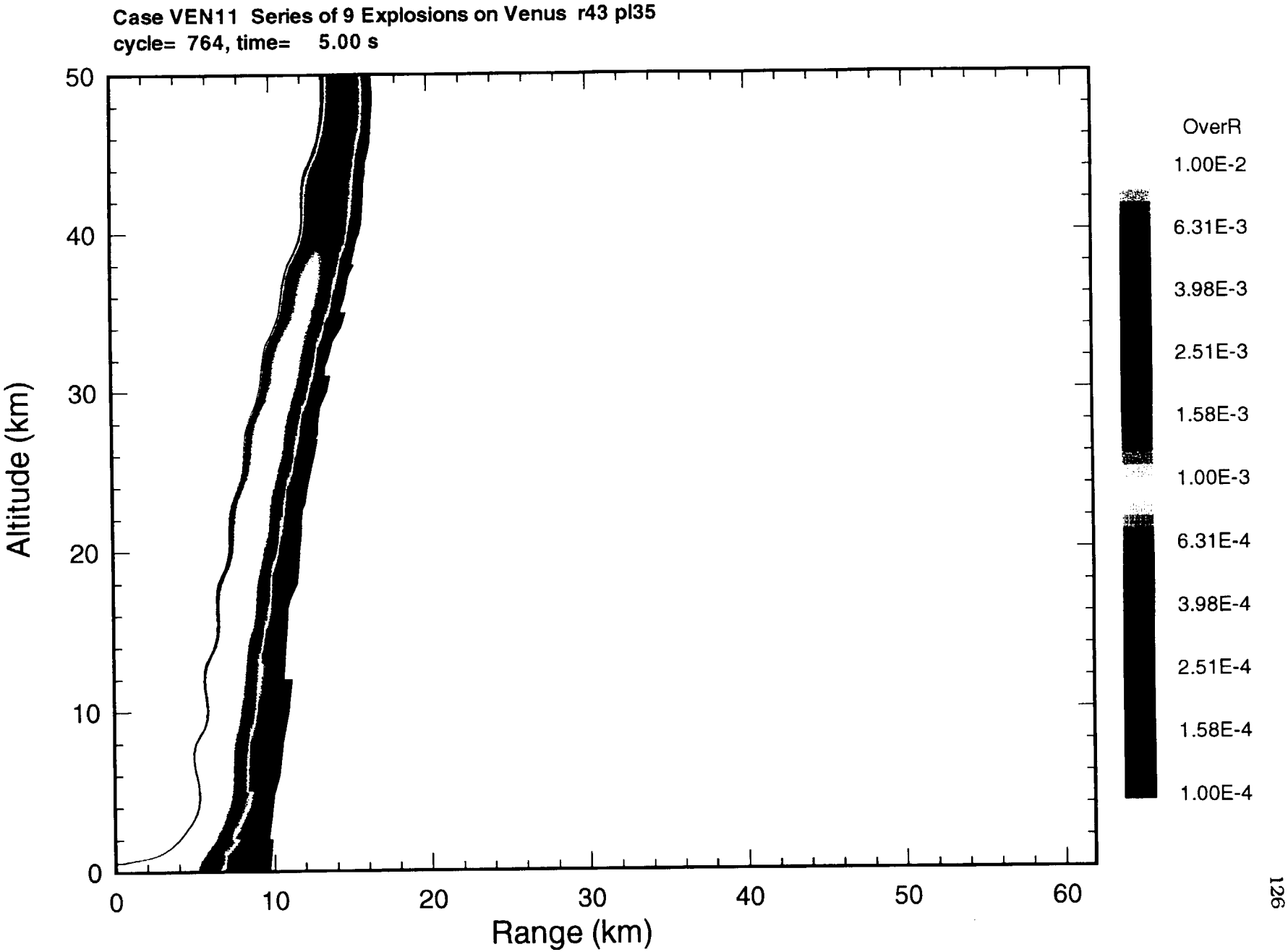
Case VEN11 Series of 9 Explosions on Venus r43 pl35
cycle= 764, time= 5.00 s
Altitude (km)
Range (km)
0
10
20
30
40
50
60
OverR
1.00E-2
6.31E-3
3.98E-3
2.51E-3
1.58E-3
1.00E-3
6.31E-4
3.98E-4
2.51E-4
1.58E-4
1.00E-4

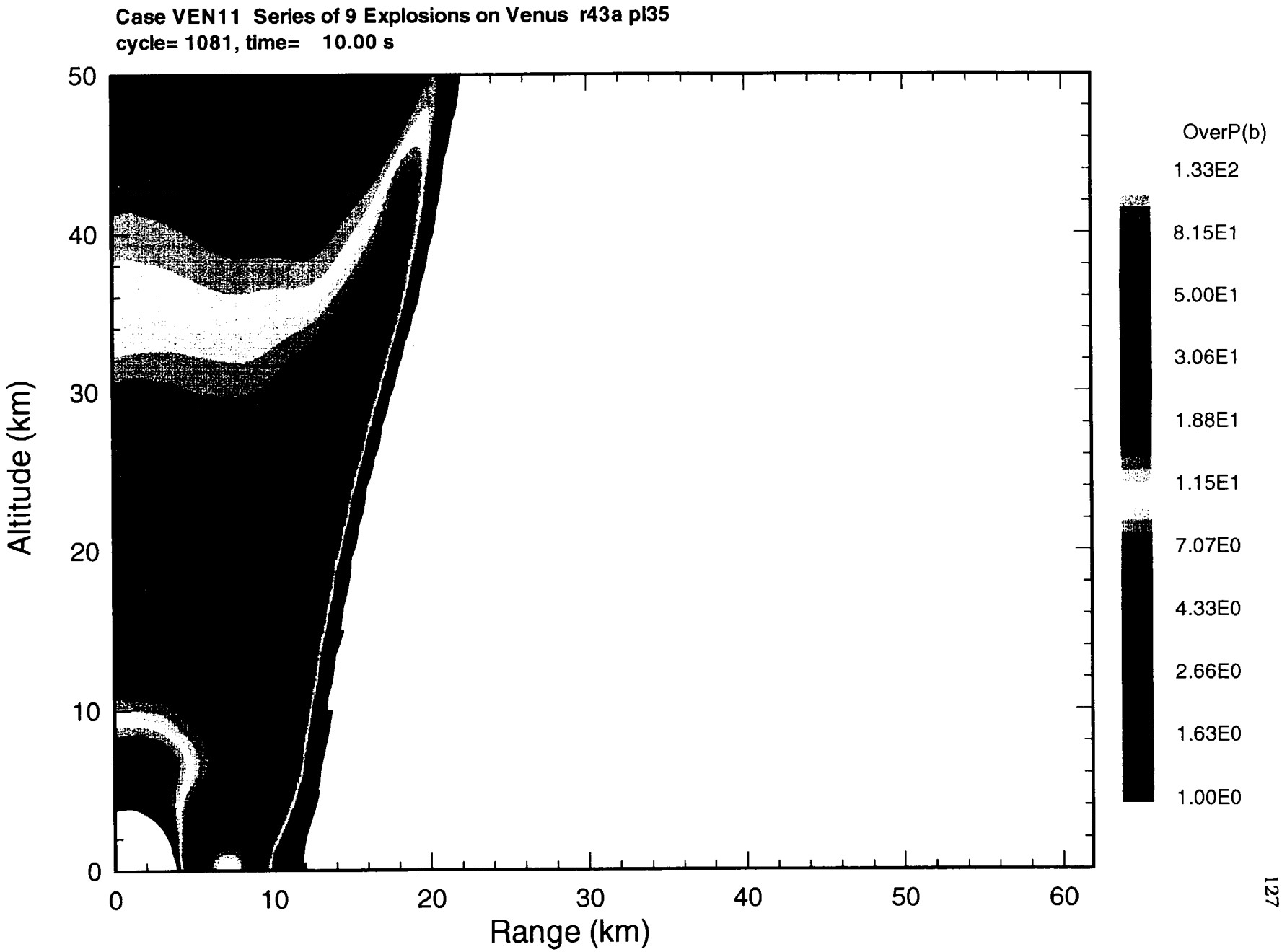
Case VEN11 Series of 9 Explosions on Venus r43a pl35
cycle= 1081, time= 10.00 s
Altitude (km)
Range (km)
0
10
20
30
40
50
60
OverP(b)
1.33E2
8.15E1
5.00E1
3.06E1
1.88E1
1.15E1
7.07E0
4.33E0
2.66E0
1.63E0
1.00E0

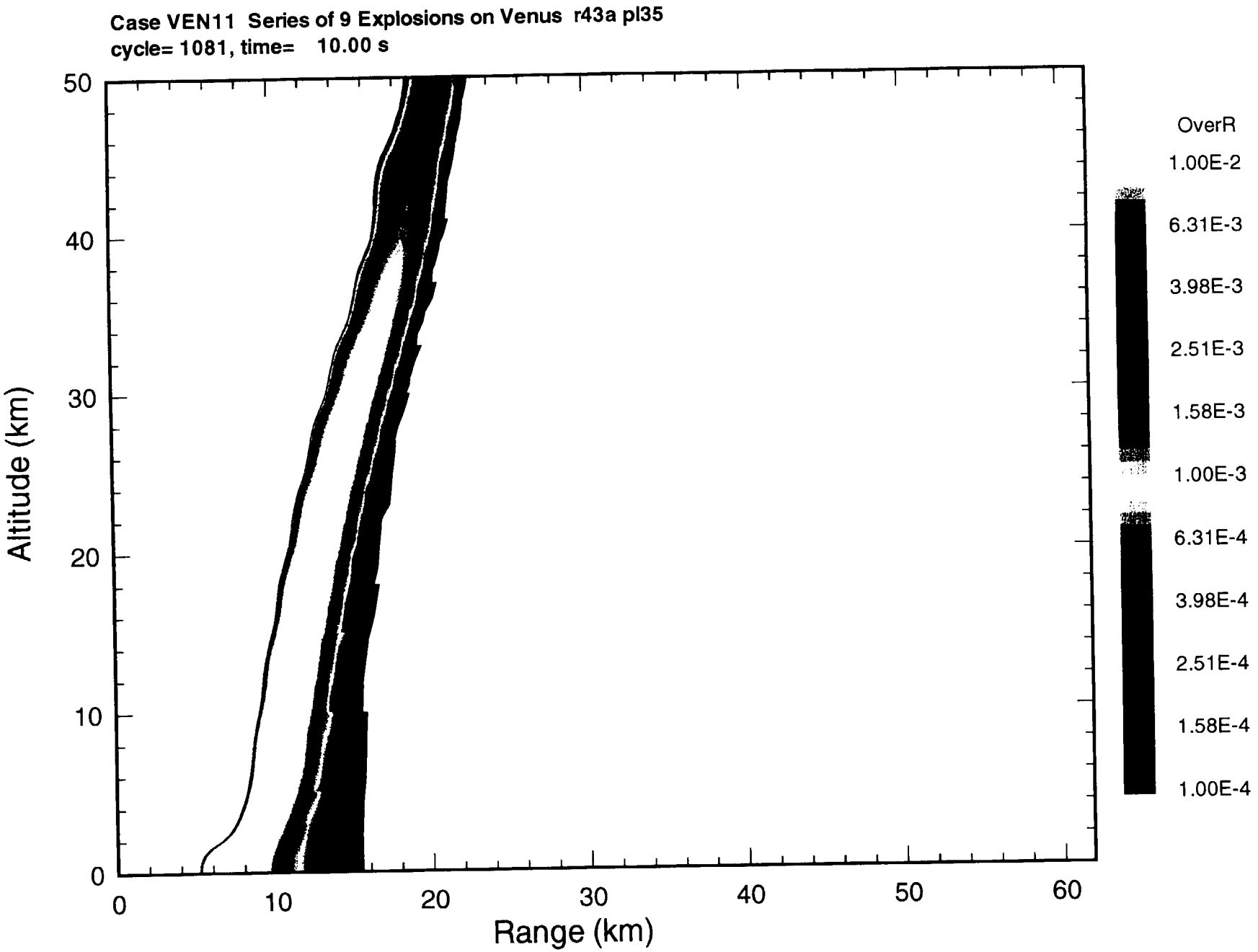
Case VEN11 Series of 9 Explosions on Venus r43a pl35
cycle= 1081, time= 10.00 s
Altitude (km)
Range (km)
0
10
20
30
40
50
60
OverR
1.00E-2
6.31E-3
3.98E-3
2.51E-3
1.58E-3
1.00E-3
6.31E-4
3.98E-4
2.51E-4
1.58E-4
1.00E-4

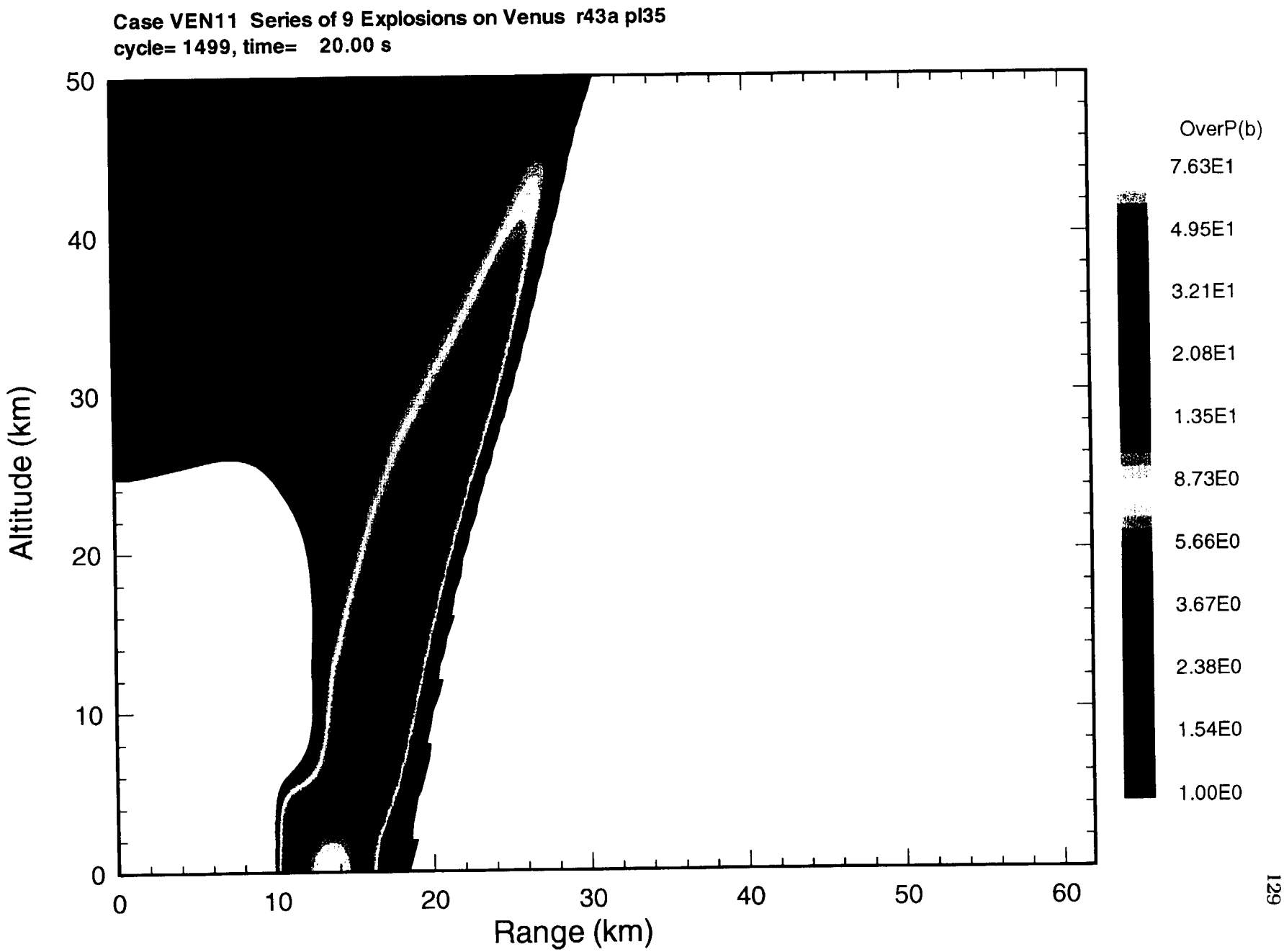
Case VEN11 Series of 9 Explosions on Venus r43a pl35
cycle= 1499, time= 20.00 s
Altitude (km)
Range (km)
0
10
20
30
40
50
60
OverP(b)
7.63E1
4.95E1
3.21E1
2.08E1
1.35E1
8.73E0
5.66E0
3.67E0
2.38E0
1.54E0
1.00E0

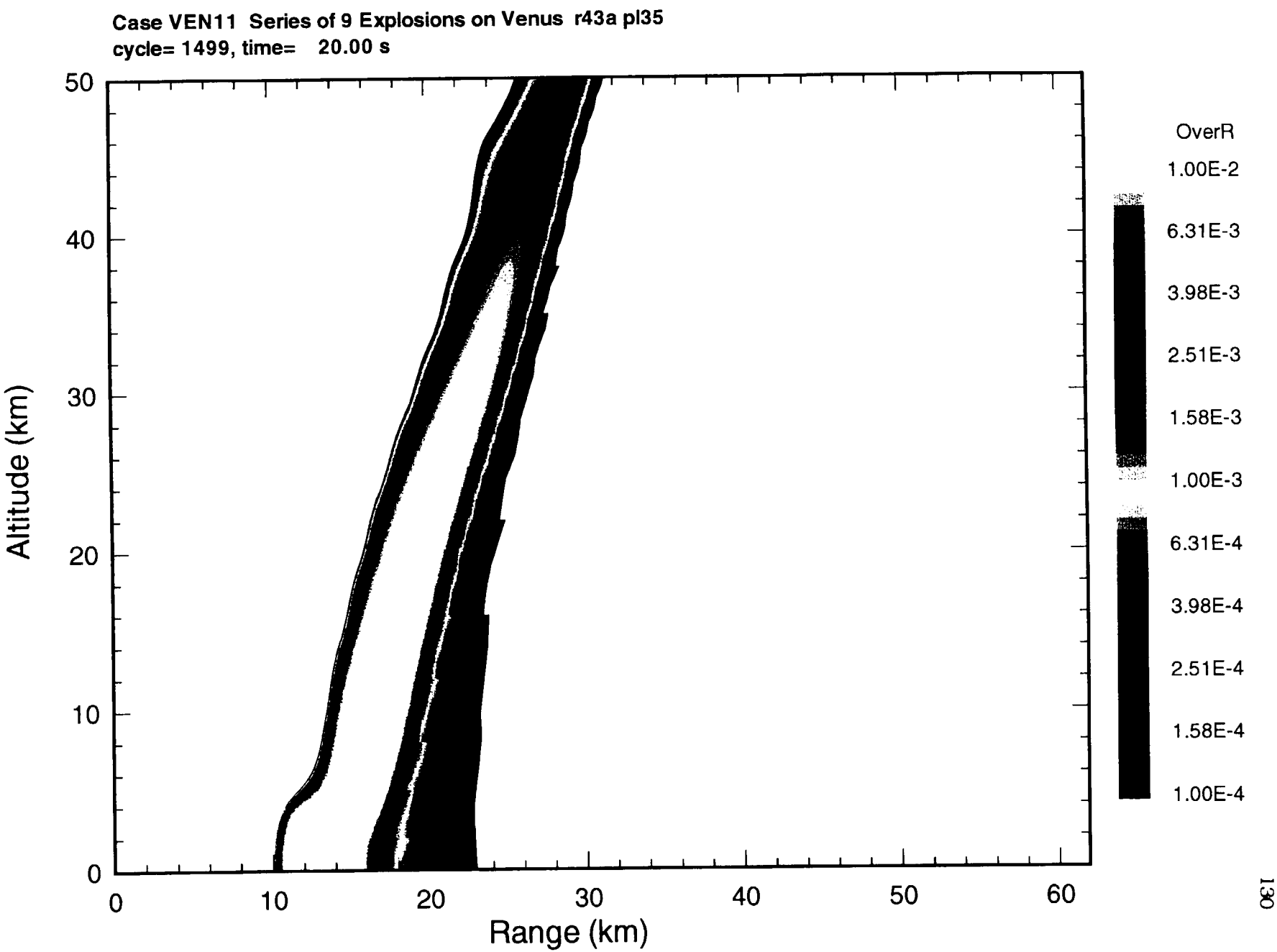
Case VEN11 Series of 9 Explosions on Venus r43a pl35
cycle= 1499, time= 20.00 s
Altitude (km)
Range (km)
0
10
20
30
40
50
60
OverR
1.00E-2
6.31E-3
3.98E-3
2.51E-3
1.58E-3
1.00E-3
6.31E-4
3.98E-4
2.51E-4
1.58E-4
1.00E-4

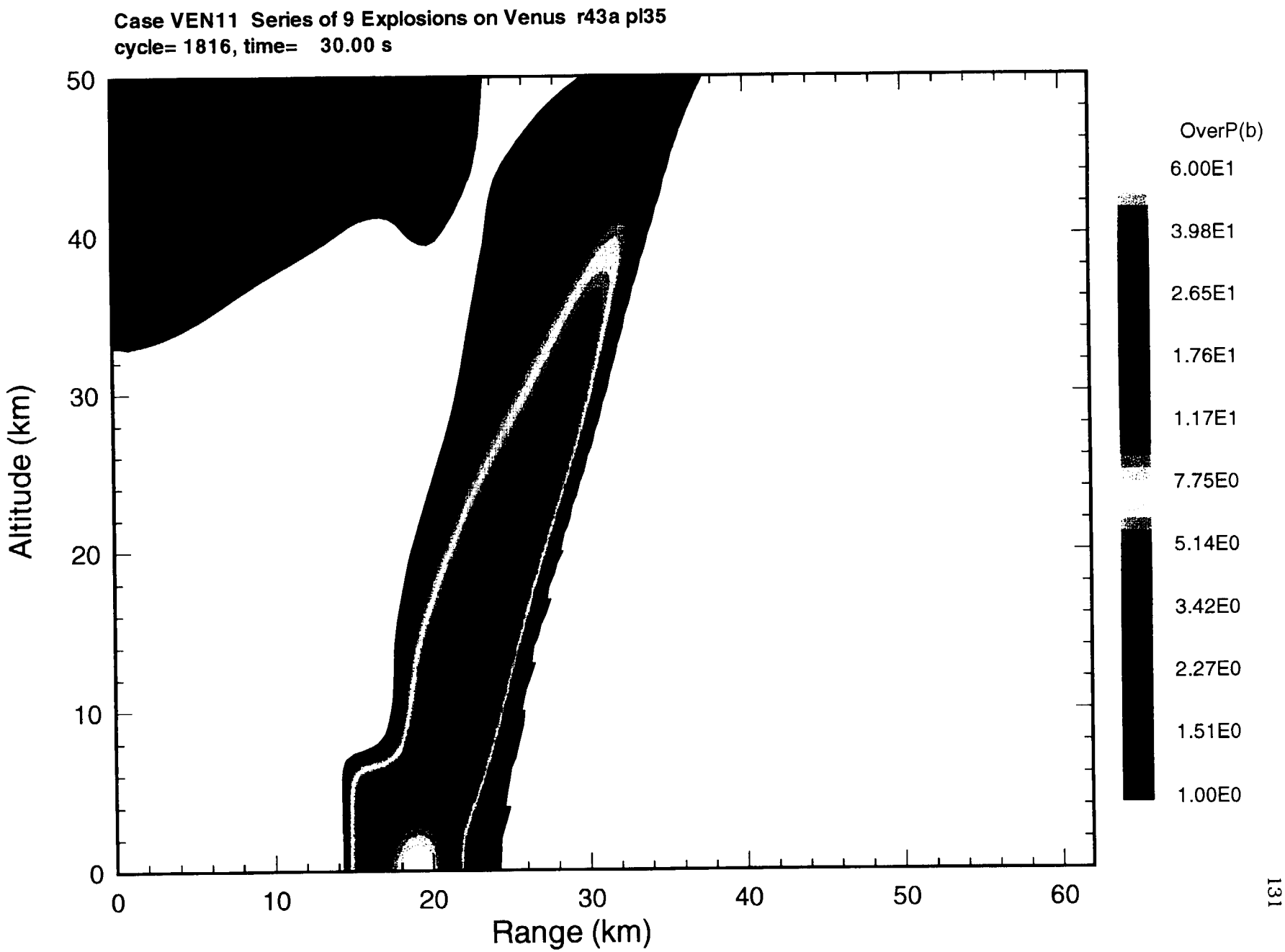
Case VEN11 Series of 9 Explosions on Venus r43a pl35
cycle= 1816, time= 30.00 s
Altitude (km)
Range (km)
0
10
20
30
40
50
60
OverP(b)
6.00E1
3.98E1
2.65E1
1.76E1
1.17E1
7.75E0
5.14E0
3.42E0
2.27E0
1.51E0
1.00E0

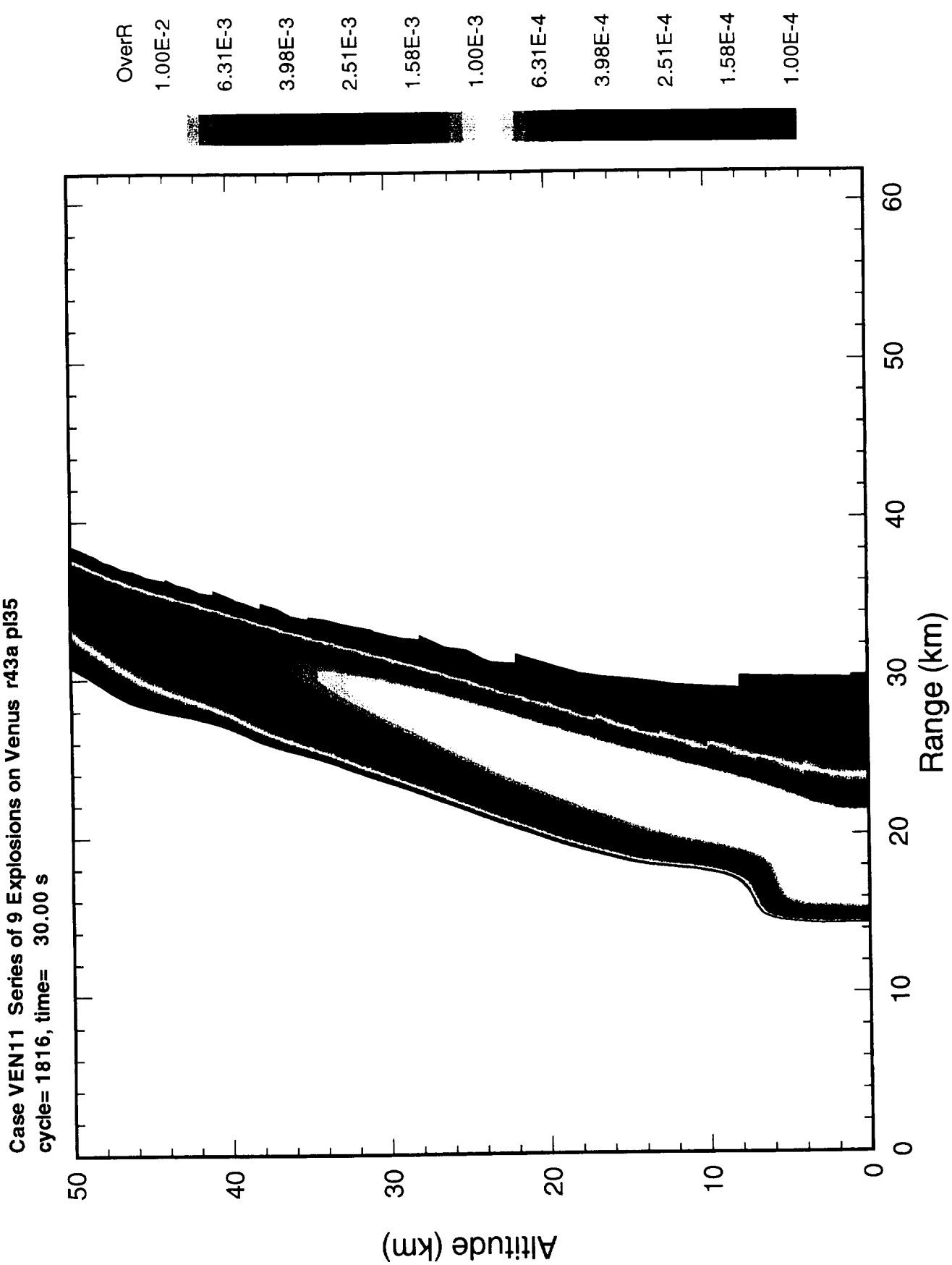
Case VEN11 Series of 9 Explosions on Venus r43a pl35
cycle= 1816, time= 30.00 s
OverR
1.00E-2
6.31E-3
3.98E-3
2.51E-3
1.58E-3
1.00E-3
6.31E-4
3.98E-4
2.51E-4
1.58E-4
1.00E-4
Altitude (km)
Range (km)
0
10
20
30
40
50
60

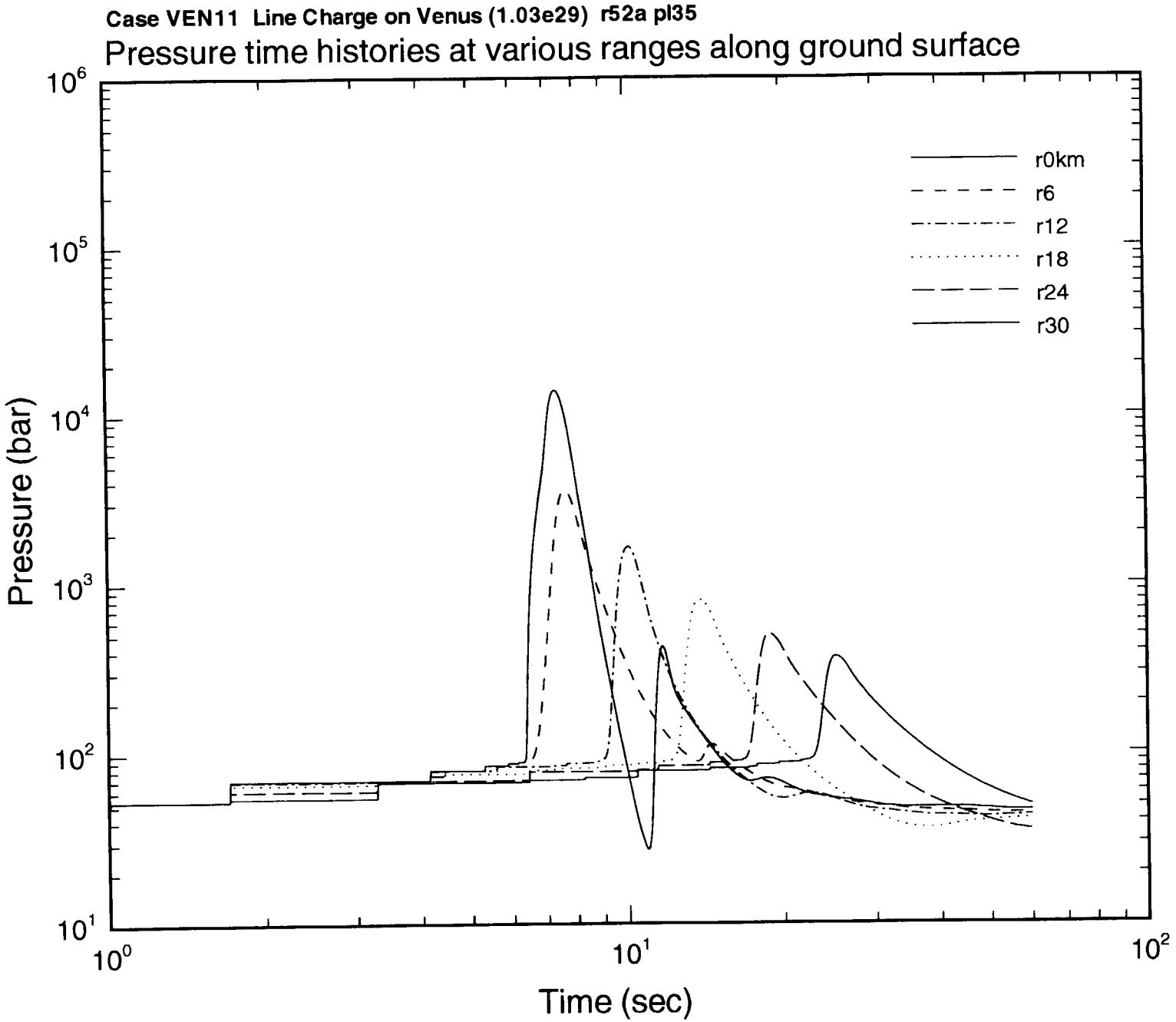
Case VEN11 Line Charge on Venus (1.03e29) r52a pl35
Pressure time histories at various ranges along ground surface
r0km
r6
r12
r18
r24
r30
Pressure (bar)
Time (sec)
10^6
10^5
10^4
10^3
10^2
10^1
10^0
10^1
10^2

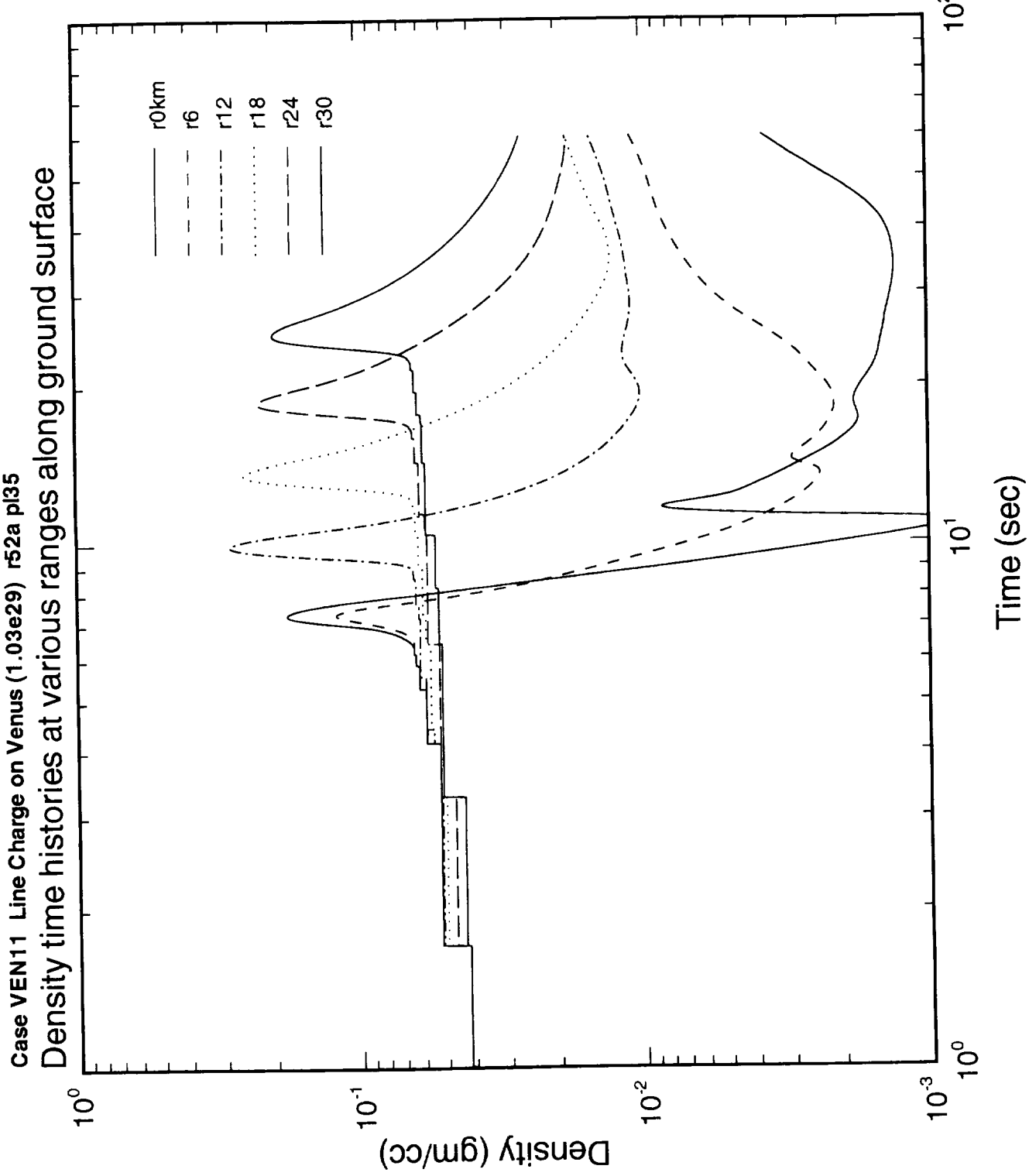
Case VEN11 Line Charge on Venus (1.03e29) r52a pl35
Density time histories at various ranges along ground surface
r0km
r6
r12
r18
r24
r30
Density (gm/cc)
Time (sec)
10^0
10^-1
10^-2
10^-3
10^0
10^1
10^2

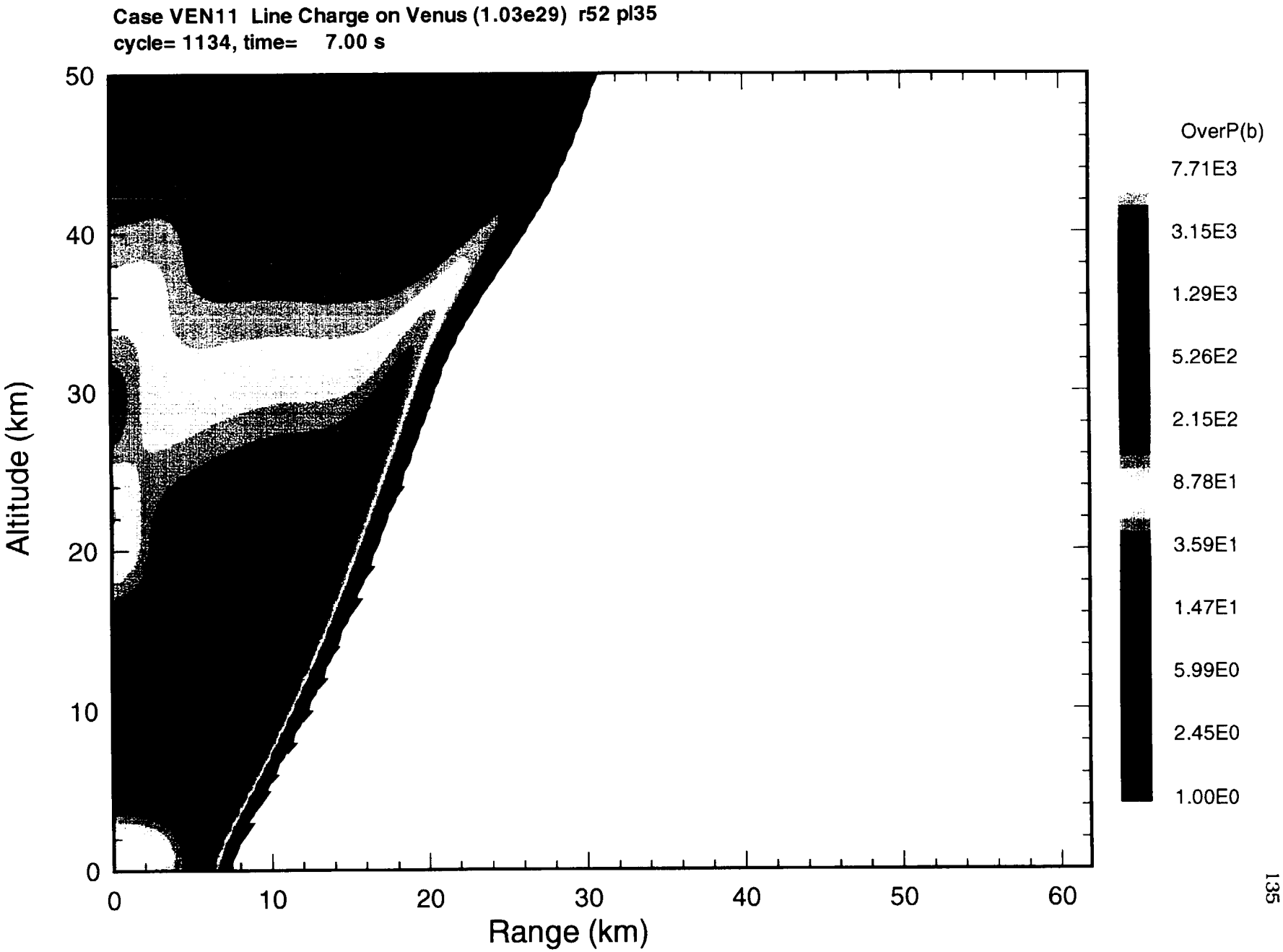
Case VEN11 Line Charge on Venus (1.03e29) r52 pl35
cycle= 1134, time= 7.00 s
Altitude (km)
Range (km)
0
10
20
30
40
50
60
OverP(b)
7.71E3
3.15E3
1.29E3
5.26E2
2.15E2
8.78E1
3.59E1
1.47E1
5.99E0
2.45E0
1.00E0

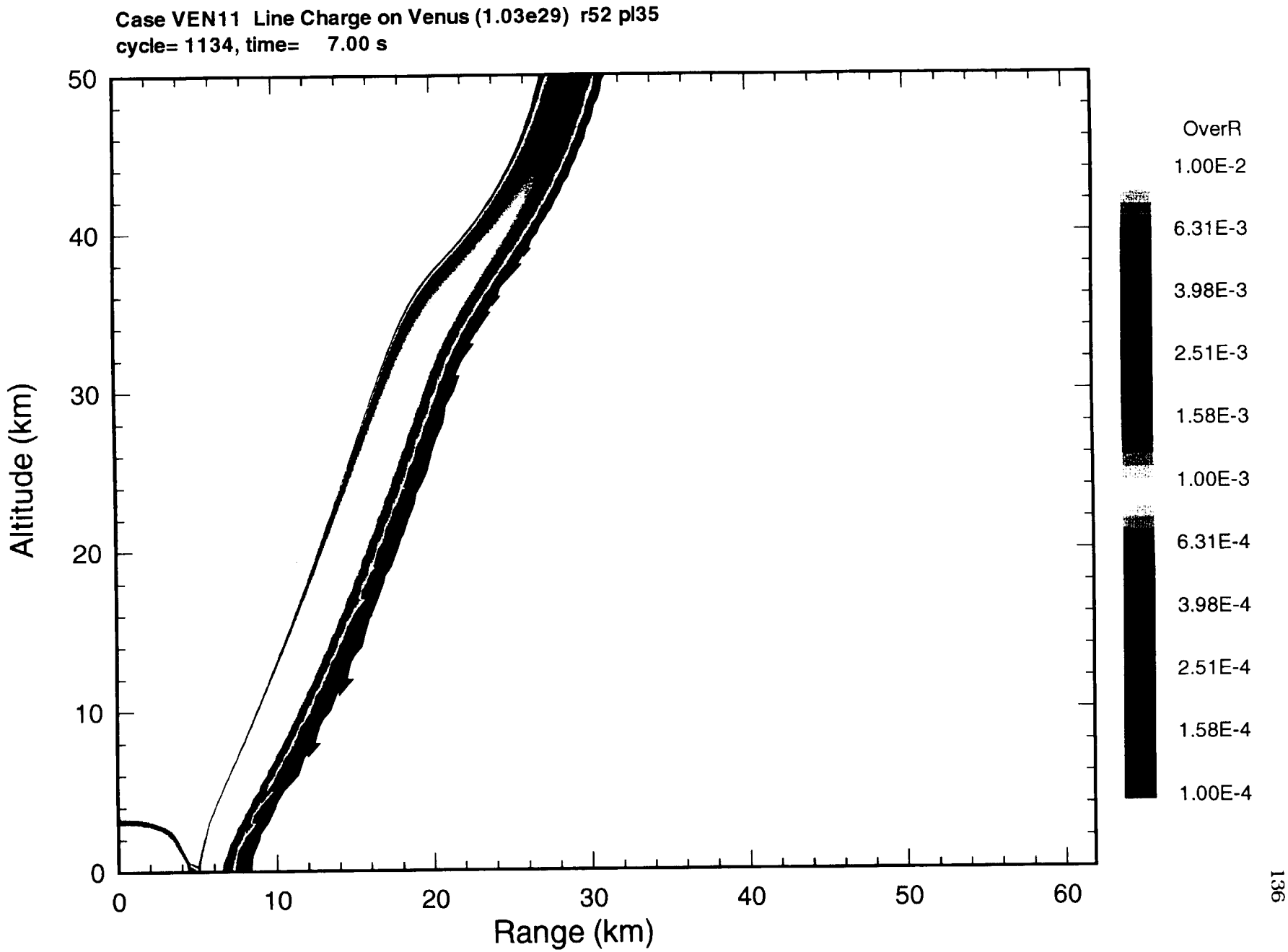
Case VEN11 Line Charge on Venus (1.03e29) r52 pl35
cycle= 1134, time= 7.00 s
Altitude (km)
Range (km)
0
10
20
30
40
50
60
OverR
1.00E-2
6.31E-3
3.98E-3
2.51E-3
1.58E-3
1.00E-3
6.31E-4
3.98E-4
2.51E-4
1.58E-4
1.00E-4

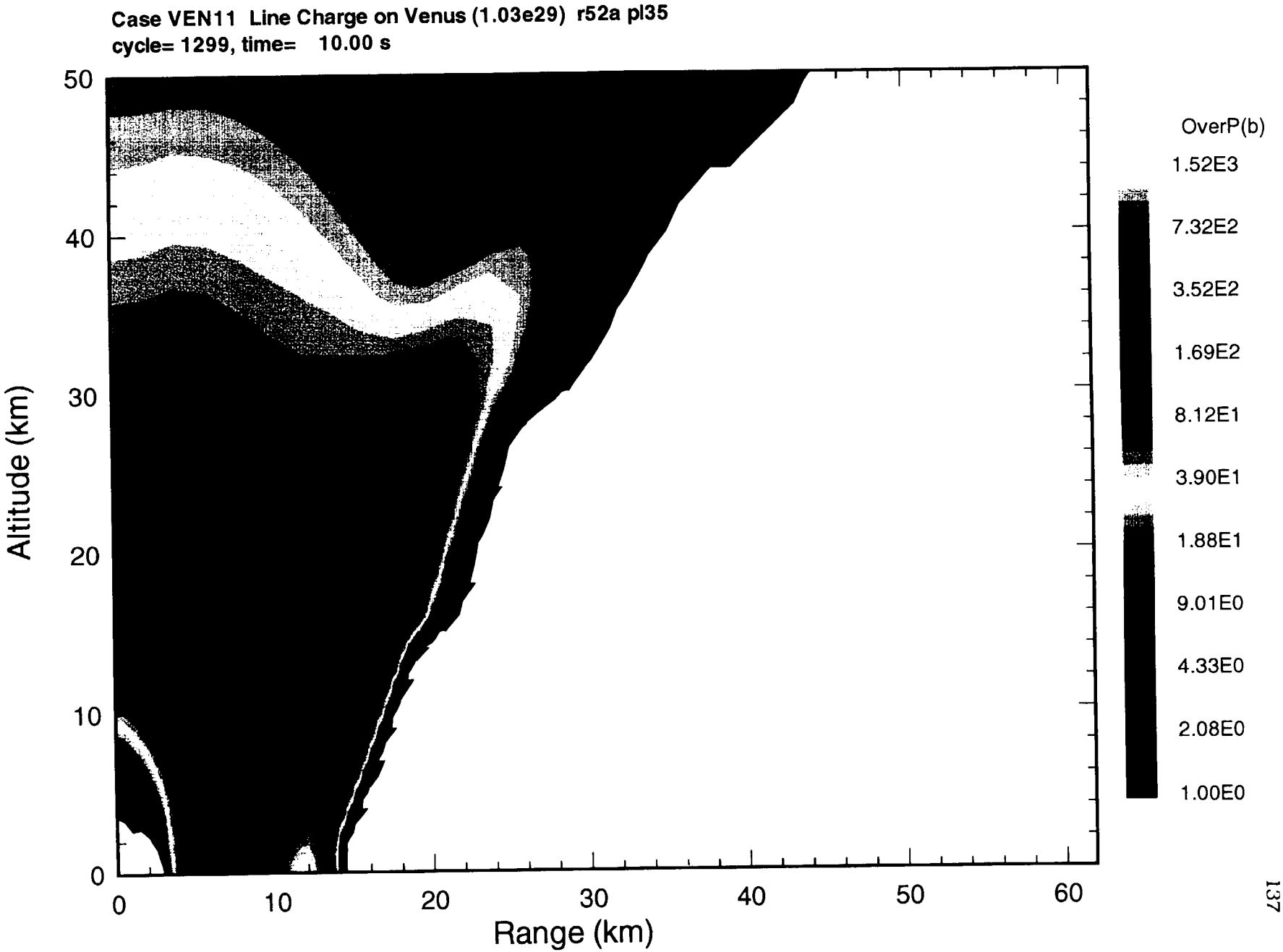
Case VEN11 Line Charge on Venus (1.03e29) r52a pl35
cycle= 1299, time= 10.00 s
Altitude (km)
Range (km)
0
10
20
30
40
50
60
OverP(b)
1.52E3
7.32E2
3.52E2
1.69E2
8.12E1
3.90E1
1.88E1
9.01E0
4.33E0
2.08E0
1.00E0

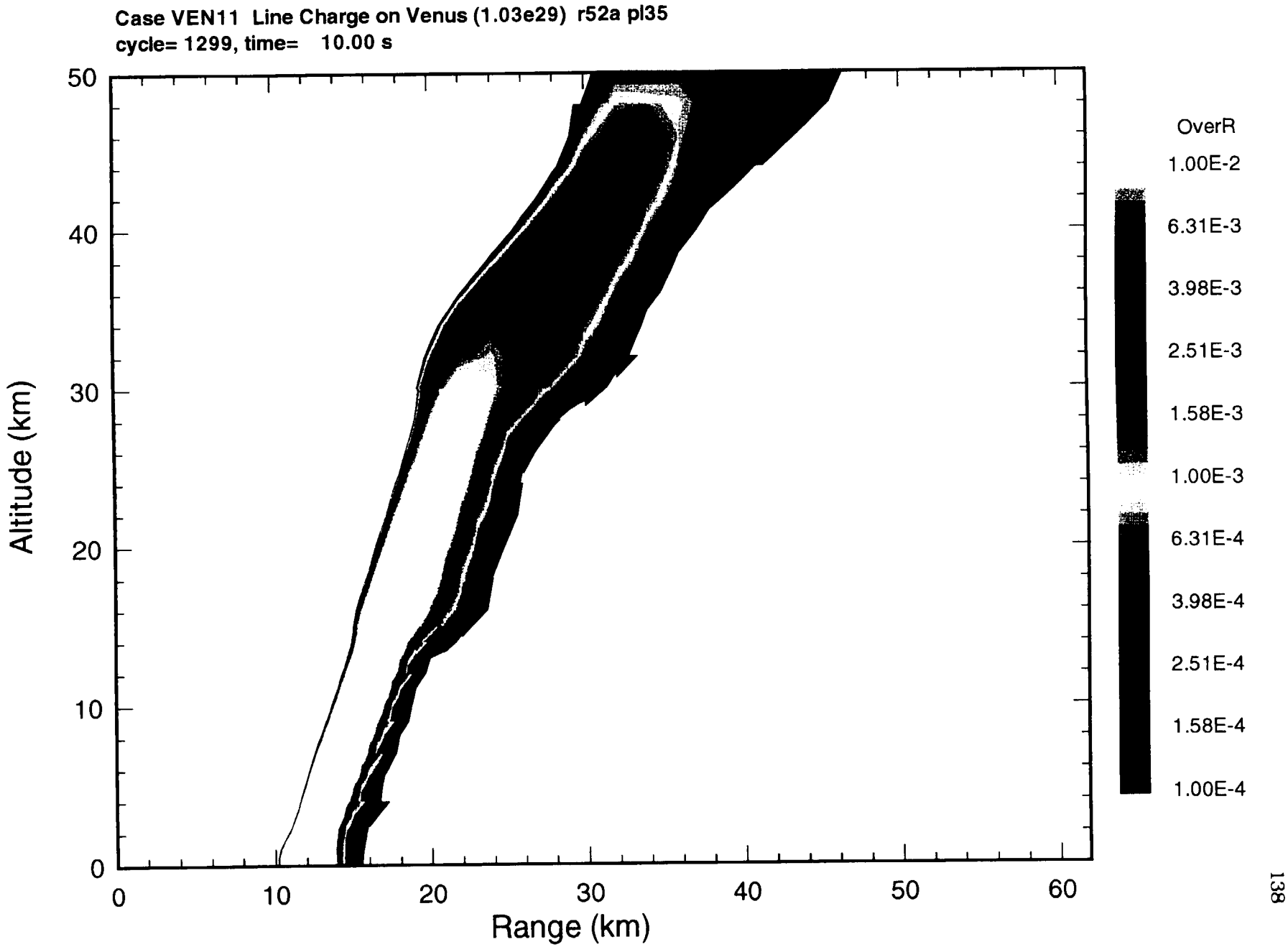
Case VEN11 Line Charge on Venus (1.03e29) r52a pl35
cycle= 1299, time= 10.00 s
Altitude (km)
Range (km)
0
10
20
30
40
50
60
OverR
1.00E-2
6.31E-3
3.98E-3
2.51E-3
1.58E-3
1.00E-3
6.31E-4
3.98E-4
2.51E-4
1.58E-4
1.00E-4

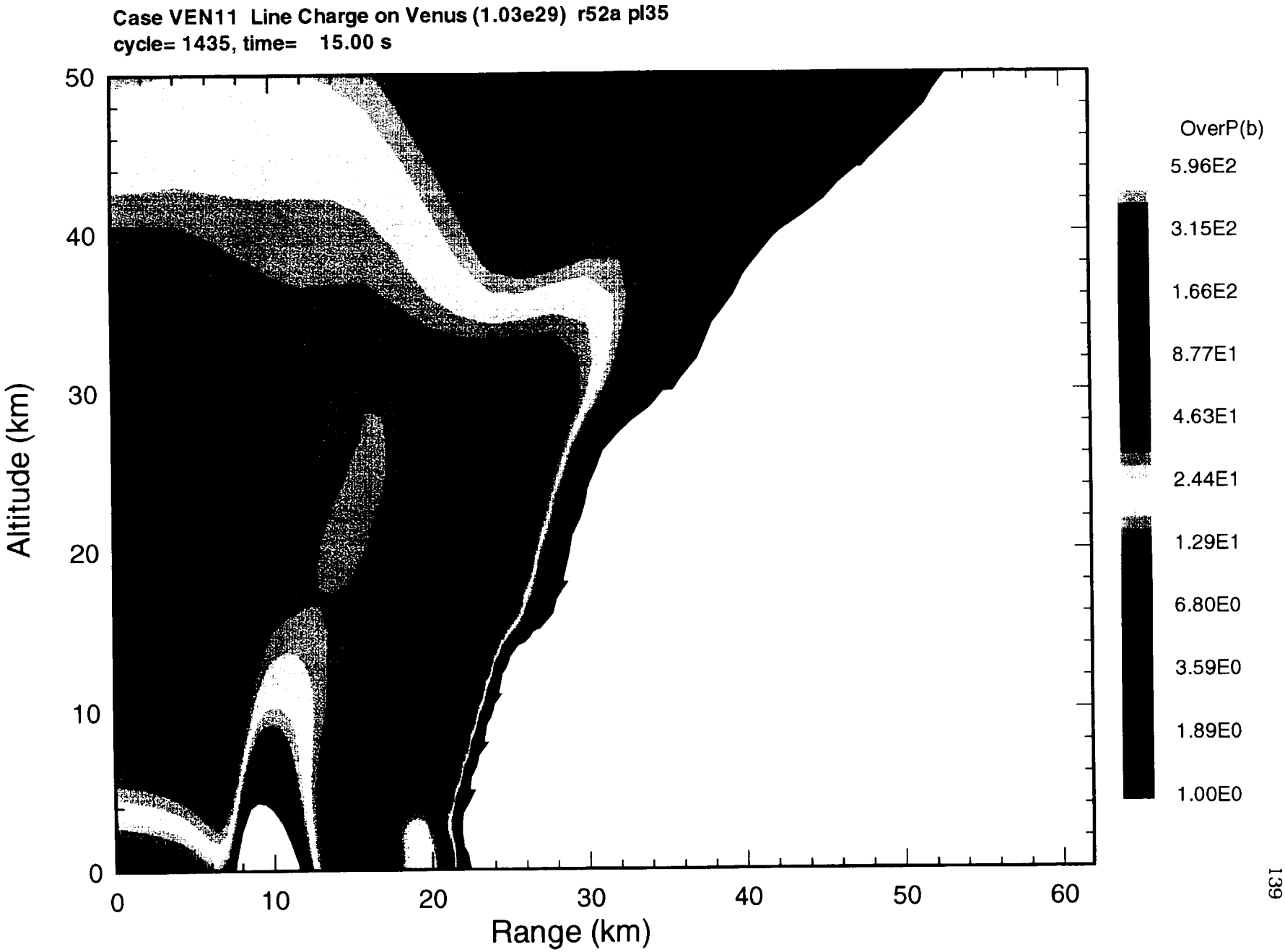
Case VEN11 Line Charge on Venus (1.03e29) r52a pl35
cycle= 1435, time= 15.00 s
Altitude (km)
Range (km)
0
10
20
30
40
50
60
OverP(b)
5.96E2
3.15E2
1.66E2
8.77E1
4.63E1
2.44E1
1.29E1
6.80E0
3.59E0
1.89E0
1.00E0

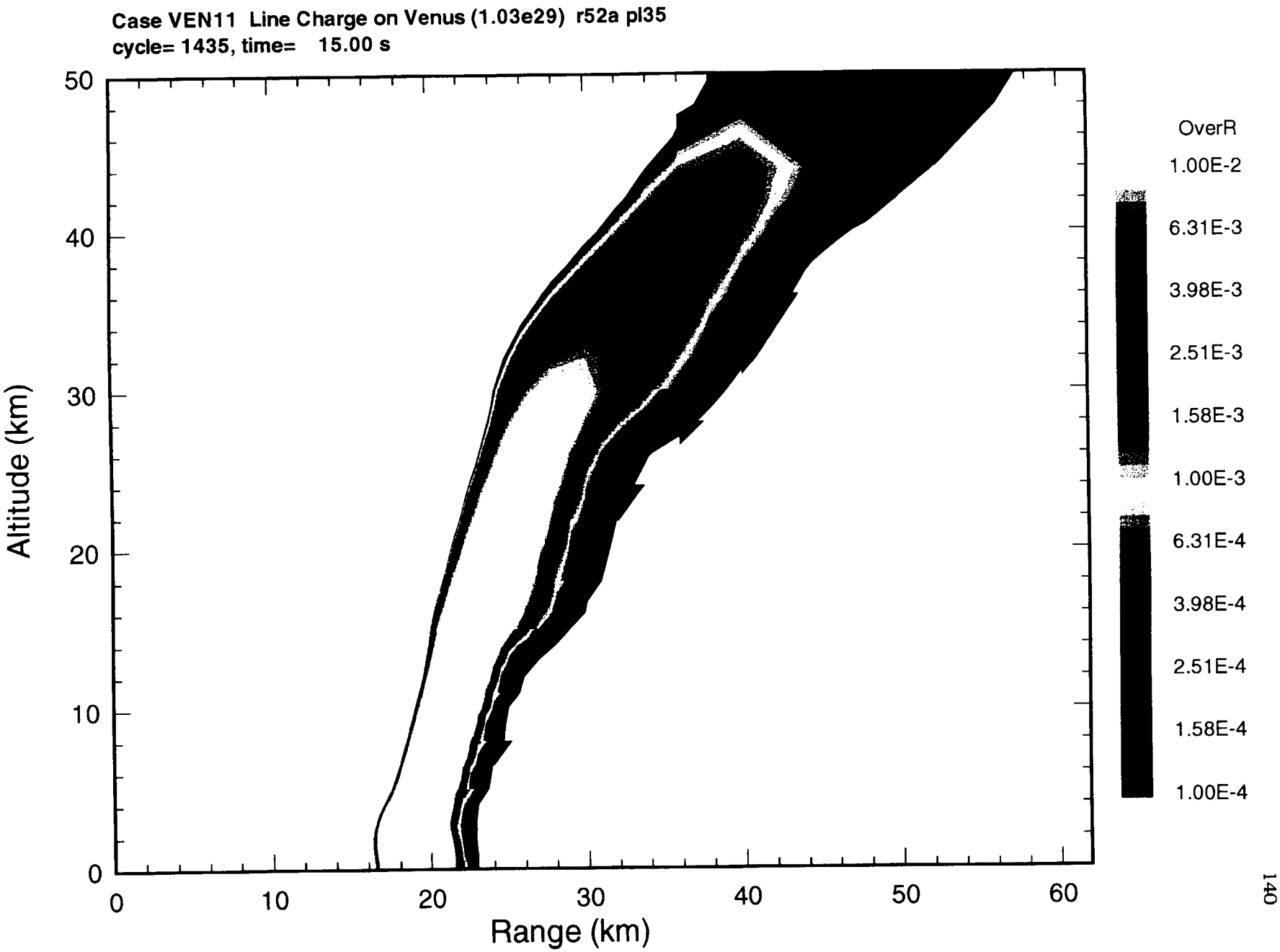
Case VEN11 Line Charge on Venus (1.03e29) r52a pl35
cycle= 1435, time= 15.00 s
Altitude (km)
Range (km)
0
10
20
30
40
50
60
OverR
1.00E-2
6.31E-3
3.98E-3
2.51E-3
1.58E-3
1.00E-3
6.31E-4
3.98E-4
2.51E-4
1.58E-4
1.00E-4

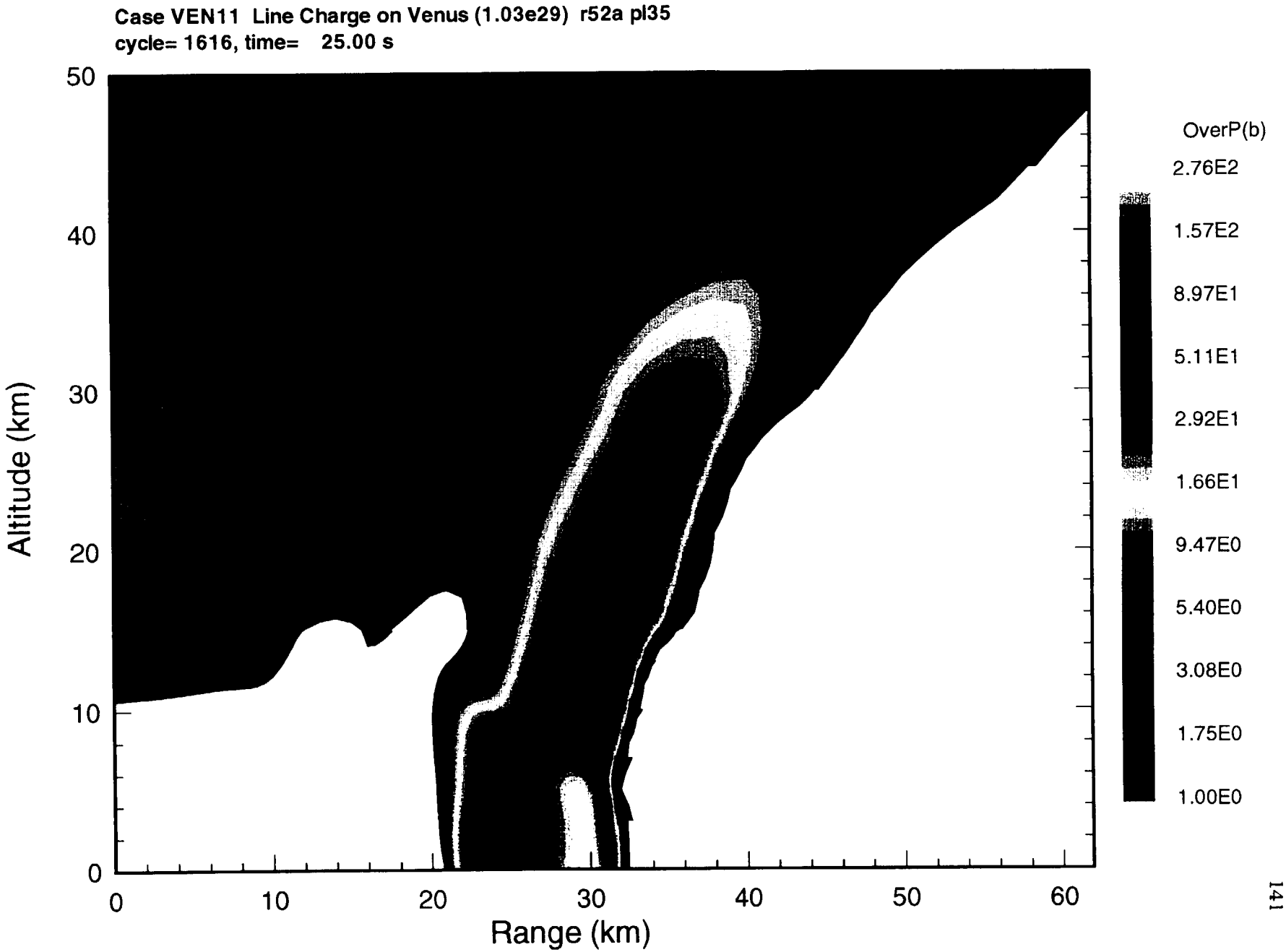
Case VEN11 Line Charge on Venus (1.03e29) r52a pl35
cycle= 1616, time= 25.00 s
Altitude (km)
Range (km)
0
10
20
30
40
50
60
OverP(b)
2.76E2
1.57E2
8.97E1
5.11E1
2.92E1
1.66E1
9.47E0
5.40E0
3.08E0
1.75E0
1.00E0

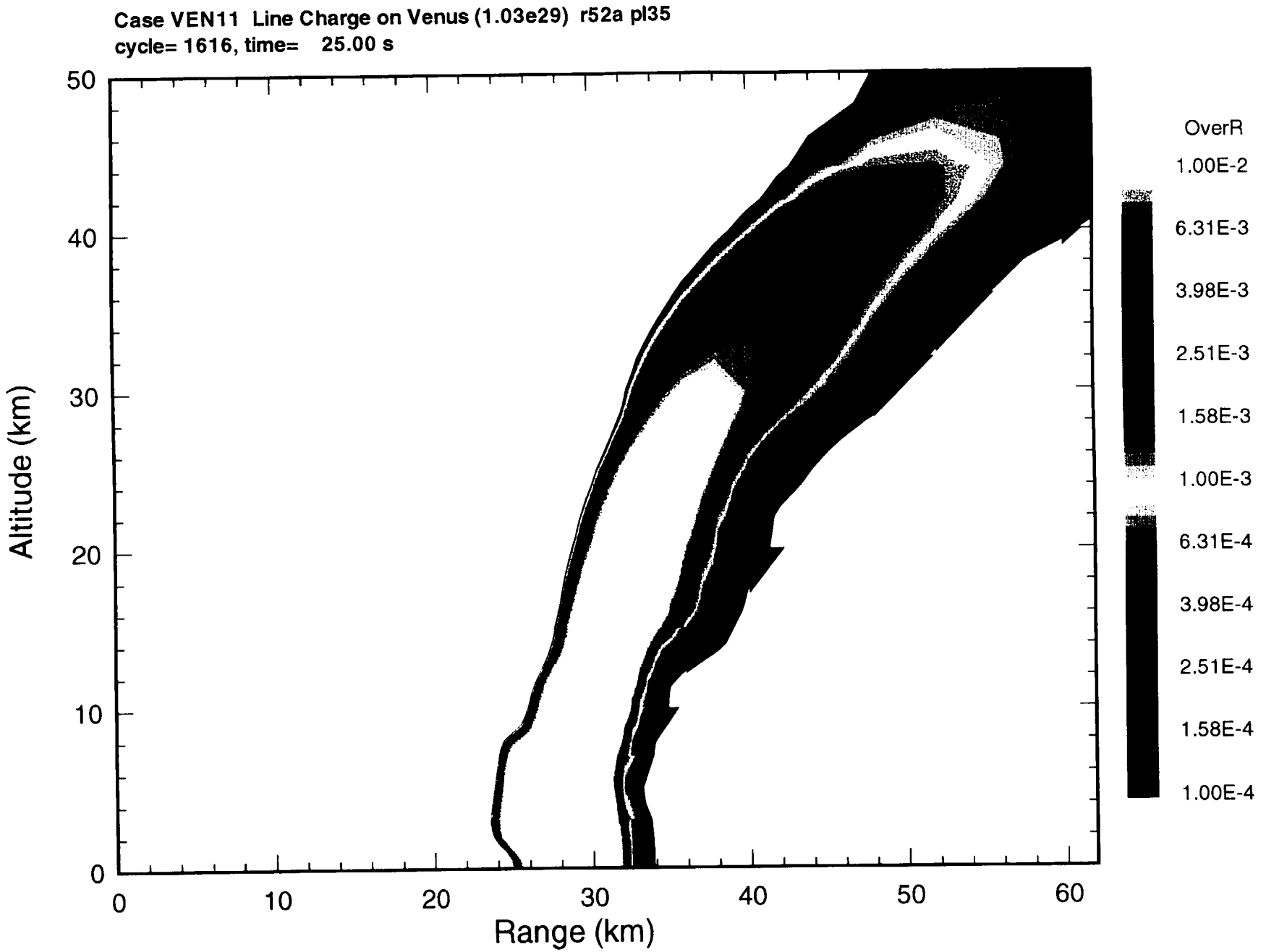
Case VEN11 Line Charge on Venus (1.03e29) r52a pl35
cycle= 1616, time= 25.00 s
Altitude (km)
Range (km)
0
10
20
30
40
50
60
OverR
1.00E-2
6.31E-3
3.98E-3
2.51E-3
1.58E-3
1.00E-3
6.31E-4
3.98E-4
2.51E-4
1.58E-4
1.00E-4

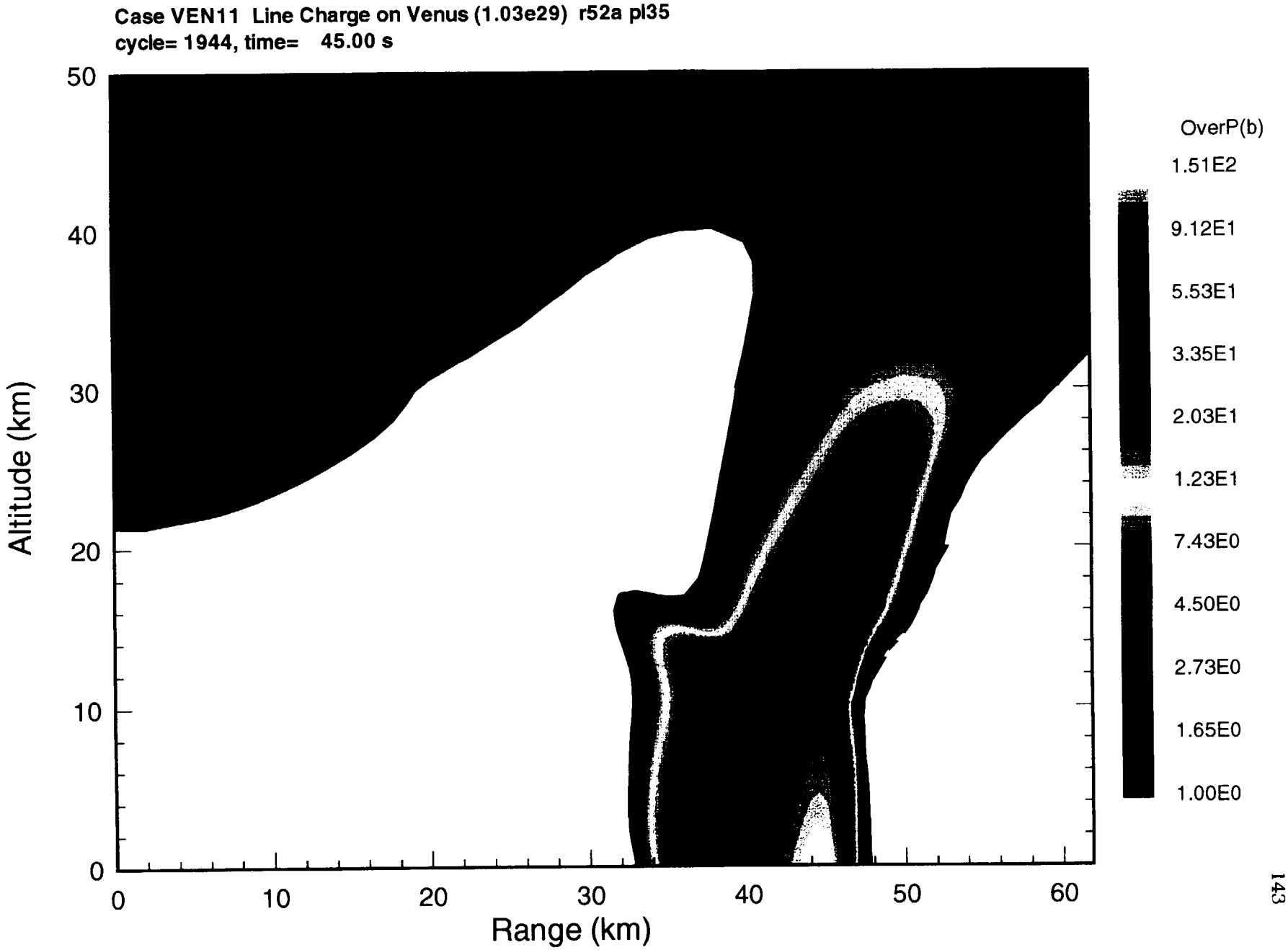
Case VEN11 Line Charge on Venus (1.03e29) r52a pl35
cycle= 1944, time= 45.00 s
Altitude (km)
Range (km)
0
10
20
30
40
50
60
OverP(b)
1.51E2
9.12E1
5.53E1
3.35E1
2.03E1
1.23E1
7.43E0
4.50E0
2.73E0
1.65E0
1.00E0

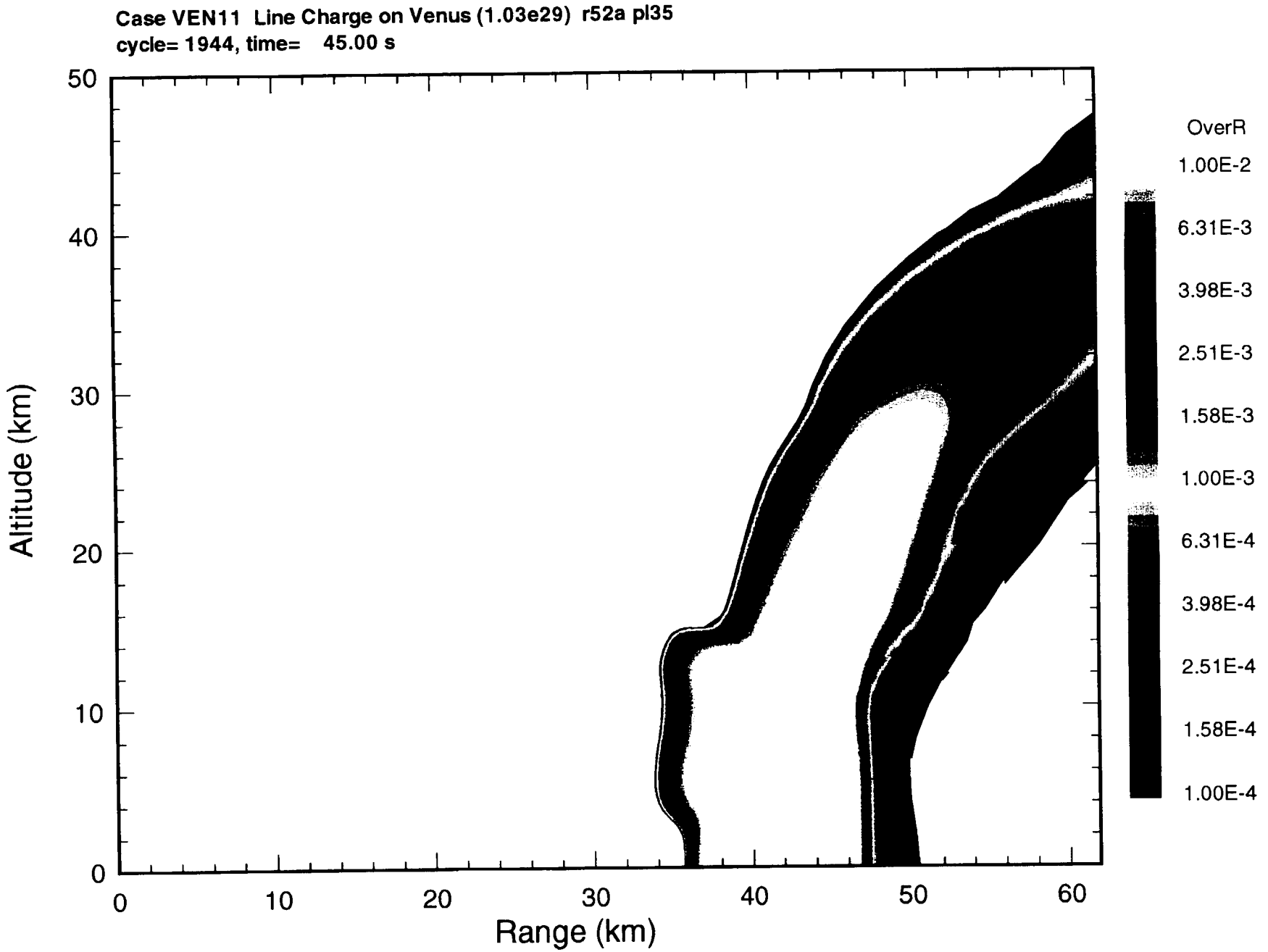
Case VEN11 Line Charge on Venus (1.03e29) r52a pl35
cycle= 1944, time= 45.00 s
Altitude (km)
Range (km)
0
10
20
30
40
50
60
OverR
1.00E-2
6.31E-3
3.98E-3
2.51E-3
1.58E-3
1.00E-3
6.31E-4
3.98E-4
2.51E-4
1.58E-4
1.00E-4

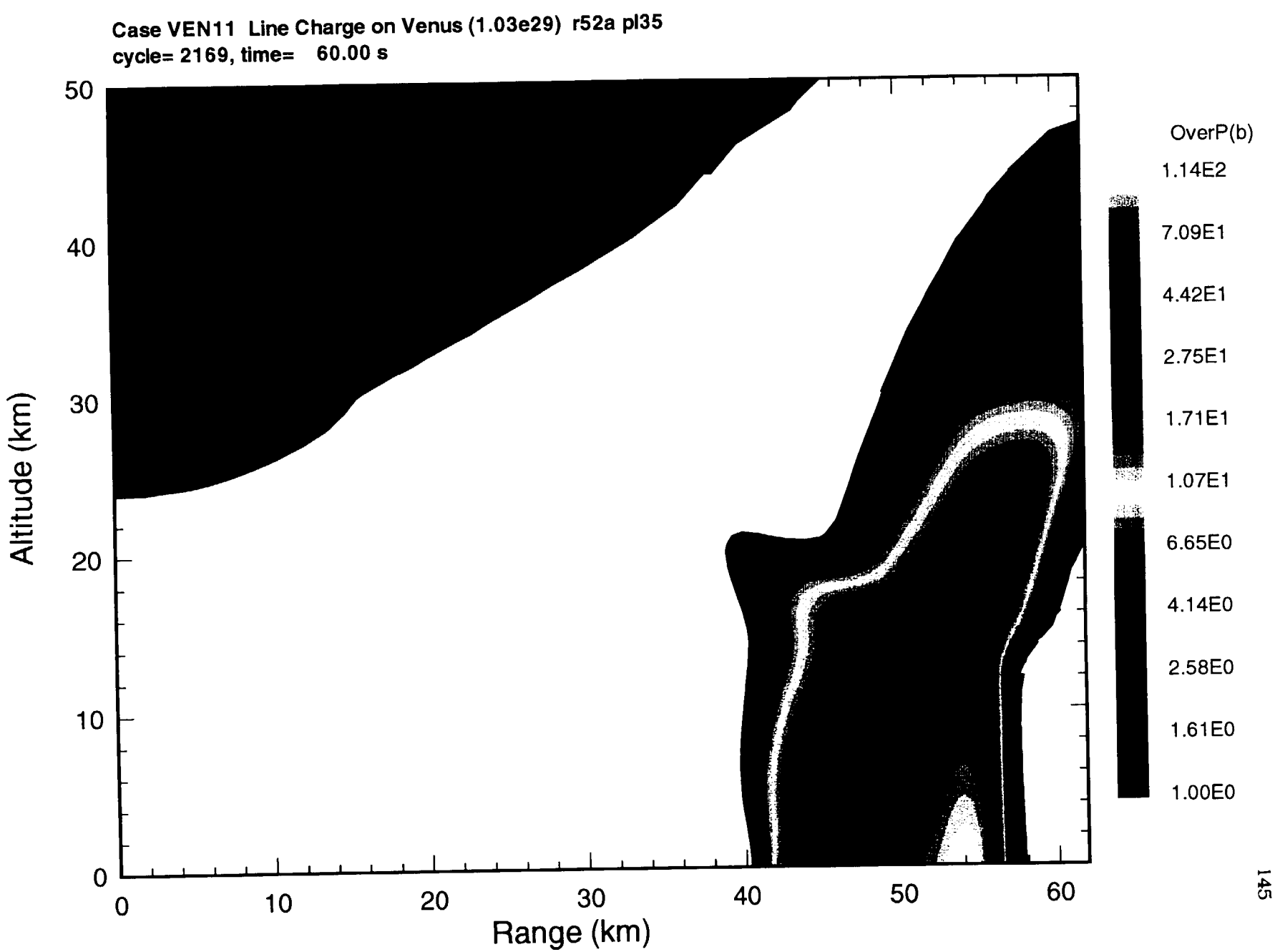
Case VEN11 Line Charge on Venus (1.03e29) r52a pl35
cycle= 2169, time= 60.00 s
Altitude (km)
Range (km)
0
10
20
30
40
50
60
OverP(b)
1.14E2
7.09E1
4.42E1
2.75E1
1.71E1
1.07E1
6.65E0
4.14E0
2.58E0
1.61E0
1.00E0

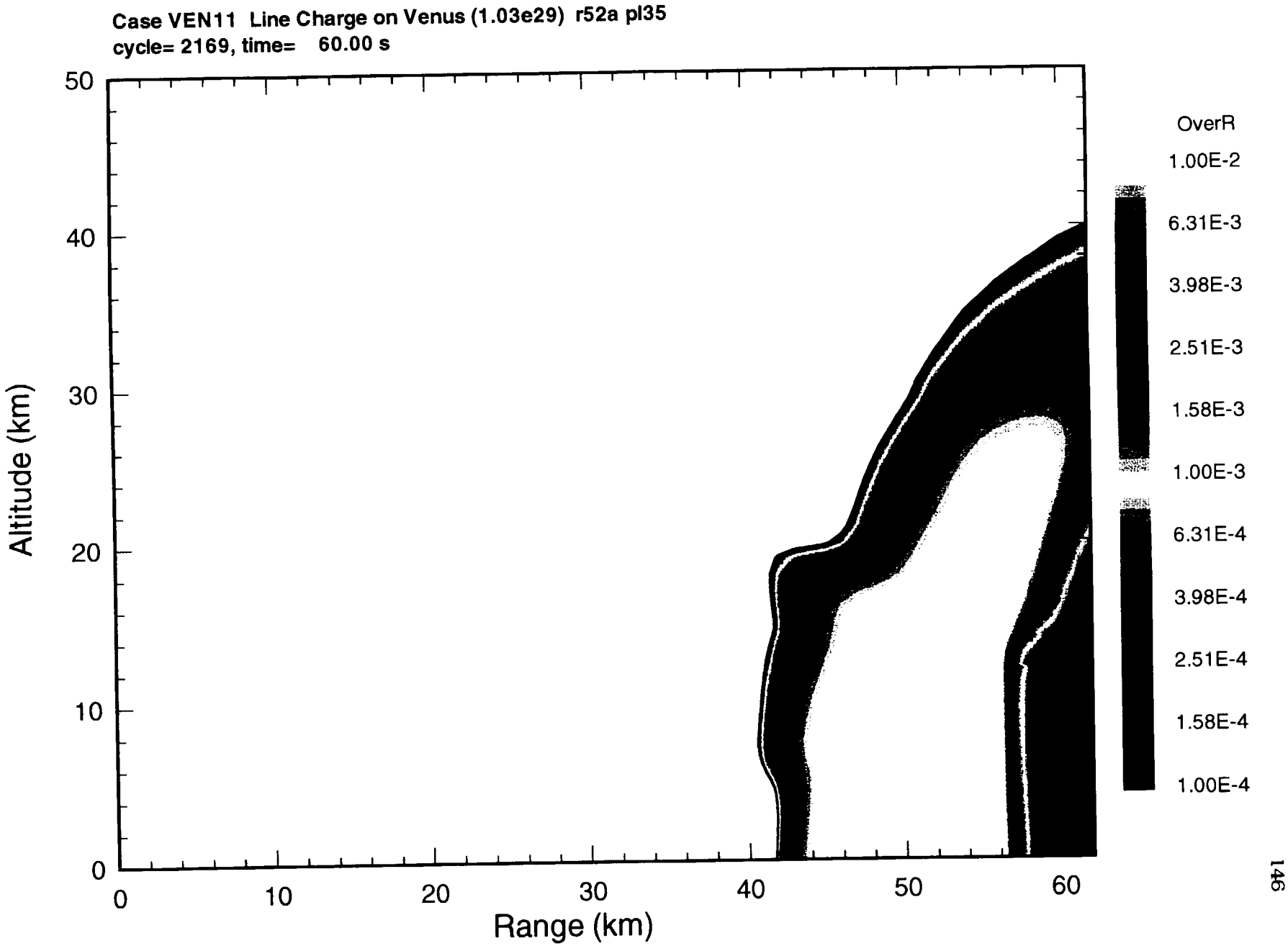
Case VEN11 Line Charge on Venus (1.03e29) r52a pl35
cycle= 2169, time= 60.00 s
Altitude (km)
Range (km)
0
10
20
30
40
50
60
OverR
1.00E-2
6.31E-3
3.98E-3
2.51E-3
1.58E-3
1.00E-3
6.31E-4
3.98E-4
2.51E-4
1.58E-4
1.00E-4

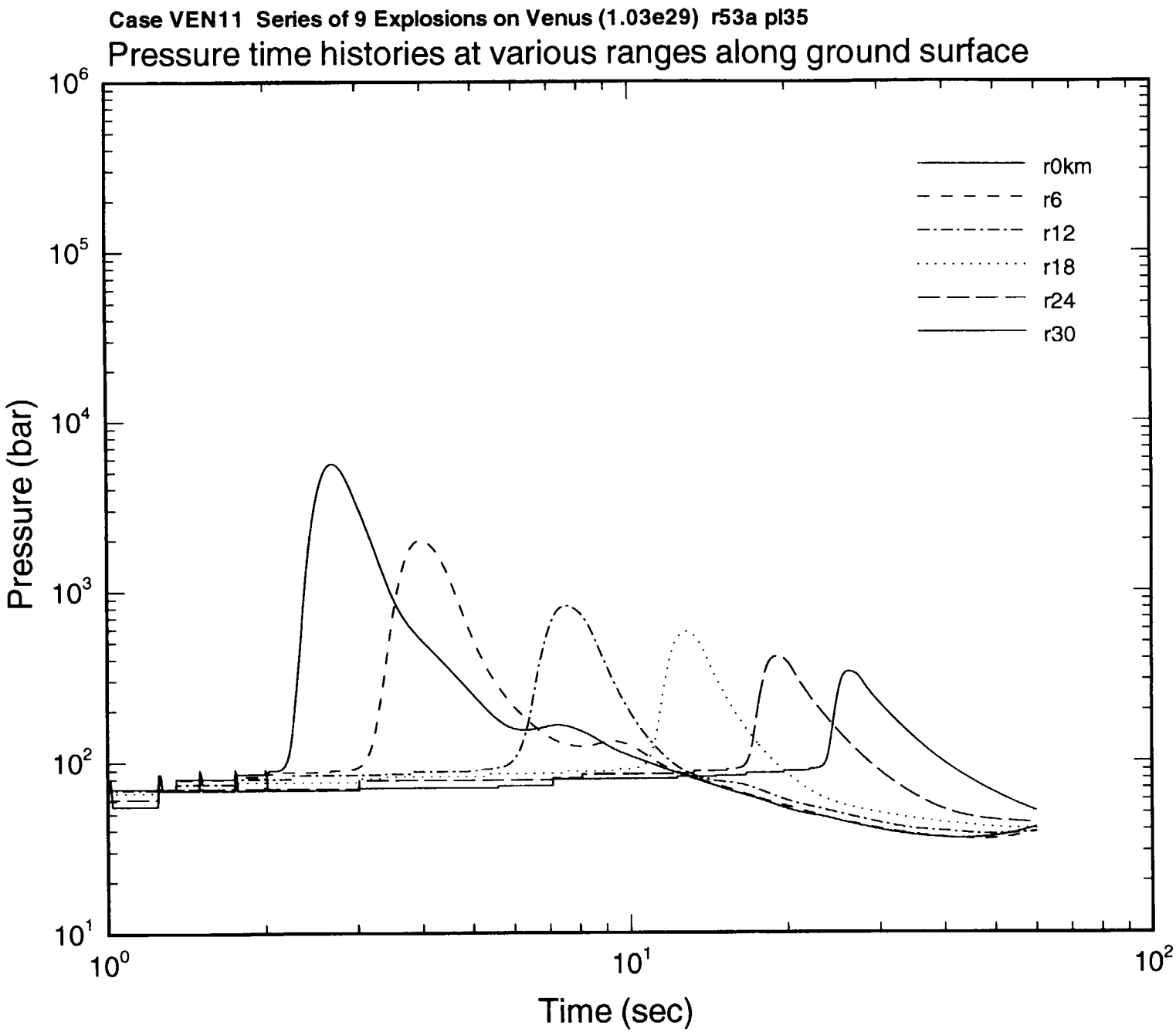
Case VEN11 Series of 9 Explosions on Venus (1.03e29) r53a pl35
Pressure time histories at various ranges along ground surface
r0km
r6
r12
r18
r24
r30
Pressure (bar)
Time (sec)
10^6
10^5
10^4
10^3
10^2
10^1
10^0
10^1
10^2

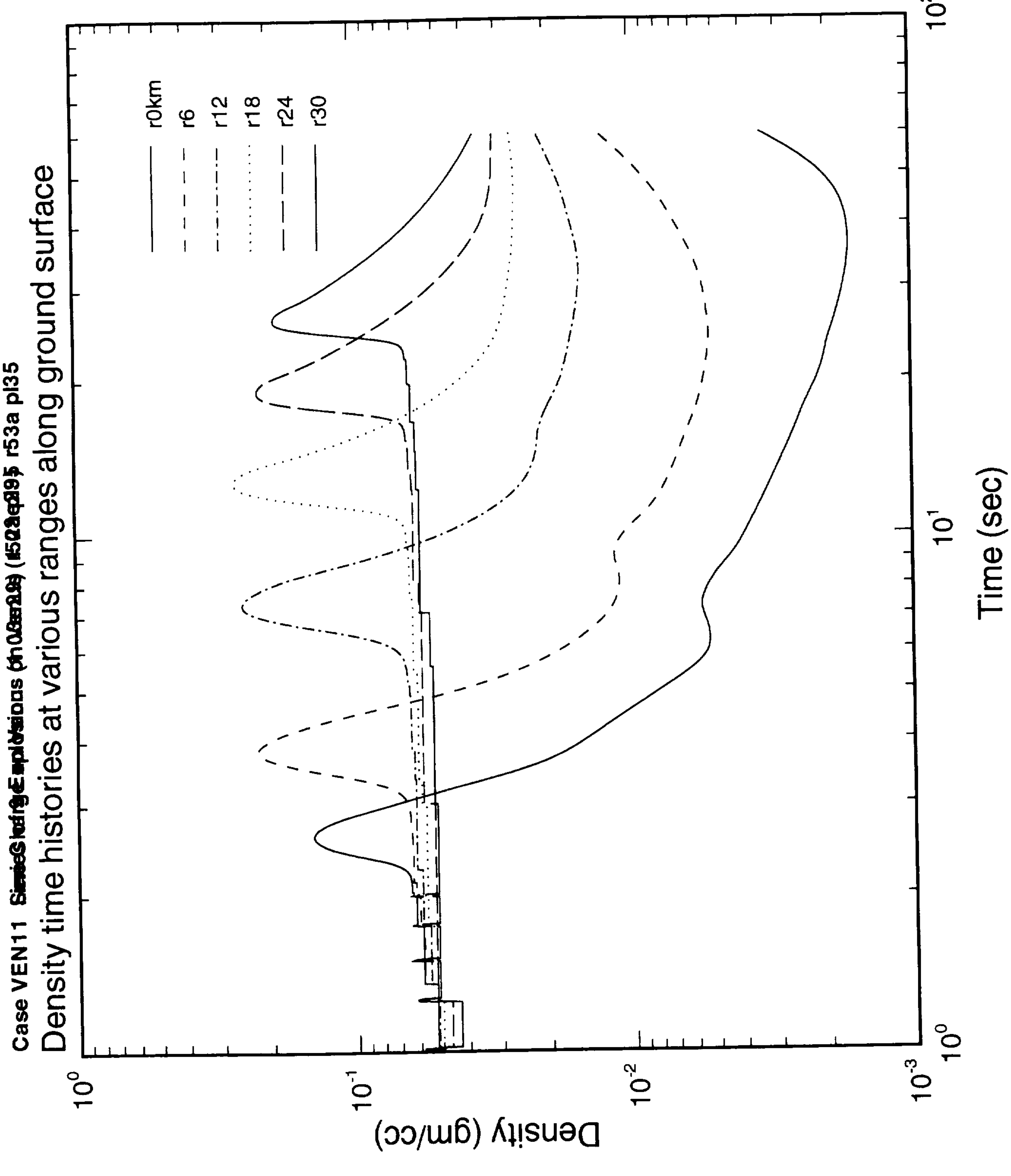
Case VEN11
r53a pl35
Density time histories at various ranges along ground surface
Density (gm/cc)
Time (sec)
10^0
10^-1
10^-2
10^-3
10^0
10^1
10^2
r0km
r6
r12
r18
r24
r30

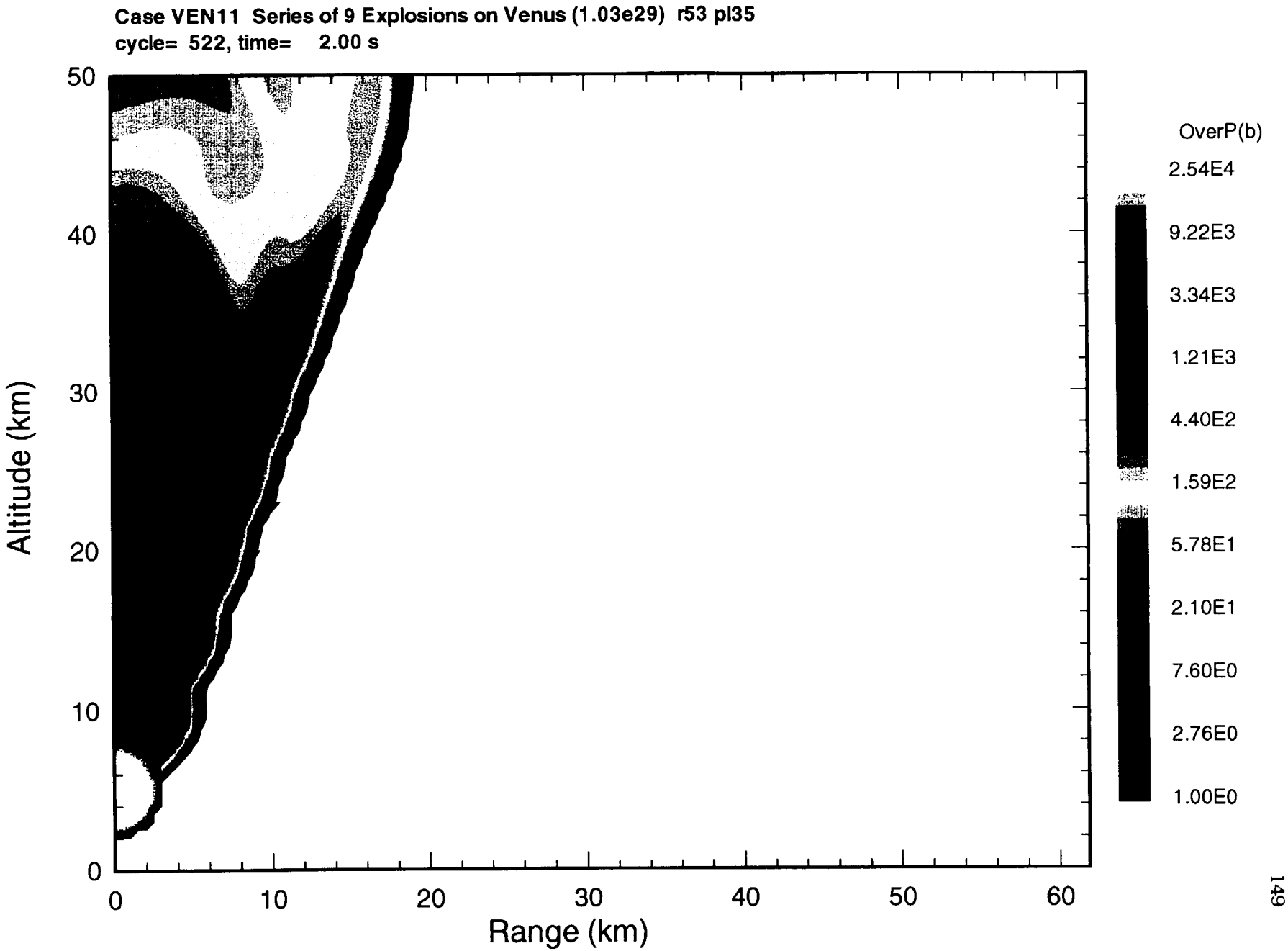
Case VEN11 Series of 9 Explosions on Venus (1.03e29) r53 pl35
cycle= 522, time= 2.00 s
Altitude (km)
Range (km)
0
10
20
30
40
50
60
OverP(b)
2.54E4
9.22E3
3.34E3
1.21E3
4.40E2
1.59E2
5.78E1
2.10E1
7.60E0
2.76E0
1.00E0

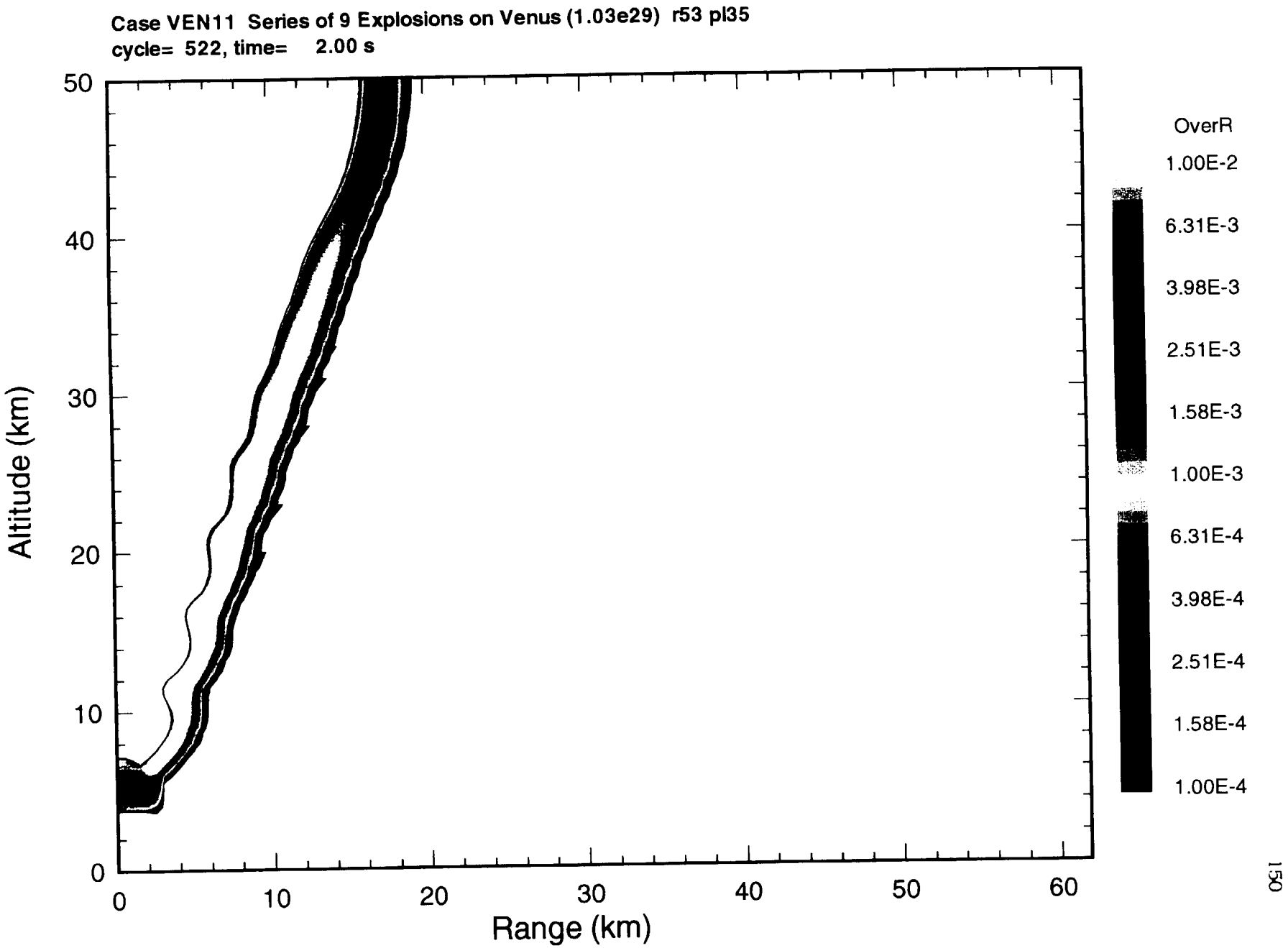
Case VEN11 Series of 9 Explosions on Venus (1.03e29) r53 pl35
cycle= 522, time= 2.00 s
Altitude (km)
Range (km)
0
10
20
30
40
50
60
OverR
1.00E-2
6.31E-3
3.98E-3
2.51E-3
1.58E-3
1.00E-3
6.31E-4
3.98E-4
2.51E-4
1.58E-4
1.00E-4

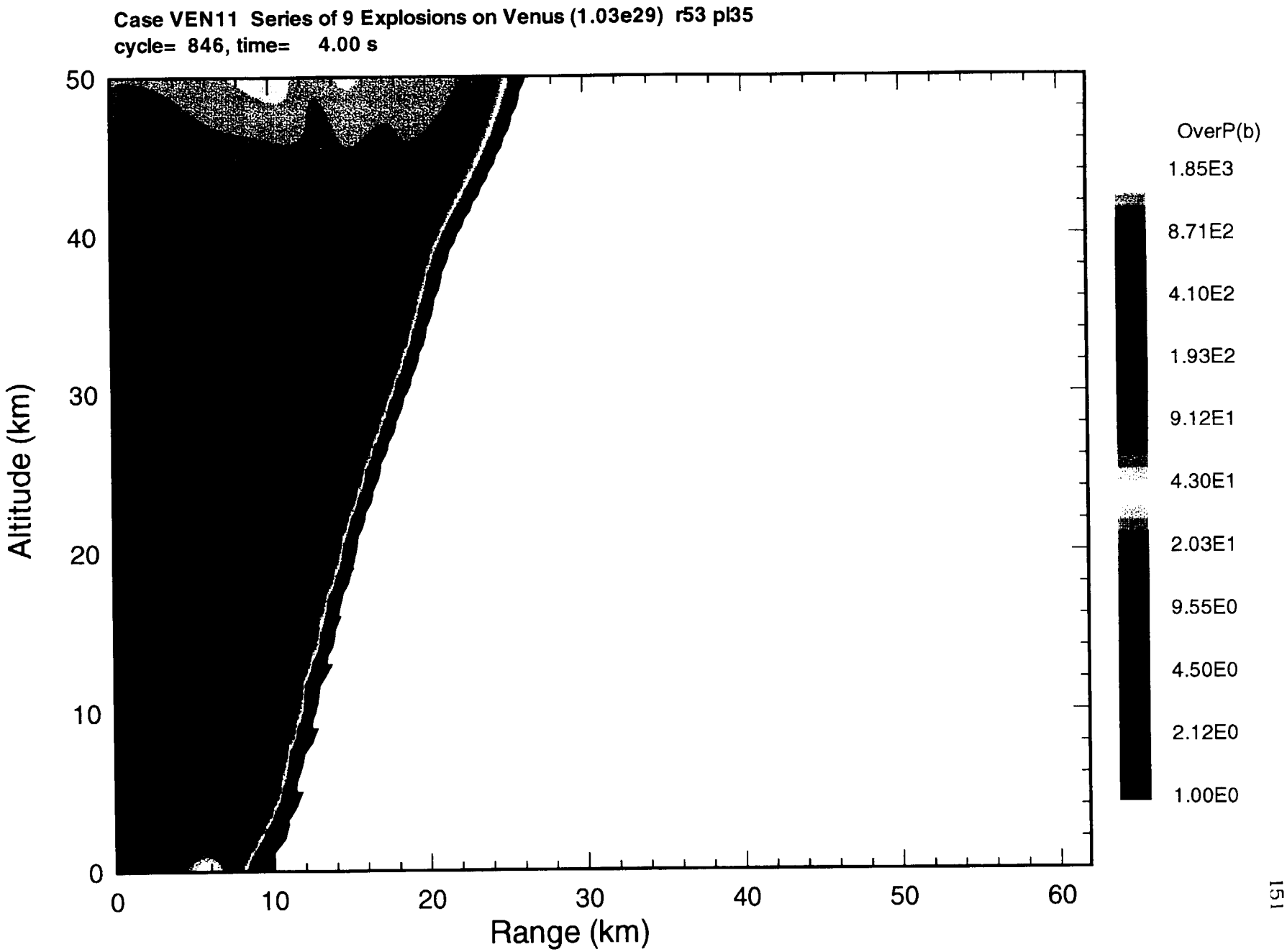
Case VEN11 Series of 9 Explosions on Venus (1.03e29) r53 pl35
cycle= 846, time= 4.00 s
Altitude (km)
Range (km)
0
10
20
30
40
50
60
OverP(b)
1.85E3
8.71E2
4.10E2
1.93E2
9.12E1
4.30E1
2.03E1
9.55E0
4.50E0
2.12E0
1.00E0

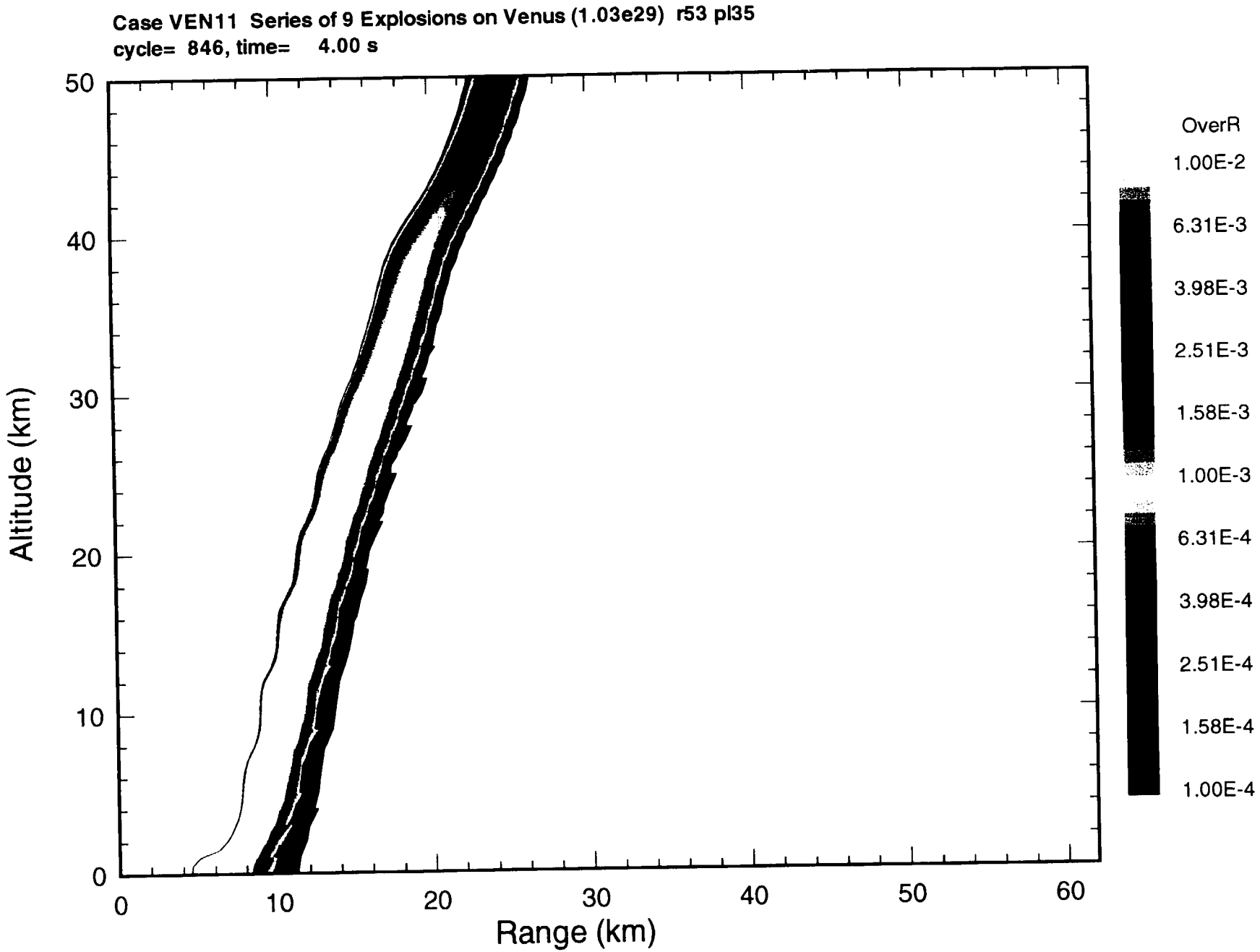
Case VEN11 Series of 9 Explosions on Venus (1.03e29) r53 pl35
cycle= 846, time= 4.00 s
Altitude (km)
Range (km)
0
10
20
30
40
50
60
OverR
1.00E-2
6.31E-3
3.98E-3
2.51E-3
1.58E-3
1.00E-3
6.31E-4
3.98E-4
2.51E-4
1.58E-4
1.00E-4

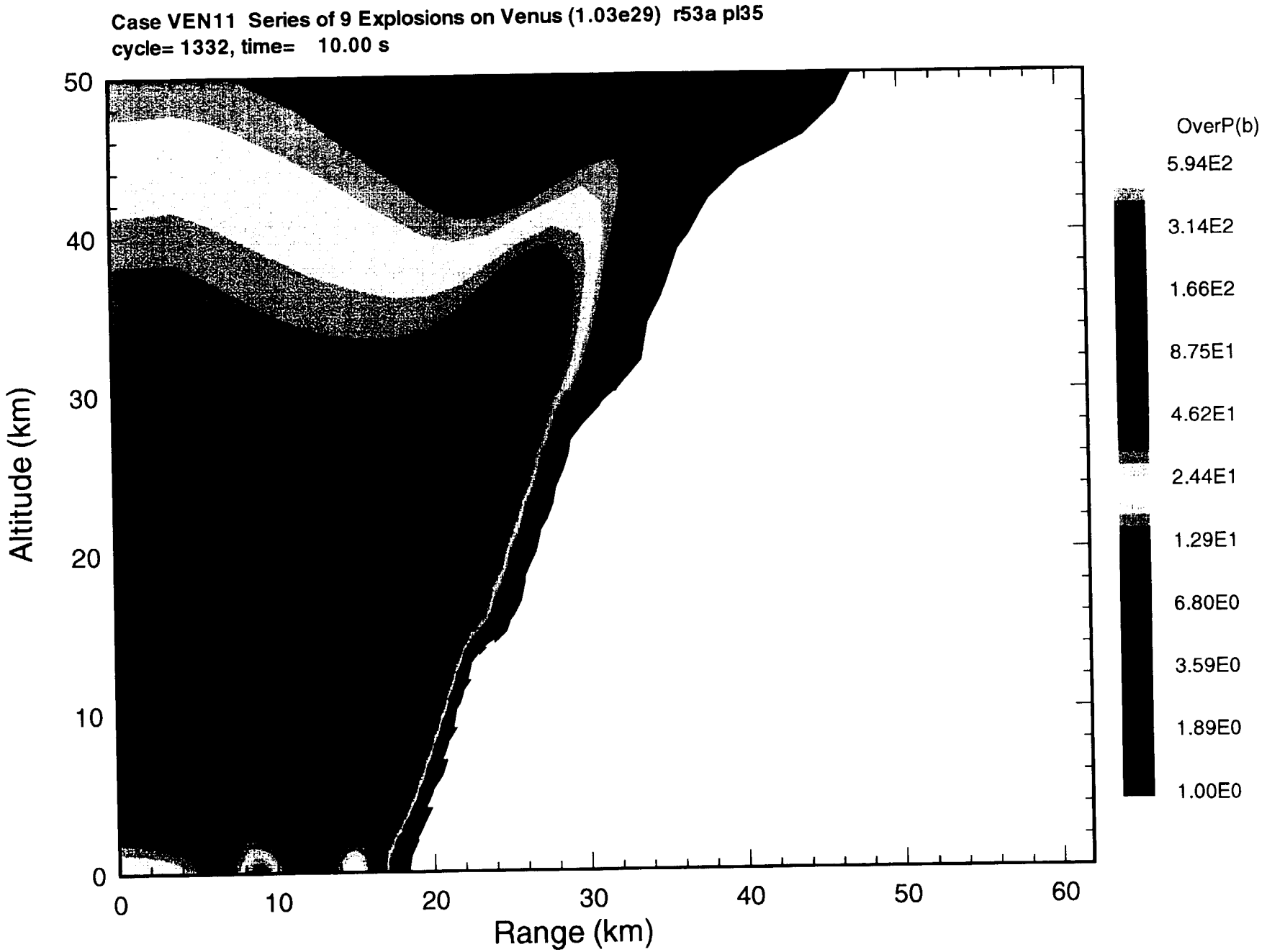
Case VEN11 Series of 9 Explosions on Venus (1.03e29) r53a pl35
cycle= 1332, time= 10.00 s
Altitude (km)
Range (km)
0
10
20
30
40
50
60
OverP(b)
5.94E2
3.14E2
1.66E2
8.75E1
4.62E1
2.44E1
1.29E1
6.80E0
3.59E0
1.89E0
1.00E0

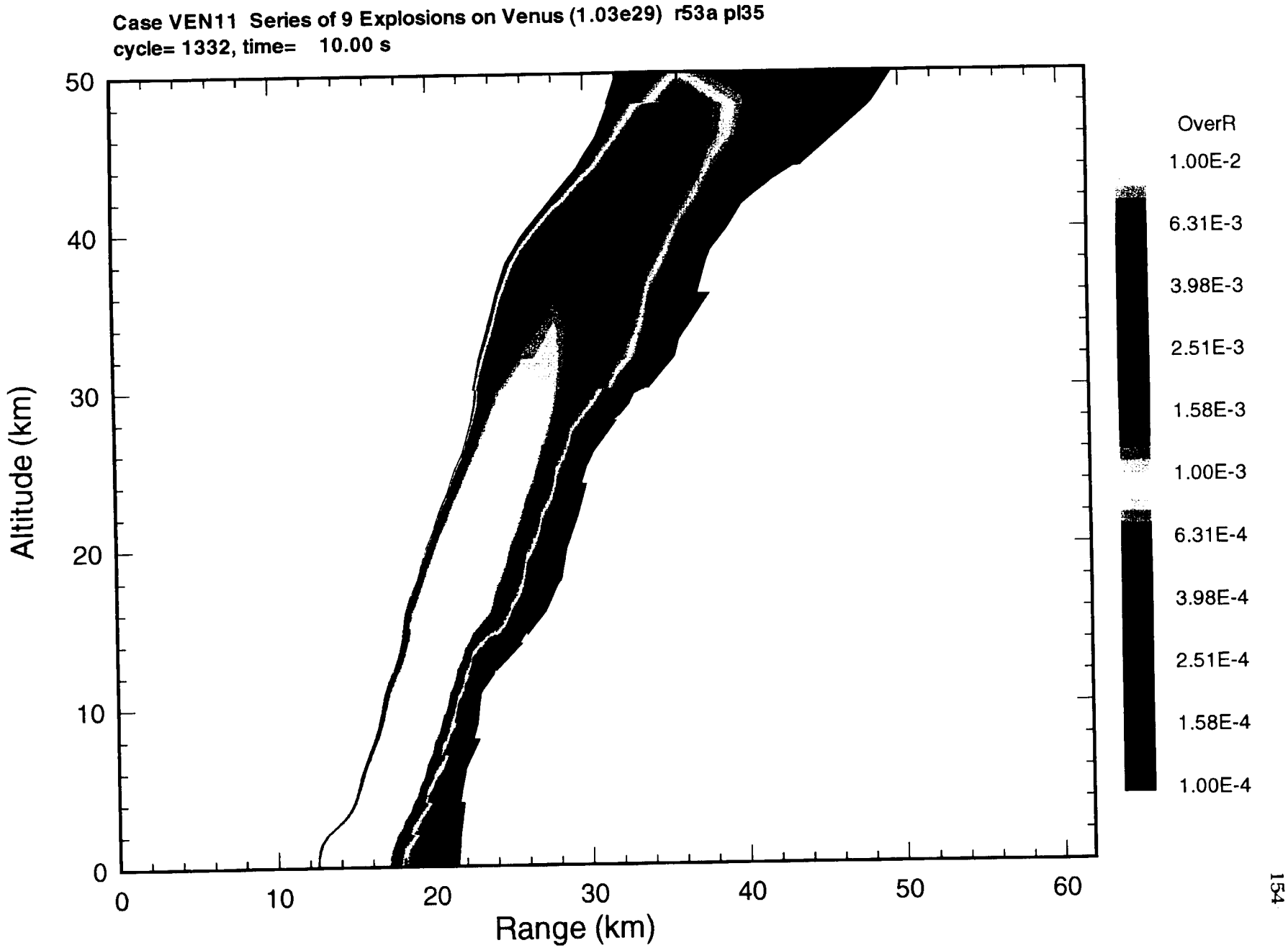
Case VEN11 Series of 9 Explosions on Venus (1.03e29) r53a pl35
cycle= 1332, time= 10.00 s
Altitude (km)
Range (km)
0
10
20
30
40
50
60
OverR
1.00E-2
6.31E-3
3.98E-3
2.51E-3
1.58E-3
1.00E-3
6.31E-4
3.98E-4
2.51E-4
1.58E-4
1.00E-4

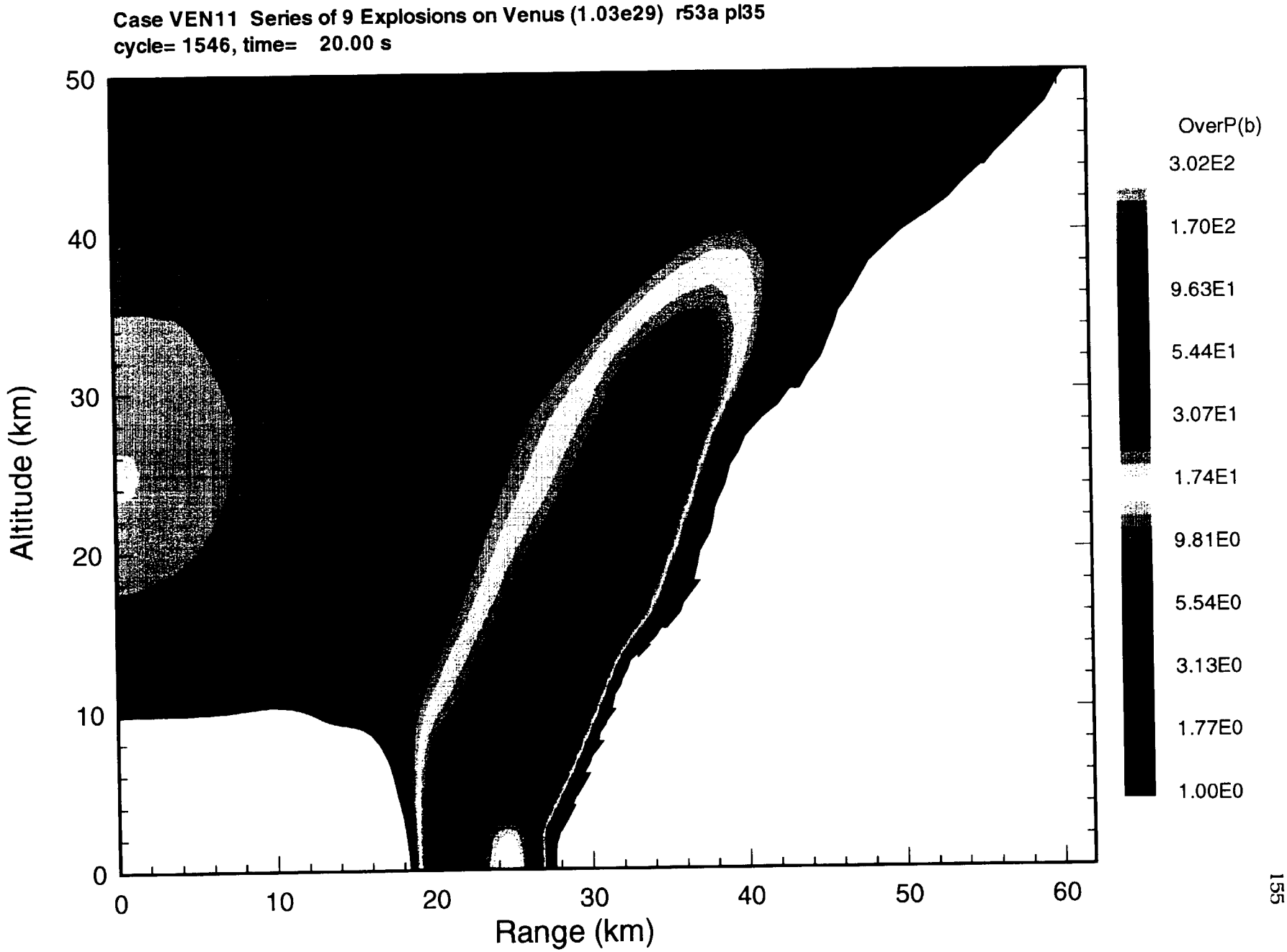
Case VEN11 Series of 9 Explosions on Venus (1.03e29) r53a pl35
cycle= 1546, time= 20.00 s
Altitude (km)
Range (km)
0
10
20
30
40
50
60
OverP(b)
3.02E2
1.70E2
9.63E1
5.44E1
3.07E1
1.74E1
9.81E0
5.54E0
3.13E0
1.77E0
1.00E0

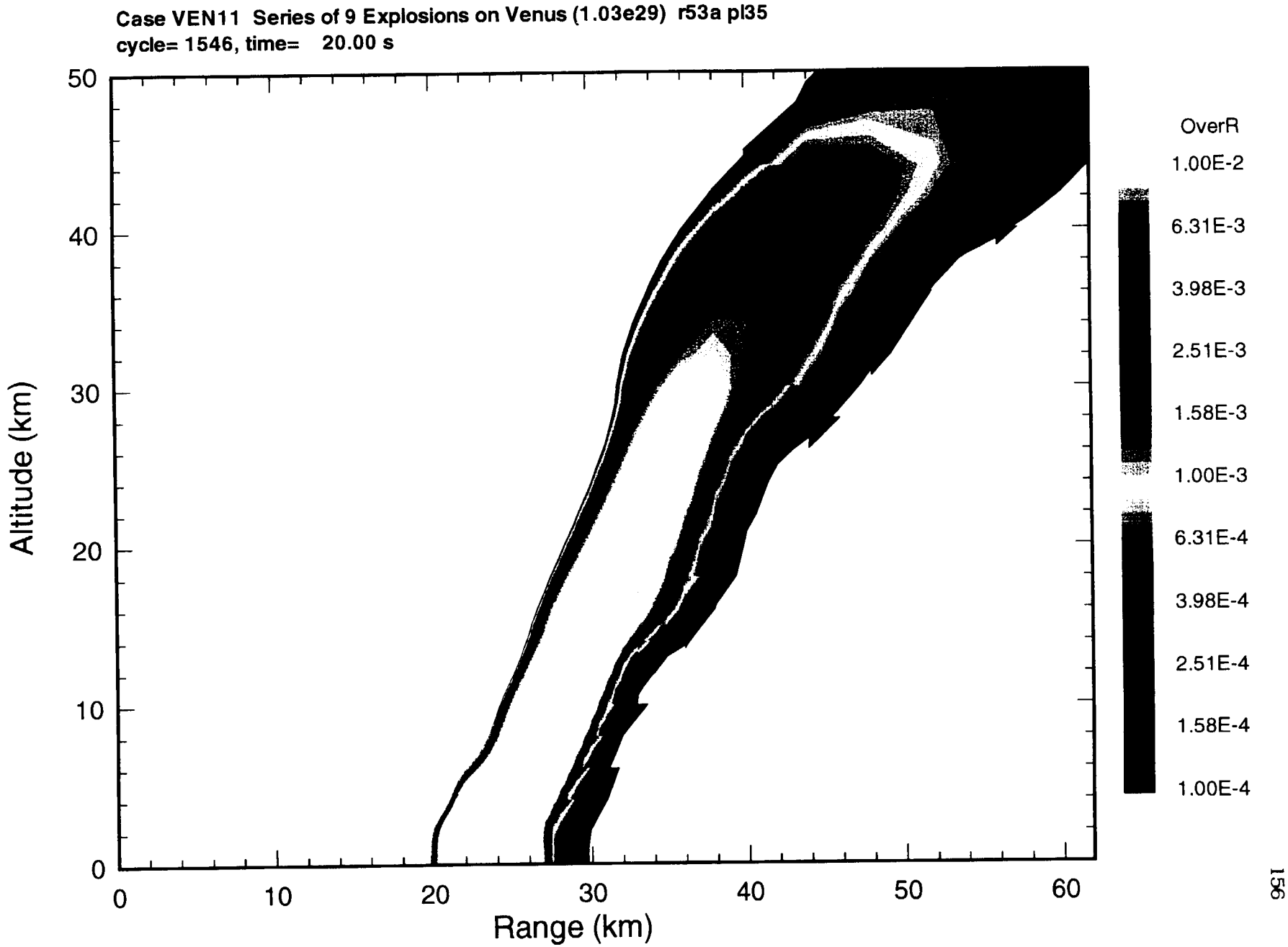
Case VEN11 Series of 9 Explosions on Venus (1.03e29) r53a pl35
cycle= 1546, time= 20.00 s
Altitude (km)
Range (km)
0
10
20
30
40
50
60
OverR
1.00E-2
6.31E-3
3.98E-3
2.51E-3
1.58E-3
1.00E-3
6.31E-4
3.98E-4
2.51E-4
1.58E-4
1.00E-4

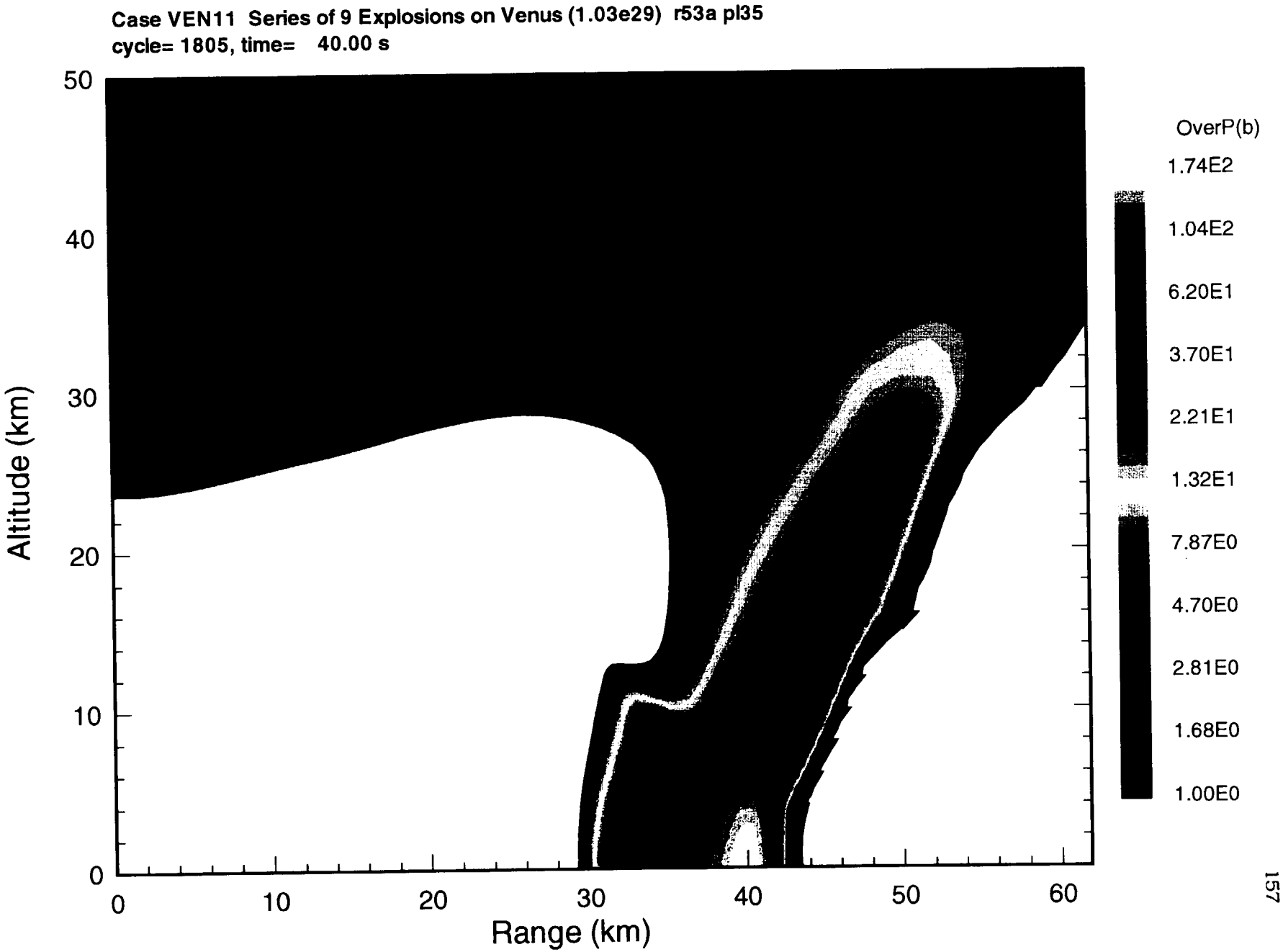
Case VEN11 Series of 9 Explosions on Venus (1.03e29) r53a pl35
cycle= 1805, time= 40.00 s
Altitude (km)
Range (km)
0
10
20
30
40
50
60
OverP(b)
1.74E2
1.04E2
6.20E1
3.70E1
2.21E1
1.32E1
7.87E0
4.70E0
2.81E0
1.68E0
1.00E0

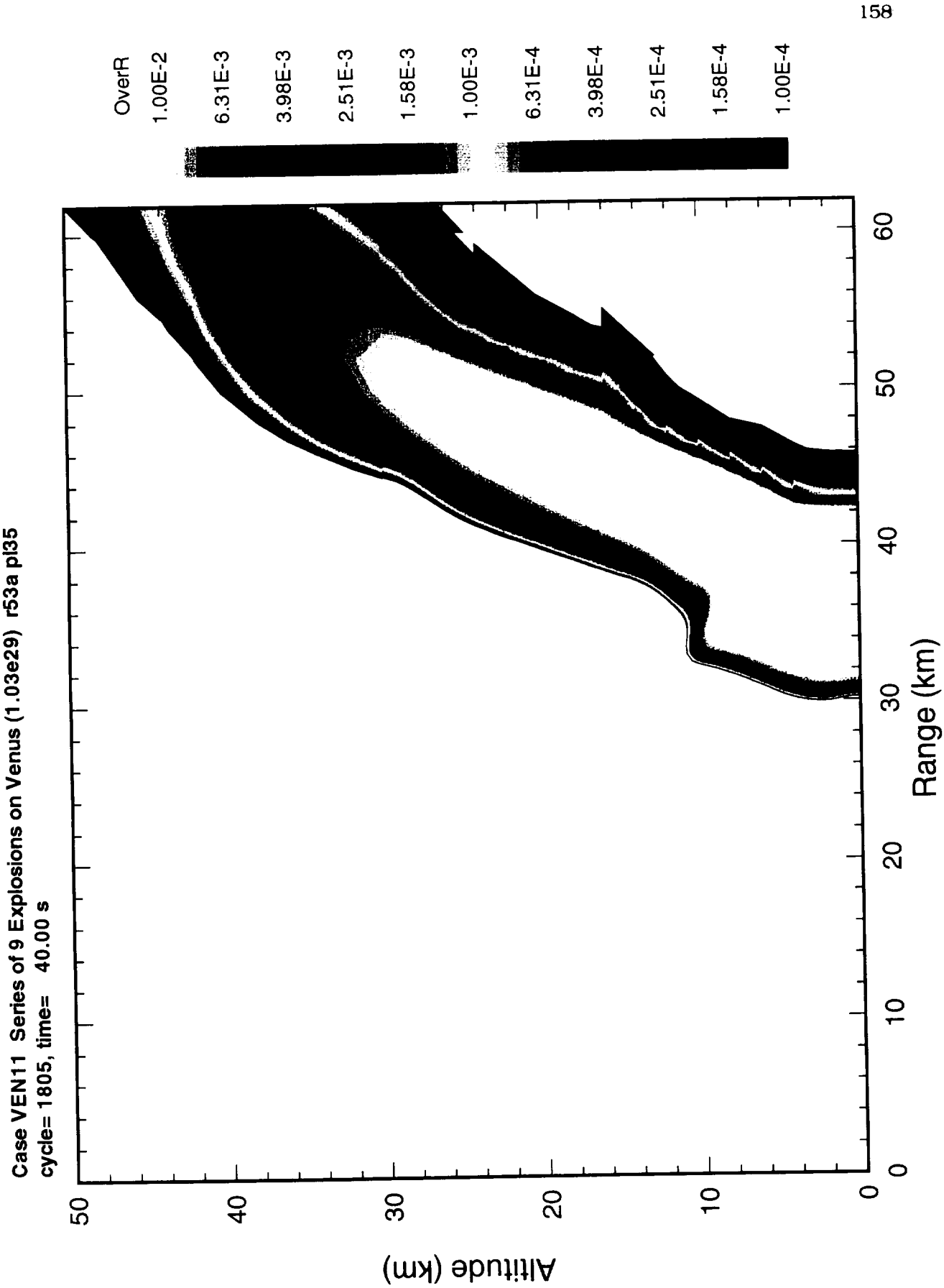
Case VEN11 Series of 9 Explosions on Venus (1.03e29) r53a pl35
cycle= 1805, time= 40.00 s
OverR
1.00E-2
6.31E-3
3.98E-3
2.51E-3
1.58E-3
1.00E-3
6.31E-4
3.98E-4
2.51E-4
1.58E-4
1.00E-4
Altitude (km)
Range (km)
0
10
20
30
40
50
60

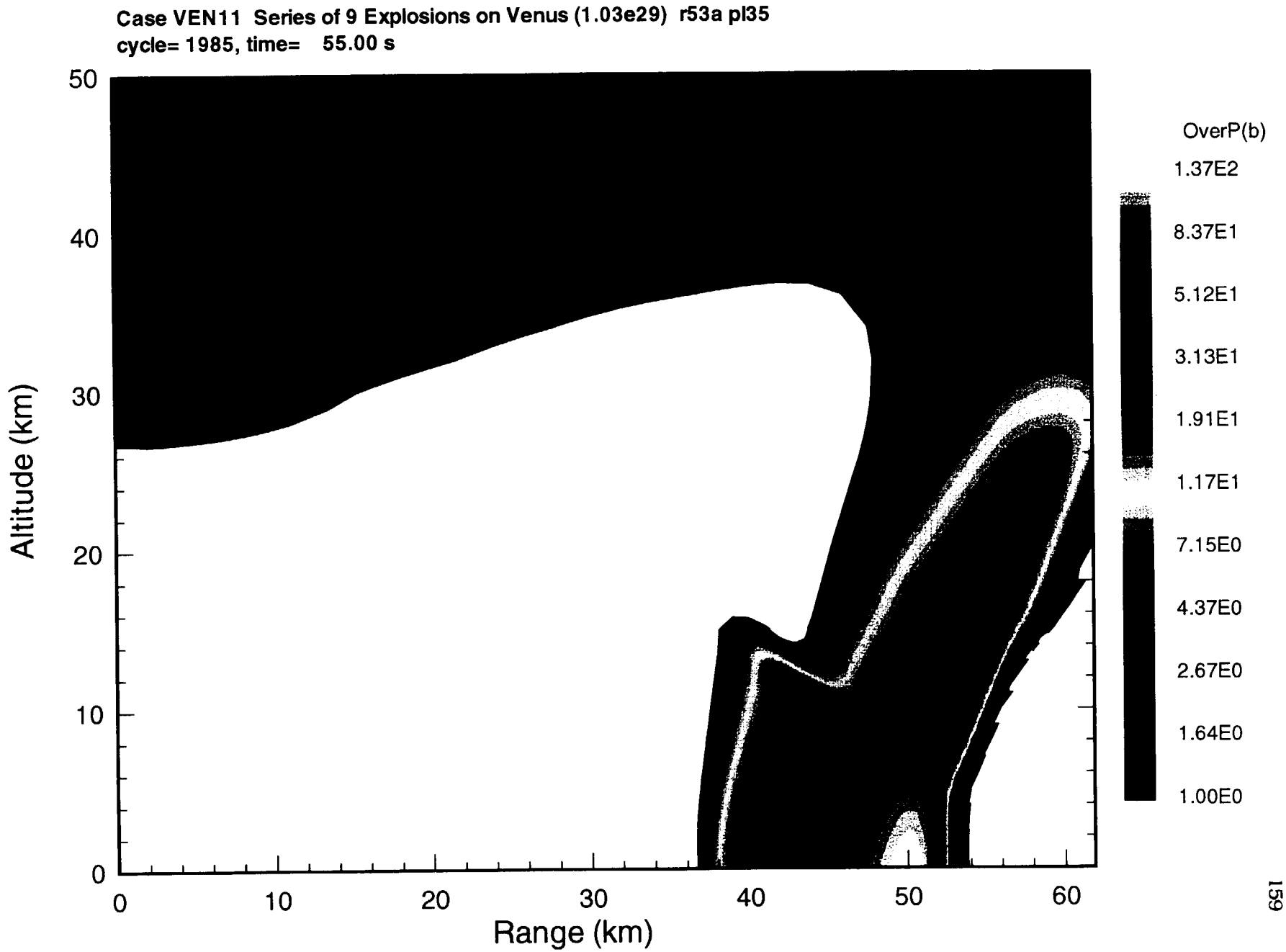
Case VEN11 Series of 9 Explosions on Venus (1.03e29) r53a pl35
cycle= 1985, time= 55.00 s
Altitude (km)
Range (km)
0
10
20
30
40
50
60
OverP(b)
1.37E2
8.37E1
5.12E1
3.13E1
1.91E1
1.17E1
7.15E0
4.37E0
2.67E0
1.64E0
1.00E0

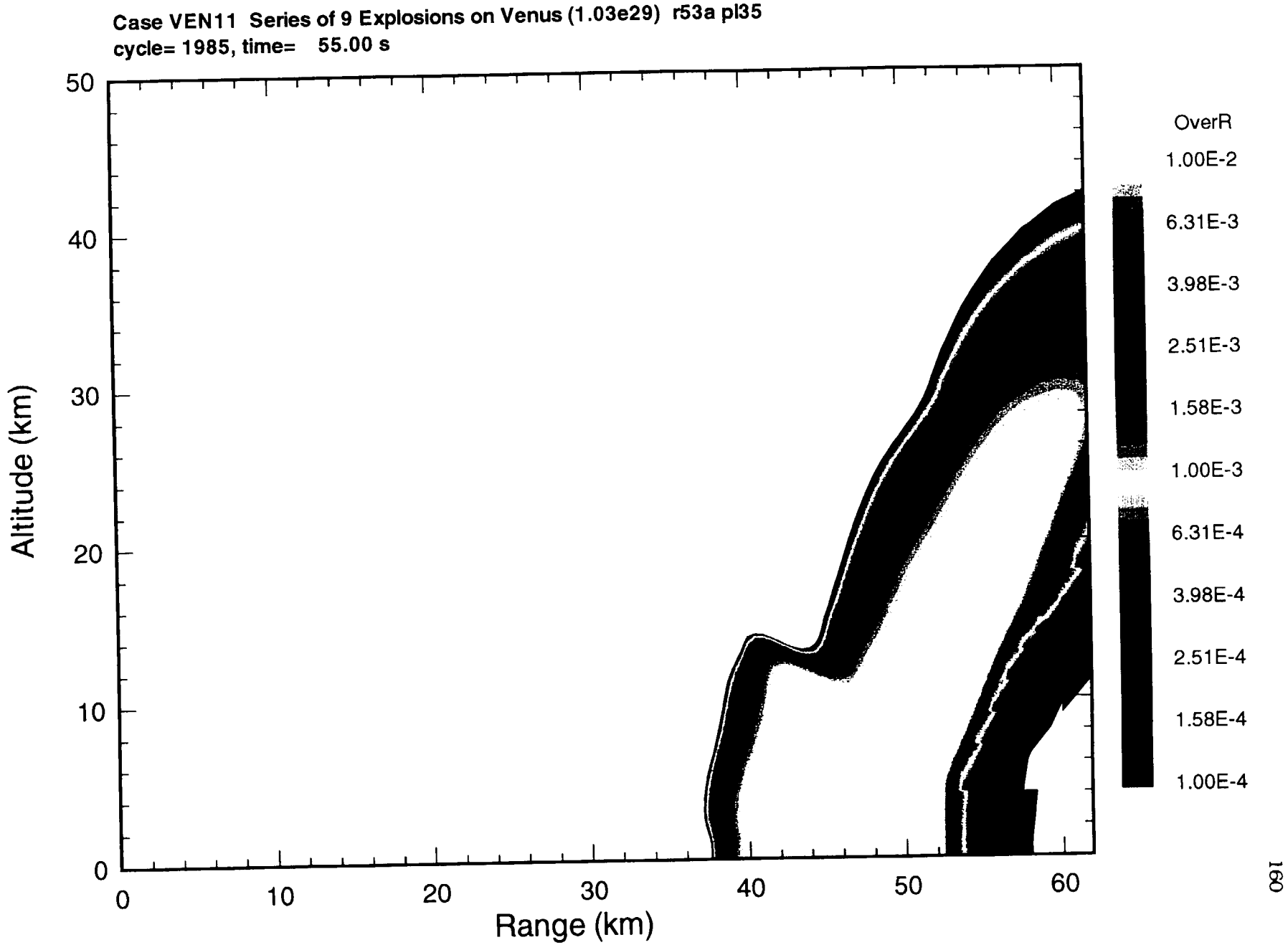
Case VEN11 Series of 9 Explosions on Venus (1.03e29) r53a pl35
cycle= 1985, time= 55.00 s
Altitude (km)
Range (km)
0
10
20
30
40
50
60
OverR
1.00E-2
6.31E-3
3.98E-3
2.51E-3
1.58E-3
1.00E-3
6.31E-4
3.98E-4
2.51E-4
1.58E-4
1.00E-4

REFERENCES

Alexopoulos J. S. and McKinnon (1992) Multiring impact craters on Venus: An overview from Arecibo and Venera imges and initial Magellan data, *Icarus* **100**. 347-363.

Alexopoulos J. S. and McKinnon (1994) Large impact craters and basins on Venus, with implications for ring mechanics on the terrestrial planets. *Geological Society of America, Special Paper 293.*

Brackett R. A. and McKinnon (1992) Cratering mechanics on Venus: Pressure enhancement by the atmospheric "ocean," Geophysical Research Letters, Vol. 19, No. 21, pp.2115-2118.

Buckingham, E. (1914) On physically similar systems; illustrations of the use of dimensional equations. *Phys. Rev. IV*, 4, 345-376.

Buckingham, E. (1915) Model Experiments and the forms of empirical equations. *Transactions ASME* **37**, 263-296.

Chabai, A. J. (1965) On Scaling of Craters Produced by Buried Explosives, *J. Geophys. Res.*, **70**, 5075-5098.

Chapman, C. R. and W. B. McKinnon (1986) Cratering of Planetary Satellites in *Satellites*, Arizona Press, Tucson, p507.

Gault D.E. (1973) Displaced mass, depth, diameter, and effects of oblique trajectories for impact craters formed in dense crystalline rocks. *The Moon*, **6**, 32-44.

Gault D.E. and J. A. Wedekind (1978) Experimental studies of oblique impact, *Proc. Lunar Planet. Sci. Conf. 9th*, 3843.

Hassig P. J., (1991) Atmospheric response to a 10-km-diameter asteroid impact on Venus, *CRT Final Report 5870FR (Prepared for Jet Propulsion Laboratory).*

Hassig P. J., Schlamp R. J., McArdle J. C., and Rosenblatt M.(1991) Numerical simulations of dust/ice clouds from nuclear bursts, *DNA-TR-90-91.*

Hassig P. J., Hatfield D. W., Schlamp R. J., Nguyen C. T., Hookham P. A., and Rosenblatt M. (1992) Advances in nuclear cloud modeling. *DNA-TR-92-23.*

Hassig, P. J., Roddy, D. and Shoemaker, E. (1994) Disintegration of the comet Shoemaker-Levy 9 in the Jovian atmosphere. *ISSW 20 Abst.* Pasadena CA.

Hatfield D., Roddy D., Hassig P. J., and Rosenblatt, M. (1992) Computer simulations of comet-like bodies passing through the Venusian atmosphere-Preliminary results on atmospheric and ground shock effects. *CRT Final Report 5871,*Chatsworth, CA.

Herr, R. W. (1971) Effects of Atmospheric-Lithostatic Pressure Ratio on Explosive Craters in Dry Soil, *NASA Tech Rept. TR-R-366.*

Holsapple, K. A. (1980) The equivalent Depth of Burst for Impact Cratering, *Proc. Lunar Planet. Sci. Conf. 11th*, 2379-2401.

Holsapple K. A. and Schmidt R. M. (1982) On the scaling of crater dimensions—2: Impact processes, *J. Geophys. Res.* **87**(B3), 1849–1870.

Holsapple K. A. and Schmidt R. M. (1987) Point-source solutions and coupling parameters in cratering mechanics, *J. Geophys. Res.* **92**(B7), 6350–6376.

Housen K. R., Schmidt R. M. and Holsapple K. A. (1983) Crater ejecta scaling laws: Fundamental forms based on dimensional analysis, *J. Geophys. Res.* **88**(B3), 2485–2499.

Housen, K.R. and R.M. Schmidt (1990) Atmospheric pressure effects on craters produced by deeply buried explosives, *EOS*, **71**, No. 6, XX.

Housen K. R. and Schmidt R. M. (1995) Ejecta velocities for cratering in rock. Submitted for publication, *Icarus.*

REFERENCES

Housen K. R. and Schmidt R. M. (1995) Whipple shields are characterized by a single geometry parameter. *Journal of Spacecraft and Rockets* **32**, 1, pp 162-168.

Housen K.R., Schmidt R. M., Voss M. E. and Watson H. E. (1993) "D.O.B. scaling and critical depth of burst for cratering (Pressure and strength effects)," DNA TR-92-24, Defense Nuclear Agency, Washington, DC.

Ivanov B. A., Basilevsky A. T., Kryuchkov V. P., and Chernaya I. M. (1986) Impact craters of Venus: Analysis of Venera 15 and 16 data, *J. Geophys. Res.* **91**(B4), D413-D430.

Ivanov B. A., Nemchinov I. V., Svetsov V. A., Provalov A. A., Khazins V. M., and Phillips R. J. (1992) Impact cratering on Venus: Physical and mechanical models, *J. Geophys. Res.* **97**(E10), 16,167-16,181.

Melosh, H. J. (1989) *Impact Cratering — A Geologic Process*, Oxford Univ. Press, New York, p.121.

Johnson, S. W. *et al.*, (1969) Gravity and atm pressure effects on crater formation in sand, *J. Geophys. Res.*, **74**, 4838.

O'Keefe J. D. and Ahrens T. J. (1982) The interaction of the Cretaceous/Tertiary Extinction Bolide with the atmosphere, ocean, and solid earth, *Geological Society of America Special Paper* **190**, 93–102.

O'Keefe J. D. and Ahrens T. J. (1987) Impact crater maximum depth of penetration and excavation, in *Lunar and Planetary Science XVIII*, p. 744-745, Lunar and Planetary Science Institute, Houston, TX.

O'Keefe J. D. and Ahrens T. J. (1993) Planetary Cratering Mechanics, *J. Geophys. Res.* **98**(E9), 17,011–17,028.

Phillips, R. J. *et al.*, (1991) Impact craters on Venus: Initial analysis from Magellan, Science, 252, No. 5003, 288.

Phillips, R. J. *et al.*, (1992) Impact craters and Venus resurfacing history, *J. Geophys. Res.* **97**(E10), 15,923–15,948.

Roddy D.J., Schuster S.H., Rosenblatt M., Grant L.B., Hassig P.J. and Kreyenhagen K.N. (1987) Computer simulations of large asteroid impacts into oceanic and continental sites--Preliminary results on atmospheric, cratering and ejecta dynamics, *Int. J. of Impact Engr.* **5**, 525–541.

Roddy D., Hatfield D. W., Hassig P., Rosenblatt M., Soderblom L., and DeJong E. (1992) Computer simulations of comet- and asteroid-like bodies through the Venusian atmosphere--Preliminary results on atmospheric and ground shock effects, *International Colloquium on Venus*, Houston TX.

Schmidt R. M. (1980) Meteor Crater: Energy of formation — implications of centrifuge scaling, *Proc. Lunar Planet. Sci. Conf. 11th*, p. 2099–2128.

Schmidt, R. M .*et al.*, (1992) Pressure/strength effects in cratering. *EOS*, **73**, 43, 324.

Schmidt, R. M. (1992) Experiments to investigate atmospheric effects on crater size, *Lunar Planet. Sci. XXIII*, 1221-1222.

Schmidt, R. M. (1993) Pressure versus drag effects on crater size, *Lunar Planet. Sci. XXIV*, 1253-1254.

Schmidt R. M. and Hassig P. J. (1995) Asteroid entry into Venusian atmosphere: Pressure and density fields. *Lun Planet. Sci. XXVI*, 1239.

Schmidt R. M. and Holsapple K. A. (1980) Theory and experiments on centrifuge cratering, *J. Geophys. Res.* **85**(B1), 235–252.

Schmidt R. M. and Holsapple K. A. (1982) Estimates of crater size for large-body impact: Gravity scaling results, *Geological Society of America Special Paper* **190**, 93–102.

Schmidt R. M. and Holsapple K. A. (1989) Planetary ejection mechanisms, *EOS*, **70**, No. 43, 1989.

Schmidt R. M. and Housen K. R. (1987) Some recent advances in the scaling of impact and explosion craters, *Int. J. of Impact Engr.* **5**, 543–560.

Schmidt R. M. and Housen K. R. (1995) Dimensional analysis provides framework for simulation experiments. *The Industrial Physicist, AIP,* Vol. 1, No. 1, 21-24.

Schmidt R. M. and Voss M. E. (1987) Shock measurement and visualization in water, *ASME Publication AMD-Vol. 83, p51.*

Schmidt R. M. and Voss M. E. (1989) Experimental investigation of shock wave propagation in shallow water, *DNA Tech. Rept., DNA-TR-89-260-V1,* Washington D. C.

Schmidt, R. M., K. R. Housen and P. J. Hassig (1995) Dynamic similarity for Venusian entry airblast. *EOS*, **76**, 46, F336.

Schmidt, R. M. and Voss, M. E. (1990) Water shock evolution in deep and shallow water, Volume 1--Small scale experimental results. Report DNA-TR-89-260-V1. Defense Nuclear Agency, Alexandria VA.

Schmidt R. M. and Watson H. E. (1988) Impact-generated stress waves and spall in water. *Lunar Planet. Sci. XIX*, 1031-1032.

Schmidt, R.M., K.A. Holsapple and K.R. Housen (1986) Gravity Effects in Cratering, *DNA Tech. Rept., DNA-TR-86-182.*

Schmidt, R. M., Voss, M. E., Housen, K. R., and Holsapple, K. A. (1994) Subscale Experiments to Measure Shock and Bubble Loading on Responding Structures. ASME Publication PVP-Vol. 272, Sloshing, Fluid-Structure Interaction and Structural Response Due to Shock and Impact Loads, Minneapolis MN.

Schmidt R., M. K. R. Housen and P. J. Hassig (1996) Effect of boundary conditions on calculations for Venusian entry shock, *Lun Planet. Sci. XXVII,* 1143.

Schultz, P. H. and D.E. Gault (1979) Atmospheric Effects on Martian Ejecta Emplacement, *J. Geophys. Res.*, **84**, 7669-7687.

Schultz, P. H. and D.E. Gault (1982) Impact Ejecta Dynamics in an Atmosphere: Experimental Results and Extrapolations, *Geological Soc. Am, Paper 190*, 153-174.

Schultz, P. H. (1982) Atmospheric Effects on Impact Cratering Efficiency, *Lunar Planet. Sci. XIII*, 694-695.

Schultz, P. H. (1988) Atmospheric Effects on Impact Cratering Efficiency, *Lunar Planet. Sci. XIX*, 1037-1038.

Schultz, P. H. (1990a) Evidence for Atmospheric Effects on Martian Crater Shape, *Lunar Planet. Sci XXI*, 1097-1098.

Schultz, P. H. (1990b) Evidence for Atmospheric Effects on Cratering Efficiency, *Lunar Planet. Sci XXI*, 1095-1096.

Schultz, P. H. (1992) Atmospheric effects on cratering efficiency, *J. Geophys. Res.*, **97**, E1 975-1005.

Schaber G. G., Strom R. G., Moore H. J., Soderblom L. A., Kirk R. L., Chadwick D. J., Dawson D. D., Gaddis L. R., Boyce J. M., and Joel Russell (1992) Geology and distribution of impact craters on Venus: Shat ar they telling us? *J. Geophys. Res.*, **97**, E8, 13,257-13,301.

Strom, R. G. (1988) Implications for the origin of the objects responsible for the period of late hearvy bombardment from the terrestrial planet cratering record. *Lunar Planet. Sci. XIX*, 1141-1142.

Takata, T., T. J. Ahrens, and R. J. and Phillips (1995) Atmospheric effects on cratering on Venus, *J. Geophys. Res.*, **100**, E11 23,329-23,348.

Voss, M. E. and Schmidt, R. M. (1993) Explosive Shock Wave Propagation in Shallow Water: Small-Scale Experiments with Rock and Layered Bottom Geologies, Volumes 1 and 2. Report DNA-TR-27-93-V1,-V2, Defense Nuclear Agency, Alexandria VA.